

The oxidation capacity of the atmosphere
-
OH and HO₂ radical measurements in a
boreal forest environment using laser
induced fluorescence spectroscopy

Dissertation

zur Erlangung des Grades
„Doktor der Naturwissenschaften“
im Promotionsfach Physik

am Fachbereich Physik, Mathematik und Informatik
der Johannes Gutenberg-Universität Mainz,
ausgeführt am
Max-Planck-Institut für Chemie, Mainz

vorgelegt von
Korbinian Hens

Oktober 2013

Abstract

The main oxidant in the degradation process of volatile organic compounds (VOCs) in the atmosphere is the hydroxyl radical (OH), which is in fast equilibrium with the hydroperoxyl radical (HO₂). Previous observation and model comparison of these radical species in forest ecosystems have unveiled a significant gap in understanding of the underlying processes.

Within the framework of this PhD thesis, OH and HO₂ were measured using laser-induced fluorescence (LIF) in a pine dominated forest in Southern Finland during the HUMPPA-COPEC-2010 (*Hyytiälä United Measurements of Photochemistry and Particles in Air – Comprehensive Organic Precursor Emission and Concentration study*) field campaign in summer 2010. Different components of the LIF instrument were optimized and a modified background signal detection method (*InletPreInjector* technique) was integrated and applied for the first time. Simultaneous side-by-side measurements of hydroxyl radicals were conducted with two instruments using chemical ionization mass spectrometry (CIMS) and LIF, showing good agreement. The instrument intercomparison proves the ability and performance of the modified LIF instrument to measure atmospheric OH concentrations accurately. Subsequently, the LIF instrument was moved to the top of a 20 m tower, above the canopy, to investigate the radical chemistry at the ecosystem-atmosphere interface. Comprehensive measurements including observations of the total OH reactivity were conducted and analysed using steady-state calculations as well as an observationally constrained box model.

Production rates of OH calculated from measured OH precursors, are under conditions of moderate OH reactivity ($k'_{\text{OH}} \leq 15 \text{ s}^{-1}$), consistent with those derived from the steady state assumption and measured total OH loss. The primary photolytic sources of OH contribute up to one third of the total OH production. It was shown that under conditions of moderate OH reactivity hydroxyl recycling occurs mainly by HO₂ reacting with NO and O₃. In periods when high total OH reactivity ($k'_{\text{OH}} > 15 \text{ s}^{-1}$) was observed, additional recycling pathways, forming OH directly, not via reaction of HO₂ with NO or O₃ were identified.

Box model simulations agree with measurements for atmospheric hydroxyl radicals ($\text{OH}_{\text{mod.}}/\text{OH}_{\text{obs.}}=1.04 \pm 0.16$), while HO₂ mixing ratios are significantly underpredicted ($\text{HO}_2^{\text{mod.}}/\text{HO}_2^{\text{obs.}}=0.3 \pm 0.2$) and simulated OH reactivity does not match the observed OH reactivity. The simultaneous underprediction of HO₂ and OH reactivity in periods in which OH concentrations were simulated well, suggests that the missing OH reactivity is an unaccounted source of HO₂. Additional RO₂/HO₂ sources that are independent of OH, such as the thermal decomposition of transported peroxyacyl nitrates (PAN) and the photolysis of glyoxal, are indicated.

Zusammenfassung

Das wichtigste Oxidationsmittel für den Abbau flüchtiger Kohlenwasserstoffverbindungen (*VOC*, engl.: *volatile organic compounds*) in der Atmosphäre ist das Hydroxylradikal (OH), welches sich in einem schnellen chemischen Gleichgewicht mit dem Hydroperoxyradikal (HO_2) befindet. Bisherige Messungen und Modellvergleiche dieser Radikalspezies in Waldgebieten haben signifikante Lücken im Verständnis der zugrundeliegenden Prozesse aufgezeigt.

Im Rahmen dieser Doktorarbeit wurden Messungen von OH- und HO_2 -Radikalen mittels laserinduzierten Fluoreszenzmesstechnik (*LIF*, engl.: *laser-induced fluorescence*) in einem Nadelwald in Süd-Finnland während der Messkampagne HUMPPA-COPEC-2010 (*Hyytiälä United Measurements of Photochemistry and Particles in Air – Comprehensive Organic Precursor Emission and Concentration study*) im Sommer 2010 durchgeführt. Unterschiedliche Komponenten des LIF-Instruments wurden verbessert. Eine modifizierte Methode zur Bestimmung des Hintergrundsignals (engl.: *InletPreInjector technique*) wurde in den Messaufbau integriert und erstmals zur Messung von atmosphärischem OH verwendet. Vergleichsmessungen zweier Instrumente basierend auf unterschiedlichen Methoden zur Messung von OH-Radikalen, chemische Ionisationsmassenspektrometrie (*CIMS* - engl.: *chemical ionization mass spectrometry*) und LIF-Technik, zeigten eine gute Übereinstimmung. Die Vergleichsmessungen belegen das Vermögen und die Leistungsfähigkeit des modifizierten LIF-Instruments atmosphärische OH Konzentrationen akkurat zu messen. Nachfolgend wurde das LIF-Instrument auf der obersten Plattform eines 20 m hohen Turmes positioniert, um knapp oberhalb der Baumkronen die Radikal-Chemie an der Schnittstelle zwischen Ökosystem und Atmosphäre zu untersuchen. Umfangreiche Messungen - dies beinhaltet Messungen der totalen OH-Reaktivität - wurden durchgeführt und unter Verwendung von Gleichgewichtszustandsberechnungen und einem Boxmodell, in welches die gemessenen Daten als Randbedingungen eingehen, analysiert. Wenn moderate OH-Reaktivitäten ($k'_{\text{OH}} \leq 15 \text{ s}^{-1}$) vorlagen, sind OH-Produktionsraten, die aus gemessenen Konzentrationen von OH-Vorläuferspezies berechnet wurden, konsistent mit Produktionsraten, die unter der Gleichgewichtsannahme von Messungen des totalen OH Verlustes abgeleitet wurden. Die primären photolytischen OH-Quellen tragen mit einem Anteil von bis zu einem Drittel zur Gesamt-OH-Produktion bei. Es wurde gezeigt, dass OH-Rezyklierung unter Bedingungen moderater OH-Reaktivität hauptsächlich durch die Reaktionen von HO_2 mit NO oder O_3 bestimmt ist. Während Zeiten hoher OH-Reaktivität ($k'_{\text{OH}} > 15 \text{ s}^{-1}$) wurden zusätzliche Rezyklierungspfade, die nicht über die Reaktionen von HO_2 mit NO oder O_3 , sondern direkt OH bilden, aufgezeigt.

Für Hydroxylradikale stimmen Boxmodell-Simulationen und Messungen gut überein ($\text{OH}_{\text{mod.}}/\text{OH}_{\text{obs.}}=1.04 \pm 0.16$), während HO_2 -Mischungsverhältnisse in der Simulation signifikant unterschätzt werden ($\text{HO}_2^{\text{mod.}}/\text{HO}_2^{\text{obs.}}=0.3 \pm 0.2$) und die simulierte OH-Reaktivität nicht mit der gemessenen OH-Reaktivität übereinstimmt. Die gleichzeitige Unterschätzung der HO_2 -Mischungsverhältnisse und der OH-Reaktivität, während OH-Konzentrationen von

der Simulation gut beschrieben werden, legt nahe, dass die fehlende OH-Reaktivität in der Simulation eine noch unberücksichtigte HO₂-Quelle darstellt. Zusätzliche, OH-unabhängige RO₂/HO₂-Quellen, wie z.B. der thermische Zerfall von herantransportiertem Peroxyacetylnitrat (PAN) und die Photolyse von Glyoxal sind indiziert.

Contents

1. The oxidation capacity of the atmosphere	1
2. HO_x photochemistry in the troposphere	5
2.1. HO _x production	5
2.2. HO _x sinks	8
2.3. Oxidation of volatile organic compounds and HO _x recycling	8
2.4. The relationship between HO _x and J _{O(1D)}	10
3. HO_x measurements using the HORUS instrument	13
3.1. Techniques for HO _x radical measurements	13
3.1.1. Techniques for the detection of atmospheric OH	13
3.1.2. Techniques for the detection of atmospheric HO ₂	18
3.2. HORUS	19
3.2.1. Measurement principle	20
3.2.2. Instrument setup	23
3.2.3. Calibration	30
3.2.4. Other dependencies of the instrument sensitivity	34
3.2.5. Interferences	35
4. HUMPPA–COPEC–2010	43
4.1. Measurement site and instrumentation	43
4.2. HO _x observations	46
4.3. Primary HO _x production	52
4.4. OH budget – calculated based on observations	54
4.5. OH / HO ₂ ratio	58
4.6. OH recycling probability and cycling-lifetime	58
4.7. HO _x recycling pathways	63
5. Box model simulations	69
5.1. Box model CAABA/MECCA	69
5.1.1. Significance and sensitivity	71

5.2. HO _x simulations using CAABA/MECCA	73
5.2.1. OH loss tuning	75
5.2.2. Significance and uncertainties	75
5.2.3. Sources and sinks of HO _x	79
6. Summary and conclusions	85
A. Measurements of trace gas species and meteorological parameters during HUMPPA-COPEC 2010	89
B. Chemical mechanism – MTM	93
C. Data sheets	123
C.1. Pen-ray line source – LOT-QuantumDesign, Europe	123
C.2. NIST NO standard	124
C.3. Dew Point Generator - LI-610 & H ₂ O-Monitor - LI-7000	125
C.4. Gas Flow Calibrator – DryCal, BIOS, USA	127
C.5. Optical Fiber – Thorlabs GmbH, Germany	130
C.6. Laser Dye Pyrromethene-597 – Exciton, USA	131
D. Abbreviations	133
Bibliography	137

List of tables

3.1. Parameters of temperature dependency for collisional quenching rate coefficients.	23
3.2. Systematic uncertainties during actinometric measurement.	34
4.1. Instrumentation applied for above canopy observations during HUMPPA-COPEC2010	47
4.2. HO _x budget under different conditions of observed radiation and total OH reactivity.	67
5.1. Deposition rates/velocities used in the model	71
5.2. Sensitivity analysis with respect to changes in observed, model constraining parameters.	78
A.1. Median levels and variability of relevant trace gases under different conditions of observed radiation and total OH reactivity.	90

List of figures

1.1. Spatial and temporal scales of variability for atmospheric constituents.	2
2.1. Schematic overview of the HO _x radical photochemistry in the troposphere. . .	6
2.2. Reaction scheme for OH and HO ₂ radical formation following 1-OH addition to isoprene by a 1,5- and a 1,6-H-shift, respectively.	10
3.1. Three pressure dependent components of the LIF sensitivity.	16
3.2. Schematic representation of the timing of photon counting process.	17
3.3. Schematic of the branches in the rotational structure of OH showing the transitions used for laser excitation ($A^2\Sigma^+ - X^2\Pi, v'=0 \leftarrow v''=0$).	21
3.4. Dye laser setup.	24
3.5. Transmission curves for isosceles brewster prisms (for p-polarized, s-polarized and mixed-polarized light) of different glass types.	25
3.6. Suppression of laser pulse backreflections and OH fluorescence signal.	26
3.7. Setup of the HORUS detection system.	27
3.8. Schematic representation of the optical path inside a White Cell.	28
3.9. Two ways to determine OH background signal.	29
3.10. Characteristics of the vacuum system.	30
3.11. Schematic of the setup used for calibration of the HORUS instrument.	31
3.12. Calibration of the NO analyzer (C42, Thermo Environmental Instruments) for NO in N ₂ and N ₂ O.	32
3.13. Actinic flux density of the mercury lamp used for calibration of the HORUS instrument.	33
3.14. Sensitivity change inside the second detection axis of HORUS as a function of the associated laser scatter signal.	36
3.15. NO dependency of the HO ₂ signal during a calibration.	38
3.16. NO dependency of the total (HO ₂ + RO ₂) signal during ambient air measurement and expected HO ₂ signal (blue line) applying the conversion efficiency derived from titration experiment during calibration.	40
3.17. Titration experiments at different water vapour mixing ratios.	41
3.18. Comparison of the measured H ₂ O ₂ with simulation based on HO ₂ measurements by LIF.	42

4.1. SMEAR II field station, Hyytiälä, Southern Finland (61° 51' N, 24° 17' E, 181 m a.s.l.)	44
4.2. Setup of the HORUS instrument on the HUMPPA tower.	45
4.3. Comparison of OH measurements by IPI-LIF-FAGE technique and by CIMS on ground (University of Helsinki, Petäjä et al., 2009).	48
4.4. Comparison of OH measurements by IPI-LIF-FAGE technique and by CIMS (University of Helsinki, Petäjä et al., 2009) based on 30-minute average data.	49
4.5. Simultaneous OH measurements on the ground and above the canopy.	50
4.6. Linear correlation of OH and $J_{O(1D)}$ during HUMPPA–COPEC–2010.	51
4.7. Contributions to the primary HO_x production.	52
4.8. Average diurnal OH production below and budget above the canopy.	55
4.9. Observed OH / HO_2 ratio vs. NO / CO ratio.	59
4.10. Expected NO dependency of the recycling probability r	60
4.11. OH recycling probability (r) as a function of the ambient NO mixing ratio in different environments.	61
5.1. Data availability for model simulations.	70
5.2. Histogram of the Monte-Carlo simulation ($N = 9999$) for the reaction rate coefficients on a single dataset in the early afternoon above canopy.	72
5.3. Simulated vs. observed OH concentrations and HO_2 mixing ratios, applying the MIM2 chemistry scheme and the recently proposed MIM3 including new additions in the isoprene chemistry.	74
5.4. Simulations including the terpene mechanism MTM.	74
5.5. Tuning the model to the observed total OH reactivity by introducing an additional α -pinene equivalent.	76
5.6. Uncertainties of HO_x simulations.	77
5.7. Simulated contributions to the OH production during HUMPPA–COPEC–2010.	80
5.8. Simulated contributions to the observed total OH reactivity during HUMPPA–COPEC–2010.	81
5.9. Simulated production and loss rates of HO_2 during HUMPPA–COPEC–2010 under conditions of different radiation and total observed OH reactivity.	83
A.1. Timeseries of trace gas species and meteorological parameters during HUMPPA–COPEC–2010.	91
A.1. (continued): Timeseries of trace gas species and meteorological parameters during HUMPPA–COPEC–2010.	92
C.1. Discontinuous spectrum of the pen-ray line source.	123

C.2. National Institute of Standards & Technology - NO standard used for actinic flux density calibration of the mercury lamp that was applied for calibration of the HORUS instrument.	124
C.3. Certificate of Calibration, Dew Point Generator Licor, LI-610.	125
C.4. Calibration of the H ₂ O-Monitor - Licor, LI-7000, using the Dew Point Generator Licor, LI-610.	126
C.5. Certificate of Calibration, DryCal, DC-LC-1 & HC-LC-1, BIOS International, USA.	127
C.6. Specifications of coated silica fiber used for transportation of the 308 nm UV light within HORUS.	130
C.7. Pyrromethene-597 laser dye, Exciton, USA, www.exciton.com	131

1. The oxidation capacity of the atmosphere

The gaseous envelope surrounding the earth - the atmosphere of earth - mainly consists of nitrogen ($\sim 78\%$ by vol.), oxygen ($\sim 21\%$ by vol.), argon ($\sim 0.93\%$ by vol.), and a variable fraction of water ($\sim 0\text{-}2\%$ by vol.). Beside those main constituents, trace gases, such as the greenhouse gases and numerous volatile organic compounds (VOCs), are significantly influencing physical and chemical properties of the earth's atmosphere. Chemical compounds are continuously emitted into the atmosphere by geological, biogenic, and anthropogenic processes (Seinfeld and Pandis, 2006; Guenther et al., 1995, and ref. therein) including substances harmful to health. Thus, environmental pollution by emissions and the capability of the atmosphere to remove pollutants strongly affects the quality of life. This fact led to an enhanced interest in understanding the underlying processes within the last decades.

Removal of pollutants and trace gases from the atmosphere is mostly initiated by oxidation processes. Products like carbon dioxide (CO_2), water (H_2O), and water soluble compounds, that can be subsequently removed from atmosphere by wet and dry deposition, are formed. Only a few species are not affected by tropospheric oxidation chemistry, such as N_2O and chlorofluorocarbons (CFCs), which reach the stratosphere by vertical transport where they finally degrade.

The most important oxidant in the troposphere during daytime is the hydroxyl radical (OH). Furthermore, the OH radical is initiating the formation of a wide variety of secondary species, e.g. ozone and secondary organic aerosol. Ozone (O_3) and hydrogen peroxide (H_2O_2) in the case of oxidation within cloud droplets are also contributing to the oxidation capacity of the atmosphere. The photolabile nitrate radical (NO_3) can be an important nighttime oxidant in the polluted atmosphere. Though, due to its outstanding reactivity the OH radical dominates the cleansing capacity of the atmosphere.

The oxidation capacity in turn defines the atmospheric lifetime and consequently affects the abundance of most trace gases. An overview of typical lifetimes and associated transport ranges for important atmospheric trace gas species is given in Figure 1.1.

Environmental changes, like increasing anthropogenic emissions, enhanced energy consumption, change in landuse, such as urbanisation and deforestation influence the physical and chemical properties of the atmosphere, leading to a continuous change of the atmospheric composition. Nonetheless, the global OH concentration remained almost constant in the past (Lelieveld et al., 2002). This indicates that the atmospheric oxidation capacity is to some extent a buffered system with respect to changes in atmospheric trace gas concentrations. OH radicals are not necessarily removed from the system by oxidation processes. In

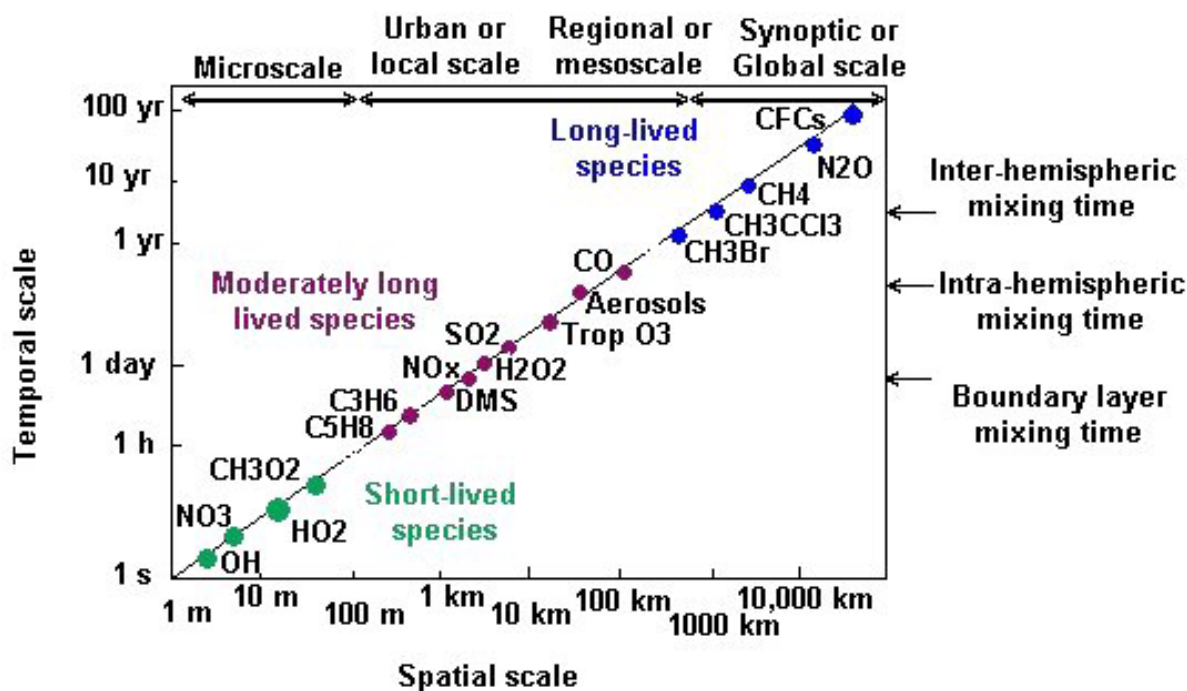


Abbildung 1.1.: Spatial and temporal scales of variability for atmospheric constituents (Taken from Seinfeld and Pandis, 2006).

fact, they are efficiently recycled, for example via the strongly linked hydroperoxyl radical (HO_2), which forms back OH in presence of nitrogen oxide (NO). Such buffering mechanisms are crucial to preserve the oxidation capacity and to prevent from catastrophic conditions, when toxic gases and gases relevant to climate would accumulate to harmful levels.

Relevance of forest ecosystems

Forests cover about one third of the earth's total land surface (FAO, 2010). They are known to be an important global source of biogenic volatile organic compounds (BVOCs) that are very reactive towards OH (Williams, 2004). A major contribution to BVOCs, such as isoprene, monoterpenes (e.g. α -pinene), and sesquiterpenes (e.g. farnesene), is emission by vegetation (Fehsenfeld et al., 1992; Guenther et al., 1995; Kesselmeier and Staudt, 1999). Therefore, forest emissions are expected to significantly influence the oxidation capacity of the atmosphere. Measurement of OH and HO_2 radicals in forest environments, however,

unveils serious deficits in our understanding of the underlying processes. Different types of forests are known to emit various characteristic BVOCs influencing the oxidation chemistry. Several studies in and above isoprene-rich forest environments have been conducted in the past. Aircraft measurements of atmospheric trace gases performed over the pristine Amazon rainforest during the GABRIEL¹ campaign (Lelieveld et al., 2008; Kubistin et al., 2010) unexpectedly showed higher OH concentrations than predicted from box and global models. Furthermore, Kubistin et al. (2010) reported that isoprene acts as a buffer for the hydroxyl radicals, which is related to an increased HO_x recycling in the oxidation mechanism of BVOCs at low NO_x conditions, when the OH recycling reaction of HO₂ with NO is inhibited. Similarly, other studies from tropical forest regions (Stone et al., 2011; Whalley et al., 2011) reported that increased recycling would be necessary to explain the measured HO_x values. An increase of the deposition rates for OH reactants, like methyl vinyl ketone (MVK) and methacrolein (MACR), can help explain the measurement results for ground-based observations during the OP3² campaign in Borneo (Pugh et al., 2010a). It is unclear if measurements of the total OH reactivity are available as the observations are not compared with observations of the reactivity in the latter study. The authors conclude that the inadequacies apparent in the model are related to the representation of detailed physical and micrometeorological effects rather than errors in the chemical scheme. Measurements conducted in a deciduous forest (Tan et al., 2001) also showed an underestimation of observed OH concentrations from box model simulations. Although two follow up studies at the same site showed model predicted OH generally being in reasonable agreement with the measured OH, the model did underestimate the OH concentrations observed by a factor of about three in the afternoon during warmer periods (Griffith et al., 2013). It remains unclear if higher biogenic VOC emissions within those periods caused an instrumental interference as recently suggested by Mao et al. (2012).

Further, Kim et al. (2013) reported reasonable agreement between observed OH and that from steady-state calculations using observations, particularly measurements of HO₂, in a monoterpene dominated forest environment. Constrained box model calculations underpredicted the observed HO₂ by as much as a factor of eight and underestimated the observed OH by a factor of four. The authors conclude that the OH recycling occurs mainly via the reaction of HO₂ with NO in this forest, which is characterized by high 2-methyl-3-buten-2-ol (MBO) and monoterpene emissions (Kim et al., 2013).

Studies on oxidation processes in monoterpene dominated environments are rare. Direct OH reactivity measurements in a boreal forest, conducted by Sinha et al. (2008) and a box model study investigating the OH reactivity budget (Mogensen et al., 2011), revealed a significant fraction of “unknown OH reactivity”. Comprehensive measurements in the same boreal forest were conducted during the HUMPPA–COPEC–2010 campaign (*Hyytiälä United Measurements of Photochemistry and Particles in Air – Comprehensive*

¹Guyanas Atmosphere-Biosphere Exchange and Radicals Intensive Experiment with the Learjet

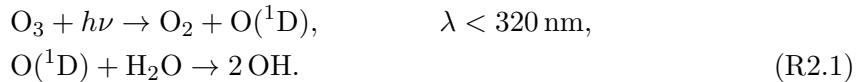
²OP3 - Oxidant and Particle photochemical processes above a South-East Asian tropical rain forest project

Organic Precursor Emission and Concentration study) (Williams et al., 2011). HUMPPA–COPEC–2010 included observations of many VOCs, HO_x and the total OH reactivity to increase our understanding of atmospheric oxidation processes based on detailed analysis of production and loss processes of the hydroxyl radical and exploring the HO_x budget in a coniferous forest, using direct calculations from measured species as well as an observationally constrained chemical box model in steady state.

The “Mainz Isoprene Mechanisms,” a set of reduced chemical reaction schemes considering only isoprene as the predominant primary BVOC (Taraborrelli et al., 2009 based on Pöschl et al., 2000; Taraborrelli et al., 2012), is compared to a preliminary terpene mechanism, also taking the most abundant terpenes measured during HUMPPA–COPEC–2010 (e.g. α -pinene, β -pinene, β -myrcene, farnesene, and Δ^3 -carene) and their oxidation products into account. The modification of the chemical mechanism is analysed and discussed.

2. HO_x photochemistry in the troposphere

In the lower troposphere, the main primary source of OH on a global scale is the photolysis of ozone (O₃) and the subsequent reaction of the excited oxygen atom with water vapour (Levy II, 1971):



Other sources of OH, e.g. photolysis of peroxides or ozonolysis of alkenes, are known as well and were described elsewhere (Jaegle et al., 2000; Ren et al., 2008, and references therein). Once formed, OH reacts rapidly - within a typical lifetime of less than one second - with many atmospheric compounds (e.g. CO or O₃) producing hydroperoxyl radicals (HO₂). The oxidation of hydrocarbons by OH leads to the formation of peroxy radicals (RO_x = RO₂ + HO₂). In the presence of nitric oxide (NO) the RO₂ is converted to HO₂, which reacts with O₃ or NO forming OH (e.g. Martinez et al., 2003). Under atmospheric background conditions the HO₂ radical occurs typically at about 100 times higher concentrations compared to OH with atmospheric lifetimes in the order of $\tau_{\text{HO}_2} \approx 100 \text{ s}$, acting as a buffer for the OH radical in catalytic cycles (Weinstock, 1969; Levy II, 1971; Crutzen, 1973). The main HO_x sinks are self reactions with radicals and the formation of acids. A schematic overview of the basic HO_x chemistry is shown in Figure 2.1.

The spatial and temporal variability of HO_x radicals is typically large. Due to the short atmospheric lifetime the radicals are produced and recycled or consumed locally, depending on solar radiation, atmospheric ozone column, absolute humidity, and various trace gas concentrations. Typical OH concentrations in the lower troposphere during daytime are in the order of $[\text{OH}] \approx 10^6 \text{ molec. cm}^{-3}$ (equivalent to mixing ratios in the sub-ppt_v range), while HO₂ concentrations are in the order of $[\text{HO}_2] \approx 10^8 \text{ molec. cm}^{-3}$ (equivalent to mixing ratios in the lower ppt_v range).

The most relevant production, loss, and recycling pathways of HO_x will be treated in detail in the following sections.

2.1. HO_x production

Ozone molecules absorbing a photon with a wavelength $\lambda < 320 \text{ nm}$ dissociate into molecular oxygen and an excited oxygen atom, O(¹D). This oxygen atom loses its excitation energy

2. HO_x photochemistry in the troposphere

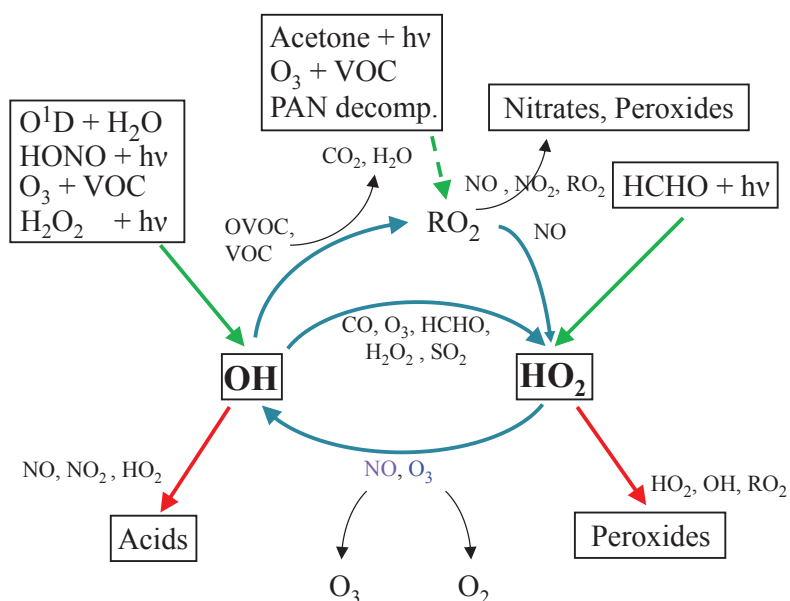


Abbildung 2.1.: Schematic overview of the HO_x radical photochemistry in the troposphere.

Radical **production** (green), **recycling** (blue), and **loss** (red) pathways are indicated by bold arrows. Some reactions are simplified. Refer to text for details.

predominantly by collision with molecular nitrogen and oxygen and returns to the ground state, O(³P). Oxygen and O(³P) recombine, forming back ozone. A minor portion of the excited oxygen atoms react with water vapour forming two OH radicals (Reaction R2.5).



The resulting primary production rate of OH radicals is given by

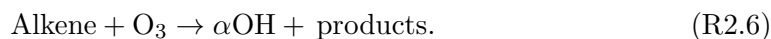
$$\frac{d [\text{OH}]}{dt} = 2b_{\text{O}(^1\text{D})\rightarrow\text{OH}}J_{\text{O}(^1\text{D})} [\text{O}_3], \quad (\text{R2.1})$$

where $J_{\text{O}(^1\text{D})}$ is the associated photolysis frequency and $b_{\text{O}(^1\text{D})\rightarrow\text{OH}}$ denotes the branching ratio

$$b_{\text{O}(^1\text{D})\rightarrow\text{OH}} = \frac{k_{\text{O}(^1\text{D})+\text{H}_2\text{O}} [\text{H}_2\text{O}]}{k_{\text{O}(^1\text{D})+\text{H}_2\text{O}} [\text{H}_2\text{O}] + k_{\text{O}(^1\text{D})+\text{O}_2} [\text{O}_2] + k_{\text{O}(^1\text{D})+\text{N}_2} [\text{N}_2]}. \quad (\text{R2.2})$$

At 298 K and 1% water vapour content about 14% of the excited O(¹D) atoms lead to the formation of OH radicals (Atkinson et al., 2006).

The ozonolysis of alkenes, and particularly terpenes, represents a non-photolytic primary OH source. A primary ozonide and subsequently a Criegee Intermediate is formed within this reaction, which can release OH radicals during its decomposition (Criegee, 1975).



The photolysis of nitrous acid (HONO) at wavelengths below 380 nm yields OH and nitric oxide (Reaction R2.7). HONO itself is formed on surfaces by reaction of nitrogen dioxide (NO₂) and water. It typically accumulates during nighttime and starts to decompose in the morning hours, when solar radiation increases (Aumont et al., 2003; Kleffmann et al., 2002, 2005).

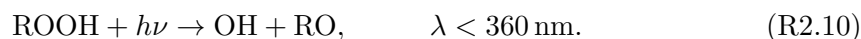
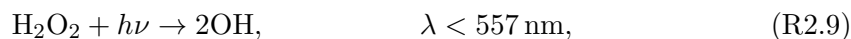


HO₂ is produced within the radical channel of the photolysis reaction of formaldehyde (HCHO):



From ozonolysis of hydrocarbons HO₂ radicals can form as well.

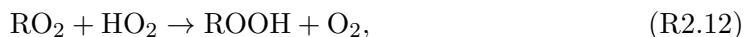
Beside those primary HO_x sources, the photolysis of hydrogen peroxide as well as organic peroxides, which are products in the oxidation process of VOCs contribute as secondary OH sources.



Especially in the upper troposphere, where the water vapour content in air is reduced and therefore, Reaction R2.5 is inhibited, hydrogen peroxide photolysis becomes more important.

2.2. HO_x sinks

HO_x radicals are primarily lost within radical-radical reactions forming peroxides and other products.



The photolysis of peroxides (see Reaction R2.9-R2.10) leads to the production of OH. However, peroxides are mainly lost by wet and dry deposition processes, thus, being removed from the HO_x cycle.

The formation of acids is another sink for OH and HO₂ radicals.



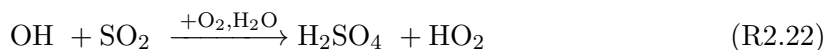
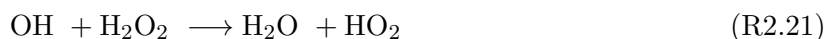
Heterogeneous chemistry and radical deposition can also contribute to the HO_x radical loss.

2.3. Oxidation of volatile organic compounds and HO_x recycling

The OH-initiated oxidation of carbon monoxide (CO) is on global average one of the most important loss reactions of the OH radical. Furthermore, HO₂ is produced when CO is converted into CO₂ by oxidation reaction.



Beside CO, ozone (O₃), formaldehyde (HCHO), hydrogen peroxide (H₂O₂), and SO₂ also react with OH radicals forming HO₂.

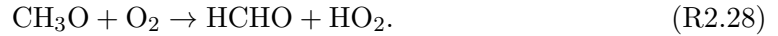
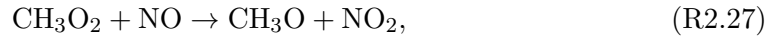


At NO levels of about 100 pptv and higher the HO₂ radicals reacting with NO can recycle the hydroxyl radical, providing it for another oxidation process. Similarly the reaction of

HO₂ with ozone forms back OH (Reactions R2.23 - R2.24).

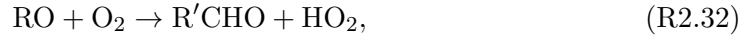
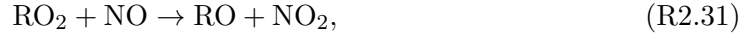
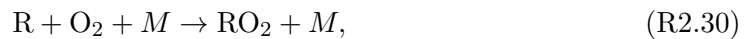


The OH-initiated oxidation of volatile organic compounds represents another HO_x recycling pathway. The most abundant atmospheric VOC is the greenhouse gas methane (CH₄). Due to its long chemical lifetime of about 8 years it is homogeneously distributed spatially within the troposphere. Methane is mainly oxidized by reaction with the OH radical, leading to the formation of methylperoxy radicals (CH₃O₂). CH₃O₂ reacting with NO yields methoxy radicals (CH₃O), which react rapidly with oxygen forming HO₂ and formaldehyde.



The HO_x-cycle is completed forming back OH radicals by Reactions R2.23 & R2.24.

The oxidation of other VOCs follows a similar reaction chain:



where R denotes an organic group.

Organic peroxy radicals (RO₂) are formed in the reaction of the hydrocarbon with OH. The subsequent reaction of RO₂ with NO leads to the formation of alkoxy radicals (RO), which rapidly react with oxygen, producing HO₂ radicals and organic aldehydes.

In close analogy to the HO_x sinks described above, RO₂ radicals can be lost from the radical cycle by reactions with other RO₂ radicals, HO₂ (Reaction R2.12), and NO_x forming peroxides and peroxy nitrates.



Peroxy nitrates thermally decompose, forming back peroxy radicals and NO₂, thus acting as a reservoir species for the peroxy radicals and NO_x.



2. HO_x photochemistry in the troposphere

The reaction of specific alkylperoxy radicals with HO₂, which was previously only considered as a radical termination process, represent an additional OH recycling pathway. Laboratory studies investigating the OH production from the reactions of ethyl peroxy, acetyl peroxy, and acetyl peroxy radicals with HO₂ revealed OH yields up to 70 % (Thornton et al., 2002; Hasson et al., 2004; Jenkin et al., 2007; Dillon and Crowley, 2008). A direct recycling mechanism, forming back OH from RO₂ in the absence of NO, by a 1,5-H-shift, was proposed by Peeters et al. (2009) for the OH-initiated degradation of isoprene. The occurrence of a 1,6-H-shift leads to the recycling of an HO₂ radical (Figure 2.2).

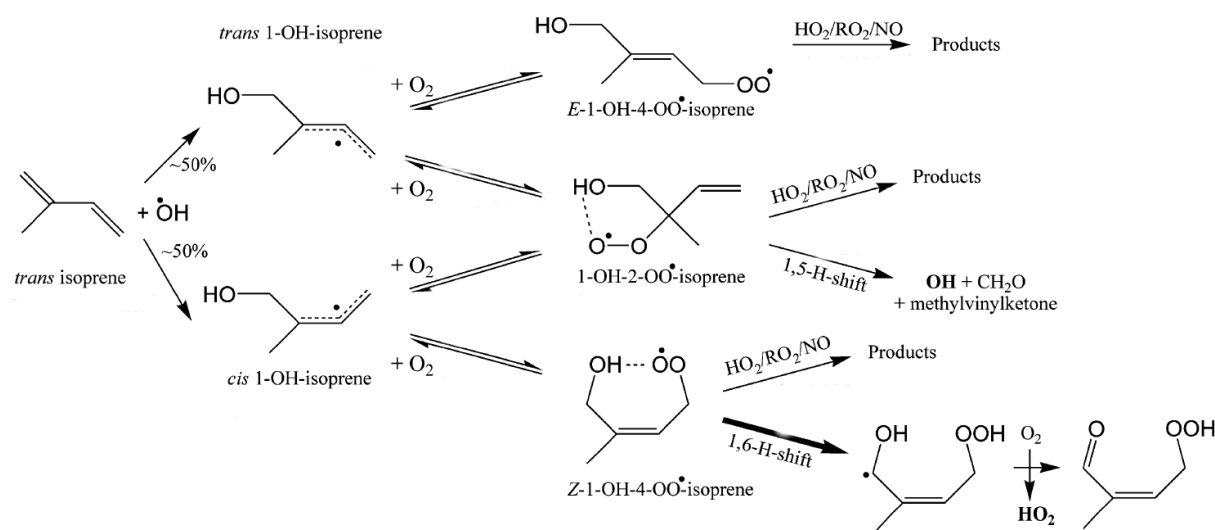


Abbildung 2.2.: Reaction scheme for OH and HO₂ radical formation following 1-OH addition to isoprene by a 1,5- and a 1,6-H-shift, respectively (Taken from Peeters et al., 2009, and modified).

2.4. The relationship between HO_x and J_{O(1D)}

When primary production is the predominant source of OH, the hydroxyl radical concentration follows the course of J_{O(1D)} (Rohrer and Berresheim, 2006). During daytime the main primary source of OH is the photolysis of O₃ and the reaction of O(¹D) with water vapour (Reaction R2.5). Under conditions of low NO, O₃, and non-methane hydrocarbon concentrations (clean background atmosphere) the secondary OH production, i.e. the recycling reactions forming back OH from HO₂ (Reactions R2.23 - R2.24), is inhibited. Stationary-

state can be assumed for OH due to its short lifetime:

$$\frac{d[\text{OH}]}{dt} = P_{\text{OH}}^{\text{total}} - L_{\text{OH}}^{\text{total}} = 0. \quad (2.3)$$

The production of OH under clean background atmosphere conditions is mainly determined by Reactions R2.5 and R2.24:

$$P_{\text{OH}}^{\text{total}} = 2b_{\text{O}(^1\text{D}) \rightarrow \text{OH}} J_{\text{O}(^1\text{D})} [\text{O}_3] + k_{\text{HO}_2 + \text{O}_3} [\text{O}_3]. \quad (2.4)$$

The most relevant OH loss processes are Reactions R2.17 and R2.25:

$$L_{\text{OH}}^{\text{total}} = k_{\text{CH}_4 + \text{OH}} [\text{CH}_4] [\text{OH}] + k_{\text{CO} + \text{OH}} [\text{CO}] [\text{OH}]. \quad (2.5)$$

When $k_{\text{O}(^1\text{D}) + \text{H}_2\text{O}} [\text{H}_2\text{O}] \ll k_{\text{O}(^1\text{D}) + \text{O}_2} [\text{O}_2] + k_{\text{O}(^1\text{D}) + \text{N}_2} [\text{N}_2]$ and $k_{\text{HO}_2 + \text{O}_3} \ll 2b_{\text{O}(^1\text{D}) \rightarrow \text{OH}} J_{\text{O}(^1\text{D})}$ the hydroxyl radical concentration is approximately

$$[\text{OH}] = \frac{2J_{\text{O}(^1\text{D})} [\text{O}_3] [\text{H}_2\text{O}] k_{\text{O}(^1\text{D}) + \text{H}_2\text{O}}{k_{\text{O}(^1\text{D}) + \text{M}} [\text{M}] + k_{\text{CH}_4 + \text{OH}} [\text{CH}_4] k_{\text{CO} + \text{OH}} [\text{CO}]}, \quad (2.6)$$

where $M = \text{O}_2, \text{N}_2$. The variability of the photolysis frequency $J_{\text{O}(^1\text{D})}$ is typically large compared to the variability of $\text{CH}_4, \text{O}_3, \text{CO}$, and H_2O concentrations resulting in a quasi-linear relationship between OH and $J_{\text{O}(^1\text{D})}$ (Holland et al., 2003; Rohrer and Berresheim, 2006).

As shown by the following equations, the HO_2 concentration is proportional to $\sqrt{J_{\text{O}(^1\text{D})}}$ under clean background atmosphere conditions. The production of HO_2 is dominated by Reaction R2.17. HO_2 is mainly lost by reaction with O_3 and in radical-radical reactions (Reactions R2.11-R2.12, R2.24):

$$P_{\text{HO}_2}^{\text{total}} = k_{\text{CO} + \text{OH}} [\text{CO}] [\text{OH}], \quad (2.7)$$

$$L_{\text{HO}_2}^{\text{total}} = k_{\text{HO}_2 + \text{O}_3} [\text{HO}_2] [\text{O}_3] + 2k_{\text{HO}_2 + \text{HO}_2} [\text{HO}_2]^2 + \dots \\ k_{\text{HO}_2 + \text{CH}_3\text{O}_2} [\text{HO}_2] [\text{CH}_3\text{O}_2]. \quad (2.8)$$

Methylperoxy radicals are formed in the OH-initiated oxidation of CH_4 (Reactions R2.25 - R2.26) and mainly lost by reaction with other radicals:

$$P_{\text{CH}_3\text{O}_2}^{\text{total}} = k_{\text{CH}_4 + \text{OH}} [\text{CH}_4] [\text{OH}], \quad (2.9)$$

$$L_{\text{CH}_3\text{O}_2}^{\text{total}} = k_{\text{HO}_2 + \text{CH}_3\text{O}_2} [\text{HO}_2] [\text{CH}_3\text{O}_2]. \quad (2.10)$$

For the sum of $\text{CH}_3\text{O}_2, \text{HO}_2$, and OH radicals the steady-state is

$$\frac{d([\text{OH}] + [\text{HO}_2] + [\text{CH}_3\text{O}_2])}{dt} = 2b_{\text{O}(^1\text{D}) \rightarrow \text{OH}} J_{\text{O}(^1\text{D})} [\text{O}_3] - 2k_{\text{HO}_2 + \text{HO}_2} [\text{HO}_2]^2 + \dots \\ - 2k_{\text{HO}_2 + \text{CH}_3\text{O}_2} [\text{HO}_2] [\text{CH}_3\text{O}_2] = 0. \quad (2.11)$$

2. HO_x photochemistry in the troposphere

The resulting HO₂ concentration is proportional to the square root of the photolysis frequency J_{O(1D)} (Penkett et al., 1997):

$$[\text{HO}_2] = \left(\frac{b_{\text{O}(1\text{D}) \rightarrow \text{OH}} J_{\text{O}(1\text{D})} [\text{O}_3]}{k_{\text{HO}_2 + \text{HO}_2} + \alpha k_{\text{HO}_2 + \text{CH}_3\text{O}_2}} \right)^{\frac{1}{2}}, \quad (2.12)$$

where α denotes the ratio $\frac{[\text{CH}_3\text{O}_2]}{[\text{HO}_2]}$.

Observed relationships between HO_x and the photolysis frequency J_{O(1D)} may differ significantly from the basic relations (Equations 2.6 & 2.12), when the assumptions are not applicable. Nonetheless, often linear correlation between OH and J_{O(1D)} is found, at which the proportionality factor is different for different chemical regimes (Holland et al., 2003).

3. HO_x measurements using the HORUS instrument

3.1. Techniques for HO_x radical measurements

Because of their high reactivity towards trace gases and surfaces, the lifetime of hydroxyl radicals in the troposphere is typically less than one second. Average OH concentrations are in the order of 10^5 to 10^7 molec. cm⁻³ during daytime. The strongly coupled HO₂ radical is about a factor of 100 times more abundant with a typical tropospheric lifetime in the range of seconds to minutes. Therefore, highly sensitive detection systems are required for measurements of these radicals. In the last decades several direct and indirect methods have been developed. The most relevant atmospheric HO_x radical measurement techniques are discussed in the following paragraphs.

3.1.1. Techniques for the detection of atmospheric OH

¹⁴CO method

Based on the assumption of carbon monoxide being mainly oxidized by hydroxyl radicals, the OH concentration in sample air can be derived by addition of isotopically labeled ¹⁴CO and subsequent freeze desalination of the CO₂ produced (Felton et al., 1988). The observed concentrations of ¹⁴CO and ¹⁴CO₂ in combination with the known reaction rate constant of the reaction of CO with OH provide access to the OH concentration in sample air. The lower limit of detection of the radiochemical ¹⁴CO method is about 2×10^5 molec. cm⁻³ at an integration time of 2 minutes. Integration times of several minutes and the elaborate sample handling are the disadvantages of this method.

Spin trapping - electron paramagnetic resonance

Electron paramagnetic resonance (EPR, also known as: electron spin resonance, ESR) spectroscopy is a method to detect substances with unpaired electrons, based on the resonant absorption of electromagnetic radiation (microwaves) by the sample substance in a magnetic field. Since the chemical lifetime of OH is short, highly resolved EPR spectroscopy is too slow for detection of hydroxyl radicals. In combination with spin trapping methods the measurement of atmospheric OH becomes feasible. Janzen et al. (1978) used this method

for measurement of OH in aqueous solution. Watanabe et al. (1982) accomplished measurements of atmospheric OH using α -4-pyridyl-N-tert-butyl-nitrone α -1-oxide (4-POBN) for spin trapping. The hydroxy-adduct of 4-POBN can subsequently be measured by EPR, to quantify the OH radicals. The lower limit of detection of this method is on the order of 5×10^5 molec. cm⁻³ at an integration time of 20 minutes.

Differential optical absorption spectroscopy – DOAS

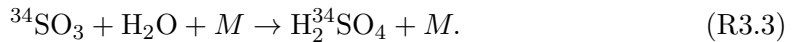
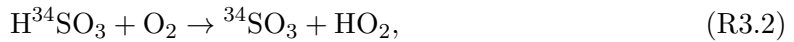
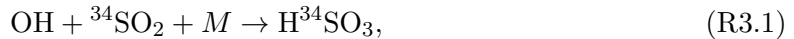
The differential optical absorption spectroscopy (DOAS) is based on the wavelength-dependent absorption of light by the molecules present in the atmosphere, following Beer-Lambert's law:

$$I(\lambda) = I_0(\lambda) \exp \left(\int_0^l -\sigma_{\text{OH}}(\lambda) [\text{OH}] dl \right). \quad (3.1)$$

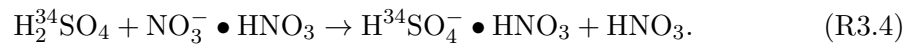
I_0 and I are the intensities of light before and after transmission through the sampled air along the path l , with the absorption cross section of the OH radical at the wavelength λ , $\sigma_{\text{OH}}(\lambda)$. Light from artificial (e.g. laser) or natural (e.g. the sun) light sources passes the atmosphere and the absorption spectrum is recorded using spectrographs with a high spectral resolution. Subsequently the OH absorption spectrum is extracted. DOAS is an absolute technique, thus, calibration of the instrument is not necessary. The biggest uncertainty in OH measurement by DOAS is due to the uncertainty in the absorption cross section, which is about 7% (Dorn et al., 1995). The lower limit of detection of this method depends on the length of the lightpath, scattering by aerosols, and absorption due to other trace gases. Typically values of about 1.5×10^6 molec. cm⁻³ at an integration time of 15 minutes (2σ) can be reached.

Chemical ionization mass spectroscopy – CIMS

Chemical ionization mass spectroscopy (CIMS) is an indirect method to determine the OH mixing ratio. The OH is titrated with isotopically labeled ³⁴SO₂ and the emerging sulfuric acid (H₂³⁴SO₄) is measured subsequently.



³⁴SO₂ is injected into the sample air in excess for efficient conversion of the OH radicals into sulfuric acid within a few milliseconds (Eisele and Tanner, 1991; Tanner and Eisele, 1995; Tanner et al., 1997; Berresheim et al., 2002; Petäjä et al., 2009). Ions of nitrate (NO₃⁻) are used for ionization of the sulfuric acid by a charge transfer reaction. The nitrate ions exist mainly in a chemical complex with HNO₃ or H₂O.



The resulting chemical complex H³⁴SO₄⁻•HNO₃ becomes fragmented in a collision chamber and the fragments are detected by mass spectroscopy. Since the stable isotope ³⁴S makes only about 4% of the naturally occurring sulfur, it can be distinguished between atmospheric H₂SO₄ and H₂³⁴SO₄ generated by OH titration. The measured concentration of H³⁴SO₄⁻ is proportional to the OH concentration in sample air. The biggest uncertainty of this method is due to the uncertainty of reaction rate constants. In order to improve the uncertainty of the CIMS technique, calibrations are conducted. The lower limit of detection is on the order of 1 × 10⁵ molec. cm⁻³ at an integration time of 5 minutes.

Laser-induced fluorescence - fluorescence assay by gas expansion – LIF-FAGE

Wang and Davis (1974) reported the first measurement of hydroxyl (OH) in air by detecting the resonance fluorescence excited by a tunable laser source in the ultraviolet. OH radicals were selectively excited at a wavelength $\lambda = 282.58$ nm on resonance with the P₁(2) line in the A²Σ⁺ – X²Π, v'₁=1 ← v''=0 transitions of OH. The transition back to the ground state occurs via various rotationally and vibrationally excited states with a high fluorescence intensity in the wavelength range between 307 – 315 nm. However, at atmospheric pressure, most of the electronically excited OH molecules lose their energy by collisional quenching due to other molecules present in air at a typical collision lifetime of about 1 ns (Heard and Pilling, 2003). The lifetime of the excited state of OH is approximately 700 ns, and hence very few of the initially excited OH molecules will fluoresce. Large background signals due to laser scatter at aerosols, other molecules in sample air and walls inside the detection system and the low yield from OH fluorescence led to a lower limit of detection of 5 × 10⁶ molec. cm⁻³ (Wang and Davis, 1974). Furthermore, the measurement of atmospheric OH by LIF technique as described by Wang and Davis (1974) is subject to severe limitations. The laser radiation at $\lambda \approx 282$ nm which is used to excite the OH molecules, leads also to photodissociation of atmospheric ozone, yielding O(¹D) atoms. The subsequent reaction of the laser-generated O(¹D) atoms with atmospheric water vapour leads analog Reaction R2.1 to the formation of hydroxyl radicals, so the laser radiation itself is a source of OH (Ortgies et al., 1980). The development of the FAGE (fluorescence assay by gas expansion) method was a major step in order to overcome the disadvantages of atmospheric OH measurements by LIF due to low fluorescence yields and the interference caused by laser radiation, ozone and water vapour. Hard et al. (1979) for the first time detected atmospheric OH at reduced pressure (~ 1 – 5 hPa). OH detection at low pressure reduces the number density of water vapour and ozone, thus, limiting the production of laser-generated OH. The reduction of pressure leads to a smaller number of OH radicals available for detection and increased wall losses, due to the larger mean free path for the OH molecules inside the detection cell. Nonetheless, there is an increase in the OH fluorescence quantum yield, as the rate of collisional quenching of the excited OH radicals is reduced. The lifetime of the excited state extends to several hundred nanoseconds inside the FAGE detection system. An overview of the combined effects is presented in Figure 3.1.

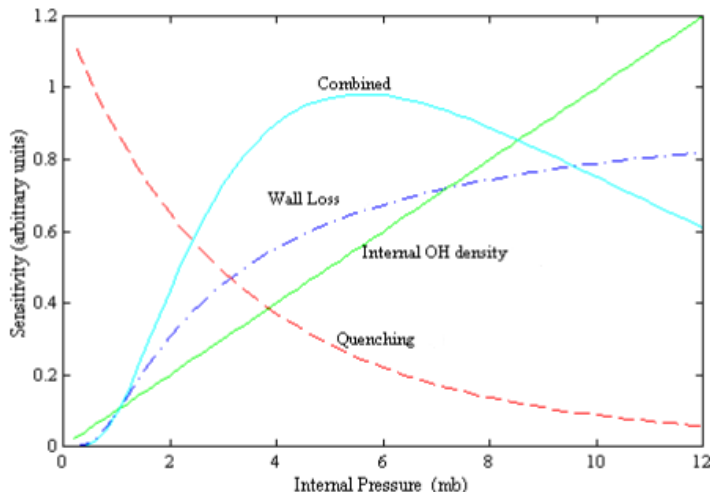


Abbildung 3.1.: Three pressure dependent components of the LIF sensitivity: the internal density (green solid line), OH transmission (blue dash-dotted line), and quenching (red dashed line). The product of these three functions (turquoise solid line) is the expected form of the pressure dependent sensitivity (Taken from Faloon et al., 2004, and modified).

Furthermore, background signals are suppressed efficiently. Background from sunlight is reduced by the sampling nozzle, used to suck ambient air into the low pressure detection cell. Baffles and black anodized walls inside the detection system are used to further suppress background photons by multiple reflections on these black surfaces. The laser-scattered background signal due to Rayleigh scattering and Mie scattering (fluorescence from aerosols) and fluorescence from the walls of the detection system can be discriminated against the OH fluorescence using a pulsed laser for excitation and a gated photon counting detection scheme (Figure 3.2). The detectors are switched off during the laser pulse by electronic gating, enabling discrimination against the much more intense background signals that exhibit the same temporal characteristics as the laser pulse (Heard and Pilling, 2003).

Present-day LIF-FAGE instruments widely use the electronic transition $A^2\Sigma^+ - X^2\Pi$, $v'=0 \leftarrow v''=0$ at around 308 nm for excitation of the OH radicals, and the fluorescence is subsequently detected at similar wavelengths. This became feasible with the introduction of gated photon counting. The interference due to laser-generated OH is about a factor of 25

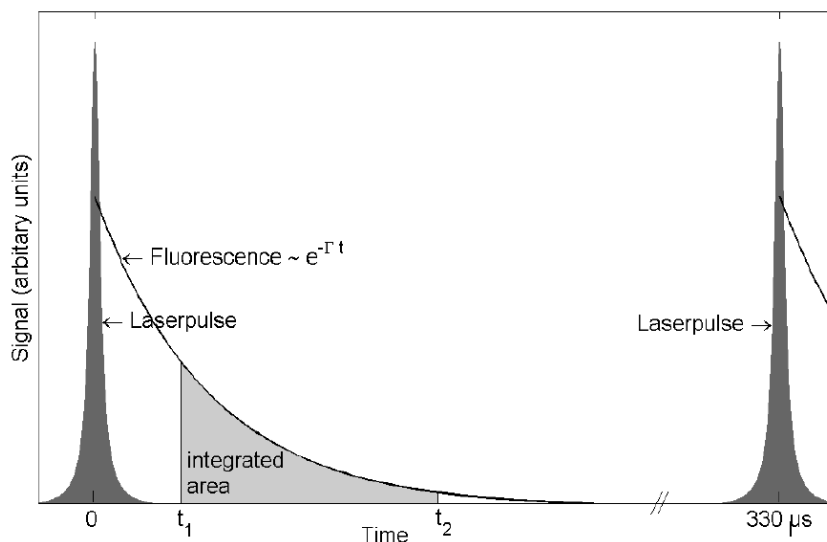


Abbildung 3.2.: Schematic representation of the timing of photon counting process that is used to quantify OH concentrations by LIF-FAGE technique. The detectors are switched off during the laser pulse by electronic gating, to discriminate against the much more intense background signals that exhibit the same temporal characteristics as the laser pulse. The integrated fluorescence signal is proportional to the number concentration of hydroxyl radicals in sample air (Taken from Faloon et al., 2004, and modified).

times smaller compared to the excitation at around 282 nm, because of the lower absorption cross section of O₃ and the reduced O(¹D) quantum yield at $\lambda = 308$ nm. The absorption cross section of OH at 308 nm is about four times larger compared to $\lambda = 282$ nm, leading to a larger OH fluorescence signal (Chan et al., 1990). The lower limit of detection of this method is typically on the order of 1×10^5 molec. cm⁻³ at an integration time of 30 seconds. Recently further development of the LIF-FAGE method in order to avoid interferences in hydroxyl radical measurements due to other atmospheric compounds is under progress and will be discussed in more detail in Section 3.2.5.

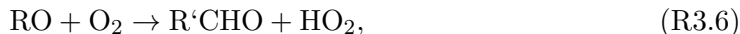
3.1.2. Techniques for the detection of atmospheric HO₂

Matrix isolation ESR

Measurement of atmospheric HO₂ radicals with Matrix isolation and electron spin resonance spectroscopy (MIESR) was developed by Mihelcic et al. (1978) and is currently the only selective method to detect HO₂ directly. The air is sampled by expansion through a nozzle into a chamber with reduced pressure (~ 10 hPa) and the radicals are subsequently frozen out in a matrix formed by D₂O molecules on a sampling finger which is cooled with liquid nitrogen in order to avoid further chemical interactions between reactive molecules. Subsequently, the measurement is accomplished by electron spin resonance (ESR) spectroscopy in the laboratory. Furthermore, MIESR spectroscopy has the capability to measure the concentrations of HO₂, RO₂, CH₃C(O)O₂, NO₃, and NO₂ simultaneously in one sample. Typical sampling times of about 30 minutes are required to collect sufficient number of HO₂ radicals. The lower limit of detection of this method is about 1×10^7 molec. cm⁻³ for HO₂. The sample handling, i.e. taking the samples and the necessity to store them cryogenically, results in a relatively low time resolution. The subsequent ESR analysis of the samples in laboratory is also time-consuming. However, the MIESR method does not require calibrations, thus, it is appointed as a reference method for intercomparison to other instruments.

Chemical ionization mass spectroscopy – CIMS

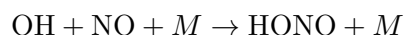
Chemical ionization mass spectroscopy can be used to detect HO₂ and RO₂ radicals indirectly by chemical conversion to OH (Reiner et al., 1997; Cantrell et al., 2003). The conversion is accomplished by addition of NO and O₂:



The resulting OH radicals can be subsequently detected by addition of SO₂, which leads to the formation of sulfuric acid (Reactions R3.1 - R3.3). Chemical ionization mass spectroscopy is used for quantification, as already described above. In contrast to measurements of atmospheric OH it is not necessary to use isotopically labeled SO₂, since the HO₂ + RO₂ radical concentration is about 100 times larger compared to OH, thus, the atmospheric H₂SO₄ background on the signal is small. The conversion efficiency from RO₂ to OH strongly depends on the amount of NO, O₂, and SO₂ injected into sample air. To detect HO₂ selectively, nitrogen instead of oxygen is injected, suppressing Reaction R3.6. Only ambient O₂ remains for conversion of RO to HO₂. Under these conditions 70 % to 75 % of the H₂SO₄ stem from atmospheric HO₂ (Heard and Pilling, 2003). The lower limit of detection of this method is about 7×10^5 molec. cm⁻³ for HO₂ at an integration time of 1 minute.

Laser induced fluorescence - fluorescence assay by gas expansion – LIF-FAGE

Another indirect method for the detection of HO₂ radicals is also based on the chemical conversion of HO₂ to OH by adding NO in excess to the sample air (Reaction R2.23). Following the conversion, the OH radicals are detected by LIF-FAGE technique (Heard and Pilling, 2003; Faloon et al., 2004). In order to achieve a high conversion efficiency within the short period (typically a few milliseconds) between injection of NO into the sample air and excitation of the resulting hydroxyl radicals by laser light and the subsequent detection of the fluorescence signal, high mixing ratios of NO ($\sim 500 - 1500 \text{ ppm}_V$) are used. Nonetheless, the conversion efficiency is limited by the efficiency of mixing the injected NO with the sample air, and wall losses. At very high NO mixing ratios the Reaction R2.14



becomes a relevant loss process. Conversion efficiencies up to 95 % were established in LIF-FAGE instruments (Heard and Pilling, 2003). According to Reaction R2.31, organic peroxy radicals quickly react with NO forming RO. These RO radicals can form additional HO₂ by reaction with atmospheric oxygen (Reaction R2.32). Due to the low pressure inside the LIF-FAGE detection system this reaction is slow compared to ambient conditions and contributes less than 10 % to the total signal (Holland et al., 2003). However, it is meanwhile known, that RO₂ radicals from OH plus alkene- and aromatic precursors including isoprene (mainly OH-addition) can form specific RO by reaction with NO. These RO radicals can decompose under low pressure conditions forming HO₂ rapidly (Fuchs et al., 2011; Dillon, 2011). Interferences from these RO₂ species can be significantly reduced by reducing the reaction time and/or the NO concentration in the detection cell at the expense of a reduced HO₂ detection sensitivity. A lower detection limit of less than $1 \times 10^6 \text{ molec. cm}^{-3}$ at an integration time of 30 seconds is typically achieved by HO₂-LIF-FAGE instruments.

3.2. HORUS

Observations of OH and HO₂ concentrations within the scope of this thesis, in particular during the HUMPPA-COPEC2010 field campaign, were conducted using the Max Planck Institute for Chemistry (Mainz, Germany) HO_x instrument based on laser-induced fluorescence, HORUS (*HydrOxyl Radical Measurement Unit based on fluorescence Spectroscopy*). The HORUS instrument is originally based on the design of GTHOS (Ground-based Tropospheric Hydrogen Oxides Sensor), the Penn State HO_x instrument described by Faloon et al. (2004). HORUS is described in detail by Martinez et al. (2010). HORUS has been deployed for a variety of campaigns on ground-based, shipborne, and airborne platforms (Schlosser et al., 2009; Hosaynali Beygi et al., 2011; Kubistin et al., 2010; Martinez et al., 2010; Regelin et al., 2012).

3.2.1. Measurement principle

The LIF-FAGE method used by HORUS is based on the resonant absorption of laser light by the OH molecules and the subsequent detection of the fluorescence signal. The intensity of the fluorescence signal is proportional to the OH radical concentration. The excitation of OH radicals used in HORUS can be explained by transitions between the ground state X²Π and the first excited state A²Σ⁺ (Figure 3.3). The electron configuration of the ground state is (1σ)² (2σ)² (3σ)² (π⁺)² (π⁻)¹ with an unpaired electron in the π-orbital (Freeman, 1958). The electron configuration of the first electronically excited state A²Σ⁺ is (1σ)² (2σ)² (3σ)¹ (π⁺)² (π⁻)². The rotational states of the ground state separate because of the spin-orbit coupling (fine structure) into two electronic substates X²Π_{1/2} and X²Π_{3/2}. There is no spin-orbit coupling in the excited electronic state A²Σ⁺ due to the lack of any angular momentum.

Quantum numbers in Figure 3.3 refer to:

- K: angular momentum (rotation+orbit)
- J: total angular momentum (including spin)

The energy levels of the substates within the ²Π state are labeled with $f_i(K)$ and $f'_i(K)$, where $i = 1$ denotes $(K + \Sigma)$ and $i = 2$ refers to $(K - \Sigma)$, in which Σ is the projection of the spin to the molecule axis (z-axis). The energetically higher level (caused by lambda doubling interaction) is labeled $f'_i(K)$. In analogy to this, the substates within the ²Σ⁺ state (γ-splitting) are labeled with $F_i(K)$ and $F'_i(K)$. Absorption lines are labeled by X_i(K) whereby X denotes the rotational branch $P(\Delta K = -1)$, $Q(\Delta K = 0)$, or $R(\Delta K = 1)$ and K is the quantum number of the angular momentum in the ground state. Subscripts i represent again the fine structure of the ground state. For transitions with changing spin projection ($K \pm \frac{1}{2}$), so-called satellite branches that occur at similar energies but show lower intensities compared to main branches, the index i' for the excited state is added in front of the ground state index (e.g. Q₂₁(2)). A more detailed description of the OH absorption spectrum can be found in Freeman (1958); Dieke and Crosswhite (1962); Langhoff et al. (1982) and references therein.

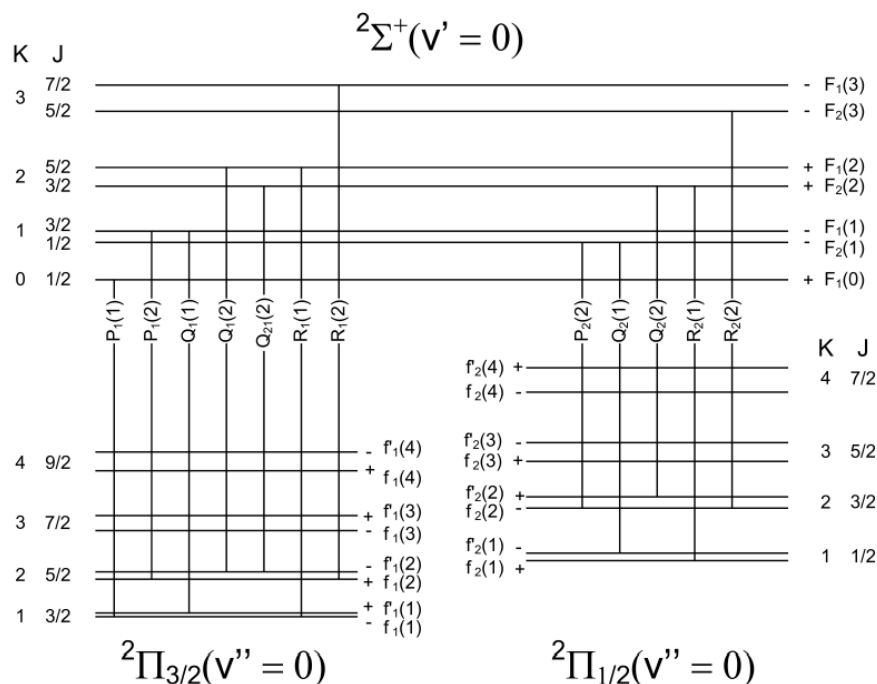


Abbildung 3.3.: Schematic of the branches in the rotational structure of OH showing the transitions used for laser excitation ($A^2\Sigma^+ - X^2\Pi, v'=0 \leftarrow v''=0$). K is the quantum number of the angular momentum (rotation + orbit) and J is the quantum number of the total angular momentum (including spin). For notation of transition lines refer to text.

In HORUS OH molecules are selectively excited at low pressure by pulsed UV light at around 308 nm on resonance with the $Q_1(2)$ transition line. Subsequently, the fluorescence signal from the excited hydroxyl radical molecules is detected at low pressure ($\sim 3 - 5$ hPa). Since the fluorescence is detected at around 308 nm, similar to the excitation wavelength, a gated photon counting technique as presented in Figure 3.2 using micro channel plate detectors (MCP) is applied. The integrated fluorescence signal is proportional to the con-

centration of hydroxyl radicals in sample air:

$$S \sim \int_{t_1}^{t_2} I(t) dt \sim [\text{OH}^*] \int_{t_1}^{t_2} e^{-\Gamma t} dt \quad (3.2)$$

The concentration of excited OH radicals $[\text{OH}^*]$ is proportional to the total OH concentration, the Boltzmann correction factor f_b and the laser power P . With the fluorescence efficiency factor

$$Q = \int_{t_1}^{t_2} e^{-\Gamma t} dt \quad (3.3)$$

and the constant of proportionality C' we obtain

$$S = C' \cdot Q f_b P [\text{OH}]. \quad (3.4)$$

The product of fluorescence efficiency factor, Boltzmann correction factor and C' is the normalized sensitivity of the LIF instrument:

$$\zeta = C' \cdot Q \cdot f_b. \quad (3.5)$$

The total instrument sensitivity is given by

$$\mathcal{E}_{\text{LIF}} = \zeta \cdot P \quad (3.6)$$

and can be determined by calibration of the HORUS instrument (see Section 3.2.3).

The decay rate of the excited OH radicals, Γ , is defined by the natural lifetime of the excited state, γ_{nat}^{-1} and the deactivation by collisional quenching due to other molecules X:

$$\Gamma = \gamma_{\text{nat}} + \sum k_X(T) [\text{X}], \quad (3.7)$$

where X=N₂, O₂, and H₂O are the most relevant collision partners in ambient air. The temperature dependency of the associated rate constants can be approximated within a temperature range of -70°C to 50°C (Faloona et al., 2004):

$$k_X(T) = aT^{\frac{1}{2}} - bT^{\frac{3}{2}} + c. \quad (3.8)$$

The coefficients a, b, c are experimentally determined (Bailey et al., 1997, 1999) and listed in Table 3.1. Particularly H₂O is an efficient quenching gas for the excited OH molecules, leading to a decrease of the fluorescence efficiency factor Q and therefore a decrease in instrument sensitivity with increasing water concentration.

Tabelle 3.1.: Parameters of temperature dependency for collisional quenching rate coefficients.

Collision gas	a (in $\text{cm}^3 (\text{molec. s K}^{\frac{1}{2}})^{-1}$)	b (in $\text{cm}^3 (\text{molec. s K}^{\frac{3}{2}})^{-1}$)	c (in $\text{cm}^3 \text{ molec.}^{-1} \text{ s}^{-1}$)
N ₂	-1.668×10^{-11}	-1.731×10^{-14}	2.313×10^{-10}
O ₂	1.008×10^{-11}	1.655×10^{-14}	5.129×10^{-11}
H ₂ O	-4.017×10^{-10}	-4.4686×10^{-14}	5.3137×10^{-9}

3.2.2. Instrument setup

HORUS consists of four main components: the laser system, the low pressure detection system, the vacuum system, and the instrument control and data acquisition unit. A comprehensive description of the HORUS instrument setup is given in Kubistin et al. (2010). The most relevant characteristics for HUMPPA–COPEC–2010 and recent instrument developments are presented in the following paragraphs.

Laser system

The UV light for excitation of the hydroxyl radicals is provided by a Nd:Yag pumped, pulsed, tunable dye laser system (Martinez et al., 2010; Wennberg et al., 1994) operated at a pulse repetition frequency of 3 kHz. A diode-pumped, quality-switched Nd:Yag laser (Type Navigator I, Spectra Physics) is applied for optical pumping of the custom-made dye laser system at 532 nm (frequency doubled). In order to focus the beam of the pump laser precisely on the dye cell the beam (with an approximate initial diameter of 0.65 mm) is expanded, using a tenfold beam expander (Linos - Qioptic) and a collecting lens ($f = 100$ mm, Thorlabs). Furthermore, the incoupling of the green laser beam is actively controlled by two piezo-actuated mirrors to compensate changes due to thermal and mechanical influences on the laser base plate.

The dye laser setup is shown in Figure 3.4. The incoming beam of the pump laser ($\lambda = 532$ nm) hits the dye cell under the brewster angle. The laser dye, Pyrromethene-597 (Exciton, USA) dissolved in high purity grade isopropanol ($> 99.9\%$), has an absorption maximum in the green and fluoresces in the green to red wavelength range. To avoid saturation of the excited states of the laser dye, the dye solution is continuously circulated through a reservoir at a high flow rate of 1.7 liters per minute in order to exchange the dye inside the dye cell between two consecutive laser pulses. The fluorescence light is collected and amplified within the cavity. The cavity is defined on one end by the end mirror and on the other by the outcoupling mirror (see Figure 3.4). Primary wavelength selection in the

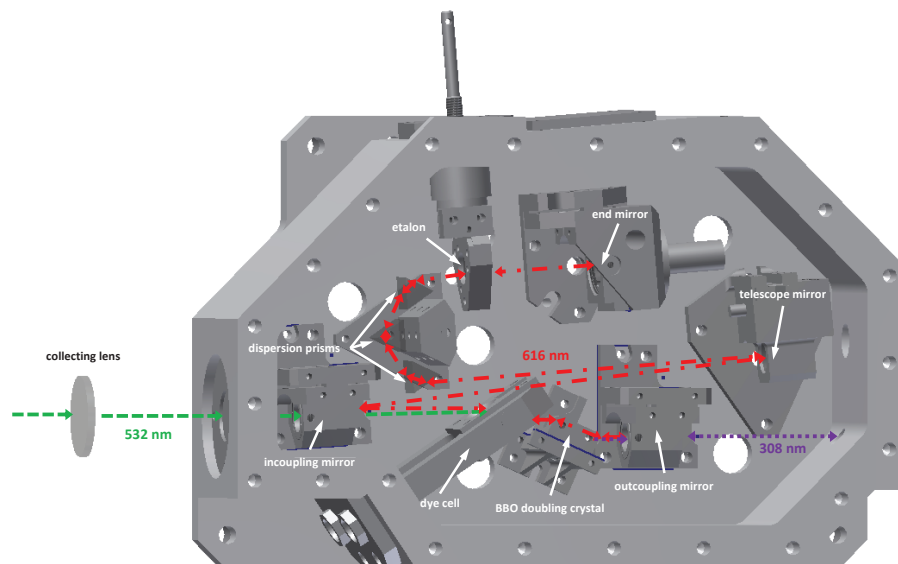


Abbildung 3.4.: Dye laser setup. The incoming beam of the pump laser ($\lambda = 532 \text{ nm}$) is focussed on the dye cell. The fluorescence from laser dye (Pyrromethene-597) at $\lambda = 616 \text{ nm}$ is amplified inside the optical resonator. UV light at $\lambda = 308 \text{ nm}$ is produced using a nonlinear doubling crystal (BBO) for intracavity frequency doubling.

cavity is achieved by means of a dispersion prism array, then further narrowed by a rotatable intracavity etalon, which is actively controlled by a stepper motor. When the intracavity power builds up sufficiently to permit frequency doubling in the doubling crystal (BBO - β -barium borate) the UV light then exits via the outcoupling mirror.

Since the instrument sensitivity \mathcal{E}_{LIF} is directly proportional to the laser power P (see Equation 3.6) it is desired to achieve high and stable laser power at the excitation wavelength of OH. Furthermore, the lower limit of detection improves at higher UV power. This is important, when long optical fibers causing high losses have to be used to transport the UV light to the detection system. To improve the UV power output of the laser system the design of the cavity was analyzed and slightly modified. The biggest positive impact on the UV power was gained by the exchange of the dispersion prisms material. The transmission of

the p-polarized light is strongly dependent on the incidence angle. Previously three isosceles brewster prisms ($\alpha = 60^\circ$) made in LaFN8 were used in the HORUS dye laser system. For the mechanical setup - three prisms with theoretical brewster angle of 60° and total deflection angle between input and output plane of 60° (for each prism) - a different material (e.g. SF10) fits the requirements better. The transmission for such a prism (for p-polarized, s-polarized and mixed-polarized light) is shown in Figure 3.5 for different glass types. During

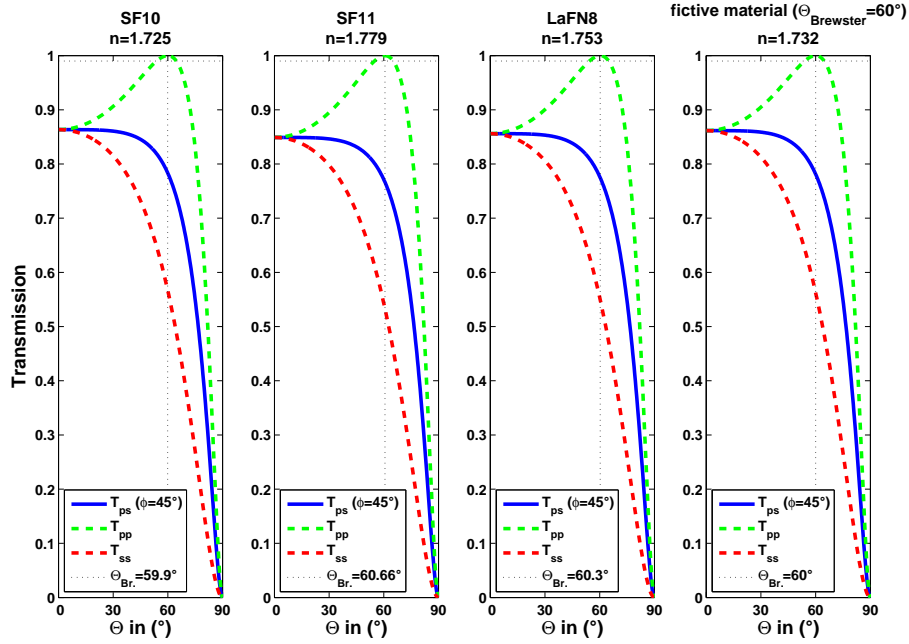


Abbildung 3.5.: Transmission curves for isosceles brewster prisms (for p-polarized, s-polarized and mixed-polarized light) of different glass types. The material SF10 fits the requirements of the HORUS dye laser system best.

the HUMPPA–COPEC–2010 campaign, optical fibers about 4 meters in length were used to transfer the 308 nm light to the detection system. Optical fibers allow complicated pathways and provide robust and stable coupling of the UV light into the detection system. However, along with the transmission losses also backreflections of the laser pulses are a disadvantage of using optical fibers. Depending on the length of the optical fiber (l) and the refractive index of the fiber material (n_{fiber}), the delay between laser pulse and its first backreflection can be calculated:

$$t = \frac{2l \cdot n_{fiber}}{c} \quad (3.9)$$

3. HO_x measurements using the HORUS instrument

where c is the speed of light in vacuum.

In case of the fibers used during HUMPPA–COPEC–2010 the first backreflection would occur approximately 40 ns after the laser pulse and a second backreflection with another 40 ns delay. Thus, backreflections of the laser pulse can (especially for long fibers, e.g. of ~ 10 meters in length) overlap parts of the fluorescence signal and reduce the instrument sensitivity. To overcome this issue, angled polished fibers were used the first time during HUMPPA–COPEC–2010. The angled polished incoupling and outcoupling surfaces helped to suppress backreflections significantly (see Figure 3.6).

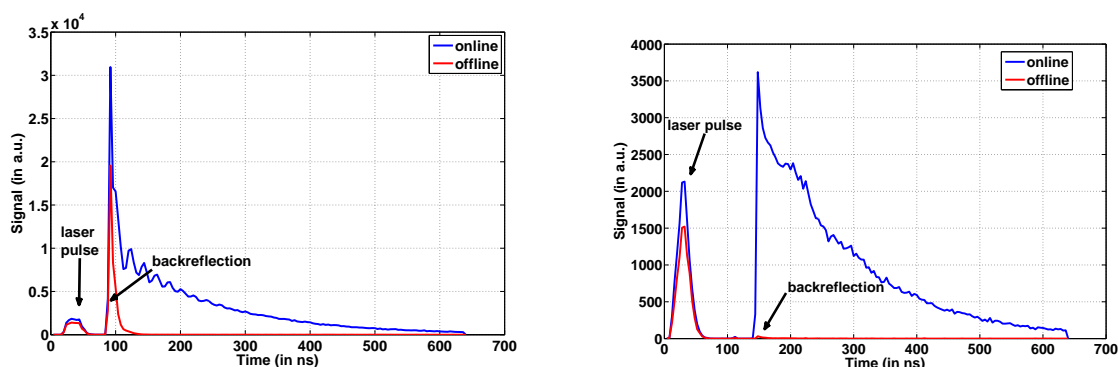


Abbildung 3.6.: Suppression of laser pulse backreflections and OH fluorescence signal. A flat polished fiber produces backreflections that can overlap the fluorescence signal (left panel). Using an angled polished fiber helps to suppress the backreflection of the laser pulse significantly (right panel).

Low pressure detection system

A schematic overview of the detection system setup of HORUS is shown in Figure 3.7. The sample air is drawn through a critical orifice (pinhole size of about 1.2 mm) into the low pressure detection cells, achieving a constant volume flow of about 10 slm ($p = 1013$ hPa, $T = 273.15$ K). The resulting exchange rate of sample air is necessary to avoid excitation of the sample air by two consecutive laser pulses, producing laser-generated OH. In order to maximize the fluorescence signal at a certain radical level (i.e. maximizing the instrument sensitivity) a White Cell setup crossing the detection volume with 32 light paths is used (see Figure 3.8), (White, 1942).

The detection of HO₂ is achieved via chemical conversion to OH by adding NO in excess to the total flow of sample air downstream of the OH detection. The sum of remaining ambient OH plus OH originating from HO₂ conversion is measured in a second detection axis (see Figure 3.7).

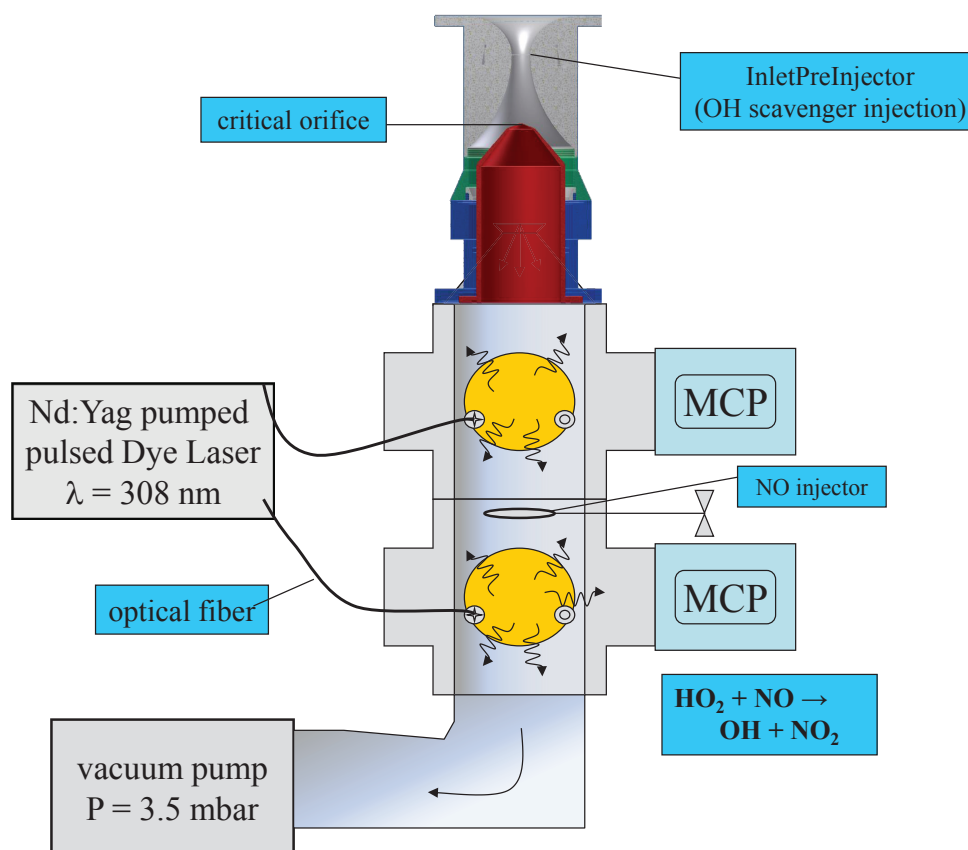


Abbildung 3.7.: Setup of the HORUS detection system. The sample air is drawn through a critical orifice into the low pressure detection cell. OH radicals are excited by laser light at around 308 nm and the fluorescence of these molecules is detected using a multi channel plate detector (MCP). In a second detection axis, placed in line with the OH detection cell, HO₂ is detected after conversion to OH by reaction with NO, which is injected between the first and the second detection cell. An InletPreInjector is mounted on top of the standard LIF inlet for chemical background detection. For details refer to text.

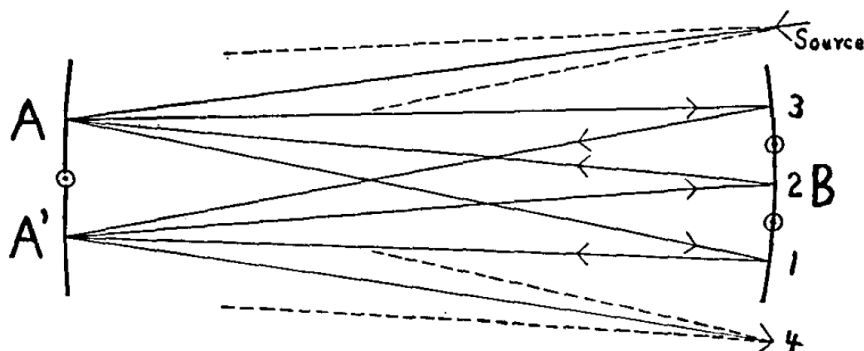


Abbildung 3.8.: Schematic representation of the optical path inside a White Cell. The incoming laser beam is multiple reflected using three mirrors before exiting the cell (Taken from White, 1942).

Taking the information from the so-called first axis OH measurement into account, the HO₂ concentration is calculated. The proportionality between fluorescence signal and hydroxyl radical concentration is given by the instrument sensitivity \mathcal{E}_{LIF} , which is normalized by laser power. Nevertheless, the sensitivity still depends on many other parameters, including the density inside the fluorescence cell, the water vapour concentration in sample air (quenching effects), the transition probability, the overlap of the laser and fluorescence transition lines, the transmissivity of the White Cell setup, as well as the sensitivity of the detector. Some of those parameters are difficult to be determined separately and might even change in time (e.g. contamination of optical surfaces or changing detector efficiency due to ageing). Therefore, calibrations of the HORUS instrument were performed on a regular basis (see Section 3.2.3).

The usual LIF method to determine the background signal is changing the excitation wavelength, to get off-resonant for the OH molecule and measure the background signal periodically. In HORUS 5 seconds of “online” measurement are followed by 5 seconds “offline”, which is 1000 etalon steps (~ 37 GHz) alternating left and right of the Q₁(2) transition line. Furthermore, the ambient OH can be removed from sample air by periodic addition of a chemical OH reactant (e.g. propane, propene, C₃F₆) to determine the background signal (Figure 3.9). Since both methods do not exclude each other the addition of a chemical reactant was done on top of the wavelength modulation method for the HORUS instrument during HUMPPA-COPEC-2010.

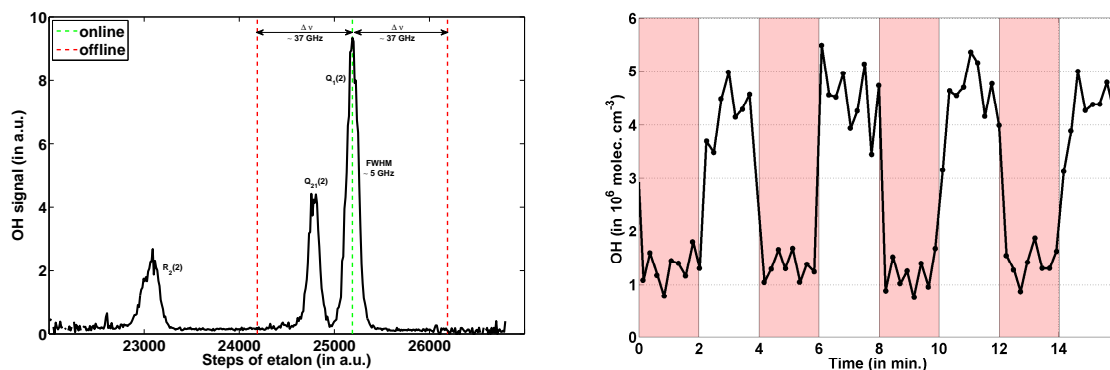


Abbildung 3.9.: Two ways to determine OH background signal: (left panel) by wavelength change and (right panel) by periodic addition of an OH reactant (periods with colored background) using an InletPreInjector (Brune et al., 2010; Novelli et al., 2012; Mao et al., 2012).

Vacuum system

The HORUS instrument requires a vacuum system to create a low pressure, forcing the sample air through a critical orifice into the detection cells. Therefore, a compressor (roots blower, Type M90, Eaton) and a vacuum pump (scroll pump, Type XDS-35, Edwards) are connected in series. With this setup the sample air is compressed and the pressure in front of the vacuum pump is enhanced, leading to an improved pumping efficiency, which is mandatory to achieve the low pressure of a few hPa inside the detection cells. The characteristics of the vacuum system are shown in Figure 3.10. It is proved to be stable within longterm measurements running continuously for several weeks.

Instrument control and data acquisition unit

The HORUS instrument is controlled using an embedded PC running a Debian LINUX operating system. Analogue and digital sensors as well as actuators, such as valves or stepper motors, are connected to the data acquisition using a modular system of electronic cards, which was developed at the Max-Planck-Institute, Mainz. The connection to the embedded PC is established via the ISA bus. The software design of HORUS is based on the client-server model, programmed in “C”. The server controls the communication with the hardware and periodically stores records from the sensors on a harddrive. UDP sockets are used to query data from clients and/or send actuator commands (e.g. move stepper motor). The graphical user interface (GUI, programmed in MatLab, Mathworks, Inc.) is also realized as a client. Thus, the data acquisition is running as an independent process and will not be

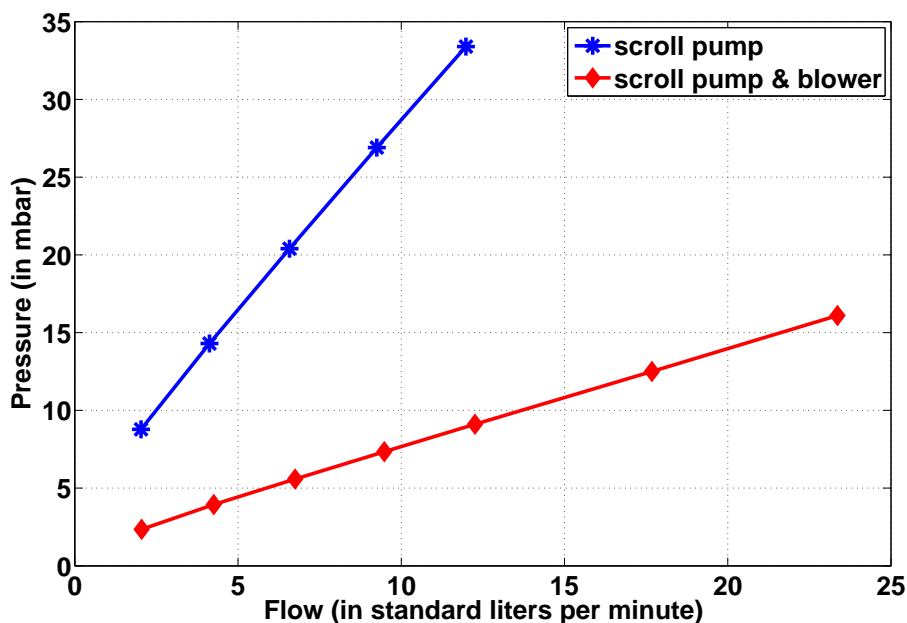


Abbildung 3.10.: Characteristics of the vacuum system. To improve the pumping efficiency of the scroll pump (Type XDS-35, Edwards) a roots blower (Type M90, Eaton) is used for precompaction.

affected by malfunctions of the GUI. Furthermore, it is possible to run the graphical user interface on a different computer (within the same network) than the data acquisition.

3.2.3. Calibration

The instrument sensitivity \mathcal{E}_{LIF} is determined by regular calibrations of the LIF system. For calibration of the HORUS instrument, different mixtures of dry and humid air was flown turbulently through a 16 mm square aluminium tube at a rate of 50 liters per minute. The resulting water vapour concentration is measured with an infrared absorption instrument (LI-7000, Licor), which is calibrated against a dew point generator (LI-610, Licor) within a typical range of 0-25 mmol mol⁻¹ of H₂O in calibration air. The dew point generator itself is calibrated against a certified primary standard (NIST). A mercury lamp (Pen-ray line source, LOT-QuantumDesign, Europe) is attached to the tube to produce equal concentrations of OH and HO₂ radicals by photolysis of water vapour. From the flow speed, which is derived from the measured mass flow (DryCal sensor, NIST traceable certified

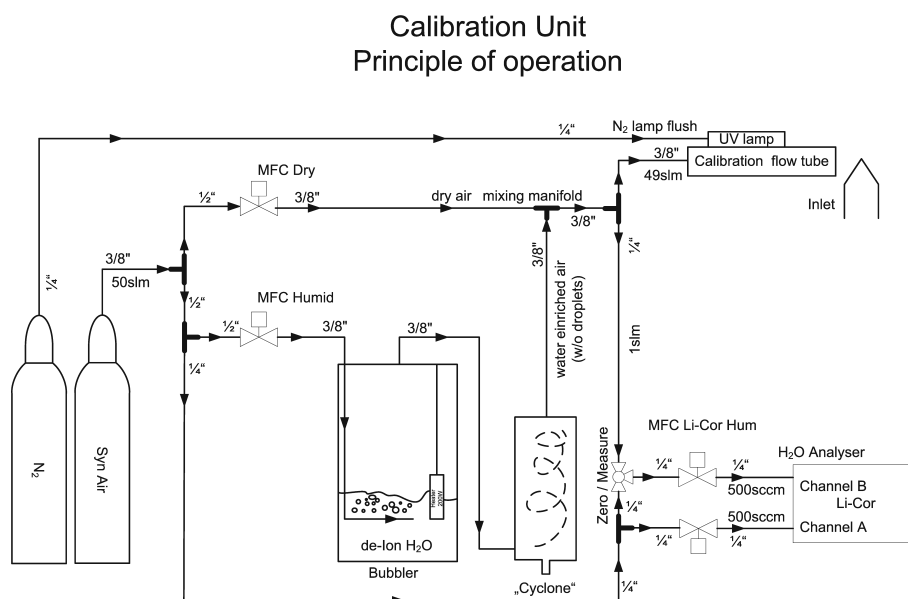


Abbildung 3.11.: Schematic of the setup used for calibration of the HORUS instrument. Different mixtures of dry and humid air are established using a bubbler device and subsequently the water vapour mixing ratio is measured by a H₂O analyser. The humidified air is flown through the calibration flow tube, where OH and HO₂ radicals are produced in equal amounts by photolysis of the water vapour at 184.9 nm (Taken from Kubistin et al., 2010).

by Westphal, Germany), and the resulting residence time, t , of calibration air within the illuminated volume, the absorption cross section of water at 185 nm, $\sigma_{\text{H}_2\text{O}}$, and the actinic flux density of the lamp, Φ_0 , the radical concentration can be calculated (Faloona et al., 2004). The absorption by oxygen and the resulting reduction of the actinic flux density across the tube height, h , is taken into account by application of a correction factor, f_{O_2} , following Beer-Lambert's law.

$$[\text{OH}] = [\text{HO}_2] = \Phi_0 \sigma_{\text{H}_2\text{O}} [\text{H}_2\text{O}] t f_{\text{O}_2}, \quad (3.10)$$

3. HO_x measurements using the HORUS instrument

with the correction factor for absorption by oxygen

$$f_{\text{O}_2} = \frac{\int_0^h e^{-\sigma_{\text{O}_2}[\text{O}_2]x} dx}{h}. \quad (3.11)$$

A schematic of the setup used for calibration of the HORUS instrument is shown in Figure 3.11.

Exact knowledge of the actinic flux density is crucial for this calibration method. The mercury lamp used for calibration of the HORUS instrument during HUMPPA–COPEC–2010 was calibrated using the actinometry method by N₂O photolysis, as described by Martinez et al. (2010), immediately before and after the campaign. N₂O photolysis produces O(¹D) molecules which partly react with N₂O producing NO. The actinic flux density of the lamp is determined by measuring NO from the photolysis of known concentrations of N₂O in nitrogen with a NO_x chemiluminescence analyzer (C42, Thermo Environmental Instruments). The analyzer itself is calibrated using a NIST standard. It is to be considered that the sensitivity of the analyzer varies with different quenching efficiency of the carrier gas, as shown in Figure 3.12.

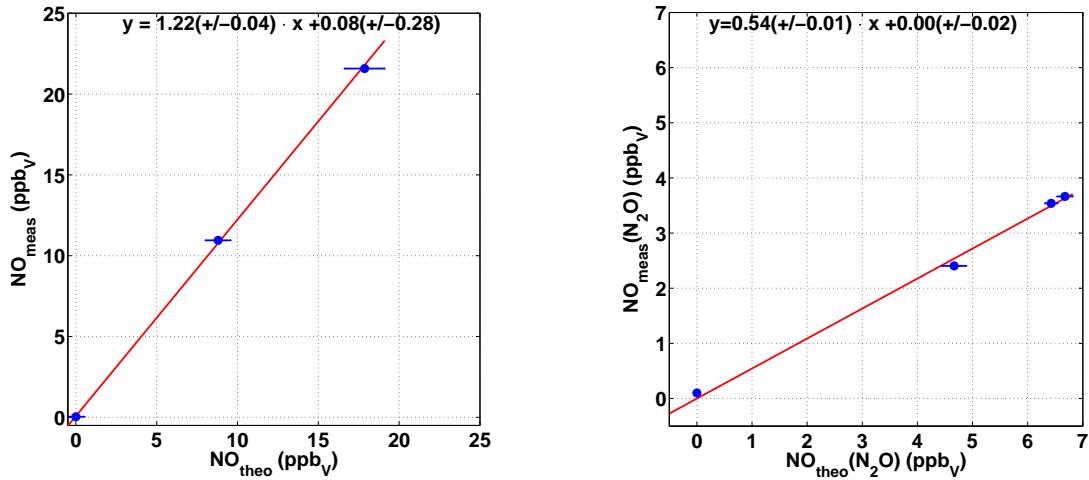


Abbildung 3.12.: Calibration of the NO analyzer (C42, Thermo Environmental Instruments) for NO in N₂ and N₂O. The sensitivity of the analyzer varies with different quenching efficiency of the carrier gas.

At mixing ratios of about 15 % N_2O , NO concentrations reach up to 5 ppb_V , well above the detection limit of the NO_x analyzer ($< 50 \text{ ppt}_V @ 120 \text{ sec}$ averaging time). The absorption of the 185 nm light across the calibrator tube increases with increasing N_2O concentration. This effect was taken into account for the calculation of the lamp actinic flux (Kubistin, 2009). The resulting actinic flux density at different N_2O mixing ratios is shown in Figure 3.13.

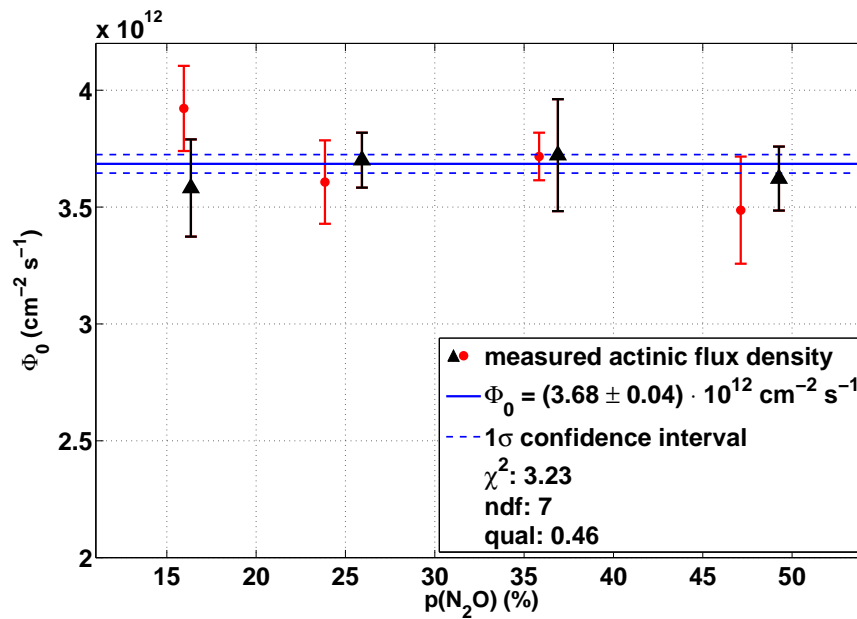


Abbildung 3.13.: Actinic flux density of the mercury lamp used for calibration of the HORUS instrument. The actinic flux density Φ_0 is derived from the photolysis of N_2O at different mixing ratios and the subsequent detection of the NO yields. The data shown here is the combined dataset from two actinometric measurements, one of them conducted before (red dots) and a second one after (black triangles) the field campaign, indicating a good long-term stability of the lamp actinic flux density. Errorbars indicate the propagated statistical variability of the calculated flux density.

3. HO_x measurements using the HORUS instrument

Both measurements of the actinic flux density, Φ_0 , before and after the field campaign, agree within uncertainties and indicate the long-term stability of the actinic flux density. From the overall fit we obtained $\Phi_0 = (3.68 \pm 0.04) \times 10^{12} \text{ cm}^{-2} \text{ s}^{-1}$ with a reasonable quality of fit. The systematic error of the actinic flux density measurement is calculated to be about 17%, similar to the value by Martinez et al. (2010) taking the contribution of all components summarized in Table 3.2 into account.

Table 3.2.: Systematic uncertainties during actinometric measurement.

Instrument/Quantity	systematic uncertainty
NO Monitor (TEI)	6 %
NO Standard (NIST)	1 %
Mass flow controller (MKS)	2 %
Absorption cross section $\sigma_{\text{H}_2\text{O}}$	2 %
Quantum yield	1 %
Kinetic rate coefficients	12 %
Dimensions of reaction chamber	3 %
Pressure sensor (MKS)	2 %
Long-term stability of act. meas.	10 %
Overall system. error estimate	17 %

3.2.4. Other dependencies of the instrument sensitivity

Furthermore, the instrument sensitivity is limited by quenching of the fluorescence, which happens mainly due to water vapour. To minimize this effect, the HORUS system is operated at low pressure ($\sim 3 - 5 \text{ hPa}$), but still high enough to keep wall losses small and provide enough molecules for excitation. The quenching effect by H₂O is considered in our calculations. An additional dependency on water vapour of about 12% and 17% decrease in sensitivity per 1% increase in water vapour mixing ratio was observed for the first and second fluorescence cell, respectively. This additional water effect indicates further losses at higher water mixing ratios possibly due to formation of OH-water clusters during the cold-adiabatic expansion of the sample air while entering the low pressure detection system. Changing instrument sensitivity with respect to water vapour mixing ratio, which is not

caused by quenching, was reported by others (Hofzumahaus et al., 1996; Holland et al., 1998) hypothesizing that condensation processes during the cold-adiabatic expansion are causing this effect. The above mentioned quantification of the additional water dependency during instrument calibration was used to correct for this dependency.

Unfortunately, the MCP detectors changed in sensitivity during the HUMPPA–COPEC–2010 field campaign, decreasing over time. Calibrations of the instrument were conducted about every second day to keep track of changes in sensitivity. Within some limitations, the behaviour of the laser scattering inside the system is an indicator of the sensitivity changes in the system. For the laser scatter signal, factors such as laser power fluctuations and background reflections have to be taken into account. Differing amounts and composition of aerosols in the sample air therefore might cause variable scatter. However, comparison of the laser scatter signal in ambient air with the quasi-simultaneous measured sensitivity during calibration shows a linear dependency. This functional dependency was applied to correct for the changing sensitivity (see Figure 3.14).

3.2.5. Interferences

Knowledge about possible interferences and avoiding those when indicated is required in order to measure OH and HO₂ reliably. Interferences can be caused by processes in the instrument itself and/or atmospheric substances which fluoresce at wavelengths similar to the hydroxyl radical. Laboratory studies testing the effect of sulfur dioxide, formaldehyde, nitrous acid, nitric acid, acetone, hydrogen peroxide, and various hydrocarbons on the OH signal did not show any significant interference for measurements in the atmosphere (Kubistin, 2009; Faloon et al., 2000; Ren et al., 2004). A negative interference on the OH signal by naphthalene was observed in polluted urban environments and can be used for the specific measurement of this compound (Martinez et al., 2004). It was recently reported that LIF measurements can be affected from internally generated OH (Mao et al., 2012; Novelli et al., 2012). Therefore, a chemical modulation method to determine the background signal for the measurement of atmospheric OH (as proposed by Brune et al., 2010) was applied to the HORUS-LIF for the first time during HUMPPA–COPEC–2010. A new injection unit IPI (*InletPreInjector*) was developed and optimized to scavenge more than 95 % of atmospheric OH by periodic injection of a chemical reactant in front of the standard inlet. In order to minimize wall losses, a bypass flow, large compared to the sample flow into the detection system, was established. Optimization of this injection system included tests using different reactants, e.g. propylene and hexafluoropropene, and varying injection and bypass flow conditions to determine the best parameters for continuous operation. A different publication on the characterisation of the OH scavenger injection device *IPI* is in preparation by Novelli et al. (2013).

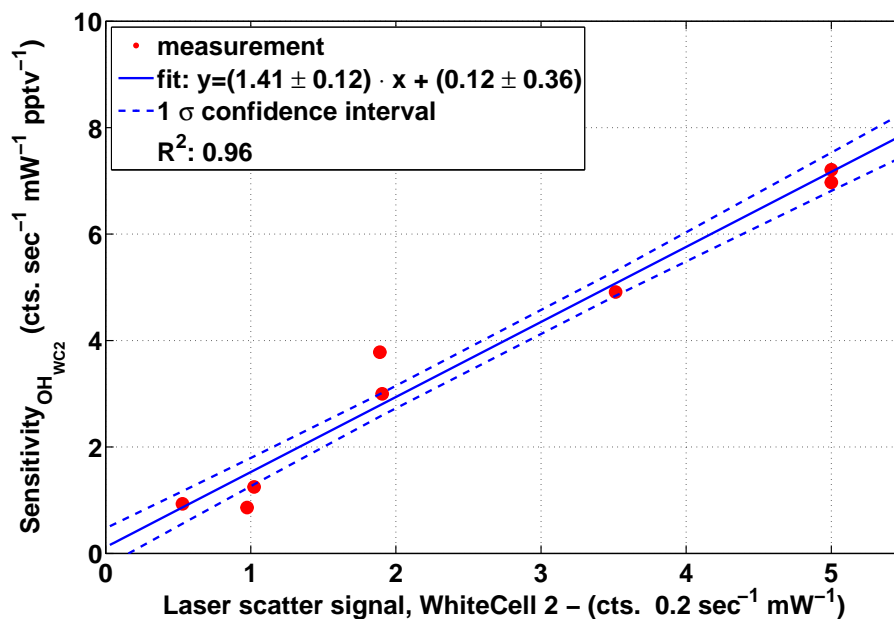
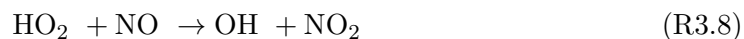


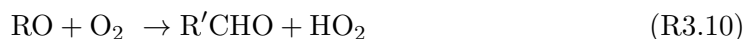
Abbildung 3.14.: Sensitivity change inside the second detection axis of HORUS as a function of the associated laser scatter signal. A linear correlation ($R^2=0.96$) with a non-significant offset was observed during instrument calibrations. The functional dependency obtained from linear regression was applied to the measurements to correct for changes in instrument sensitivity by continuously monitoring the laser scatter signal. A similar correction function for the change in sensitivity of the first detection cell has also been determined empirically and applied.

Measurements of HO₂ concentrations are conducted using chemical conversion into OH via the reaction with NO and the subsequent detection of the hydroxyl radicals by the LIF technique (Reaction R3.8):



In the atmosphere, RO₂ is also converted into HO₂ in the presence of NO (Reactions R3.9 - R3.10). These reactions were expected to be negligible in low pressure FAGE detection systems due to the reduced oxygen concentration and the short reaction time between

injection of NO and detection of OH within the system (Heard and Pilling, 2003).



We observed a small interference (<10%) originating from methyl peroxy radicals in the laboratory for the HORUS instrument, comparable to the results reported by Holland et al. (2003), who detected an interference smaller than 5% for their LIF-FAGE instrument. Significant interferences in HO₂ measurements by the LIF-FAGE technique from RO₂ species resulting from the OH-initiated oxidation of alkenes and aromatics have been observed by Fuchs et al. (2011) and others (Dillon, 2011). In contrast to alkane-based peroxy radicals, which are formed in the reaction of VOC + OH via H-atom abstraction, alkene-based peroxy radicals (mainly produced via OH-addition on the C-C double bond) form specific RO by reaction with NO, that can decompose under the low pressure conditions forming HO₂ rapidly. The conversion efficiency is limited by Reaction R3.9. The ratio of HO₂ to RO₂ converted by reaction with NO under excess conditions (see Reactions R3.8 & R3.9) is given by the pseudo-first-order approximation

$$\frac{[\text{HO}_2](t)}{[\text{RO}_2](t)} = \frac{[\text{HO}_2]_0}{[\text{RO}_2]_0} \cdot \frac{e^{-k_{R3.8} [\text{NO}]t}}{e^{-k_{R3.9} [\text{NO}]t}} = \frac{[\text{HO}_2]_0}{[\text{RO}_2]_0} \cdot e^{-(k_{R3.8}-k_{R3.9}) [\text{NO}]t}, \quad (3.12)$$

while $k_{R3.8} > k_{R3.9}$.

The ratio in Equation 3.12 becomes small, i.e. HO₂ is converted more efficiently compared to RO₂ when the product $[\text{NO}] \cdot t$ is small. Thus, any potential interference from alkenes on HO₂ can be reduced by reducing reaction time and/or NO concentration. During HUMPPA-COPEC-2010 NO mixing ratios of about 400 ppm_v occurred inside the detection system of HORUS by injection of pure NO into sample air, yielding a conversion efficiency from HO₂ to OH of more than 95% at the operating conditions of the instrument. This could also have caused a high conversion efficiency for interfering RO₂ species as described above. Nevertheless, this interference depends strongly on the available VOCs for the production of RO₂ in the investigated environment as well as on the instrumental setup which defines the conversion efficiency of those peroxy radicals inside the instrument. The observed HO₂ can be interpreted as the sum of atmospheric HO₂ and a contribution from the effective interference by specific RO₂:

$$[\text{HO}_2]^{\text{obs.}} = [\text{HO}_2]^{\text{atm.}} + \sum_i (\alpha_{\text{RO}_2}^i \times [\text{RO}_2]_i) \quad (3.13)$$

The relative detection sensitivities $\alpha_{\text{RO}_2}^i$ for the specific RO₂ compared to HO₂ are strongly dependent on the instrumental setup and can reach values up to about 0.9 (Fuchs et al., 2011; Lu et al., 2012; Whalley et al., 2013). However, the speciation of RO₂ in the observed environment strongly influences the effective interference. Based on model simulations the

3. HO_x measurements using the HORUS instrument

magnitude of the RO₂ interference on HO₂ measurements by some LIF instruments in different environments was estimated between 10 % up to about 30 % (Lu et al., 2012; Fuchs et al., 2011; Mao et al., 2012; Whalley et al., 2013; Griffith et al., 2013).

NO titration experiments during calibration and ambient air measurements in two forest environments in Germany have been conducted after HUMPPA–COPEC–2010, quantifying the maximum interference by RO₂ in the HORUS instrument in these environments to be less than 20 % (Tatum Ernest et al., 2012). For the purpose of these titrations the NO injection of HORUS was varied to accomplish internal NO mixing ratios of approximately 1 to 1600 ppm_v. The resulting NO dependency of the signal caused by a constant HO₂ concentration during a calibration is presented in Figure 3.15.

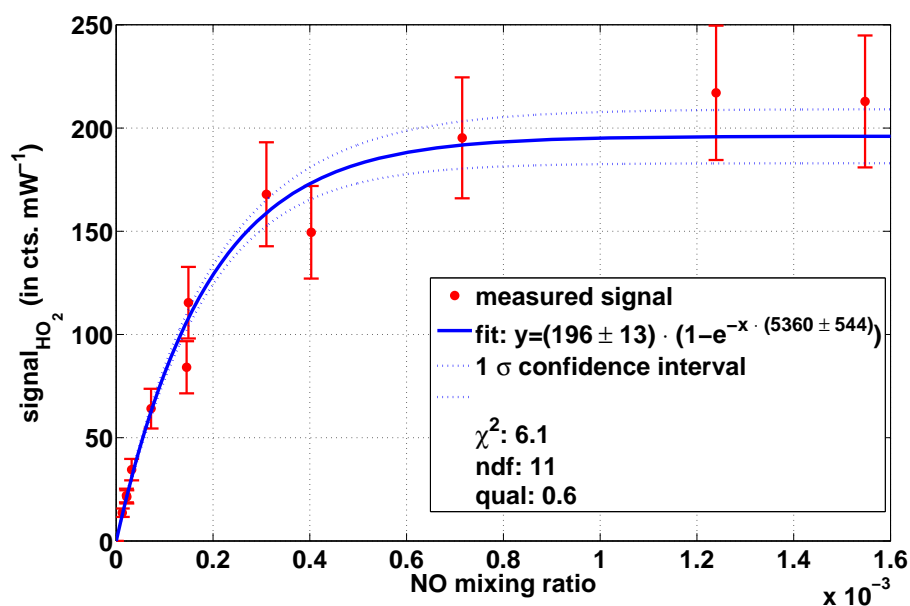


Abbildung 3.15.: NO dependency of the HO₂ signal during a calibration. A constant HO₂ concentration is provided to the LIF instrument by the calibrator unit. The NO mixing ratio for conversion from HO₂ to OH inside HORUS is varied from approximately 1 to 1600 ppm_v. Above ~ 800 ppm_v a rather constant conversion efficiency is found.

From this dependency a conversion efficiency from HO₂ to OH as a function of the NO mixing ratio is derived. The observed signal can be expressed by

$$S_{\text{HO}_2}(\text{NO}) = \mathcal{E}_{\text{LIF}}^{\text{NO}_{\text{Cal}}} \cdot \epsilon'(\text{NO}) \cdot [\text{HO}_2]^{\text{Cal}}, \quad (3.14)$$

where $\mathcal{E}_{\text{LIF}}^{\text{NO}_{\text{Cal}}}$ is the instrument sensitivity at the NO level during HORUS calibration and $\epsilon'(\text{NO})$ represents the NO-dependent conversion efficiency, fulfilling the constraint

$$\epsilon'(\text{NO}_{\text{Cal}}) = 1. \quad (3.15)$$

The signal during a titration experiment using ambient air shows a similar NO dependency, representing the conversion efficiency for the sum of HO₂ and interfering RO₂ species, assuming constant conditions, i.e. only minor changes in HO₂ and RO₂ concentrations during the titration. It can be written as

$$\begin{aligned} S_{\text{HO}_2+\text{RO}_2}(\text{NO}) &= S_{\text{HO}_2}(\text{NO}) + S_{\text{RO}_2}(\text{NO}) \\ &= \mathcal{E}_{\text{LIF}}^{\text{NO}_{\text{Cal}}} \cdot \epsilon'(\text{NO}) \cdot [\text{HO}_2] + S_{\text{RO}_2}(\text{NO}). \end{aligned} \quad (3.16)$$

At a very low reference NO level, NO_{ref} , the contribution from RO₂ to the total signal is assumed to be less than 10%, which is the upper limit for the RO₂ interference by methyl peroxy radicals determined in laboratory experiments. Under these conditions Equation 3.16 simplifies to

$$\begin{aligned} 0.9 \cdot S_{\text{HO}_2+\text{RO}_2}(\text{NO}_{\text{ref}}) &= S_{\text{HO}_2}(\text{NO}_{\text{ref}}) \\ &= \mathcal{E}_{\text{LIF}}^{\text{NO}_{\text{Cal}}} \cdot \epsilon'(\text{NO}_{\text{ref}}) \cdot [\text{HO}_2]. \end{aligned} \quad (3.17)$$

Therefore, it is possible to quantify the HO₂ concentration as well as the contribution from RO₂ interference to the total signal at a certain NO level. The result of a titration in ambient air and the expected HO₂ signal are shown in Figure 3.16. The difference between the two curves provides the magnitude of the interference. In the presented titration (Figure 3.16) this difference makes $\sim 12\%$ of the total signal at the maximum NO level. However, even the expected HO₂ curve is systematically lower compared to the total observed signal, the observed deviation is not significant.

Furthermore, titration experiments were conducted at different water vapour mixing ratios within the calibration air, to rule out a potential dependency of the conversion efficiency on the water vapour mixing ratio. Between 20% and 90% of the calibration air were flushed through the bubbler of the calibration unit, yielding H₂O mixing ratios of 3.7 – 12.5 mmole mole⁻¹. The normalized instrument sensitivities are plotted in Figure 3.17.

There is no clear water dependency observed on the HO₂ conversion efficiency. Nonetheless, the titration curves show at the highest NO level a variability of $\sim 20\%$, which provides an estimate on the precision of these titration experiments.

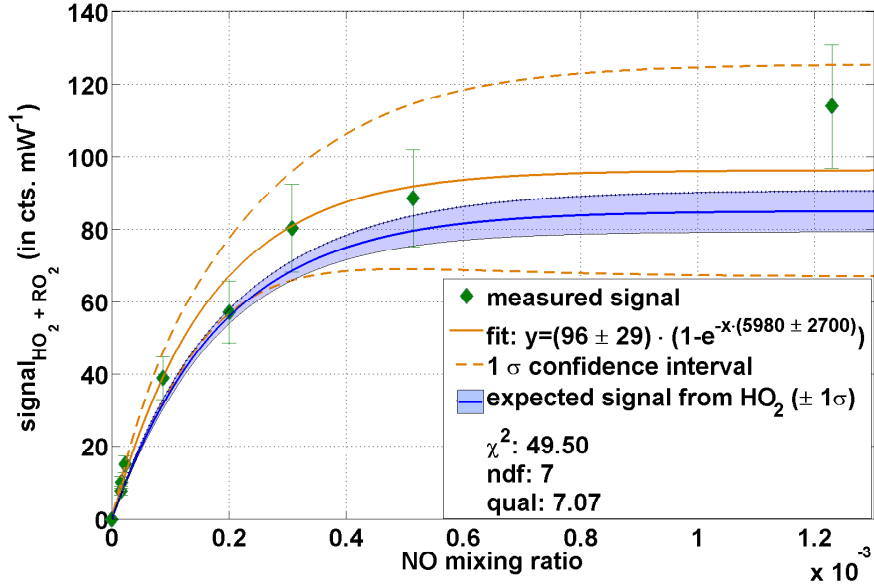


Abbildung 3.16.: NO dependency of the total (HO₂+ RO₂) signal during ambient air measurement and expected HO₂ signal (blue line) applying the conversion efficiency derived from titration experiment during calibration. At maximum NO mixing ratio the signals differ by ~ 12 %. However, even the expected HO₂ curve is systematically lower compared to the total observed signal, the observed deviation is not significant.

To further investigate the effect of RO₂ interference on the measurement of HO₂ concentrations during HUMPPA–COPEC–2010, we calculated the H₂O₂ budget taking the production by the self-reaction of HO₂ and the loss via photolysis and deposition into account and compared the calculated hydrogen peroxide with the measurements (Figure 3.18). The production of H₂O₂ by HO₂ shows a quadratic dependency and is therefore highly sensitive to the HO₂ concentration. The decay of hydrogen peroxide in the afternoon is mainly determined by the deposition process. A reasonable deposition rate of $4 \times 10^{-5} \text{ s}^{-1}$, corresponding to a deposition velocity of 4 cm s^{-1} in a 1 km high boundary layer, was used for the calculation. This is comparable to values reported by Hall and Claiborn (1997) for a boreal forest, ranging from 1 to 5 cm s^{-1} . Removal of hydrogen peroxide by photolysis makes up to

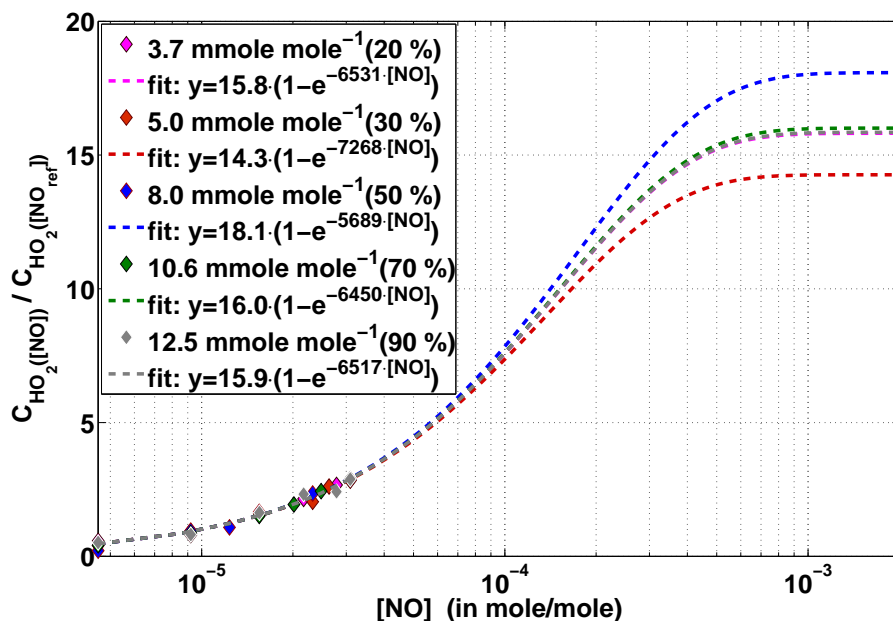


Abbildung 3.17.: Titration experiments at different water vapour mixing ratios within the calibration air, to rule out a potential water dependency on the HO₂ conversion efficiency. The titration curves show at the highest NO level a variability of $\sim 20\%$, which provides an estimate on the precision of these titration experiments. Percentages in parentheses denote the portion of humidified air to the total flow of calibration air.

10% of the total H₂O₂ loss. Hydrogen peroxide concentrations derived using the measured HO₂ is in reasonable agreement with the measured H₂O₂. In some cases measured HO₂ is still not sufficient to explain the measured H₂O₂ concentrations. Even though under some conditions hydrogen peroxide measurements might be affected by mixing with different air masses, e.g. from the residual layer, which have not been considered in our calculation, the comparison gives confidence that the measurements of HO₂ are not subject to a major interference. Although the magnitude of the RO₂ interference during HUMPPA-COPEC-2010 cannot be conclusively derived there is no evidence for an extraordinary large interference in the HORUS instrument compared to other LIF systems. Therefore, a contribution of 30% to the observed HO₂ signal (presently the maximum value observed in LIF instruments) is considered as an upper limit estimate of the RO₂-interference for further analysis.

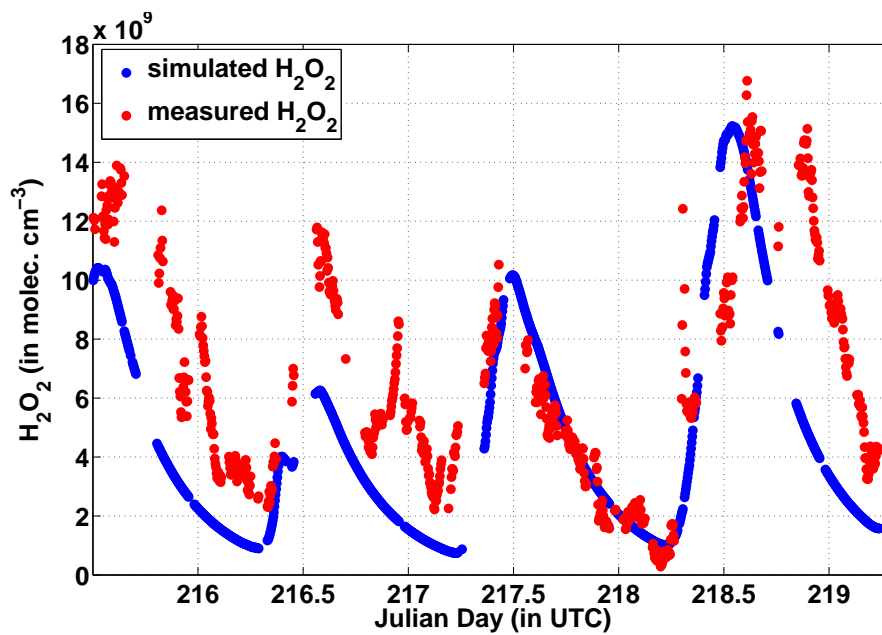


Abbildung 3.18.: Comparison of the measured H₂O₂ with simulation based on HO₂ measurements by LIF. The measured HO₂ is needed to explain the observed hydrogen peroxide.

4. HUMPPA–COPEC–2010

The boreal forest ecosystem represents the world largest interconnected woodland. It extends over an area of about $15 \times 10^6 \text{ km}^2$ between 50 and 65° N and makes up 27% of the world's forest (FAO, 2010). Hence, the boreal forest is expected to influence significantly the chemistry and physics of the atmosphere. The vegetation of the boreal forest comprises mainly coniferous trees, such as pine and spruce, that are known to emit significant quantities of reactive biogenic volatile organic compounds (e.g. monoterpenes) to the atmosphere as a function of temperature and to a lesser extent light (Williams et al., 2011, and references therein).

During HUMPPA-COPEC (*Hyytiälä United Measurements of Photochemistry and Particles in Air – Comprehensive Organic Precursor Emission and Concentration* study) a comprehensive dataset including measurements of the main oxidants OH, O₃, and NO₃; important trace gases such as CO, NO_x, H₂O₂, HCHO, HONO; anthropogenic and biogenic VOCs, and their oxidation products, inorganic chemical constituents, aerosol properties, aerosol size distributions, as well as photolysis frequencies and other meteorological parameters was collected at the boreal forest field station SMEAR II (*Station for Measuring Forest Ecosystem-Atmosphere Relations*). An overview can be found in Williams et al. (2011).

The general objective of the HUMPPA–COPEC–2010 campaign was to comprehensively characterize the atmospheric physics and chemistry over a boreal forest site in summer. This includes the characterization and speciation of volatile organic compounds, investigation of the formation and growth mechanisms of secondary organic aerosol, and the observation and analysis of radical chemistry as well as the extent of OH recycling processes.

In order to measure OH and HO₂ radicals the HORUS instrument was deployed during the intensive HUMPPA-COPEC field experiment in summer 2010.

4.1. Measurement site and instrumentation

The field site is located in a boreal forest in Hyytiälä, Southern Finland ($61^\circ 51' \text{ N}$, $24^\circ 17' \text{ E}$, 181 m a.s.l.) (Vesala et al., 1998). The largest city near the station is Tampere (about 200 000 inhabitants), located about 60 km S-SW of the measurement site (Figure 4.1), (Hari and Kulmala, 2005). The SMEAR II station is equipped with several masts and towers surrounded by a more than 40-year-old pine dominated forest (*Pinus Sylvestris L.*). The canopy height during the measurement period was about 20 meters (For more detailed

information about the continuous measurements and the infrastructure see Vesala et al., 1998; Kulmala et al., 2001; Hari and Kulmala, 2005).

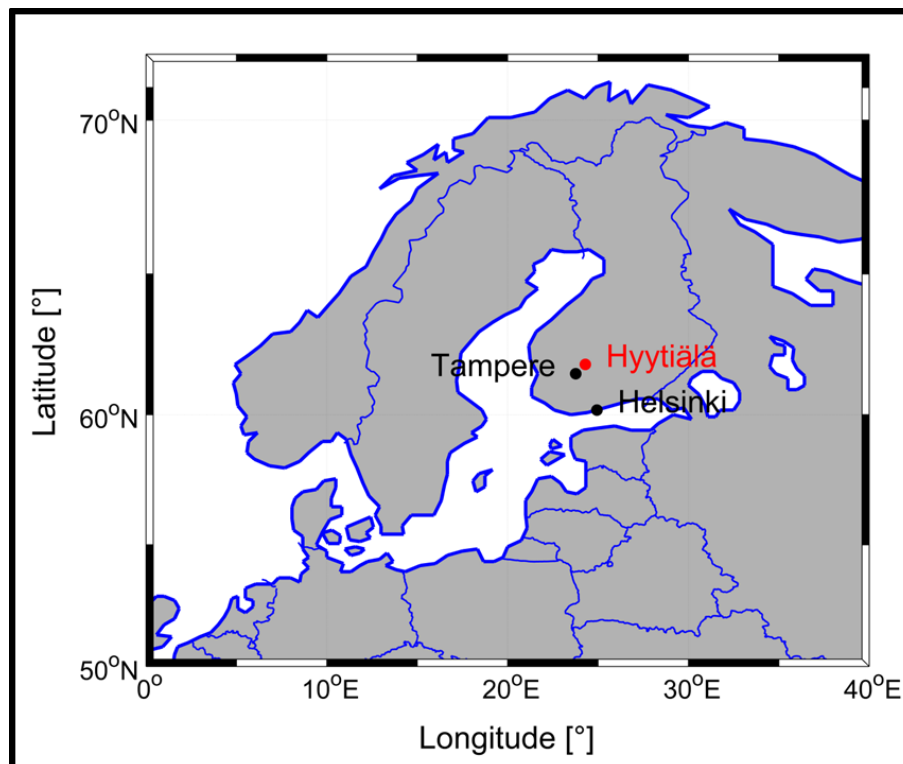


Abbildung 4.1.: SMEAR II field station, Hyytiälä, Southern Finland (61° 51' N, 24° 17' E, 181 m a.s.l.)

During the intensive measurement period of the HUMPPA–COPEC–2010 campaign an additional scaffolding tower was set up at the field site within a clearing (the HUMPPA tower, ~ 24 m high), reaching about 2-3 m above the canopy top. The sensors and inlet lines of instruments measuring reactive species like OH, HO₂, O₃, NO_x, NO₃, HONO, H₂O₂, organic peroxides, HCHO, monoterpenes, as well as the associated photolysis frequencies (J_{NO₂}, J_{O(1D)}), and the total OH reactivity were collocated on the top platform of the HUMPPA tower to investigate the photochemistry at the ecosystem-atmosphere interface (see Figure 4.2).

Since the campaign instrumentation and meteorological conditions are described elsewhere (Williams et al., 2011), only a brief description of the instruments used in this study is given here; time resolution and lower limits of detection are summarized in Table 4.1.



Abbildung 4.2.: Setup of the HORUS instrument on the HUMPPA tower. Simultaneous side-by-side measurements of hydroxyl radicals were conducted at the start of the campaign with two instruments using chemical ionization mass spectrometry (CIMS) and laser induced fluorescence within the forest. The two instrument inlets (shown on the pictures in the lower right corner) were co-located at the side of the container, about 1m a.g.l. .

Ozone was measured using a UV instrument, sharing an inlet line with the chemiluminescence detection system (CLD) for measuring NO and NO₂. NO₂ was measured indirectly by conversion to NO using a blue light converter. The instrument setup was similar to the well-established one described by Hosaynali Beygi et al. (2011) for a different field campaign. NO₃ and N₂O₅ were measured by cavity-ring-down spectroscopy (Schuster et al., 2009; Crowley et al., 2010). Two long path absorption photometer systems (LOPAP) were set up within the forest and on the HUMPPA tower, measuring HONO (Kleffmann et al., 2002). Hydrogen peroxide and the sum of organic peroxides were observed with a wet chemical system based on derivatisation and fluorescence enzyme (DEF) described by Klippel et al.

(2011). Measurements of carbon monoxide were conducted using a commercial vacuum-UV resonance fluorescence CO instrument (AeroLaser GmbH, Garmisch-Partenkirchen, Germany). Detection of HCHO was based on the Hantzsch reaction and subsequent quantification of the reaction product via fluorescence detection. BVOCs were measured by several mass spectrometers. Gas chromatograph mass spectrometry (GC-MS) was used to investigate alkanes, alkenes, and particularly isoprene and monoterpenes (Yassaa et al., 2012). Proton transfer reaction mass spectrometry (PTR-MS) was applied for the observation of methanol, acetone, acetonitrile, isoprene, total monoterpenes, benzene and toluene. In the case of isoprene measurements, GC-MS data is used for further analysis, due to higher uncertainty in PTR-MS measurements, probably caused by a cold-trap connected to the PTR-MS instrument. Furthermore, the PTR-MS isoprene data might be affected by an interference due to 2-methyl-3-buten-2-ol (MBO) which is detected at the same mass to charge ratio as isoprene using conventional H_3O^+ ionization (Goldan et al., 1997; Williams et al., 2001; Karl et al., 2012).

Photolysis frequencies (J_{NO_2} , $J_{\text{O}(^1\text{D})}$) were measured within the clearing at the forest ground, as well as on top of the HUMPPA tower with a set of filter radiometers at each position (Junkermann et al., 1989; Bohn et al., 2008; B.Bohn, personal communication, 2012). Water vapour, temperature, and pressure were recorded at several different levels on a 75 m meteorological mast located about 100 m away. The total reactivity towards OH was determined by a comparative reactivity method (Sinha et al., 2008; Nölscher et al., 2012). This method is based on the competitive scavenging of OH by a reference gas (pyrrole) and atmospheric trace gases. A chemical ionization mass spectrometry (CIMS) instrument was deployed to measure OH on ground (Petäjä et al., 2009).

4.2. HO_x observations

During the HUMPPA–COPEC–2010 field experiment gradients of the hydroxyl radical were measured using the CIMS instrument from University of Helsinki on ground (Petäjä et al., 2009) and the HORUS-LIF instrument above the canopy. To assure the comparability of both instruments and techniques they had to be compared side-by-side under ambient conditions. The HORUS-LIF instrument already participated in the international HO_x Comp 2005 project, a ground-based intercomparison of six OH instruments (4 LIF, 1 CIMS, 1 DOAS) performing measurements in the atmosphere simulation chamber SAPHIR as well as in ambient air. The HORUS-LIF showed good agreement with CIMS measurements ($R^2 = 0.96$) during daytime. However, we were expecting from that study to see a nighttime signal in ambient air whereas the CIMS method usually does not detect nighttime OH (Schlosser et al., 2009).

During HUMPPA–COPEC–2010 the two OH instruments were intercompared at the beginning of the field experiment (27th–30th of July) before starting the gradient measurement of OH concentrations. The inlet system of the LIF was placed next to the CIMS inlet on

Tabelle 4.1.: Instrumentation applied for above canopy observations during HUMPPA-COPEC2010

Species/Quantity	Time re- solution	Accuracy (1 σ)	Precision (1 σ)	Lower limit of detecti- on	Technique [†]
OH	~4 min	30 % (2 σ)	$\sim 5 \times 10^5$ molec. cm ⁻³	$\sim 9 \times 10^5$ molec. cm ⁻³	IPI-LIF-FAGE
HO ₂	~15 s	30 % (2 σ)	< 0.8 pptv	0.4 pptv	LIF-FAGE
OH	30 s	32 %	—	$\sim 5 \times 10^4$ molec. cm ⁻³	CIMS
O ₃	3 s	1 %	—	~1 ppbv	UV
NO, NO ₂	1 s	~5 %	~14 pptv	5 pptv	CLD (+Bluelight converter)
NO ₃	5 s	—	—	2-4 pptv	CRD
N ₂ O ₅	5 s	—	—	5-10 pptv	CRD
HONO	30 s	10 %	~1-2 %	< 5 pptv	LOPAP
H ₂ O ₂ and ROOH	5 min	25-30 %	8 pptv (3 σ)	15 pptv	Dual enzyme
CO	1 s	< 10 %	< 10 %	~1 ppbv	UV
HCHO	5 min	19 %	~700 pptv (3 σ)	9 pptv	Hantsch
Alkanes, alkenes, isopre- ne, monoterpenes	60 min	—	—	1 pptv	GC-MS
Methanol, acetone, ace- tonitrile, total terpenes, benzol, toluene isoprene*	6 min	—	—	~50 pptv	PTR-MS
Total OH reactivity	1 min	16 %	3-4 s ⁻¹	3 s ⁻¹	CRM
J _O (^{1D}), J _{NO₂}	1 s	~15 %	1 %	—	Filterradiometer

* Isoprene measurements might be affected by 2-methyl-3-buten-2-ol (MBO) detected at the same mass to charge ratio.

[†] IPI-LIF-FAGE = InletPreInjector - Laser Induced Fluorescence - Fast Gas Expansion; CIMS = Chemical Ionization Mass Spectrometry; UV = UltraViolet absorption/fluorescence; CLD=Chemiluminescence Detector; CRD= Cavity Ring Down; LOPAP = Long Path Absorption Photometer; GC-MS = Gas Chromatography - Mass Spectrometry; PTR-MS = Proton Transfer-Reaction Mass Spectrometer; CRM = Comparative Reactivity Method.

ground. The meteorological conditions at the field site within the four days of instrument intercomparison were dominated by above average temperatures, exceeding 25°C during noon, and mainly south-easterly winds, without rainy periods. Timeseries of meteorological parameters and trace gas concentrations can be found in Appendix A.

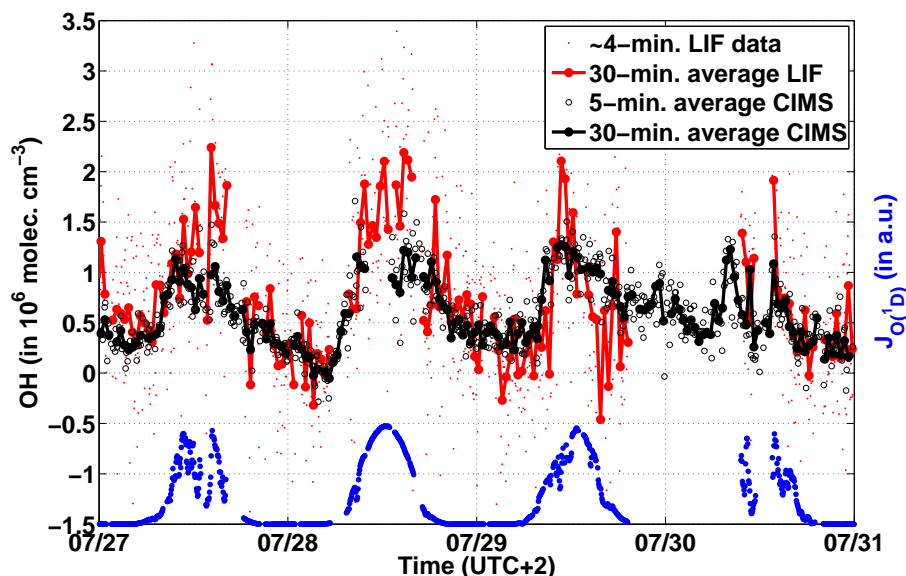


Abbildung 4.3.: Comparison of OH measurements by IPI-LIF-FAGE technique and by CIMS on ground (University of Helsinki, Petäjä et al., 2009). Nighttime OH was observed by both techniques.

The result of these four days of instrument intercomparison is shown in Figure 4.3. OH radical concentrations observed by both techniques are generally in agreement. The LIF data shows stronger fluctuations compared to the measurements by CIMS on the same averaging interval timescale of 30 minutes. Daytime maximum OH concentrations reached about $(1.5 - 2) \times 10^6 \text{ molec. cm}^{-3}$. During nighttime, both instruments observed OH concentrations below $5 \times 10^5 \text{ molec. cm}^{-3}$, but still well above the lower limit of detection of the CIMS, which was $5 \times 10^4 \text{ molec. cm}^{-3}$ at a time resolution of 30 s. For the LIF the detection limit was $4.8 \times 10^5 \text{ molec. cm}^{-3}$ at a time resolution of 60 minutes. The larger limit of detection as well as the increased fluctuations in the LIF observation compared to CIMS is mainly caused by application of the chemical modulation method. To determine atmospheric OH the interference signal is subtracted from the total observed signal. The detection limit is therefore not only given by instrument properties, like laser power, optical properties, and detector efficiency. It is also prone to the atmospheric variability both of

OH and of the species causing the interference inside the detection unit. Nevertheless, the good agreement during the intercomparison (Figure 4.4) provides confidence in the chemical modulation method and that the LIF measurements are not affected by additional unknown OH interferences resulting from the laser fluorescence technique (Novelli et al., 2012).

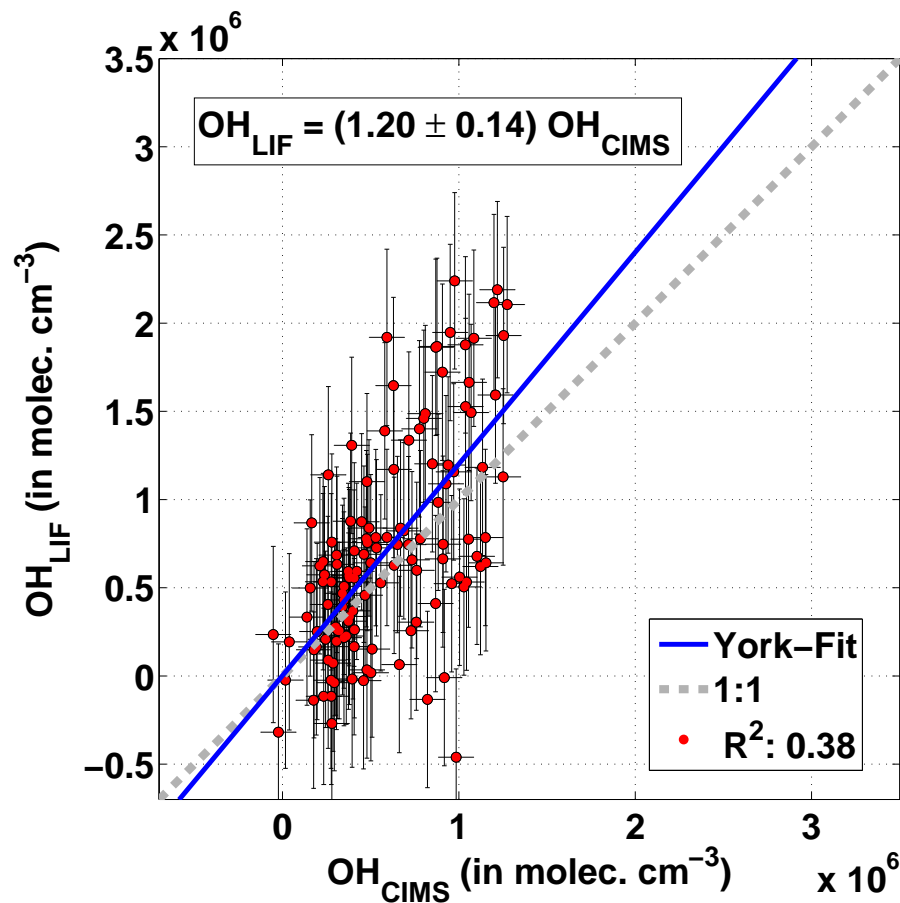


Abbildung 4.4.: Comparison of OH measurements by IPI-LIF-FAGE technique and by CIMS (University of Helsinki, Petäjä et al., 2009) based on 30-minute average data. Errorbars indicate the precision of the associated measurements. Linear regression following the method by York et al. (2004) yields a slope of 1.20 ± 0.14 and an insignificant offset (Offset: $(2 \pm 93) \times 10^3$ molec. cm^{-3}).

Finally, the LIF instrument was moved to the top of the HUMPPA tower to investigate the radical chemistry at the interface between atmosphere and ecosystem while the CIMS stayed on the ground. The resulting hydroxyl radical measurements are presented in Figure 4.5.

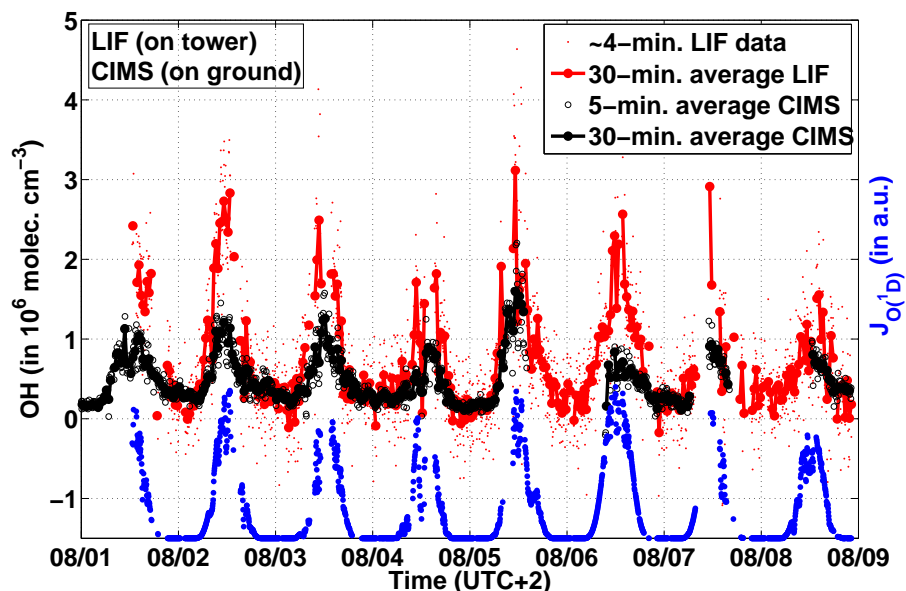


Abbildung 4.5.: Simultaneous OH measurements on the ground and above the canopy. Concentration maxima observed on the tower are up to a factor of 3 times higher than on the ground. Both instruments measured similar values during night.

Simultaneous OH measurements on ground and above canopy revealed a factor of 2-3 difference in observed concentration maxima, reaching values up to about 3×10^6 molec. cm^{-3} on the tower. During nighttime, the hydroxyl radical observations above canopy and on ground showed similar values. Linear correlation of OH and photolysis frequency $J_{\text{O}(^1\text{D})}$ was previously found during ground-based campaigns (Rohrer and Berresheim, 2006). However, the slope varies with location, depending on the abundance of VOCs and NO_x (see Section 2.4). The comparison of the correlation on ground and above canopy shows that higher OH values on the tower are driven by higher radiation but does not suggest differences in the chemical regime (Figure 4.6).

The nighttime OH, which was occasionally well above the detection limit of both instruments, can not be explained by the supporting observations, with known sources accounting for about 20% of the total OH production necessary to explain the measured concentrations. NO_3 was always below the lower limit of detection of about 1 ppt_v (at 5 min. time

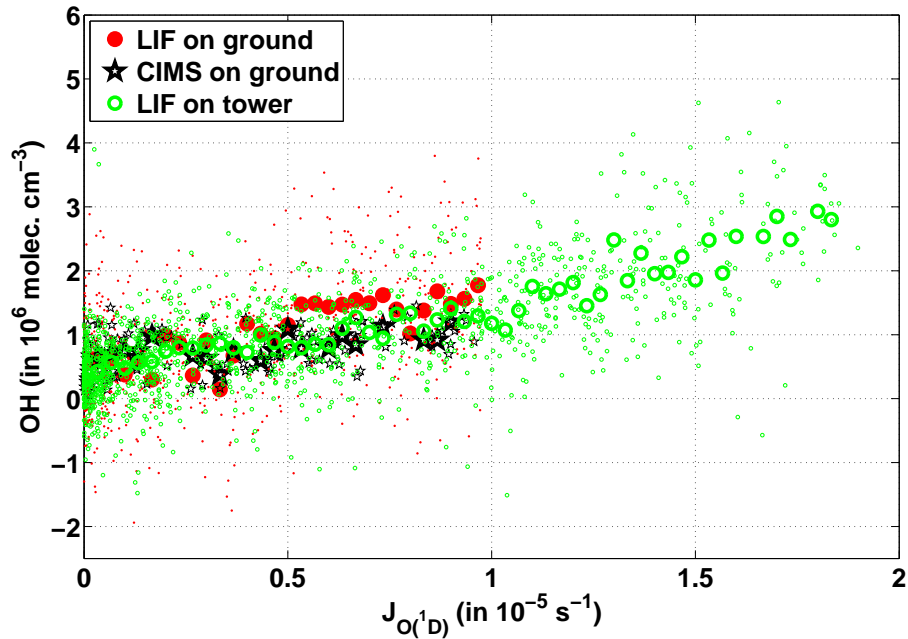
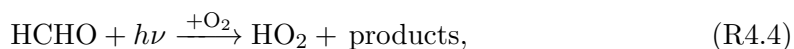
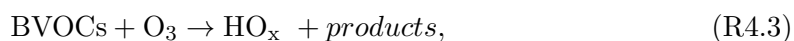
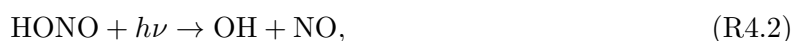


Abbildung 4.6.: Linear correlation of OH and $J_{O(1D)}$ is found during HUMPPA–COPEC–2010. The comparison of the correlation on ground and above canopy shows that higher OH values on the tower are driven by enhanced radiation. Similar slopes, mainly depending on the abundance of VOCs and NO_x, do not suggest differences in the chemical regime. Small symbols show 5-minute dataset, large symbols are means of data binned in steps of $3 \times 10^{-7} \text{ s}^{-1}$.

resolution) for the CRD instrument (Rinne et al., 2012). However, the production rate for NO₃ from the reaction of NO₂ and O₃ is of the order of $1 \times 10^6 \text{ molec. cm}^{-3} \text{ s}^{-1}$. Assuming this would directly cause an equally high OH production in the oxidation process of VOCs, which is an unlikely high upper estimate, this would still only explain an additional 10 to 15 % of the missing production during nighttime. The ozonolysis of unmeasured VOCs and their oxidation products, as well as enhanced HO_x recycling are potential candidates to explain the missing OH production. A more detailed analysis of the most relevant OH production terms is given in Section 4.4.

4.3. Primary HO_x production

Subsequent to the ground-level comparison with the OH-CIMS (1st – 8th of August), the HORUS instrument was moved to the top of the HUMPPA tower to investigate the photochemistry at the ecosystem-atmosphere interface. Making use of the comprehensive measurements of atmospherically relevant species, described in section 4.1, the known primary production rates of HO_x can be calculated considering the Reactions R4.1 - R4.5.



The contributions to the primary HO_x production during HUMPPA–COPEC–2010 are presented in Figure 4.7.

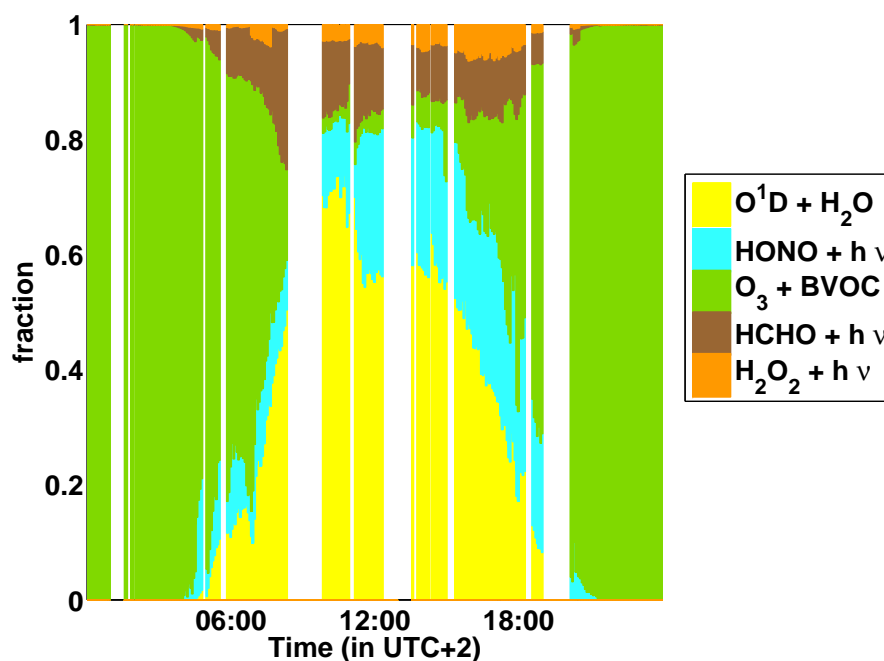


Abbildung 4.7.: Contributions to the primary HO_x production.

During daytime the photolytic production from O(¹D) + H₂O emerges as the most important HO_x source with a contribution of more than 50% around noon. The photolysis of hydrogen peroxide contributes less than 10% at maximum in the late afternoon hours. Slightly more relevant for the primary HO_x production is the direct formation of HO₂ from formaldehyde photolysis. The contribution to the HO_x production by photolysis of HONO is remarkable. The steady-state concentration of HONO due to reaction of NO with OH and photolysis backreaction (Reaction R4.2) was calculated and subtracted from the measured HONO concentration, to separate the primary OH production by HONO. This starts earlier in the morning and lasts longer in the evening hours compared to the production via O(¹D) + H₂O. Furthermore, it is comparable in magnitude in the early morning and late afternoon hours. During nighttime, when the photolytic sources vanish, the ozonolysis of BVOCs remains. During daytime the contribution due to O₃ + BVOC is negligible.

The primary HO_x production seems to be dominated by the primary OH production. Nonetheless, other direct HO₂ sources, such as RO₂ radicals produced from acetone photolysis reacting with NO or the photolysis of glyoxal, forming hydroperoxyl radicals, were not considered. Acetone photolysis provides only a RO₂ production rate on the order of $1 \times 10^4 \text{ molec. cm}^{-3} \text{ s}^{-1}$. This rate, considered as an upper limit of the additional HO₂ production does not contribute significantly to the total HO_x production. Glyoxal was not measured during HUMPPA-COPEC-2010. However, glyoxal is detected at the same mass like acetone in the PTR-MS instrument. Therefore, the acetone mixing ratio (Median: $\sim 3 \text{ ppb}_V$) can be assumed as an upper limit estimate for the glyoxal mixing ratio. A HO₂ production rate on the order of $1 \times 10^6 \text{ molec. cm}^{-3} \text{ s}^{-1}$ by photolysis of glyoxal is feasible, which is equivalent to a contribution of about 10 to 30% to the total HO_x production. Similarly peroxyacyl nitrates (PAN) that can be transported, i.e. it is not necessarily locally produced, decompose forming peroxyacyl radicals. These peroxy radical species can react with HO₂ forming OH (see Section 2.3). Thus, PAN does not directly contribute to the HO_x production, but it can represent a radical source, driving additional OH recycling processes.

4.4. OH budget – calculated based on observations

Similarly to the primary HO_x production, the budget of hydroxyl radicals is derived using the comprehensive measurements of atmospheric species. Besides the photolytic sources (Reaction R4.6 - R4.7), ozonolysis of different biogenic VOCs (Reaction R4.8) contributes to the primary production of OH. Secondary sources, e.g. the recycling of HO_2 by NO and O_3 (Reaction R4.11 - R4.12) and peroxide photolysis (Reaction R4.9 - R4.10), additionally play an important role in OH radical production. Based on available observations we define:

Primary production



Secondary production/Recycling



Under steady-state conditions, which can be assumed for short-lived compounds like OH, the sum of these production rates should equal the total loss of hydroxyl radicals, which can be derived from the product of the measured OH concentration and the measurements of the total OH reactivity (k'_{OH}).

$$P_{\text{OH}}^{\text{total}} = \sum_i P_{\text{OH},i} \quad (4.1)$$

$$L_{\text{OH}}^{\text{total}} = \sum_i L_{\text{OH},i} = k'_{\text{OH}} [\text{OH}] = \tau^{-1} [\text{OH}] \quad (4.2)$$

$$P_{\text{OH}}^{\text{total}} \stackrel{!}{=} L_{\text{OH}}^{\text{total}} \quad (4.3)$$

The calculated hydroxyl radical production reaches a maximum of about $1 \times 10^7 \text{ molec. cm}^{-3} \text{ s}^{-1}$ on ground and $1.4 \times 10^7 \text{ molec. cm}^{-3} \text{ s}^{-1}$ above canopy around local solar noon as shown in Figure 4.8. Since NO and NO_2 were not measured at ground level, they were derived from the above canopy measurements assuming constant NO_x with height, using the filter radiometer measurements of the photolysis frequency J_{NO_2} on ground and above the canopy to calculate partitioning between NO_2 and NO. The enhanced radical production above canopy is caused by higher $J_{\text{O}(^1\text{D})}$ observed on the tower and the enhanced recycling (Figure 4.8). The dominant primary source of OH (21%) is the reaction of $\text{O}(^1\text{D})$ with water. HONO photolysis, with a contribution during noon time of about 7%,

is also significant. However, the conversion of HO_2 to OH via the reactions with NO and O_3 dominates the total production of hydroxyl radicals (60–80 %). The ozonolysis of measured biogenic VOCs plays a minor role as a source of OH during daytime but becomes more important during nighttime.

The budget of steady-state OH was calculated as described above, using the available measurements of the chemical species contributing to the production rates and the total OH reactivity observed above canopy as constraints. Mean OH reactivity measured during this period was 11.5 s^{-1} varying typically between the lower limit of detection ($3\text{--}4 \text{ s}^{-1}$) and about 30 s^{-1} , with some peaks reaching above 70 s^{-1} (Nölscher et al., 2012). The known

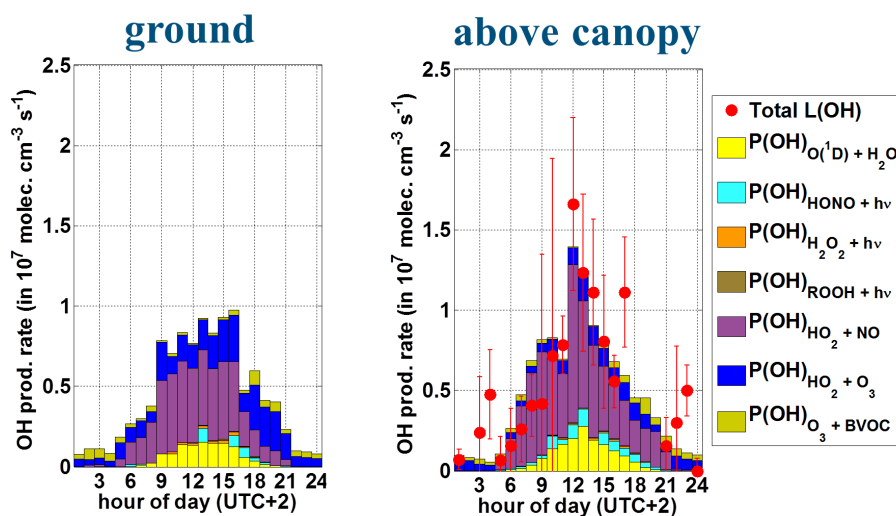
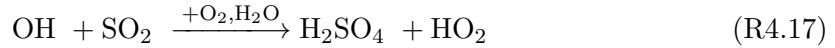


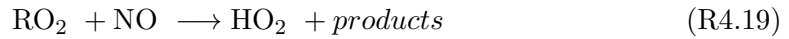
Abbildung 4.8.: Average diurnal OH production below (left panel) and budget above (right panel) the canopy. The whiskers indicate the variability of the total loss rate, calculated from total OH reactivity and hydroxyl radical measurement using LIF data.

OH sources are almost sufficient to close the budget above the canopy. Isoprene contributes less than 10% at maximum to the total OH reactivity measured during HUMPPA–COPEC–2010 due to its low mixing ratio (typically below 200 ppt_V). Measured terpenes, being similar or slightly less reactive than isoprene, e.g. α –pinene (up to 5%), β –pinene (up to 4%), β –myrcene (up to 6%), and Δ^3 –carene (up to 9%) were more abundant, thus providing in sum a higher reactivity towards OH.

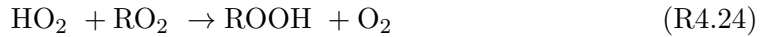
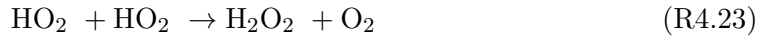
The reactions of OH with CO, O₃, HCHO, H₂O₂, and SO₂ are important sources of HO₂ radicals:



In addition, HCHO photolysis is a direct radical source, also contributing to HO₂ production during daytime. The cycling reactions of RO₂ species with NO can become the largest contributor to hydroperoxyl radical production, depending on the abundance of organic peroxy radicals and NO.



The loss of HO₂ is dominated by reactions with NO and O₃, which are at the same time the predominant source of OH. Radical-radical termination reactions (Reactions R4.22-R4.24) yielding peroxides and water act as a sink for HO_x radicals.



Unfortunately, RO₂ was not measured during HUMPPA-COPEC-2010 prohibiting the calculation of a HO₂ budget from observations in a similar manner as the OH budget. Nevertheless, assuming steady-state conditions for HO₂ and taking the hydroperoxyl radical measurements into account, the RO₂ concentration can be estimated.

$$\begin{aligned} \frac{d[\text{HO}_2]}{dt} &= 0 & (4.4) \\ &= P_{\text{HO}_2}^{\text{total}} - L_{\text{HO}_2}^{\text{total}} \\ &= P_{\text{HO}_2}^{\text{known}} + bk_{\text{R4.19}} [\text{NO}] [\text{RO}_2] - L_{\text{HO}_2}^{\text{known}} - k_{\text{R4.24}} [\text{HO}_2] [\text{RO}_2] \\ &= P_{\text{HO}_2}^{\text{known}} - L_{\text{HO}_2}^{\text{known}} + (bk_{\text{R4.19}} [\text{NO}] - k_{\text{R4.24}} [\text{HO}_2]) [\text{RO}_2] \end{aligned}$$

where b is a branching ratio and k_i denotes the reaction rate constant associated with Reaction i . From this it follows

$$[\text{RO}_2] = \frac{L_{\text{HO}_2}^{\text{known}} - P_{\text{HO}_2}^{\text{known}}}{bk_{R4.19} [\text{NO}] - k_{R4.24} [\text{HO}_2]}. \quad (4.5)$$

Typically there was about twice as much RO_2 as HO_2 (RO_2/HO_2 : median 1.8; min. 0.5; max. 4.5). This result was confirmed by calculation of the modified Leighton ratio (RO_2/HO_2 : median 1.8; min. 0.1; max. 6.3) (Leighton, 1961).

$$\Phi := \frac{J_{\text{NO}_2} [\text{NO}_2]}{[\text{NO}](k_{\text{NO} + \text{O}_3} [\text{O}_3] + k_{R4.19}([\text{RO}_2] + [\text{HO}_2]))}, \quad (4.6)$$

$$[\text{RO}_2]_{\Phi=1} = \frac{J_{\text{NO}_2} [\text{NO}_2]}{k_{R4.19} [\text{NO}]} - \frac{k_{\text{NO} + \text{O}_3}}{k_{R4.19}} [\text{O}_3] - [\text{HO}_2]. \quad (4.7)$$

Thus, organic peroxy radicals seem to play a major role in the radical photochemistry in the observed boreal forest environment, providing a strong link between OH and HO_2 .

The importance of radical cycling via HO_2 shown in the budget demands careful examination of the reliability of HO_2 measurements. The measurement of HO_2 by conversion to OH using NO can be severely affected by RO_2 reacting with NO also producing hydroxyl radicals (Fuchs et al., 2011). However, this interference depends on the instrumental setup (Whalley et al., 2013). It is to be quantified specifically for each instrument and depends on the composition of RO_2 in ambient air. The HO_2 observed during HUMPPA–COPEC–2010 therefore gives an upper limit for the atmospheric HO_2 including an unknown contribution from RO_2 . To put limits on the atmospheric HO_2 , the budget of H_2O_2 was analyzed. The H_2O_2 intercomparison (Figure 3.18) does not suggest that the HO_2 measurements by HORUS during HUMPPA–COPEC–2010 were affected by a major RO_2 interference (see Section 3.2.5). Nevertheless, assuming an interference by RO_2 species on the HO_2 measurements during HUMPPA–COPEC–2010 of 30 % would increase the gap between total OH production and total loss of OH. Recycling via HO_2 would still be the predominant source of OH. Not yet considered in the budget is the reaction of specific alkylperoxy radicals with HO_2 forming back OH (see Section 2.3). Assuming, as an upper limit, all RO_2 reacts with HO_2 like the peroxy acetyl radical does, this causes an additional OH production rate of up to $1 \times 10^7 \text{ molec. cm}^{-3} \text{ s}^{-1}$. The speciation of RO_2 for HUMPPA–COPEC–2010 is unknown, thus the contribution of RO_2 species forming OH in the reaction with HO_2 cannot be estimated. Nonetheless, as shown above such recycling mechanisms have the potential to close the hydroxyl radical budget.

4.5. OH / HO₂ ratio

The chemistry of OH and HO₂ in the atmosphere is closely linked by various hydroxyl recycling mechanisms. The ratio OH / HO₂ can be used to describe the state of equilibrium between both radicals. The equilibrium shifts depending on the concentrations of NO, O₃, CO, VOCs, and radiation. Typically during daytime a minimum of about 100 to 200 times more HO₂ was abundant compared to OH. During the dark ($J_{O(1D)} < 10^{-6} \text{ s}^{-1}$) the HO₂ concentrations were up to three orders of magnitude higher than the hydroxyl radical concentrations observed. The observed radical ratio (Figure 4.9) shows a good correlation ($R^2 = 0.80$) with the NO / CO ratio for average and high photolysis frequencies ($J_{O(1D)} > 10^{-6} \text{ s}^{-1}$). Increasing NO concentrations and decreasing CO shift the equilibrium towards the hydroxyl radical, as it is expected for an environment dominated by classical HO_x recycling pathways. The variability of CO is typically small compared to the variability of NO which therefore dominates the variability of the NO / CO ratio. At lower photolysis frequencies, when classical recycling via HO₂ + NO is no longer the predominant hydroxyl radical source (see Figure 4.8) the OH / HO₂ ratio shows no clear dependency on the ratio of NO and CO.

4.6. OH recycling probability and cycling-lifetime

The hydroxyl radical concentration significantly defines the oxidation capacity of the atmosphere. Beside primary production of the oxidant, recycling mechanisms are of major importance in hydroxyl radical production. The stability of tropospheric HO_x chemistry strongly depends on the occurrence of such processes. Self-amplifying radical production (auto-catalytic conditions) would cause the chemical system to be unstable. Similarly, total absence of recycling processes might lead to an accumulation of reduced gases in the atmosphere (catastrophic conditions) (Lelieveld et al., 2002). Thus, the probability for an OH radical to be recycled can be interpreted as a measure for the stability of tropospheric hydroxyl radical chemistry. Furthermore, a lifetime for the hydroxyl radical in units of cycles completed - the “cycling-lifetime” - can be derived from this quantity.

During HUMPPA-COPEC-2010 primary production (P) of hydroxyl radicals by photolysis of ozone and HONO together with ozonolysis of biogenic VOCs only contributes up to one third of the total OH production (Figure 4.8). Regeneration of OH from recycling reactions (Reaction R4.11 - R4.12) and photodissociation of peroxides (Reaction R4.9 - R4.10), which are products in the OH oxidation chain, can play an important role in the total OH formation. The ratio of these secondary OH sources (S) to the total hydroxyl radical production was defined by Lelieveld et al. (2002) as the OH recycling probability r :

$$r = \frac{S}{P + S} \quad (4.8)$$

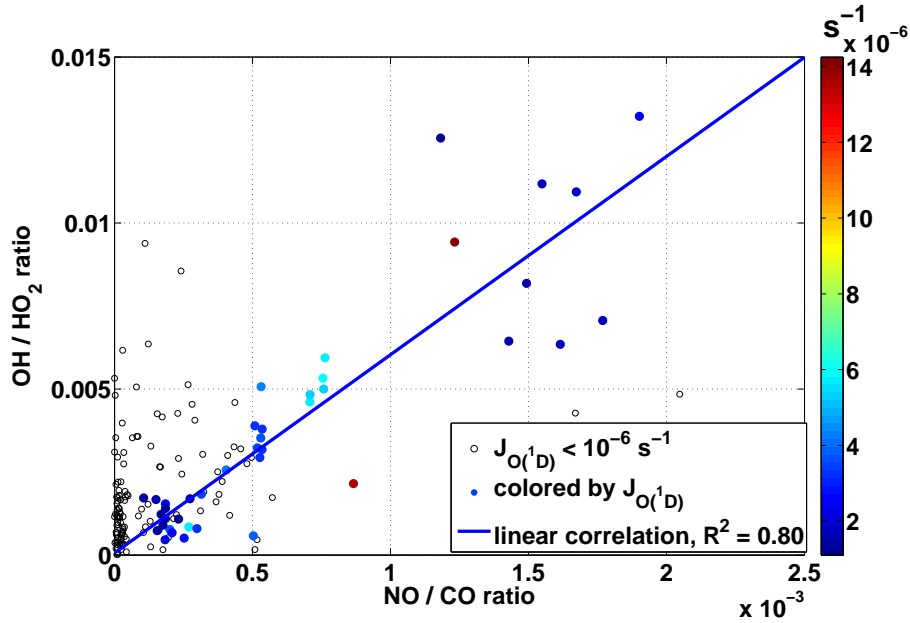


Abbildung 4.9.: Observed OH / HO₂ ratio vs. NO / CO ratio. For $J_{O(^1D)} > 10^{-6} \text{ s}^{-1}$ a linear correlation was found ($R^2 = 0.80$). At lower photolysis frequencies the radical ratio does not show a clear dependency on the ratio of NO and CO.

The recycling probability as a function of the NO concentration can be approximated considering only the predominant contributions to P and S :

$$r(\text{[NO]}) = \frac{S(\text{[NO]})}{P + S(\text{[NO]})} \approx \frac{k_{R4.11} [\text{NO}] [\text{HO}_2] + k_{R4.12} [\text{O}_3] [\text{HO}_2]}{2b_{O(^1D) \rightarrow OH} J_{O(^1D)} [\text{O}_3] + k_{R4.11} [\text{NO}] [\text{HO}_2] + k_{R4.12} [\text{O}_3] [\text{HO}_2]}. \quad (4.9)$$

The expected NO dependency of the recycling probability r (Equation 4.9) is shown in Figure 4.10. In case of high NO levels the secondary production terms exceed the magnitude of the primary production due to ozone photolysis, yielding high recycling probability values close to unity. The course of the NO dependency of r in Equation 4.9 is influenced by three parameters; the HO₂ concentration, the O₃ concentration and the photolysis frequency $J_{O(^1D)}$. The latter one only acts on the production term P . Increasing photolysis causes an increased primary production and thus, a diminished r -value. O₃ shows the same influence

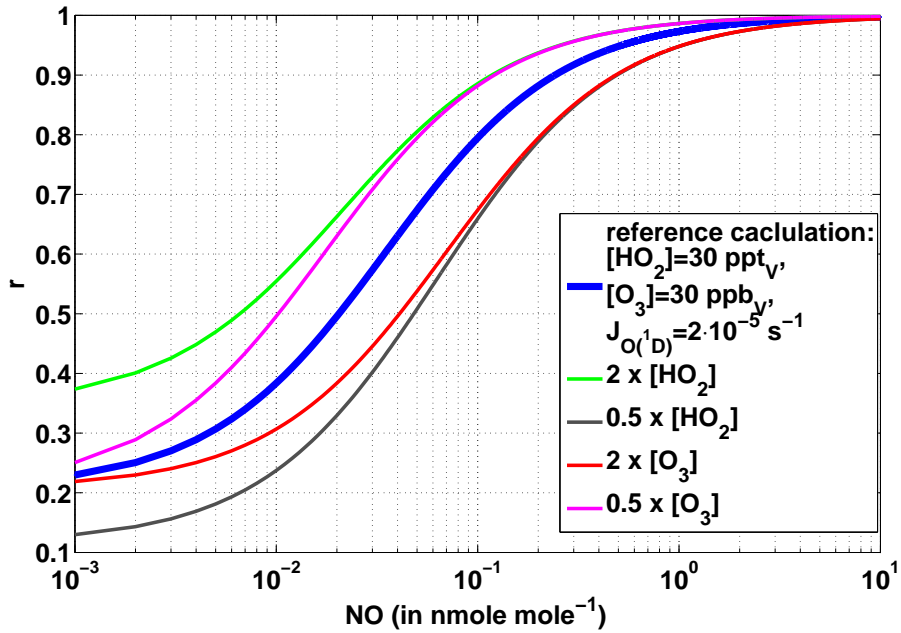


Abbildung 4.10.: Expected NO dependency of the recycling probability r at constant levels of HO_2 , O_3 and photolysis frequency $J_{\text{O}(^1\text{D})}$ (blue line). Sensitivity to these parameters is presented in different colors (see legend). Doubling the photolysis frequency (not shown in Figure) leads to a similar dependency like reducing the HO_2 concentration by 50 %.

on the primary production. Furthermore, the secondary OH production includes the term $k_{R4.12} [\text{O}_3] [\text{HO}_2]$, which is important, when $k_{R4.12} [\text{O}_3]$ is similar or large in magnitude compared to $k_{R4.11} [\text{NO}]$. Therefore, the overall sensitivity on O_3 is strongly depending on the NO level (see Figure 4.10). At very low NO mixing ratios $k_{R4.11} [\text{NO}]$ can be small compared to $k_{R4.12} [\text{O}_3]$. When NO converges to zero, Equation 4.9 yields:

$$\begin{aligned}
 r([\text{NO}]) &\approx \frac{k_{R4.12} [\text{O}_3] [\text{HO}_2]}{2b_{\text{O}(^1\text{D})\rightarrow\text{OH}} J_{\text{O}(^1\text{D})} [\text{O}_3] + k_{R4.12} [\text{O}_3] [\text{HO}_2]} \\
 &\approx \frac{k_{R4.12} [\text{HO}_2]}{2b_{\text{O}(^1\text{D})\rightarrow\text{OH}} J_{\text{O}(^1\text{D})} + k_{R4.12} [\text{HO}_2]} \\
 &\approx \frac{k_{R4.12}}{2b_{\text{O}(^1\text{D})\rightarrow\text{OH}} \frac{J_{\text{O}(^1\text{D})}}{[\text{HO}_2]} + k_{R4.12}} \quad (4.10)
 \end{aligned}$$

The recycling probability is no longer dependent on the concentration of O_3 and the limit of r is defined by the ratio of $J_{O(1D)}$ and the concentration of HO_2 (see Equation 4.10).

OH recycling probabilities calculated from observations as a function of the ambient NO mixing ratio for different environments are shown in Figure 4.11.

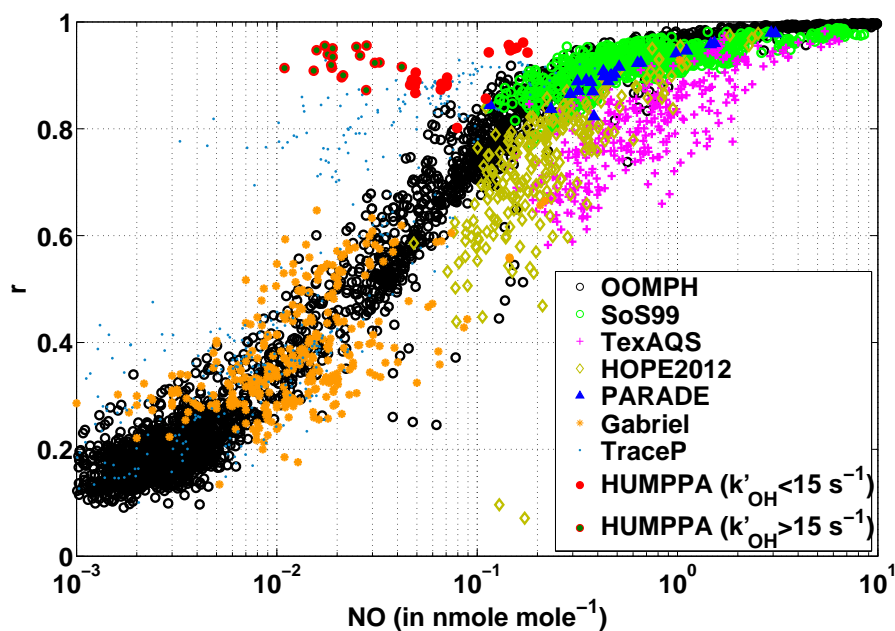


Abbildung 4.11.: OH recycling probability (r) as a function of the ambient NO mixing ratio in different environments. OOMPH – marine boundary layer, ship stack plume; SOS99 – metropolitan, biogenic VOCs; HOPE12 and PARADE – biogenic and anthropogenic VOCs; TexAQS – metropolitan, anthropogenic VOCs; Gabriel – tropical rainforest; Trace-P – east asia and western pacific; HUMPPA–COPEC–2010 – boreal forest.

Nighttime data ($J_{O(1D)} < 1 \times 10^{-5} s^{-1}$) is omitted for this calculation. Data from aircraft campaigns is filtered for observations below 2 km altitude. Measurements in the marine boundary layer (OOMPH³) are typically characterized by low NO mixing ratios and low concentrations of biogenic and/or anthropogenic VOCs. However, during the OOMPH ship cruise depending on the wind direction sometimes the chemistry in the stack plume of the

³Organics over the Ocean Modifying Particles in both Hemispheres.

ship was observed, rather than uninfluenced air from the marine boundary layer. Therefore, the OOMPH dataset includes also conditions of high NO_x levels. When the emissions from the ship stack plume perturb the chemical system of the marine boundary layer, a strong sensitivity of the recycling probability to the NO_x concentration is observed. The enhanced NO leads to a stronger conversion from HO_2 to OH , finally reaching values of r close to unity for high NO_x levels. Measurements in an environment with enhanced NO levels ($\text{NO} > 100 \text{ ppt}_V$), dominated by biogenic VOC emissions (SOS99⁴) the recycling probability is slightly reduced compared to the observations during OOMPH. Another field campaign at similar NO mixing ratios in an anthropogenically polluted environment (TexAQS⁵) show even lower calculated recycling probabilities, i.e. at the same primary production (P), the secondary production of OH (S) is reduced under the influence of additional VOCs. The reduced S at one NO level is equivalent to a reduced HO_2 concentration due to weaker production and/or enhanced destruction of the hydroperoxyl radicals, caused by the biogenic as well as anthropogenic influences. Measurements in two German forests during HOPE12⁶ and PARADE⁷ are influenced by biogenic as well as anthropogenic VOC emissions. The resulting recycling probabilities lie in between the observations from SOS99 and TexAQS. At low NO mixing ratios (ppt_V -range) observed above the tropical rainforest during Gabriel⁸ the calculated recycling probabilities are similar to the values calculated for the marine boundary layer. However, the recycling probability considering the reactions of HO_2 with NO and O_3 as secondary OH production pathways is not representative for this environment. Direct OH recycling mechanisms, not via HO_2 , as proposed for Gabriel (Kubistin et al., 2010; Lelieveld et al., 2008) are not taken into account. Efficient OH recycling in isoprene chemistry of the order of 40 to 80 % was reported by Lelieveld et al. (2008). Observations from an aircraft campaign over the Pacific (Trace-P⁹) are in large part consistent with the results from OOMPH. Nonetheless, for a part of the measurements during Trace-P enhanced recycling probabilities were calculated compared to OOMPH at similar NO levels. This might be caused by two different effects. Higher values of r occur, when the primary production P is not well represented by the reaction of $\text{O}(^1\text{D})$ with water vapour, since other primary sources that are not considered are dominant. An additional direct HO_2 source, i.e. not from $\text{OH} + \text{VOC}$, would lead to an increase of S and thus, yield elevated r values that do not necessarily represent a pure recycling probability of OH . The enhanced recycling probabilities during Trace-P were observed above the East China Sea and the Sea of Japan, southwest of Korea and Japan, respectively, where enhanced alanyl nitrate concentrations were measured. As already mentioned in Section 4.3 PAN decomposes forming RO_2 radi-

⁴Southern Oxidants Study.

⁵Texas Air Quality Study

⁶HOhenpeissenberg Photochemistry Experiment 2012

⁷PArticles and RAdicals: Diel observations of the impact of urban and biogenic Emissions

⁸Guyanase Atmosphere-Biosphere Exchange and Radicals Intensive Experiment with the Learjet

⁹TRAnsport and Chemical Evolution over the Pacific

cals. By reaction of these RO₂ species with NO, this radical source can act as a source of HO₂, which is not due to OH. Furthermore, the reaction of alcyperoxy radicals with HO₂ represent an additional OH source. In case of HUMPPA–COPEC–2010 the dataset, separates for moderate and high observed total OH reactivity into two regimes. When moderate conditions prevail ($k'_{OH} \leq 15$), the recycling probabilities are in line with the observations from SOS99, dominated by biogenic VOC emissions that reduce the recycling probability only slightly compared to the results from OOMPH. Under conditions of high observed total OH reactivity ($k'_{OH} > 15$) and lower NO levels enhanced recycling probabilities were calculated compared to OOMPH. This points to a missing primary OH production rate in the calculation, which is important compared to the photolytic production from O₃ and H₂O. Including HONO photolysis and the photolysis of H₂O₂ decreases r . It is also possible that an additional direct HO₂ source, e.g. ozonolysis of terpenes producing RO₂ that are converted by reaction with NO to HO₂, leads to the enhanced recycling probabilities under these conditions.

Recycling probabilities calculated from the observations during HUMPPA–COPEC–2010 considering all known primary and secondary production pathways are in the range $0.7 < r < 0.95$. These high values of r are consistent with the importance of radical recycling in the OH budget.

The recycling probability r can be used to calculate the cycling-lifetime, which is the number of cycles n the OH radicals completed until only $1/e$ of the initial radical concentration remains:

$$n = -\frac{1}{\ln(r)} \quad (4.11)$$

The observed median OH recycling probability of $r = (0.86 \pm 0.05)$ results in typical cycling-lifetimes of about $n = (6.6 + 4.0 / -1.9)$ cycles. Due to their relevance in the observed boreal forest environment, recycling pathways are further investigated by rate calculations based on observations.

4.7. HO_x recycling pathways

Production, loss, and recycling pathways of HO_x above the canopy under various conditions are shown in Table 4.2. Average rates calculated from observations highlight once more the importance of OH recycling via HO₂. Ozonolysis of BVOCs is an important primary radical source at low radiation levels. Photolytic OH production from O₃ as well as HONO photolysis are more relevant primary radical sources during daytime. The contribution of acetone photolysis to HO₂ formation is small at the surface, typically less than 1% of the total direct radical sources. The main sink terms are radical self-reactions, particularly HO₂ + RO₂. Since RO₂ was not measured during HUMPPA–COPEC–2010, it is estimated from HO₂ steady-state (see Section 4.4). The total OH production, P_{OH}^{total} ,

is calculated from total OH reactivity data and the hydroxyl radical measurements assuming steady-state (Equations 4.2 & 4.3). The loss rate of OH via reaction with VOCs and oxygenated VOCs (OVOCs) is derived by subtracting the known OH loss rates caused by CO, O₃, HCHO, H₂O₂, NO₂, NO, SO₂, and HO₂ from the total loss observed ($k'_{\text{OH}} [\text{OH}]$).

The dataset can be grouped by conditions of low and high radiation, and moderate and high observed total OH reactivity. The resulting four cases (see Table 4.2) are described in more detail in the following paragraphs. Associated average trace gas concentrations and variabilities are summarized in Section A, Table A.1.

Assuming steady-state, the total OH production is equal to the product of the measured total OH reactivity and the OH concentration (Equation 4.2, 4.3). Under **daylight** conditions ($J_{\text{O}(^1\text{D})} > 3 \times 10^{-6} \text{ s}^{-1}$), at **moderate** observed total **OH reactivity** ($k'_{\text{OH}} \leq 15 \text{ s}^{-1}$) (Table 4.2, upper left) $L_{\text{OH}}^{\text{total}} \approx 3.3 \times 10^6 \text{ molec. cm}^{-3} \text{ s}^{-1}$ is calculated from observations. Primary production of OH radicals is on average $1.2 \times 10^6 \text{ molec. cm}^{-3} \text{ s}^{-1}$. The reactions of HO₂ with NO ($\chi(\text{NO}) \approx 46 \text{ ppt}_V$) and O₃ produce about $3.3 \times 10^6 \text{ molec. cm}^{-3} \text{ s}^{-1}$ OH, which is 73% of the known summed OH production. The known OH sources are more than sufficient to close the OH budget. An OH loss rate of about $1.2 \times 10^6 \text{ molec. cm}^{-3} \text{ s}^{-1}$ is missing under these conditions, which is close to the combined uncertainty of 40%. OH is directly lost at a rate of $0.1 \times 10^6 \text{ molec. cm}^{-3} \text{ s}^{-1}$ by radical termination reactions with NO₂, NO, and HO₂. OH reacts with CO, O₃, HCHO, SO₂, and H₂O₂ yielding HO₂ radicals at a rate of $0.8 \times 10^6 \text{ molec. cm}^{-3} \text{ s}^{-1}$. The remaining observed total OH reactivity (equivalent to an average OH loss rate of $2.4 \times 10^6 \text{ molec. cm}^{-3} \text{ s}^{-1}$) constrains the maximum production of RO₂ from the reaction of OH with VOCs. However, this is only 75% of the RO₂ loss rate via reaction with NO, which is the dominant source of HO₂. This indicates a missing RO₂ source. Besides the ozonolysis of unmeasured BVOCs, reservoir species such as PAN, which thermally decompose (showing a strong temperature dependency), could contribute to the missing RO₂ production rate of the order of $1.2 \times 10^6 \text{ molec. cm}^{-3} \text{ s}^{-1}$. The photolytic HO₂ production by HCHO + $h\nu$ contributes with a rate of $0.2 \times 10^6 \text{ molec. cm}^{-3} \text{ s}^{-1}$. Radical-radical termination reactions govern the HO₂ loss (on average about $0.9 \times 10^6 \text{ molec. cm}^{-3} \text{ s}^{-1}$).

Under conditions of **low radiation** ($J_{\text{O}(^1\text{D})} \leq 3 \times 10^{-6} \text{ s}^{-1}$) and **moderate** observed total **OH reactivity** ($k'_{\text{OH}} \leq 15 \text{ s}^{-1}$) (Table 4.2, upper right) the known primary production of OH radicals is only $0.3 \times 10^6 \text{ molec. cm}^{-3} \text{ s}^{-1}$. Also, the classical recycling of HO₂ to OH by reaction with NO ($\chi(\text{NO}) \approx 3 \text{ ppt}_V$) and O₃ is inhibited ($0.9 \times 10^6 \text{ molec. cm}^{-3} \text{ s}^{-1}$), mainly due to the low NO concentration. Comparison with the derived total production rate (Equation 4.3) reveals a missing fraction of 40% ($P_{\text{OH}}^{\text{missing}} \approx 1 \times 10^6 \text{ molec. cm}^{-3} \text{ s}^{-1}$). This is in the same order of magnitude of the observed NO₃ production rate of $1 \times 10^6 \text{ molec. cm}^{-3} \text{ s}^{-1}$. Since the NO₃ concentration always remained below the lower limit of detection its reactivity had to be fast, potentially to some extent producing OH. Also ozonolysis of unmeasured BVOCs could directly produce OH and possibly close the OH budget.

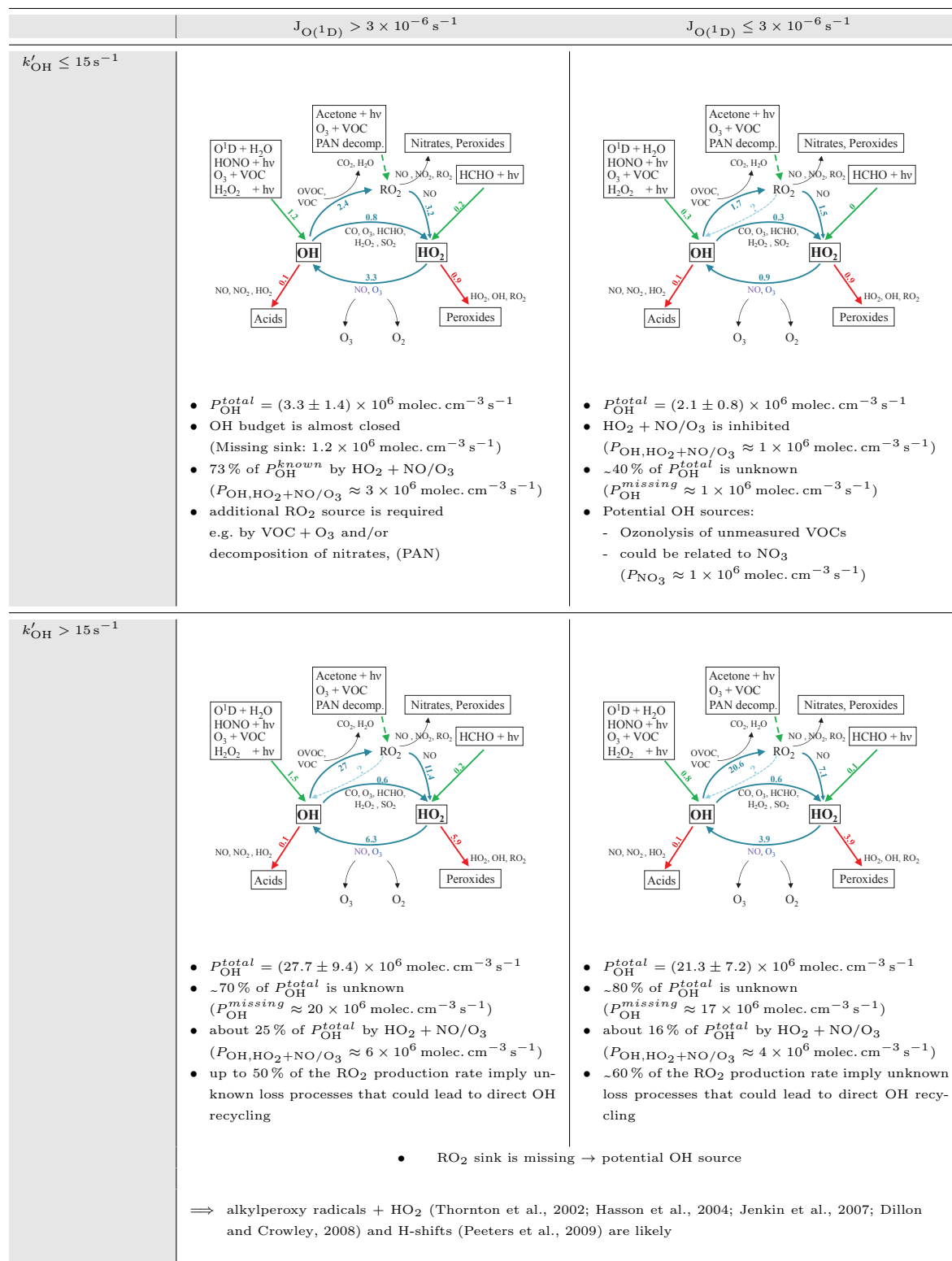
Under **daylight** conditions ($J_{\text{O}(^1\text{D})} > 3 \times 10^{-6} \text{ s}^{-1}$), with **high** observed total **OH reactivity** ($k'_{\text{OH}} > 15 \text{ s}^{-1}$) (Table 4.2, lower left) the primary production of OH radicals is

on average 1.5×10^6 molec. cm⁻³ s⁻¹. Less than 10 % of these primary produced OH radicals are directly lost by radical termination reactions with NO₂, NO, or HO₂, forming acids and H₂O. The largest known source of OH is again HO₂ recycling by reaction with NO ($\chi(\text{NO}) \approx 28\text{ppt}_V$) and O₃ with an average OH production rate of 6.3×10^6 molec. cm⁻³ s⁻¹. However, only about 30 % of the total OH production is known. The excess OH reactivity (equivalent to an average OH loss rate of 27×10^6 molec. cm⁻³ s⁻¹) is available for production of RO₂ radicals. RO₂ radicals react with NO forming HO₂ with a yield of about 90 %, representing the main source of HO₂. In comparison to this, the direct production of HO₂ radicals from HCHO photolysis is negligible (0.2×10^6 molec. cm⁻³ s⁻¹). Through the relationship between the RO₂ loss (forming HO₂) and the potential production rate of RO₂ by unaccounted observed total OH reactivity it can be estimated that about 50 % of the remaining OH reactivity, equivalent to a rate of 14×10^6 molec. cm⁻³ s⁻¹, is from other processes, e.g. direct OH recycling, not via the reaction of HO₂ + NO/O₃. Furthermore, an OH production rate of the order of 20×10^6 molec. cm⁻³ s⁻¹ is missing, to close the OH budget under these conditions. The reaction of specific alkylperoxy radicals with HO₂ could represent an additional RO₂ sink and OH source. Laboratory studies investigating the OH production from the reactions of ethyl peroxy, acetyl peroxy, and acetyl peroxy radicals with HO₂ revealed OH yields up to 70 % (Thornton et al., 2002; Hasson et al., 2004; Jenkin et al., 2007; Dillon and Crowley, 2008). Assuming that all RO₂ species, as an upper limit, would react with HO₂ forming OH, this would contribute an additional 10×10^6 molec. cm⁻³ s⁻¹ to the OH production. However, this would still not be sufficient to close the OH budget under these conditions of high radiation and high OH reactivity. A direct recycling mechanism, returning OH from RO₂ in the absence of NO, by a 1,5-H-shift, was proposed by Peeters et al. (2009) for the OH-initiated degradation of isoprene. A recent chamber study suggests a reduced reaction rate constant by about a factor of two with respect to the value given by Peeters et al. (2009) for this 1,5-H-shift (Fuchs et al., 2013). Nevertheless, at low NO levels ($\chi(\text{NO}) \approx 100\text{ppt}_V$) these isomerization reactions for isoprene-related RO₂ radicals forming OH directly become competitive with the traditional reactions of RO₂ with HO₂, RO₂, and NO. Similarly, other RO₂ radicals, specifically all conjugated alkadienes, e.g. myrcene, many mono-cyclic monoterpenes, and also sesquiterpenes, can undergo a fast H-shift isomerization (Peeters et al., 2001; Vereecken et al., 2007, 2012). Monoterpenes and sesquiterpenes have many more pathways to oxidise than isoprene, and the channels that allow for H-migration are therefore a smaller percentage than in isoprene. Still, an OH production rate of the order of 6×10^6 molec. cm⁻³ s⁻¹ is missing. A direct OH source or additional RO₂ production, balanced by an equivalent loss of RO₂ forming OH via mechanisms like the ones mentioned above could close the OH budget.

Similarly, at **low radiation** ($J_{\text{O}(^1\text{D})} \leq 3 \times 10^{-6} \text{ s}^{-1}$) and **high** observed total **OH reactivity** ($k'_{\text{OH}} > 15 \text{ s}^{-1}$) (Table 4.2, lower right) the known production of OH radicals is on average only about 20 % of the total OH production. HO₂ reacts with NO ($\chi(\text{NO}) \approx 17\text{ppt}_V$) and O₃ producing about 3.9×10^6 molec. cm⁻³ s⁻¹ OH, the largest known contribution to $P_{\text{OH}}^{\text{total}}$. For the production of RO₂ radicals the remaining observed total OH reactivity sug-

gests a rate of 20.6×10^6 molec. $\text{cm}^{-3} \text{s}^{-1}$. About 7×10^6 molec. $\text{cm}^{-3} \text{s}^{-1}$ of the RO_2 radicals react with NO forming HO_2 . An RO_2 loss rate of about 12×10^6 molec. $\text{cm}^{-3} \text{s}^{-1}$ remains, e.g. for direct recycling mechanisms, recycling OH as proposed above, i.e. alkylperoxy radicals reacting with HO_2 and/or H-shift isomerization or similar mechanisms are likely, potentially providing a large fraction of the missing OH production rate of 17×10^6 molec. $\text{cm}^{-3} \text{s}^{-1}$.

Tabelle 4.2.: HO_x budget under different conditions of observed radiation (high, left; low, right panels) and total OH reactivity (moderate, upper; high, bottom panels). Radical **production** (green), **recycling** (blue), and **loss** (red) pathways are indicated by bold arrows. All rates are given in 10⁶ molec. cm⁻³ s⁻¹.



5. Box model simulations

Numerical models are applied to describe the complex nonlinear chemistry and physical processes in the atmosphere. For short-lived trace gas species, such as radicals, transport and mixing processes that typically occur on larger time-scales can be neglected. Zero-dimensional box models are used to simulate the chemistry disregarding the coupling to physical processes. Despite the chemical reactions, emission and deposition processes are usually represented in these models. In order to analyse the observations during HUMPPA–COPEC–2010, box model simulations using the CAABA/MECCA box model were conducted.

5.1. Box model CAABA/MECCA

To investigate the influence of unmeasured intermediate reaction products, the observations were compared to simulations with version 3.0 of the chemical box model CAABA/MECCA (*Chemistry As A Boxmodel Application / Module Efficiently Calculating the Chemistry of the Atmosphere*) by Sander et al. (2011a). The model was constrained with observed, complete 5-minute datasets. Each simulation was terminated when both OH and HO₂ reached steady-state, typically after about 48 hours.

MECCA contains a comprehensive atmospheric chemistry reaction scheme. However, since we focus on organics, we switched off halogen and sulfur chemistry, as well as heterogeneous and aqueous phase reactions. A list of the chemical reactions used in this study, including rate coefficients and references, is available in the appendix (Section B). In the base configuration, version 2 of the isoprene chemistry from the “Mainz Isoprene Mechanism” (MIM2) was used, considering 68 species and 195 reactions (Taraborrelli et al., 2009 based on Pöschl et al., 2000). For sensitivity studies, the recently developed isoprene mechanism MIM3 (Taraborrelli et al., 2012), which includes additions to the isoprene chemistry; such as the photo-oxidation of unsaturated hydroperoxy-aldehydes; and a preliminary version of the monoterpene mechanism MTM (Taraborrelli et al., in preparation) were also used. The latter is based on a MIM2-like version of MIM3 (MIM3*), i.e. hydroperoxy-aldehyde chemistry, H-shifts, and RO₂ + HO₂ reactions are considered the way of MIM2, while updated estimates of rate constants from MIM3 were retained. Furthermore, it has a representation for the oxidation of the major terpenes during HUMPPA–COPEC–2010 that being α -pinene, β -pinene, β -myrcene, Δ^2 -carene, Δ^3 -carene, and α -farnesene chemistry. The oxidation

5. Box model simulations

of the first two monoterpenes is taken from the MCM¹⁰, with updates based on recent literature. Carene is assumed to yield the same products as α -pinene. Finally the oxidation of β -myrcene and α -farnesene is simplified and partially follows an isoprene-like oxidation. Deposition was included for the species listed in Table 5.1, according to values given in literature or derived from measurements. For the numerical integration of the resulting set of ordinary differential equations (ODEs), the KPP software (Sandu and Sander, 2006) with a positive definite Rosenbrock solver and automatic time-step control was used. For the photolysis frequencies of NO_2 and $\text{O}(^1\text{D})$, measured values (as described above) were used. Photolysis frequencies for other observed photolabile species are calculated based on measured $J_{\text{O}(^1\text{D})}$ and J_{NO_2} and will be presented in a separate publication by B. Bohn et al. Therefore effects of cloud coverage and aerosols are considered implicitly. In case of missing methane (CH_4) data, box model simulations were conducted using the median value of CH_4 observed, $1.79 \mu\text{mol mol}^{-1}$. The 1σ variability in CH_4 measurements during the entire campaign was $0.03 \mu\text{mol mol}^{-1}$. Measured photolysis frequencies below the lower limit of detection were set to zero, which affects the derived photolysis frequencies from other species accordingly. The uncertainty of simulated HO_x caused by these assumptions is less than 10 %. Datasets missing any other of the species used as model input were omitted from this study. An overview of the data availability and the resulting model input datasets are shown in Figure 5.1.

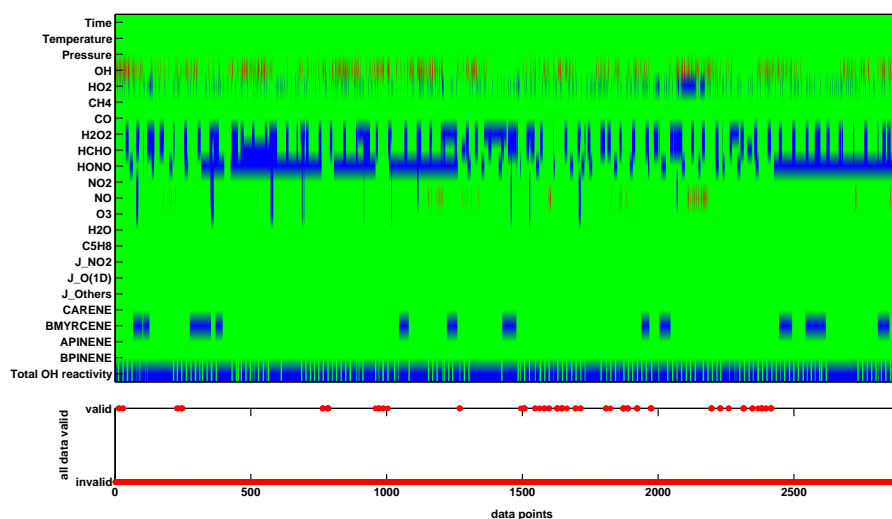


Abbildung 5.1.: Data availability for model simulations:

OK (green), missing (blue), negative (red).

¹⁰Master Chemical Mechanism, MCM v3.2

Tabelle 5.1.: Deposition rates/velocities used in the model

Species	v_D (cm s^{-1})	Deposition rate (s^{-1})	Reference
O ₃	0.56	-	mean value derived from measurements during HUMPPA-COPEC-2010
NO	0.44	-	Evans et al. (2000)
NO ₂	0.44	-	Evans et al. (2000)
HCHO	0.50	-	Evans et al. (2000)
HNO ₃ , org. nitrates	3.50	-	Evans et al. (2000)
PAN	0.29	-	Evans et al. (2000)
H ₂ O ₂ , org. peroxides	-	4×10^{-5}	estimated by best fit of calculated to measured H ₂ O ₂ mixing ratio

5.1.1. Significance and sensitivity

The significance of the discrepancies between observed and simulated HO_x concentrations depends on the uncertainty of the HO_x measurements as well as on the uncertainty of the model simulation. The latter comprises the uncertainties of all measured input variables such as trace gas concentrations and meteorological parameters as well as the uncertainties due to the chemical mechanism applied. Sensitivity analysis on measured species by varying constraint parameters within their uncertainty can be used to identify the impact on the model result. In the case of unmeasured species, e.g. oxidation products and intermediates, the uncertainties depend on the uncertainty of their production and destruction pathways as well as the uncertainty of the chemical mechanism. The uncertainties of the simulated OH and HO₂ concentrations related to the reaction rate coefficients were estimated by Monte-Carlo simulations as described by Sander et al. (2011a). Each Monte-Carlo simulation consists of 9999 model runs using a slightly different set of reaction rate coefficients for the individual runs. Different sets of rate coefficients are achieved by multiplying the original reaction rate coefficients from literature with a random uncertainty factor distributed around one and scaled on the uncertainty of the measured or estimated rate coefficient. This value

5. Box model simulations

can usually be found in publications of laboratory studies or summaries like the JPL or Atkinson evaluation (Sander et al., 2011b; Atkinson et al., 2006). If no value from literature is available a relative uncertainty of 25 % is assumed, which corresponds to a scaling factor of 1.25 (Sander et al., 2011a). The result of one Monte-Carlo simulation in case of OH applying the isoprene mechanism (MIM2) is shown as an example in Figure 5.2. The histogram shows a binned frequency distribution of the model OH resulting from the individual Monte-Carlo runs, simulated with diverse sets of rate coefficients. This yields a 1σ -uncertainty of the simulated OH resulting from the uncertainty of rate coefficients of 15%.

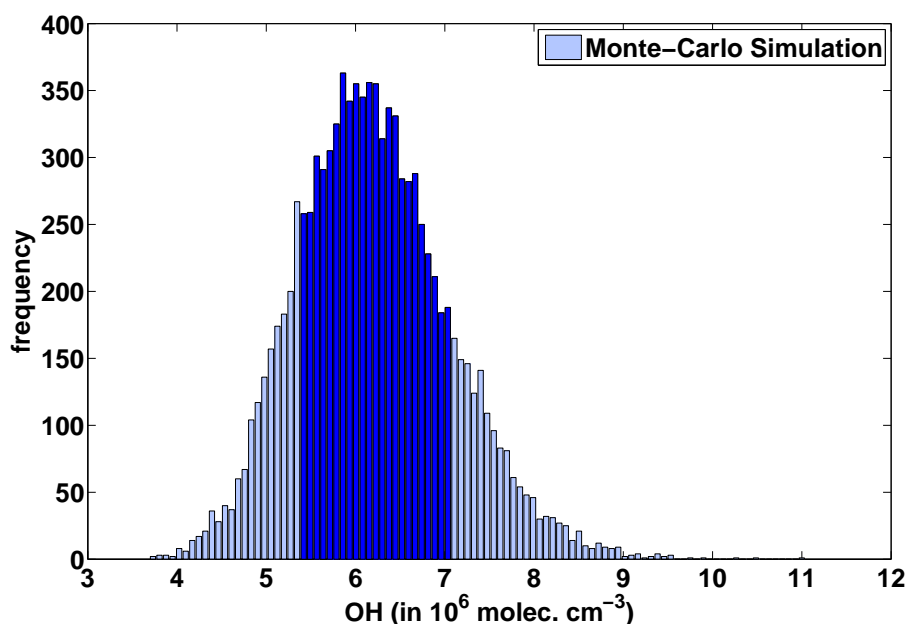


Abbildung 5.2.: Histogram of the Monte-Carlo simulation ($N = 9999$) for the reaction rate coefficients on a single dataset in the early afternoon above canopy. The resulting distribution shows a slight skewness with a median of $6.15 \times 10^6 \text{ molec. cm}^{-3}$ and a mean of $(6.21 \pm 0.86) \times 10^6 \text{ molec. cm}^{-3}$. The dark blue bars indicate the $\pm 1\sigma$ range.

5.2. HO_x simulations using CAABA/MECCA

The discussion of the observations in Section 4 indicates, that under conditions of low reactivity and high radiation, recycling of OH in this environment occurs mainly by HO₂. In order to identify the influence of unmeasured oxidation products on the HO_x budget and to examine the current understanding of the underlying processes box model simulations have been conducted.

The CAABA/MECCA box model was applied in steady-state mode with concentrations of NO, CO, O₃, H₂O₂, organic peroxides, isoprene (C₅H₈), terpenes, HONO, HCHO, and H₂O as well as photolysis frequencies constrained to measured values. Simulations were only done when data of all key constraints were available (see Section 5.1).

Applying the chemistry scheme from the “Mainz Isoprene Mechanism” (MIM2), OH concentrations are overestimated by the model by about 40% on average (Figure 5.3). HO₂ is underestimated in the simulation. The model-measurement discrepancy can be divided into two groups: The ratio of simulated to observed HO₂ concentrations is about 0.7 for a minor part of the dataset, while the simulation significantly underestimates the observed total OH reactivity for the rest of the dataset. The ratio between simulated and observed HO₂ concentrations in this case is only about 0.3. A recently published chemical reaction scheme (MIM3) including new additions to the isoprene chemistry, such as the photo-oxidation of unsaturated hydroperoxy-aldehydes (Taraborrelli et al., 2012), produces even more hydroxyl radicals leading to an overestimation by a factor of up to three in the simulation as compared to the observations. The ratio between simulated and observed hydroperoxyl radicals increases to $\text{HO}_2^{\text{mod.}}/\text{HO}_2^{\text{obs.}}=0.6$ on average, still separating into two regimes with a minor part of the dataset showing a ratio of $\text{HO}_2^{\text{mod.}}/\text{HO}_2^{\text{obs.}}=1.5$, while most of the data shows a ratio of $\text{HO}_2^{\text{mod.}}/\text{HO}_2^{\text{obs.}}=0.6$.

Since isoprene was not the predominant biogenic VOC during HUMPPA–COPEC–2010, contributing less than 10% to the total OH reactivity measured, the terpene mechanism MTM was added to the chemistry mechanism. Inclusion of terpene chemistry helped to reproduce the OH reasonably in the simulation (Figure 5.4). The ratio between simulated and observed HO₂ slightly increased compared to the isoprene chemistry reference run, but still separates into two regimes. At lower observed HO₂ levels, a ratio of up to $\text{HO}_2^{\text{mod.}}/\text{HO}_2^{\text{obs.}}=0.8$ is reached for a minor fraction of the dataset. Only about 30% of the observed HO₂ concentration can be reproduced by the model on average, when the simulated total OH reactivity does not match the observed reactivity.

The underprediction of HO₂, when OH reactivity is missing in the model while OH is reproduced accurately, indicates that the missing reactivity is an unaccounted source of HO₂. Furthermore, the recycling reaction of NO and O₃ with the missing HO₂ has the potential under most conditions to compensate for the additional OH loss, which has not been considered yet. This preserves the good agreement of simulated and observed OH even when the model accounts for all the observed total OH reactivity.

5. Box model simulations

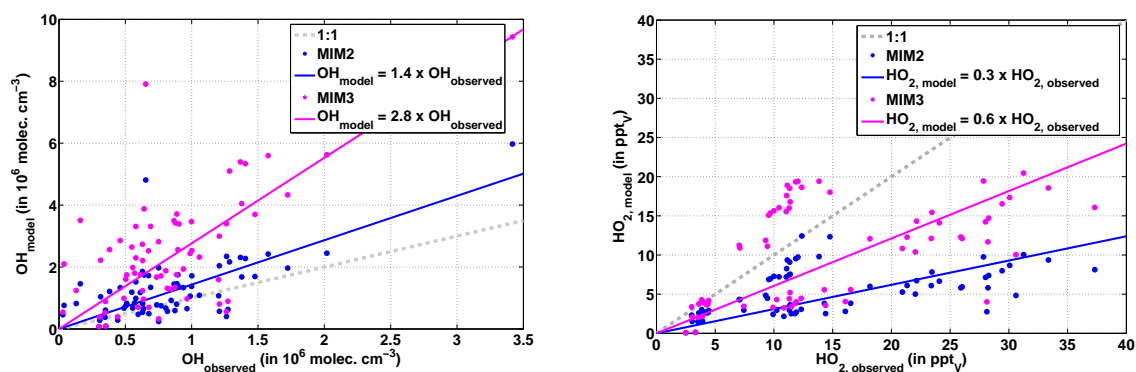


Abbildung 5.3.: Simulated vs. observed OH concentrations and HO₂ mixing ratios, applying the MIM2 chemistry scheme and the recently proposed MIM3 including new additions in the isoprene chemistry.

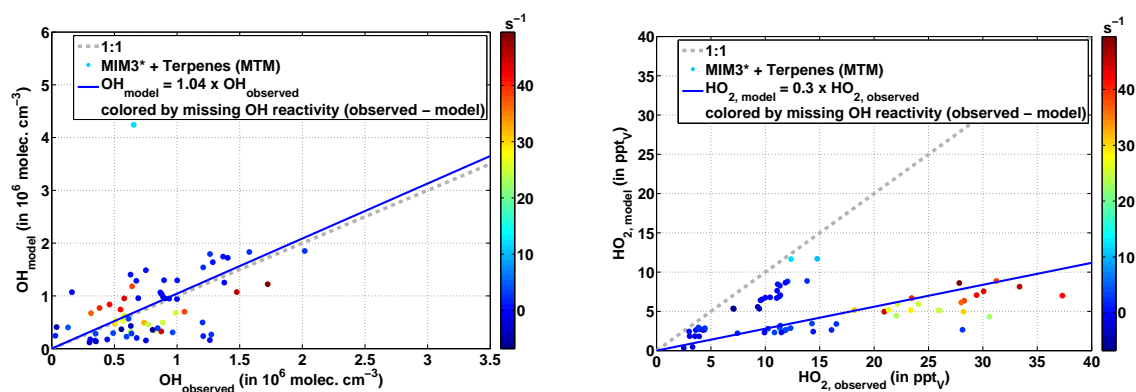


Abbildung 5.4.: Inclusion of the terpene mechanism MTM. HO₂ is still underpredicted in cases when the model reactivity does not match the measured reactivity. This indicates that the missing reactivity is an unaccounted source of HO₂. The OH is reproduced reasonably well, suggesting that the missing source of OH due to the underpredicted HO₂ is compensated by the missing OH reactivity in the simulation.

However, when high total OH reactivities ($> 20 \text{ s}^{-1}$) were observed, the enhanced HO₂ recycling is not sufficient to reproduce the observed OH. Additional mechanisms, e.g. direct OH recycling as discussed for isoprene-dominated, low-NO_x environments, or an additional primary source of OH is required to explain the observed hydroxyl radical concentrations under these conditions.

5.2.1. OH loss tuning

To investigate the hypothesis that the OH reactivity missing in the model using the terpene mechanism acts as a source of HO₂, additional reactivity towards OH was introduced by adding the surrogate molecule X which behaves chemically identically to α -pinene and its concentration was iteratively tuned for each dataset in such a way that the total OH reactivity in the model agreed with the observed OH reactivity. To match the observed total OH reactivity, up to 3 ppb_v of X (typically a factor of 5 to 10 times the measured α -pinene) had to be added. Tuning the simulation to the observed total OH reactivity improves the HO₂ agreement slightly ($\text{HO}_2^{\text{mod.}}/\text{HO}_2^{\text{obs.}}=0.4$), as shown in Figure 5.5. The production of OH from the additional HO₂, however, is not sufficient to compensate for the enhanced reactivity in the model, leading to underprediction of hydroxyl radicals in the simulation. The unaccounted OH reactivity in the simulation might still be linked to the missing source of HO₂, nevertheless, this shows that α -pinene-like chemistry for the compound X does not suffice to provide this connection. A direct HO₂/RO₂ source like decomposition of transported PAN, which is not represented in the box model simulation, could explain the underprediction of HO₂, independent of the unaccounted OH reactivity in the simulation.

5.2.2. Significance and uncertainties

To quantify the significance of model-measurement discrepancies the uncertainties in both, observations and simulations, have to be considered. The uncertainties of HO_x measurements are listed in Table 4.1. The uncertainties of simulated HO_x related to the reaction rate coefficients were determined via Monte-Carlo simulations as described in Section 5.1.1. Monte-Carlo-Analysis using the terpene mechanism yields uncertainties of 14 % and 11 % for the simulated OH and HO₂, respectively. Measured and simulated HO_x concentrations including their 1σ -uncertainties are compared in Figure 5.6. Modelled and observed OH within their uncertainties partly agree within a factor of two. Significant discrepancies by more than a factor of two are present for a minor part of the dataset (22 %). For HO₂ the underestimation by more than a factor of two in the model is significant for a large part of the dataset (52 %).

The uncertainties in observed trace gas species and photolysis frequencies used to constrain the model can also have a direct impact on the uncertainty of simulated HO_x. Even

5. Box model simulations

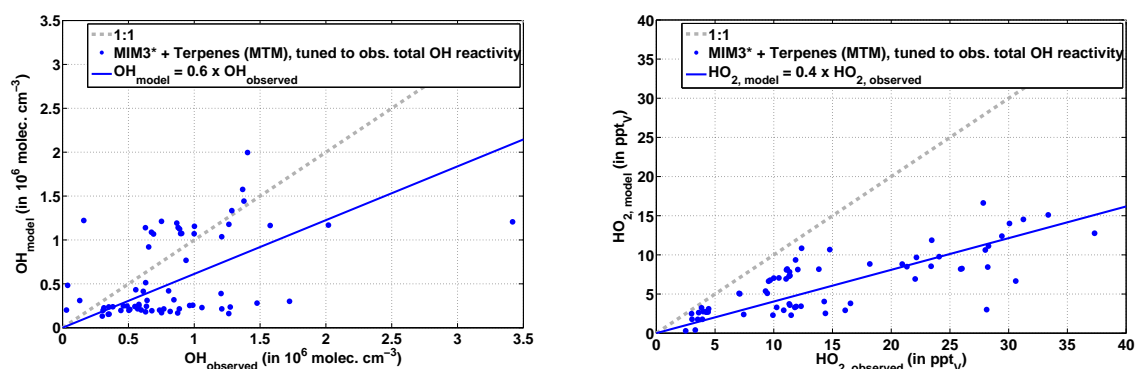


Abbildung 5.5.: Tuning the model to the observed total OH reactivity by introducing an additional α -pinene equivalent slightly improves the HO_2 agreement. The production of OH from the additional HO_2 is not sufficient to compensate for the enhanced reactivity in the model.

less obviously these parameters which are kept fixed at the observed values within the simulation, influence the abundance of unmeasured trace gases and intermediate products, therefore also showing an indirect effect on the resulting calculation of HO_x concentrations. Sensitivity studies were conducted by varying the observed trace gas concentrations separately by a factor between 0.5-10 to investigate the overall influence on the simulated HO_x (Table 5.2) with the terpene mechanism.

Substances relevant for primary production of HO_x show the highest impact in this sensitivity study. Doubling the O_3 or water vapour concentration leads to about 25 % increase in simulated OH and about 15 % enhanced HO_2 . An even larger effect (OH: +37 %, HO_2 : + 26 %) is found for photolysis elevated by a factor of two. Constraining the model with twice the amount of NO observed causes 24 % more hydroxyl radicals in the simulation. The simulated HO_2 decreases by 23 %. Reducing the CO concentration by a factor of two leads to a 8 % increase in simulated OH and a 8 % decrease in simulated HO_2 while doubling the observed CO yields a 13 % decrease in OH and a 13 % increase in HO_2 . Doubling formaldehyde or H_2O_2 only has a minor influence on the simulated HO_x . Changing the deposition rates by a factor of two causes at most a 12 % change in HO_x . None of these input parameter variations yield a change in OH and/or HO_2 of a factor of two or more. All photolysis frequencies multiplied by a factor of ten could cause such changes in simulated HO_x . Unless the uncertainties of the species used to constrain the simulation (Table 4.1) exceed the variation intervals, these uncertainties individually can neither explain the discrepancies between observation and modelled HO_2 , nor cause a significant disagreement for OH.

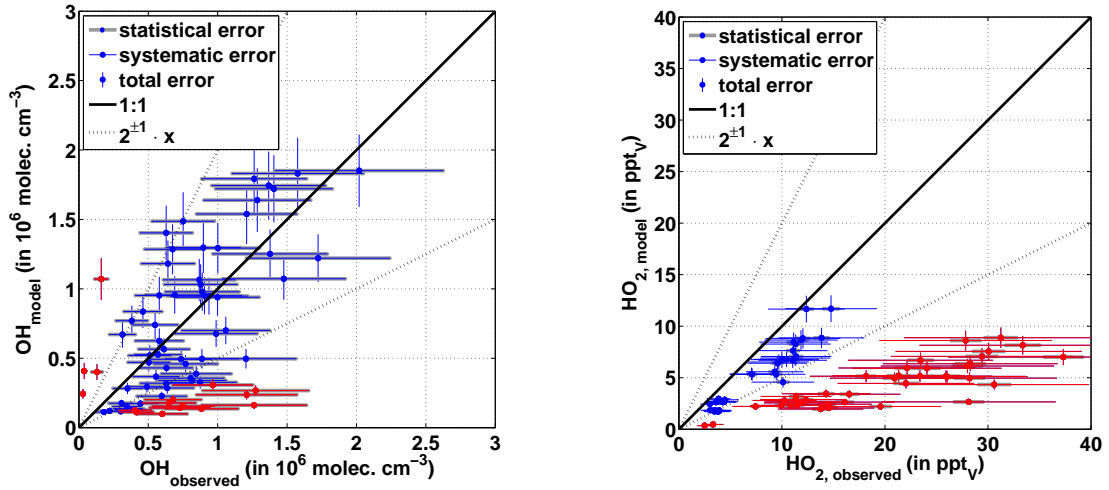


Abbildung 5.6.: Uncertainties of HO_x simulations (using the terpene mechanism) with respect to measurement uncertainties. The solid line represents the 1:1 ratio of observed and simulated HO_x. Data points showing significant discrepancies within their uncertainties by more than a factor of 2^{±1} (dashed lines) are shown in red.

Free running HCHO, i.e. not constraining the simulation to the HCHO observations, leads to enhanced OH and HO₂ concentrations (up to 30%), which is for a minor part of the dataset sufficient to produce good agreement between measured and simulated HO₂, while OH is overestimated in these simulations. Formaldehyde concentrations in the free running model are up to four times higher than observed levels. This suggests a formaldehyde sink not represented in the box model, possibly due to transport processes or uptake by plants (Lowe and Schmidt, 1983; Benning and Wahner, 1998). However, it was shown that changes in the deposition velocity have only a small impact on the simulated HO_x. The overprediction of formaldehyde in this case is more likely due to inadequate representation of the HCHO sources in the simulation. Another sensitivity simulation by also constraining the model to estimated 2-methyl-3-buten-2-ol (MBO) concentrations was conducted. Unfortunately, MBO, which is often referred to as “the isoprene of coniferous forests” was not directly measured during HUMPPA–COPEC–2010, though PTR-MS measurements of isoprene were affected by an MBO interference, as described in section 4.1. Previous measurements in this forest showed that MBO accounts only for 1-3% of the total monoterpene emission rate (Tarvainen et al., 2005). In American pine forests it can be more important. However, the

5. Box model simulations

Tabelle 5.2.: Sensitivity analysis with respect to changes in observed, model constraining parameters. The values presented refer to a dataset around local solar noon (1pm in UTC+2).

	OH (molec. cm ⁻³)		HO ₂ (molec. cm ⁻³)	
		mod/mod _{reference}		mod/mod _{reference}
Observation	3.42×10 ⁶		3.63×10 ⁸	
Reference simulation	5.20×10 ⁶	1	2.87×10 ⁸	1
2x NO	6.47 ×10 ⁶	1.24	2.22 ×10 ⁸	0.77
2x O ₃	6.42 ×10 ⁶	1.23	3.32 ×10 ⁸	1.16
2x H ₂ O	6.62 ×10 ⁶	1.27	3.31 ×10 ⁸	1.15
0.5x CO	5.63 ×10 ⁶	1.08	2.65 ×10 ⁸	0.92
2x CO	4.55 ×10 ⁶	0.88	3.23 ×10 ⁸	1.13
2x H ₂ O ₂	5.27 ×10 ⁶	1.01	2.92 ×10 ⁸	1.02
2x HCHO	5.30 ×10 ⁶	1.02	3.07 ×10 ⁸	1.07
0.5x deposition	5.59×10 ⁶	1.08	3.17×10 ⁸	1.10
2x deposition	5.83×10 ⁶	1.12	3.12×10 ⁸	1.09
2x photolysis	7.11 ×10 ⁶	1.37	3.63 ×10 ⁸	1.26
10x photolysis	1.77 ×10 ⁷	3.40	6.88 ×10 ⁸	2.40

PTR-MS signal was used as an upper limit estimate of MBO for this simulation to investigate the influence on the simulated HO_x. This MBO causes, on average, about 0.5 s⁻¹ additional reactivity towards OH, similar to the reactivity by methane. Only about 20 % of the observed HO₂ can be explained by the model and the observed OH is underpredicted by 40-60 % in this simulation. Considering the results from the above mentioned sensitivity tests and significance analysis, the discrepancy between measured and simulated HO₂ is significant, thus, the chemical mechanism applied in the simulations needs further improvement to reproduce the HO₂ for the observed boreal forest environment.

5.2.3. Sources and sinks of HO_x

The production rates of the hydroxyl radical in the box model using the terpene mechanism are shown in Figure 5.7, with respect to their contribution to the total OH production derived from measurements. The dataset is again grouped by conditions of different radiation and total OH reactivity (see Table 4.2). When the total OH reactivity is high ($k'_{\text{OH}} > 15 \text{ s}^{-1}$), the total production rate of hydroxyl radicals in the simulation accounts only for about 10% of the observed production. This is mainly due to the strong underestimation of HO₂ by the model under these conditions (see Sections 4.4 & 4.7). Photolytic production accounts for one third of the OH formation in the simulation. A similar contribution is found by HO₂ recycling via reaction with NO and O₃. Ozonolysis of BVOCs and a minor contribution by other species produced in the model account for the remaining OH production. At lower radiation ($J_{\text{O}(1\text{D})} \leq 3 \times 10^{-6} \text{ s}^{-1}$), the ozonolysis of BVOCs becomes relatively more important and the recycling reaction of HO₂ with O₃ more relevant in comparison to the reaction with NO. Under conditions of moderate total OH reactivity ($k'_{\text{OH}} \leq 15 \text{ s}^{-1}$) and low radiation ($J_{\text{O}(1\text{D})} \leq 3 \times 10^{-6} \text{ s}^{-1}$) about 33% of the observed total OH production is represented by the box model simulation. Ozonolysis of observed biogenic VOCs accounts for on average 15% of the total production rate. Even though the hydroxyl radical production rates due to recycling of HO₂ via the reactions with NO and O₃ are based on the underestimated HO₂ by the box model, they are relevant source terms contributing 13% to the total OH production. Photolytic sources and production due to other species play a minor role. By assuming observed rather than model calculated HO₂, this contribution would increase to 30%.

Almost one quarter of the OH during periods characterized by high radiation values ($J_{\text{O}(1\text{D})} > 3 \times 10^{-6} \text{ s}^{-1}$) and moderate total OH reactivity ($k'_{\text{OH}} \leq 15 \text{ s}^{-1}$) is produced by photolytic sources. Ozonolysis of BVOCs and other sources in the simulation contribute 4% each to the total observed OH production. HO₂ recycling via NO dominates the OH production (37%). Nonetheless, about 30% of the total OH observed production is not represented in the simulation, due to the underestimation of HO₂ and the associated recycling pathways.

OH reactivity contributions calculated from individually measured compounds compared to directly measured OH reactivity revealed 58% missing OH reactivity under “normal” boreal conditions and up to about 90% under “stressed” boreal conditions (i.e. prolonged high temperature) during HUMPPA–COPEC–2010 (Nölscher et al., 2012). About 50% of missing OH reactivity was reported from the same site during summer in 2008 by Sinha et al. (2010) when more typical boreal conditions at lower temperatures than in 2010 prevailed. The loss of OH in terms of OH reactivity in the simulation is presented in Figure 5.8. Similar to the findings of another modeling study based on different measurements conducted at the field station SMEAR II (Mogensen et al., 2011), the inorganic contribution (CO, O₃, H₂, H₂O₂, NO, NO₂, HO₂, and HONO) is significant (15%). A large sink for OH is due to organic compounds, most importantly monoterpenes (5%), methane (4%), and

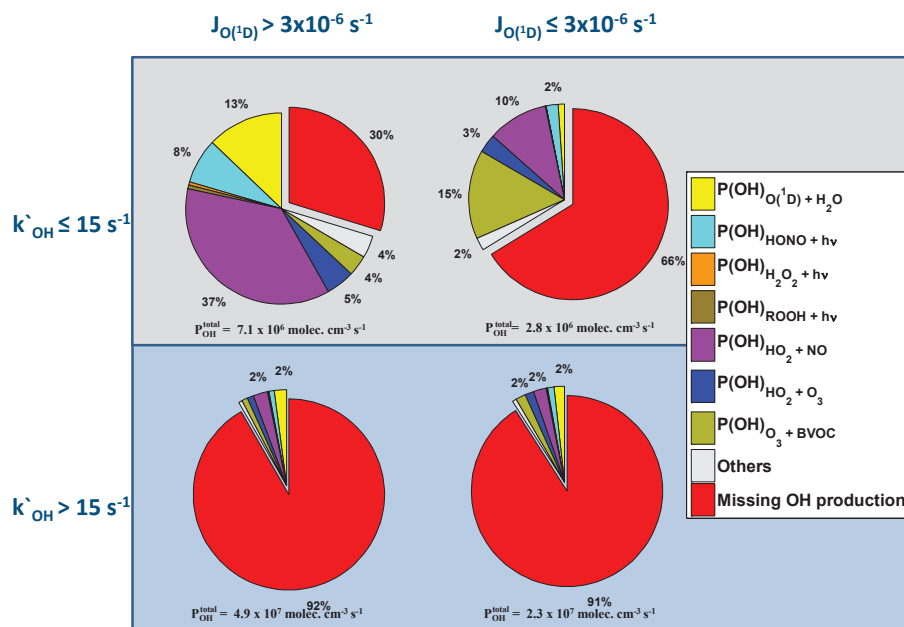


Abbildung 5.7.: Simulated contributions to the OH production during HUMPPA–COPEC–2010. Partitioning at different conditions of radiation and observed total OH reactivity with respect to the total OH production derived from measured OH concentrations and the total OH reactivity.

isoprene (2%). In contrast to the study by Mogensen et al. (2011), second and higher order organic reaction products by the model contribute an additional 42% to the total OH reactivity. On average, almost one third of the observed total OH reactivity remains unexplained. The large contribution by second and higher order organic reaction products in the model is mainly caused by aldehydes coming from monoterpene oxidation ($\sim 30\%$) and secondary products of isoprene oxidation (MVK + MACR $\sim 4\%$). Primary biogenic emissions, e.g. unmeasured monoterpenes and sesquiterpenes, photooxidation products, as well as anthropogenic pollutants occasionally transported to the measurement site are likely candidates causing the “missing” fraction of total OH reactivity.

HO_2 radicals are lost by reaction with other radicals as well as recycled towards OH by reaction with NO and O_3 (Figure 5.9). The biggest contribution to the loss of HO_2 under all conditions is the reaction with nitrogen dioxide yielding peroxyntic acid (HNO_4).

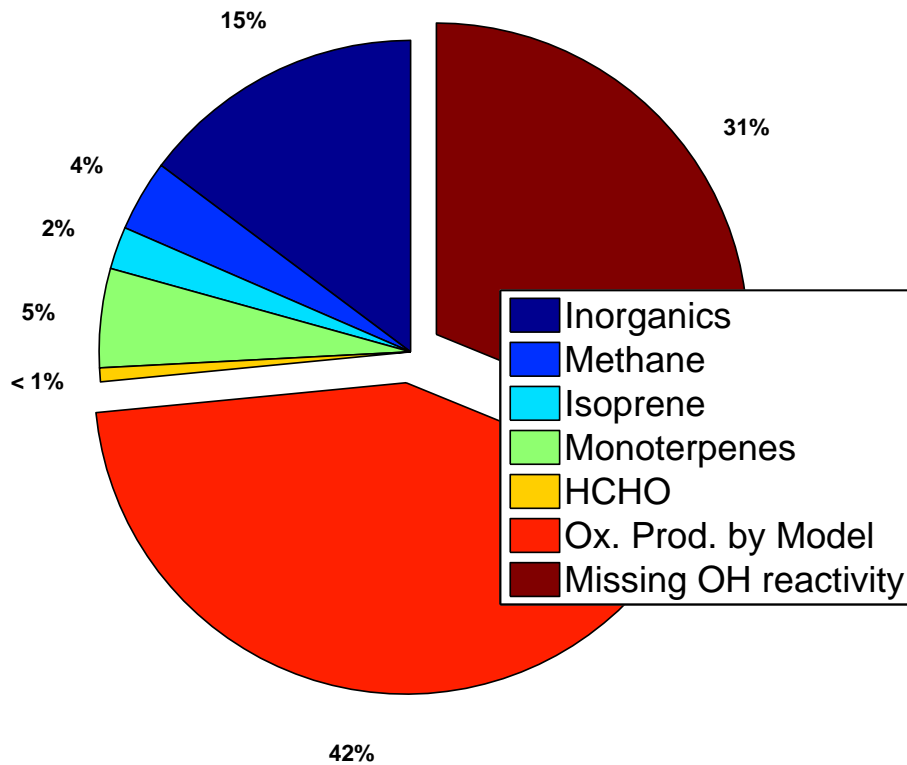


Abbildung 5.8.: Simulated contributions to the observed total OH reactivity during HUMPPA-COPEC-2010.

However, under standard conditions, HNO₄ is rather unstable and decomposes typically within a few seconds. This creates an equilibrium between HNO₄ and HO₂ + NO₂ which is strongly temperature dependent (Dentener et al., 2002). In the simulation the production and decomposition of HNO₄ occur at the same rate, thus HNO₄ acts as a reservoir species for the hydroperoxyl radicals.

At conditions of low radiation ($J_{O(^1D)} \leq 3 \times 10^{-6} \text{ s}^{-1}$) hydroperoxyl radicals reacting with RO₂ and HO_x contribute to the total loss of HO₂ in a similar amount as the recycling reactions with NO and O₃. This is still the case at conditions of enhanced observed OH reactivity and low radiation. The higher absolute HO₂ loss is caused by enhanced recycling as well as enhanced loss by radical-radical reactions.

At high photolysis frequencies ($J_{O(^1D)} > 3 \times 10^{-6} \text{ s}^{-1}$) both the total HO₂ production and loss increase by about a factor of two compared to nighttime. The HO₂ loss contribu-

5. Box model simulations

tion from the recycling reaction with NO is predominant (41 %) at a total OH reactivity $k'_{\text{OH}} \leq 15 \text{ s}^{-1}$. This is followed by the reaction with RO₂ contributing about 12 %. Other reactions, e.g. HO₂ + NO₃ or HO₂ + HO_x, contribute only a few percent. When the total OH reactivity is high, $k'_{\text{OH}} > 15 \text{ s}^{-1}$, the OH recycling reaction of HO₂ with NO becomes less important (23 %) in the simulation, whereas the reaction with RO₂ contributes about 20 % to the total HO₂ loss. In addition to HNO₄ decomposition, the reaction of OH with carbon monoxide and the reaction of RO₂ with NO are the main sources of HO₂ in the model. The photolysis of formaldehyde contributes less than 1 % to the total HO₂ production under all conditions. Ozonolysis of monoterpenes yields up to 8 % when photolysis is low but is rather unimportant at higher J-values. OH reactions with O₃, HCHO, and H₂O₂ are minor contributors (typically in total about 4 %) in HO₂ production. Differences between conditions of moderate and high total OH reactivity show up in the reactions of OH + CO and RO₂ + NO, forming HO₂. The absolute HO₂ production under conditions of enhanced radiation and high observed total OH reactivity is smaller compared to the case with enhanced radiation and moderate total OH reactivity. Under these conditions, the simulation underestimates the observed HO₂ most, indicating that important species and HO₂ production pathways are missing in the chemical mechanism, very likely including unmeasured BVOCs and their oxidation products. Unfortunately, there were no direct observations of RO₂ during HUMPPA–COPEC–2010. Thus, we are lacking the possibility to constrain the model by RO₂ observations, which would improve our understanding of the underlying processes. The hydroperoxyl radical as well as organic peroxy radicals play an important role in the production of ozone. Ozone is mainly formed and destroyed in the photochemical cycle of NO and NO₂:



For O₃ Reactions R5.1 - R5.3 represent a “null-cycle”, i.e. net ozone production and destruction is zero. However, NO is also consumed in the reaction with peroxy radicals (see Reactions R2.23 & R2.31). Thus, NO₂ is formed without consumption of O₃, leading to a net ozone production in the photolysis of NO₂ (Reaction R5.1). Whereas ozone is produced in radical reactions in polluted environments, it is destroyed by radicals in very clean airmasses, when the reaction of HO₂ with O₃ becomes dominant compared to the reaction with NO. The radical mechanism of ozone production is the major O₃ source in the polluted troposphere (Seinfeld and Pandis, 2006). Therefore, the underestimation of HO₂ in the box model simulations for HUMPPA–COPEC–2010 has a direct impact on the ozone formation in the observed and other boreal forest environments.

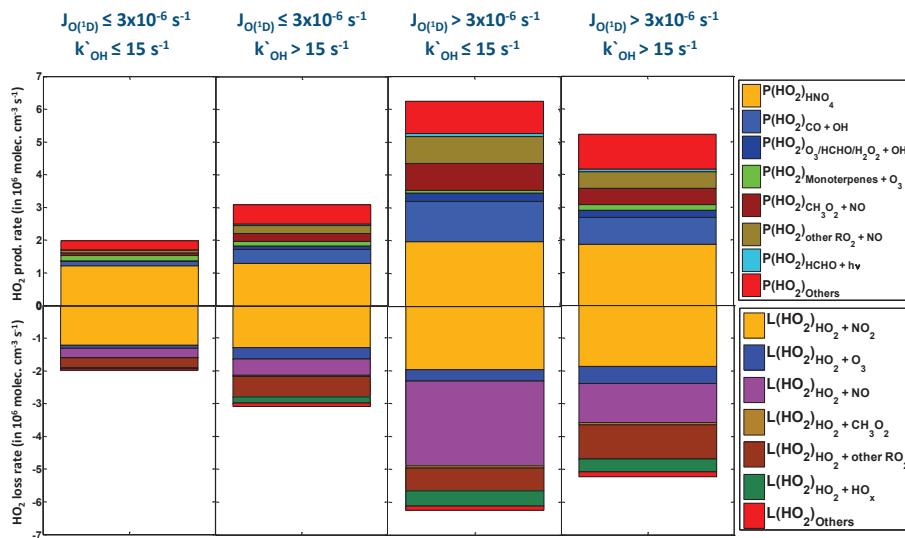


Abbildung 5.9.: Simulated production and loss rates of HO₂ during HUMPPA–COPEC–2010 under conditions of different radiation and total observed OH reactivity.

6. Summary and conclusions

Recent efforts to model HO_x concentrations in forest environments characterized by high concentrations of BVOCs and low concentrations of NO_x revealed serious discrepancies with observations of OH and HO₂ (Tan et al., 2001; Lelieveld et al., 2008; Kubistin et al., 2010; Martinez et al., 2010; Pugh et al., 2010b; Whalley et al., 2011). In contrast to well-known OH recycling pathways via HO₂ by reaction with NO and O₃, various mechanisms recycling OH directly in the absence of NO have been proposed and tested in different studies to improve the understanding of HO_x-chemistry influenced by forest emissions (Paulot et al., 2009; Peeters et al., 2009; Hofzumahaus et al., 2009; Crouse et al., 2011). Griffith et al. (2013) measured OH during two subsequent summers in a deciduous forest in northern Michigan during the PROPHET 2008 and CABINEX 2009 campaigns. The authors found good model-to-measurement agreement during the colder summer of CABINEX 2009 campaign, when lower temperatures led to lower observed mixing ratios of isoprene, its oxidation products MVK and MACR, and formaldehyde. During the warmer summer of PROPHET 2008 the model underestimates the OH concentration in the afternoon. Kim et al. (2013) reported reasonable agreement between observed OH and that from steady-state calculations using observations, particularly measurements of HO₂, in a forest environment dominated by emissions of monoterpenes and MBO. Constrained box model simulations underpredicted the observed HO₂ and OH concentrations significantly in this forest. Mao et al. (2012), addressing the impact of measurement artefacts in LIF measurements, showed reasonable agreement between model predictions and observations using their new “chemical removal method” for detection of OH in a California ponderosa pine forest during the BEARPEX09¹¹ campaign.

Within the framework of this thesis the HORUS instrument was operated for the first time using the IPI-LIF-FAGE technique to measure OH during HUMPPA–COPEC–2010. To identify possible measurement interferences an instrument intercomparison between the CIMS and HORUS-LIF instruments was conducted at the beginning of the campaign on the ground. The hydroxyl radical measurements by the two independent techniques show generally good agreement. During daytime, OH concentrations up to 3.5×10^6 molec. cm⁻³ were observed above canopy, a factor of two to three times higher than the measurements on ground. Higher OH concentrations above canopy were driven by higher radiation. There is no evidence for differences in the chemical regime on ground and above the canopy on a timescale comparable to, or less than the timescale of mixing processes.

¹¹BEARPEX09 = Biosphere Effects on AeRosols and Photochemistry EXperiment

6. Summary and conclusions

Comparison of the calculated total OH production rate with the total loss rate calculated from observed OH concentrations and total OH reactivity measurements showed that the known OH sources are almost sufficient to close the budget above the canopy. Detailed analysis of the radical production, loss, and recycling pathways revealed that OH recycling in the observed boreal forest environment occurs mainly by recycling via HO₂ under conditions of high radiation and moderate observed total OH reactivity ($J_{O(1D)} > 3 \times 10^{-6} \text{ s}^{-1}$, $k'_{OH} \leq 15 \text{ s}^{-1}$). Under conditions of enhanced total OH reactivity ($k'_{OH} > 15 \text{ s}^{-1}$) recycling mechanisms of OH, not via reaction of HO₂ with NO/O₃, are likely in addition. Furthermore, a source of HO₂ is missing under these conditions.

During some nights both instruments, CIMS (on ground) and IPI-LIF-FAGE (above canopy), detected significant amounts of OH that cannot be explained by known production rates calculated from observations. The missing OH source during nighttime of the order of $1 \times 10^6 \text{ molec. cm}^{-3} \text{ s}^{-1}$ could partly be related to NO₃. The NO₃ mixing ratio during HUMPPA-COPEC-2010 was always below the lower limit of detection of the CRD instrument (Rinne et al., 2012). However, it was produced at a rate of up to $1 \times 10^6 \text{ molec. cm}^{-3} \text{ s}^{-1}$ from the reaction of NO₂ with O₃. RO₂ radicals from NO₃-initiated VOC oxidation potentially undergo isomerization reactions or react with HO₂ as well, forming OH. Thus, NO₃ might, at least under some conditions, contribute to the missing OH source during nighttime. Ozonolysis of unmeasured VOCs is also likely to contribute.

The role of potentially undetected VOCs and oxidation products in the chemistry of HO_x can not be understood from observations alone. Hence, box model simulations have been considered for further investigation. The chemistry of the condensed isoprene mechanism (“Mainz Isoprene Mechanism”) is shown to be deficient for the observed monoterpene-dominated boreal forest environment. Isoprene levels of typically less than 200 ppt_v contributed at most 10% to the total observed OH reactivity thus leading to an overprediction of OH due to the missing sinks by a factor of up to 3 and HO₂ being significantly underpredicted ($\text{HO}_2^{\text{mod.}}/\text{HO}_2^{\text{obs.}}=0.3$). Inclusion of the Mainz Terpene Mechanism (MTM) to account for the reactivity towards OH due to observed terpene species and their oxidation products leads to much better agreement between observed and simulated OH concentrations. However, this is due to two compensating effects. On average about one third of the observed total OH reactivity is not reproduced in the simulation, thus leading to underestimation of the total sink of OH. On the other hand, the production of OH is significantly underestimated due to the underpredicted HO₂ available for recycling by reaction with NO and O₃ which was shown to be an important source of OH by direct calculation from observations. Tuning the simulation on the observed total OH reactivity by adding an unknown compound which behaves like α -pinene produced a somewhat better $\text{HO}_2^{\text{mod.}}/\text{HO}_2^{\text{obs.}}$ agreement. Nevertheless, the additional HO₂ being recycled towards OH was not sufficient to compensate for the resulting enhanced OH loss. The biggest model-observation discrepancies for HO₂ occurred when “missing” OH reactivity was highest. Therefore, this provides evidence that the “missing” OH reactivity in the simulation is a source of HO₂. However, a single terpene following the chemical mechanism of α -pinene as described in the preliminary terpene mechanism

cannot account for this alone. Additional RO₂/HO₂ sources that are independent of OH, such as the thermal decomposition of transported peroxyacyl nitrates and the photolysis of glyoxal, are indicated.

HO₂ being underestimated in simulations for terpene dominated environments implies that the net O₃ production in global model simulations using the state-of-the-art chemical reaction schemes is potentially underestimated in boreal regions.

The OH production in this forest environment seems to be understood reasonably well under moderate total OH reactivity conditions (Table 4.2). In periods of high observed total OH reactivity a source of OH is missing. Only a small fraction of the loss of OH can be explained, even through inclusion of higher order oxidation products by application of a box model. HO₂ is underestimated in simulations, indicating missing BVOCs, which could also account for the missing reactivity in the model. Additional recycling processes of OH, not via HO₂ + NO/O₃ are indicated under conditions of high observed total OH reactivity by detailed analysis of the HO_x budget calculated from observations.

Future observations in forest environments should include RO₂ measurements, that could help constrain simulations better and further improve the understanding of the radical cycling processes in this boreal forest (and elsewhere). Particularly, identification of the fraction of acyl peroxy radical species that can directly recycle OH by reaction with HO₂ would enable a more detailed analysis of radical recycling processes under conditions of enhanced OH reactivity. Observations of additional HO₂ and RO₂ precursor species, such as glyoxal, PAN, and acetone, would enhance the capabilities to investigate the oxidation capacity. Chemical mechanisms used in simulations need to include a comprehensive representation of the most abundant biogenic VOCs, e.g. in this case monoterpenes and their oxidation chemistry in order to reproduce the radical photochemistry when isoprene is not the predominant BVOC.

A. Measurements of trace gas species and meteorological parameters during HUMPPA-COPEC 2010

Tabelle A.1.: Median levels and variability of relevant trace gases under different conditions of observed radiation and total OH reactivity.

	$J_{O(^1D)} > 3 \times 10^{-6} \text{ s}^{-1}$	$J_{O(^1D)} \leq 3 \times 10^{-6} \text{ s}^{-1}$
$k'_{OH} \leq 15 \text{ s}^{-1}$	<p>OH $\approx (1.0 \pm 0.8) \times 10^6 \text{ molec. cm}^{-3}$</p> <p>HO₂ $\approx (10 \pm 1) \text{ ppt}_V$</p> <p>O₃ $\approx (33 \pm 2) \text{ ppb}_V$</p> <p>NO $\approx (46 \pm 16) \text{ ppt}_V$</p> <p>NO₂ $\approx (280 \pm 40) \text{ ppt}_V$</p> <p>CO $\approx (85 \pm 1) \text{ ppb}_V$</p> <p>C₅H₈ $\approx (145 \pm 30) \text{ ppt}_V$</p> <p>$\alpha$-pinene $\approx (63 \pm 15) \text{ ppt}_V$</p> <p>$\beta$-pinene $\approx (16 \pm 4) \text{ ppt}_V$</p> <p>$\beta$-myrcene $\approx (5 \pm 1) \text{ ppt}_V$</p> <p>$\Delta^3$-carene $\approx (30 \pm 8) \text{ ppt}_V$</p>	<p>OH $\approx (3.8 \pm 3.0) \times 10^5 \text{ molec. cm}^{-3}$</p> <p>HO₂ $\approx (10 \pm 6) \text{ ppt}_V$</p> <p>O₃ $\approx (35 \pm 7) \text{ ppb}_V$</p> <p>NO $\approx (3 \pm 39) \text{ ppt}_V$</p> <p>NO₂ $\approx (570 \pm 210) \text{ ppt}_V$</p> <p>CO $\approx (96 \pm 5) \text{ ppb}_V$</p> <p>C₅H₈ $\approx (62 \pm 65) \text{ ppt}_V$</p> <p>$\alpha$-pinene $\approx (68 \pm 67) \text{ ppt}_V$</p> <p>$\beta$-pinene $\approx (20 \pm 17) \text{ ppt}_V$</p> <p>$\beta$-myrcene $\approx (5 \pm 4) \text{ ppt}_V$</p> <p>$\Delta^3$-carene $\approx (44 \pm 44) \text{ ppt}_V$</p>
$k'_{OH} > 15 \text{ s}^{-1}$	<p>OH $\approx (6.4 \pm 5.6) \times 10^5 \text{ molec. cm}^{-3}$</p> <p>HO₂ $\approx (27 \pm 2) \text{ ppt}_V$</p> <p>O₃ $\approx (51 \pm 1) \text{ ppb}_V$</p> <p>NO $\approx (28 \pm 7) \text{ ppt}_V$</p> <p>NO₂ $\approx (320 \pm 20) \text{ ppt}_V$</p> <p>CO $\approx (93 \pm 1) \text{ ppb}_V$</p> <p>C₅H₈ $\approx (112 \pm 13) \text{ ppt}_V$</p> <p>$\alpha$-pinene $\approx (80 \pm 4) \text{ ppt}_V$</p> <p>$\beta$-pinene $\approx (17 \pm 1) \text{ ppt}_V$</p> <p>$\beta$-myrcene $\approx (5.0 \pm 0.3) \text{ ppt}_V$</p> <p>$\Delta^3$-carene $\approx (38 \pm 2) \text{ ppt}_V$</p>	<p>OH $\approx (6.3 \pm 2.0) \times 10^5 \text{ molec. cm}^{-3}$</p> <p>HO₂ $\approx (22 \pm 4) \text{ ppt}_V$</p> <p>O₃ $\approx (51.0 \pm 0.3) \text{ ppb}_V$</p> <p>NO $\approx (17 \pm 5) \text{ ppt}_V$</p> <p>NO₂ $\approx (290 \pm 30) \text{ ppt}_V$</p> <p>CO $\approx (92 \pm 1) \text{ ppb}_V$</p> <p>C₅H₈ $\approx (110 \pm 5) \text{ ppt}_V$</p> <p>$\alpha$-pinene $\approx (61 \pm 8) \text{ ppt}_V$</p> <p>$\beta$-pinene $\approx (14 \pm 1) \text{ ppt}_V$</p> <p>$\beta$-myrcene $\approx (4.0 \pm 0.5) \text{ ppt}_V$</p> <p>$\Delta^3$-carene $\approx (27 \pm 5) \text{ ppt}_V$</p>

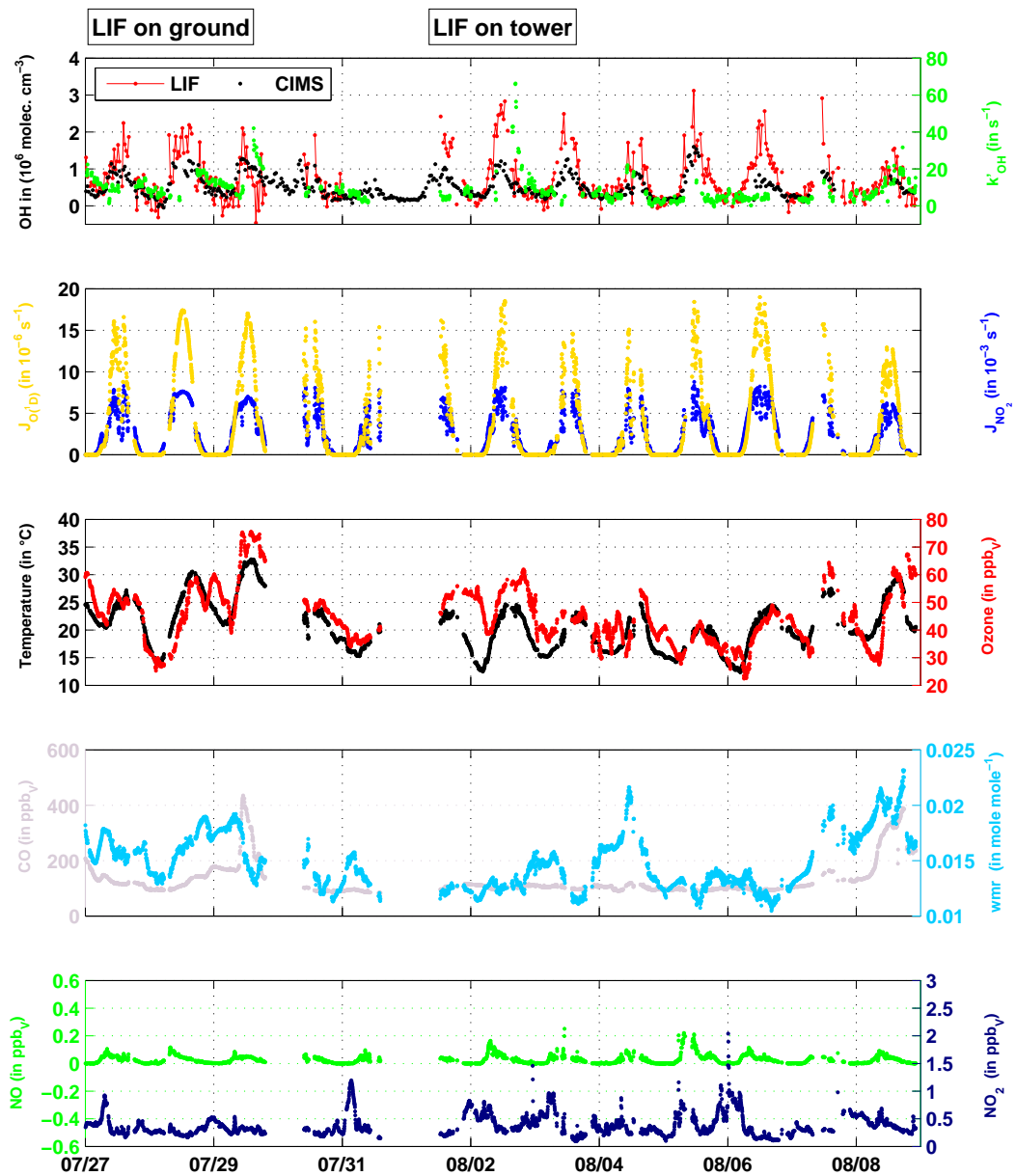


Abbildung A.1.: Timeseries of trace gas species and meteorological parameters during HUMPPA-COPEC-2010.

A. Measurements of trace gas species and meteorological parameters during HUMPPA-COPEC 2010

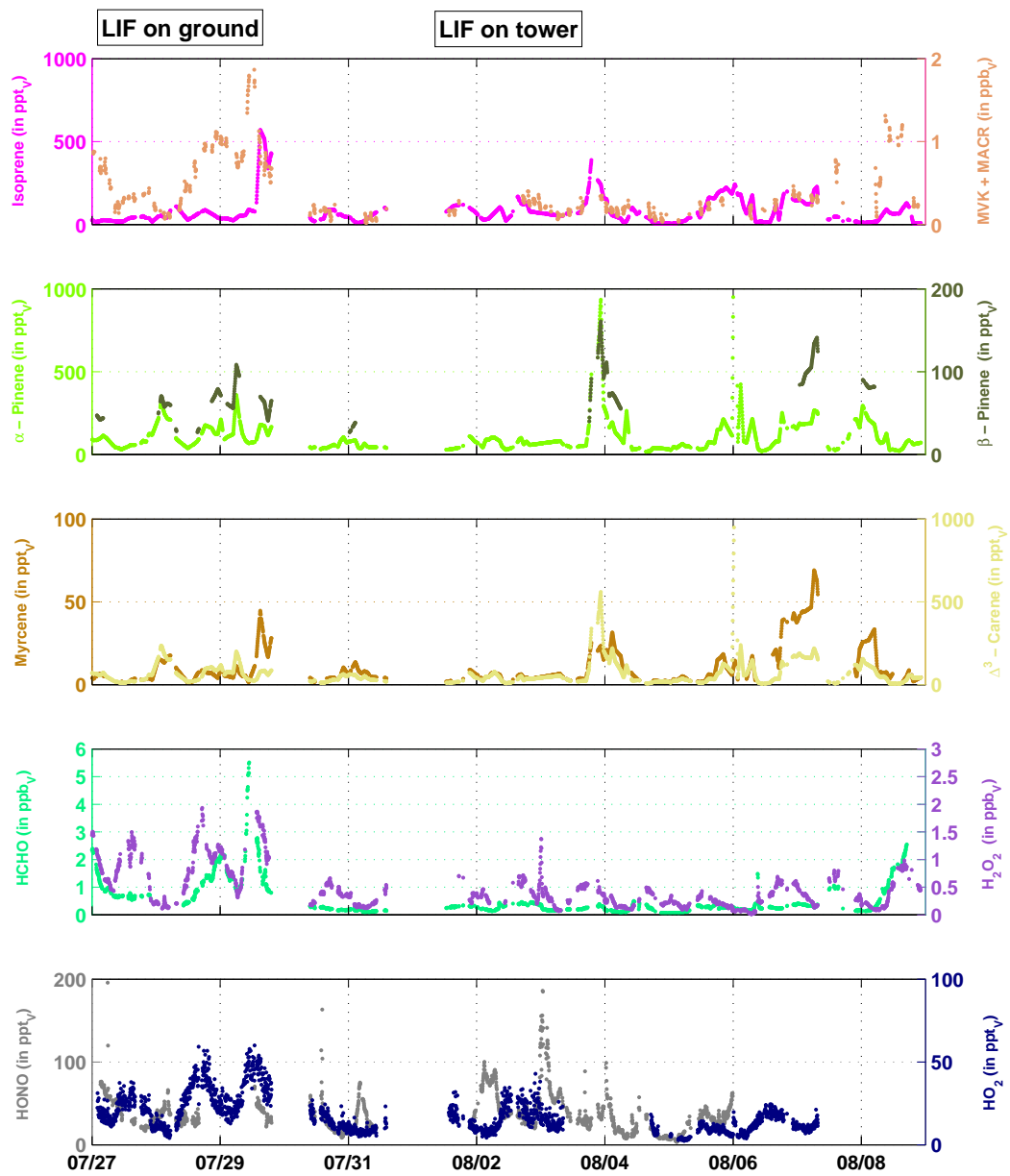


Abbildung A.1.: (continued): Timeseries of trace gas species and meteorological parameters during HUMPPA-COPEC-2010.

B. Chemical mechanism – MTM

The Chemical Mechanism of MECCA

KPP version: 2.2.1_rs5

MECCA version: 3.3

Date: October 9, 2013.

Selected reactions:

"Tr && G && !S && !Cl && !Br && !I && !Hg"

Number of aerosol phases: 0

Number of species in selected mechanism:

Gas phase: 394

Aqueous phase: 0

All species: 394

Number of reactions in selected mechanism:

Gas phase (Gnn): 952

Aqueous phase (Ann): 0

Henry (Hnn): 0

Photolysis (Jnn): 102

Heterogeneous (HETnn): 0

Equilibria (EQnn): 0

Isotope exchange (DGnn): 0

Dummy (Dnn): 0

All equations: 1054

B. Chemical mechanism – MTM

Table 1: Gas phase reactions

#	labels	reaction	rate coefficient	reference
G1000	SrTrG	$O_2 + O(^1D) \rightarrow O(^3P) + O_2$	$3.2E-11 \cdot \text{EXP}(70./\text{temp})$	Sander et al. (2003)
G1001	SrTrG	$O_2 + O(^3P) \rightarrow O_3$	$6.E-34 \cdot (\text{temp}/300.)^{*} \cdot (-2.4) \cdot \text{cair}$	Sander et al. (2003)
G2100	SrTrG	$H + O_2 \rightarrow HO_2$	$k_3rd(\text{temp}, \text{cair}, 5.7E-32, 1.6, 7.5E-11, 0., 0.6)$	Sander et al. (2003)
G2104	SrTrG	$OH + O_2 \rightarrow HO_2 + LOHOX$	$1.7E-12 \cdot \text{EXP}(-940./\text{temp})$	Sander et al. (2003)
G2105	SrTrG	$OH + H_2 \rightarrow H_2O + H + LOHOX$	$2.8E-12 \cdot \text{EXP}(-1800./\text{temp})$	Sander et al. (2006)
G2107	SrTrG	$HO_2 + O_3 \rightarrow OH + POHOX$	$1.E-14 \cdot \text{EXP}(-490./\text{temp})$	Sander et al. (2003)
G2109	SrTrG	$HO_2 + OH \rightarrow H_2O + LOHOX$	$4.8E-11 \cdot \text{EXP}(250./\text{temp})$	Sander et al. (2003)
G2110	SrTrG	$HO_2 + HO_2 \rightarrow H_2O_2$	k_HO2_HO2	Christensen et al. (2002), Kircher and Sander (1984)*
G2111	SrTrG	$H_2O + O(^1D) \rightarrow 2 OH + 2 POHOX + 2 POHPR$	$2.2E-10$	Sander et al. (2003)
G2112	SrTrG	$H_2O_2 + OH \rightarrow H_2O + HO_2 + LOHOX$	$2.9E-12 \cdot \text{EXP}(-160./\text{temp})$	Sander et al. (2003)
G3101	SrTrG	$N_2 + O(^1D) \rightarrow O(^3P) + N_2$	$1.8E-11 \cdot \text{EXP}(110./\text{temp})$	Sander et al. (2003)
G3103	SrTrGN	$NO + O_3 \rightarrow NO_2 + O_2$	$3.E-12 \cdot \text{EXP}(-1500./\text{temp})$	Sander et al. (2003)
G3106	SrTrGN	$NO_2 + O_3 \rightarrow NO_3 + O_2$	$1.2E-13 \cdot \text{EXP}(-2450./\text{temp})$	Sander et al. (2003)
G3108	SrTrGN	$NO_3 + NO \rightarrow 2 NO_2$	$1.5E-11 \cdot \text{EXP}(170./\text{temp})$	Sander et al. (2003)
G3109	SrTrGN	$NO_3 + NO_2 \rightarrow N_2O_5$	k_NO3_NO2	Sander et al. (2003)*
G3110	SrTrGN	$N_2O_5 \rightarrow NO_2 + NO_3$	$k_NO3_NO2 / (3.E-27 \cdot \text{EXP}(10990./\text{temp}))$	Sander et al. (2003)*
G3200	TrG	$NO + OH \rightarrow HONO + LONOX$	$k_3rd(\text{temp}, \text{cair}, 7.E-31, 2.6, 3.6E-11, 0.1, 0.6)$	Sander et al. (2003)
G3201	SrTrGN	$NO + HO_2 \rightarrow NO_2 + OH + PONOX$	$3.5E-12 \cdot \text{EXP}(250./\text{temp})$	Sander et al. (2003)
G3202	SrTrGN	$NO_2 + OH \rightarrow HNO_3 + LONOX$	$k_3rd(\text{temp}, \text{cair}, 1.48E-30, 3., 2.58E-11, 0., 0.6)$	Mollner et al. (2010)
G3203	SrTrGN	$NO_2 + HO_2 \rightarrow HNO_4$	k_NO2_HO2	Sander et al. (2003)
G3204	TrGN	$NO_3 + HO_2 \rightarrow NO_2 + OH + O_2 + PONOX$	$3.5E-12$	Sander et al. (2003)
G3205	TrG	$HONO + OH \rightarrow NO_2 + H_2O + LONOX$	$1.8E-11 \cdot \text{EXP}(-390./\text{temp})$	Sander et al. (2003)
G3206	SrTrGN	$HNO_3 + OH \rightarrow H_2O + NO_3 + LONOX$	k_HNO3_OH	Sander et al. (2003)*
G3207	SrTrGN	$HNO_4 \rightarrow NO_2 + HO_2$	$k_NO2_HO2 / (2.1E-27 \cdot \text{EXP}(10900./\text{temp}))$	Sander et al. (2003)*
G3208	SrTrGN	$HNO_4 + OH \rightarrow NO_2 + H_2O + LONOX$	$1.3E-12 \cdot \text{EXP}(380./\text{temp})$	Sander et al. (2003)
G4101	SrTrG	$CH_4 + OH \rightarrow CH_3O + H_2O + POHORG$	$1.85E-20 \cdot \text{EXP}(2.82 \cdot \log(\text{temp}) - 987./\text{temp})$	Atkinson (2003)
G4102	TrG	$CH_3OH + OH \rightarrow HCHO + HO_2 + POHORG$	$7.3E-12 \cdot \text{EXP}(-620./\text{temp})$	Sander et al. (2003)
G4103a	SrTrG	$CH_3O_2 + HO_2 \rightarrow CH_3OOH$	$4.1E-13 \cdot \text{EXP}(750./\text{temp}) / (1.+1./497.7 \cdot \text{EXP}(1160./\text{temp}))$	Sander et al. (2003)*

2

Table 1: Gas phase reactions (... continued)

#	labels	reaction	rate coefficient	reference
G4103b	SrTrG	$CH_3O_2 + HO_2 \rightarrow HCHO + H_2O + O_2$	$4.1E-13 \cdot \text{EXP}(750./\text{temp}) / (1.+497.7 \cdot \text{EXP}(-1160./\text{temp}))$	Sander et al. (2003)*
G4104	SrTrGN	$CH_3O_2 + NO \rightarrow HCHO + NO_2 + HO_2$	$2.8E-12 \cdot \text{EXP}(300./\text{temp})$	Sander et al. (2003)
G4105	TrGN	$CH_3O_2 + NO_3 \rightarrow HCHO + HO_2 + NO_2$	$1.3E-12$	Atkinson et al. (1999)
G4106a	SrTrG	$CH_3O_2 \rightarrow HCHO + HO_2$	$2 \cdot R02 \cdot 9.5E-14 \cdot \text{EXP}(390./\text{temp}) / (1.+1./26.2 \cdot \text{EXP}(1130./\text{temp}))$	Sander et al. (2003)
G4106b	SrTrG	$CH_3O_2 \rightarrow .5 HCHO + .5 CH_3OH$	$2 \cdot R02 \cdot 9.5E-14 \cdot \text{EXP}(390./\text{temp}) / (1.+26.2 \cdot \text{EXP}(-1130./\text{temp}))$	Sander et al. (2003)
G4107	SrTrG	$CH_3OOH + OH \rightarrow .6 CH_3O_2 + .4 HCHO + .4 OH + H_2O + .4 POHORG + POHORG$	k_CH3OOH_OH	see note
G4108	SrTrG	$HCHO + OH \rightarrow CO + H_2O + HO_2 + POHORG$	$9.52E-18 \cdot \text{EXP}(2.03 \cdot \log(\text{temp}) + 636./\text{temp})$	Sivakumaran et al. (2003)
G4109	TrGN	$HCHO + NO_3 \rightarrow HNO_3 + CO + HO_2$	$3.4E-13 \cdot \text{EXP}(-1900./\text{temp})$	Sander et al. (2003)*
G4110	SrTrG	$CO + OH \rightarrow H + CO_2 + POHORG$	$1.57E-13 + \text{cair} \cdot 3.54E-33$	McCabe et al. (2001)
G4111	TrG	$HCOOH + OH \rightarrow CO_2 + H_2O + POHORG$	$4.5E-13$	IUPAC (2013)
G4112e	TrGC	$HCHO + HO_2 \rightarrow HOCH_2O_2$	$7.7E-15 \cdot \text{EXP}(625./\text{temp})$	IUPAC (2013)
G4113e	TrGC	$HOCH_2O_2 \rightarrow HCHO + HO_2$	$2.E12 \cdot \text{EXP}(-7000./\text{temp})$	IUPAC (2013)
G4114e	TrGC	$HOCH_2O_2 + HO_2 \rightarrow .5 HOCH_2OOH + .5 HCOOH + .2 OH + .2 HO_2 + .3 H_2O + .2 POHORG$	$5.6E-15 \cdot \text{EXP}(2300./\text{temp})$	Jenkin et al. (2007)
G4115e	TrGC	$HOCH_2O_2 + NO \rightarrow NO_2 + HO_2 + HCOOH$	$2.8E-12 \cdot \text{EXP}(300./\text{temp})$	Sander et al. (2003)
G4116e	TrGC	$HOCH_2O_2 + NO_3 \rightarrow NO_2 + HO_2 + HCOOH$	$1.2E-12$	see note
G4117e	TrGC	$HOCH_2O_2 \rightarrow HCOOH + .62 HO_2$	$1.4E-12 \cdot R02$	see note
G4118e	TrGC	$HOCH_2OOH + OH \rightarrow HOCH_2O_2 + H_2O + POHORG$	$0.6 \cdot k_CH3OOH_OH + \text{krohiro}$	see note
G4119e	TrGC	$HOCH_2OOH + OH \rightarrow OH + HCOOH + H_2O + POHORG + POHORG$	$ks \cdot fsoh \cdot fsooh$	see note
G4200	TrGC	$C_2H_6 + OH \rightarrow C_2H_5O_2 + H_2O + POHORG$	$1.49E-17 \cdot \text{temp} \cdot \text{temp} \cdot \text{EXP}(-499./\text{temp})$	Atkinson (2003)
G4201e	TrGC	$C_2H_4 + O_3 \rightarrow HCHO + .63 CO + .13 HO_2 + 0.37 HOCH_2OOH + .13 OH + .13 POHORG$	$1.2E-14 \cdot \text{EXP}(-2630./\text{temp})$	Sander et al. (2003)*
G4202	TrGC	$C_2H_4 + OH \rightarrow HOCH_2CH_2O_2 + H_2O + POHORG$	$k_3rd(\text{temp}, \text{cair}, 1.E-28, 0.8, 8.8E-12, 0., 0.6)$	Sander et al. (2003)
G4203	TrGC	$C_2H_5O_2 + HO_2 \rightarrow C_2H_5OOH$	$7.5E-13 \cdot \text{EXP}(700./\text{temp})$	Sander et al. (2003)
G4204	TrGNC	$C_2H_5O_2 + NO \rightarrow CH_3CHO + HO_2 + NO_2$	$2.6E-12 \cdot \text{EXP}(365./\text{temp})$	Sander et al. (2003)
G4205	TrGNC	$C_2H_5O_2 + NO_3 \rightarrow CH_3CHO + HO_2 + NO_2$	$2.3E-12$	Atkinson et al. (1999)
G4206	TrGC	$C_2H_5O_2 \rightarrow .98 CH_3CHO + .38 HO_2 + .02 HOCH_2CH_2O_2$	$3.1E-13 \cdot R02$	Rickard and Pascoe (2009)*
G4207	TrGC	$C_2H_5OOH + OH \rightarrow .43 C_2H_5O_2 + .43 H_2O + .57 CH_3CHO + .57 OH + .57 POHORG + POHORG$	$0.6 \cdot k_CH3OOH_OH + 8.01E-12$	see note

3

Table 1: Gas phase reactions (... continued)

#	labels	reaction	rate coefficient	reference
G4208ea	TrGC	$\text{CH}_3\text{CHO} + \text{OH} \rightarrow \text{CH}_3\text{C(O)OO} + \text{H}_2\text{O} + \text{POHORG}$	$4.4\text{E}-12 \cdot \text{EXP}(365./\text{temp}) \cdot 0.95$	Atkinson et al. (2006)
G4208eb	TrGC	$\text{CH}_3\text{CHO} + \text{OH} \rightarrow .84 + .1 \text{HCHO} + .1 \text{CO} + .06 \text{GLYOX} + .16 \text{OH} + \text{H}_2\text{O} + .16 \text{POHORG} + \text{POHORG}$	$4.4\text{E}-12 \cdot \text{EXP}(365./\text{temp}) \cdot 0.05$	Atkinson et al. (2006)
G4209	TrGNC	$\text{CH}_3\text{CHO} + \text{NO}_3 \rightarrow \text{CH}_3\text{C(O)OO} + \text{HNO}_3$	KN03AL	Sander et al. (2003)
G4210e	TrGC	$\text{CH}_3\text{COOH} + \text{OH} \rightarrow \text{CH}_3\text{O}_2 + \text{CO}_2 + \text{H}_2\text{O} + \text{POHORG}$	$4.2\text{E}-14 \cdot \text{exp}(850./\text{temp})$	IUPAC (2013)
G4211et1	TrGC	$\text{CH}_3\text{C(O)OO} + \text{HO}_2 \rightarrow \text{OH} + \text{CH}_3\text{O}_2 + \text{CO}_2 + \text{POHORG}$	KAPH02*0.70	Taraborrelli (2013a)*
G4211et2	TrGC	$\text{CH}_3\text{C(O)OO} + \text{HO}_2 \rightarrow \text{CH}_3\text{C(O)OOH}$	KAPH02*0.12	Taraborrelli (2013a)*
G4211et3	TrGC	$\text{CH}_3\text{C(O)OO} + \text{HO}_2 \rightarrow \text{CH}_3\text{COOH} + \text{O}_3$	KAPH02*0.18	Taraborrelli (2013a)*
G4212	TrGNC	$\text{CH}_3\text{C(O)OO} + \text{NO} \rightarrow \text{CH}_3\text{O}_2 + \text{CO}_2 + \text{NO}_2$	$8.1\text{E}-12 \cdot \text{EXP}(270./\text{temp})$	Tyndall et al. (2001)
G4213	TrGNC	$\text{CH}_3\text{C(O)OO} + \text{NO}_2 \rightarrow \text{PAN}$	k_CH3C03_NO2	Tyndall et al. (2001)
G4214	TrGNC	$\text{CH}_3\text{C(O)OO} + \text{NO}_3 \rightarrow \text{CH}_3\text{O}_2 + \text{NO}_2 + \text{CO}_2$	4.E-12	Canosa-Mas et al. (1996)
G4217	TrGC	$\text{CH}_3\text{C(O)OO} \rightarrow .7 \text{CH}_3\text{O}_2 + .7 \text{CO}_2 + .3 \text{CH}_3\text{COOH}$	1.00E-11*RD2	Rickard and Pascoe (2009)
G4218	TrGC	$\text{CH}_3\text{C(O)OOH} + \text{OH} \rightarrow \text{CH}_3\text{C(O)OO} + \text{H}_2\text{O} + \text{POHORG}$	0.6*k_CH300H_OH	Rickard and Pascoe (2009)*
G4220	TrGNC	$\text{PAN} + \text{OH} \rightarrow \text{HCHO} + \text{CO} + \text{NO}_2 + \text{H}_2\text{O} + \text{POHORG}$	$9.50\text{E}-13 \cdot \text{EXP}(-650./\text{temp})$	Rickard and Pascoe (2009)
G4221	TrGNC	$\text{PAN} \rightarrow \text{CH}_3\text{C(O)OO} + \text{NO}_2$	k_PAN_M	Sander et al. (2003)*
G4223e	TrGC	$\text{HOCH}_2\text{CHO} + \text{OH} \rightarrow .84 + .16 + .2 \text{HO}_2 + \text{H}_2\text{O} + \text{POHORG}$	8.00E-12	Rickard and Pascoe (2009)
G4224e	TrGNC	$\text{HOCH}_2\text{CHO} + \text{NO}_3 \rightarrow \text{HNO}_3$	KN03AL	Rickard and Pascoe (2009)
G4235et2	TrGC	$\rightarrow \text{HOCH}_2\text{CO}_3$	KDEC*.97	Taraborrelli (2013a)*
G4235et3	TrGC	$\rightarrow \text{OH} + \text{HCHO} + \text{CO} + \text{POHORG}$	KDEC*.03	Taraborrelli (2013a)*
G4236et2	TrGC	$\rightarrow \text{GLYOX} + \text{HO}_2$	KDEC	Taraborrelli (2013a)
G4225	TrGC	$\text{HOCH}_2\text{CO}_3 \rightarrow .7 \text{HCHO} + .7 \text{CO}_2 + .7 \text{HO}_2 + .3 \text{HOCH}_2\text{CO}_2\text{H}$	1.00E-11*RD2	Rickard and Pascoe (2009)
G4226ea	TrGC	$\text{HOCH}_2\text{CO}_3 + \text{HO}_2 \rightarrow \text{HCHO} + \text{HO}_2 + \text{OH} + \text{CO}_2 + \text{POHORG}$	KAPH02*rco3_oh	Taraborrelli (2013a)*
G4226eb	TrGC	$\text{HOCH}_2\text{CO}_3 + \text{HO}_2 \rightarrow \text{HOCH}_2\text{CO}_3\text{H}$	KAPH02*rco3_ohh	Taraborrelli (2013a)*
G4226ec	TrGC	$\text{HOCH}_2\text{CO}_3 + \text{HO}_2 \rightarrow \text{HOCH}_2\text{CO}_2\text{H} + \text{O}_3$	KAPH02*rco3_o3	Taraborrelli (2013a)*
G4227	TrGNC	$\text{HOCH}_2\text{CO}_3 + \text{NO} \rightarrow \text{NO}_2 + \text{HO}_2 + \text{HCHO} + \text{CO}_2$	KAPNO	Rickard and Pascoe (2009)
G4228	TrGNC	$\text{HOCH}_2\text{CO}_3 + \text{NO}_2 \rightarrow \text{PHAN}$	k_CH3C03_NO2	Rickard and Pascoe (2009)
G4229	TrGNC	$\text{HOCH}_2\text{CO}_3 + \text{NO}_3 \rightarrow \text{NO}_2 + \text{HO}_2 + \text{HCHO} + \text{CO}_2$	KR02N03*1.60	Rickard and Pascoe (2009)
G4230e	TrGC	$\text{HOCH}_2\text{CO}_2\text{H} + \text{OH} \rightarrow .09 \text{HCHO} + .09 \text{CO}_2 + .91 \text{HCOCO}_2\text{H} + \text{HO}_2 + \text{POHORG}$	kco2h*ks*fsoh*fco2h	Taraborrelli (2013a)
G4231ea	TrGC	$\text{HOCH}_2\text{CO}_3\text{H} + \text{OH} \rightarrow \text{HOCH}_2\text{CO}_3 + \text{H}_2\text{O} + \text{POHORG}$	0.6*k_CH300H_OH	Taraborrelli (2013a)
G4231eb	TrGC	$\text{HOCH}_2\text{CO}_3\text{H} + \text{OH} \rightarrow \text{HCOCO}_3\text{H} + \text{HO}_2 + \text{POHORG}$	ks*fsoh*fco2h	Taraborrelli (2013a)
G4232	TrGNC	$\text{PHAN} \rightarrow \text{HOCH}_2\text{CO}_3 + \text{NO}_2$	k_PAN_M	Rickard and Pascoe (2009)

4

Table 1: Gas phase reactions (... continued)

#	labels	reaction	rate coefficient	reference
G4233	TrGNC	$\text{PHAN} + \text{OH} \rightarrow \text{HCHO} + \text{CO} + \text{NO}_2 + \text{H}_2\text{O}$	1.12E-12	Rickard and Pascoe (2009)
G4234e	TrGC	$\text{GLYOX} + \text{OH} \rightarrow 1.2 \text{CO} + .6 \text{HO}_2 + .4 + \text{H}_2\text{O} + \text{POHORG}$	$3.1\text{E}-12 \cdot \text{EXP}(340./\text{temp})$	IUPAC (2013)
G4235e	TrGNC	$\text{GLYOX} + \text{NO}_3 \rightarrow 1.2 \text{CO} + .6 \text{HO}_2 + .4 + \text{HNO}_3$	KN03AL	Rickard and Pascoe (2009)
G4235et2	TrGNC	$\rightarrow 1.5 \text{CO} + .5 \text{HO}_2 + .5 \text{OH} + .5 \text{CO}_2 + .5 \text{POHORG}$	KDEC	Taraborrelli (2013a)
G4236	TrGC	$\text{HCOCO}_3 \rightarrow .7 \text{CO} + .7 \text{HO}_2 + .7 \text{CO}_2 + .3 \text{HCOCO}_2\text{H}$	1.00E-11*RD2	Rickard and Pascoe (2009)
G4237e	TrGC	$\text{HCOCO}_3 + \text{HO}_2 \rightarrow \text{HO}_2 + \text{CO} + \text{CO}_2 + \text{OH} + \text{POHORG}$	KAPH02	Feierabend et al. (2008), Taraborrelli (2013a)
G4238	TrGNC	$\text{HCOCO}_3 + \text{NO} \rightarrow \text{HO}_2 + \text{CO} + \text{NO}_2 + \text{CO}_2$	KAPNO	Rickard and Pascoe (2009)
G4239	TrGNC	$\text{HCOCO}_3 + \text{NO}_3 \rightarrow \text{HO}_2 + \text{CO} + \text{NO}_2 + \text{CO}_2$	KR02N03*1.60	Rickard and Pascoe (2009)
G4239t2	TrGNC	$\text{HCOCO}_3 + \text{NO}_2 \rightarrow \text{HO}_2 + \text{CO} + \text{NO}_3 + \text{CO}_2$	k_CH3C03_NO2	Orlando and Tyndall (2001), Taraborrelli (2013a)*
G4240	TrGC	$\text{HCOCO}_2\text{H} + \text{OH} \rightarrow \text{CO} + \text{HO}_2 + \text{CO}_2 + \text{H}_2\text{O} + \text{POHORG}$	kco2h*kt*fo*fco2h	Taraborrelli (2013a)
G4241	TrGC	$\text{HCOCO}_3\text{H} + \text{OH} \rightarrow .2 \text{HCOCO}_3 + .8 \text{CO} + .8 \text{OH} + .8 \text{CO}_2 + \text{H}_2\text{O} + \text{POHORG} + .8 \text{POHORG}$	$0.6 \cdot k_{\text{CH300H_OH}} \cdot kt \cdot fo \cdot fco2h$	Taraborrelli (2013a)
G4242	TrGC	$\text{HOCH}_2\text{CH}_2\text{O}_2 \rightarrow .6 \text{HOCH}_2\text{CH}_2\text{O} + .2 \text{HOCH}_2\text{CHO} + .2 \text{ETHGLY}$	2.00E-12*RD2	Rickard and Pascoe (2009)
G4244	TrGC	$\text{HOCH}_2\text{CH}_2\text{O}_2 + \text{HO}_2 \rightarrow \text{HYETHO}_2\text{H}$	$2.00\text{E}-13 \cdot \text{EXP}(1250./\text{temp})$	Rickard and Pascoe (2009)
G4243	TrGNC	$\text{HOCH}_2\text{CH}_2\text{O}_2 + \text{NO} \rightarrow .24875 \text{HO}_2 + .4975 \text{HCHO} + .74625 \text{HOCH}_2\text{CH}_2\text{O} + .995 \text{NO}_2 + .005 \text{ETHOHO}_3$	KR02N0	Orlando et al. (1998)
G4245	TrGNC	$\text{ETHOHO}_3 + \text{OH} \rightarrow .93 + .93 \text{HO}_2 + .07 \text{HOCH}_2\text{CHO} + .07 \text{NO}_2 + \text{H}_2\text{O} + \text{POHORG}$	ks*(fsoh*fch2ono2+fono2*fpch2oh)+krohro	Taraborrelli (2013a)
G4246a	TrGC	$\text{HYETHO}_2\text{H} + \text{OH} \rightarrow \text{HOCH}_2\text{CH}_2\text{O}_2 + \text{H}_2\text{O} + \text{POHORG}$	0.6*k_CH300H_OH	Rickard and Pascoe (2009)
G4246b	TrGC	$\text{HYETHO}_2\text{H} + \text{OH} \rightarrow \text{HOCH}_2\text{CHO} + \text{OH} + \text{H}_2\text{O} + \text{POHORG} + \text{POHORG}$	ks*fsoh*fpch2oh	Taraborrelli (2013a)
G4246c	TrGC	$\text{HYETHO}_2\text{H} + \text{OH} \rightarrow \text{H}_2\text{O} + \text{H}_2\text{O}$	ks*fsoh*fpch2oh+krohro	Taraborrelli (2013a)
G4247a	TrGC	$\text{HOCH}_2\text{CH}_2\text{O} \rightarrow \text{HO}_2 + \text{HOCH}_2\text{CHO}$	$6.00\text{E}-14 \cdot \text{EXP}(-550./\text{temp}) \cdot C(\text{ind_O}_2)$	Orlando et al. (1998)
G4247b	TrGC	$\text{HOCH}_2\text{CH}_2\text{O} \rightarrow \text{HO}_2 + \text{HCHO} + \text{HCHO}$	$9.50\text{E}+13 \cdot \text{EXP}(-5988./\text{temp})$	Orlando et al. (1998)
G4248	TrGC	$\text{ETHGLY} + \text{OH} \rightarrow \text{HOCH}_2\text{CHO} + \text{HO}_2 + \text{H}_2\text{O} + \text{POHORG}$	$2 \cdot ks \cdot fsoh \cdot fpch2oh + 2 \cdot krohro$	Taraborrelli (2013a)
G4249e	TrGC	$\rightarrow 0.6 \text{HCHO} + 0.6 \text{CO} + 0.6 \text{HO}_2 + 0.2 \text{GLYOX} + 0.2 \text{HOCH}_2\text{CHO}$	2.00E-12*RD2	Taraborrelli (2013a)
G4250e	TrGC	$+ \text{HO}_2 \rightarrow 0.85 + 0.15 \text{HCHO} + 0.15 \text{CO} + 0.15 \text{HO}_2 + 0.15 \text{OH} + .15 \text{POHORG}$	KR02H02*0.387	Taraborrelli (2013a)

5

B. Chemical mechanism – MTM

Table 1: Gas phase reactions (... continued)

#	labels	reaction	rate coefficient	reference
G4251e	TrGC	+ NO → NO ₂ + HCHO + CO + HO ₂	KR02ND	Taraborrelli (2013a)
G4252e	TrGC	+ NO ₃ → HCHO + CO + HO ₂ + NO ₂	KR02ND3	Taraborrelli (2013a)
G4253e	TrGC	+ OH → .71 OH + .31 HCHO + .31 CO + .40 GLYOX + .29 + .71 POHORG + POHORG	0.6*k_CH300H_OH+ks*fsooh*fcho+.8*6E-12	Taraborrelli (2013a)
G4254e	TrGNC	+ NO ₂ → OH + HCHO + CO + HNO ₃ + POHORG	KNG3AL	Rickard and Pascoe (2009)
G4257e	TrGC	+ OH → HCHO + CO ₂ + NO ₂ + H ₂ O + POHORG	1.E-11	Paulot et al. (2009a),Taraborrelli (2013a)
G4258e	TrGNC	+ NO → NO ₂ + OH + HCHO + CO ₂ + POHORG	KAFND	Taraborrelli (2013a)
G4259e	TrGNC	+ NO ₃ → NO ₂ + OH + HCHO + CO ₂ + POHORG	KR02ND3*1.60	Taraborrelli (2013a)
G4260e	TrGC	+ HO ₂ → 2 OH + HCHO + CO ₂ + 2 POHORG	KAPH02*rco3_oh	Taraborrelli (2013a)
G4260et2	TrGC	+ HO ₂ →	KAPH02*rco3_ooH	Taraborrelli (2013a)*
G4260et3	TrGC	+ HO ₂ → + O ₃	KAPH02*rco3_o3	Taraborrelli (2013a)*
G4261e	TrGC	→ .7 OH + .7 HCHO + .7 CO ₂ + .3 + .7 POHORG	1.00E-11*RD2	Taraborrelli (2013a)
G4262e	TrGC	+ OH → + H ₂ O + POHORG	2.*0.6*k_CH300H_OH	Taraborrelli (2013a)
G4263e	TrGC	+ OH → HCOCO ₂ H + OH + H ₂ O + POHORG + POHORG	ks*fsooh*fco2h	Taraborrelli (2013a)
G4265e	TrGC	+ OH → HCOCO ₂ H + OH + H ₂ O + POHORG + POHORG	ks*fsooh*fco2h+kco2h	Taraborrelli (2013a)
G4266e	TrGC	+ OH → .6 HCHO + .6 HO ₂ + .6 CO + .4 + POHORG	2.8E-12*exp(510./temp)	Baulch et al. (2005),Taraborrelli (2013a)*
G4267e	TrGC	+ OH → CH ₃ COOH + OH + POHORG + POHORG	kt*ftooh*ftoh + krohro	Taraborrelli (2013a)
G4268e	TrGC	+ OH → + POHORG	0.6*k_CH300H_OH	Taraborrelli (2013a)
G4269e	TrGC	→ CH ₃ CHO + HO ₂	3.46E12*EXP(-12500./(1.98*temp))	Hermans et al. (2005),Taraborrelli (2013a)
G4270e	TrGC	CH ₃ CHO + HO ₂ →	3.46E12*EXP(-12500./(1.98*temp)) /(6.34E26*EXP(-14700./(1.98*temp)))	Hermans et al. (2005),Taraborrelli (2013a)
G4271e	TrGC	+ HO ₂ → .5 + .3 CH ₃ COOH + .2 CH ₃ O ₂ + .2 HCOOH + .2 OH	5.6E-15*EXP(2300./temp)	Taraborrelli (2013a)
G4272e	TrGC	→ CH ₃ O ₂ + HCOOH + OH	1.4E-12*RD2	Taraborrelli (2013a)
G4273e	TrGC	+ NO → CH ₃ O ₂ + HCOOH + OH + NO ₂	KR02ND	Taraborrelli (2013a)
G4300	TrGC	C ₃ H ₈ + OH → .736 iC ₃ H ₇ O ₂ + .264 C ₂ H ₅ O ₂ + .264 CO ₂ + .264 HO ₂ + H ₂ O + POHORG	1.55E-17*temp*temp*EXP(-61./temp)	Rickard and Pascoe (2009)*

6

Table 1: Gas phase reactions (... continued)

#	labels	reaction	rate coefficient	reference
G4301et2	TrGC	C ₂ H ₆ + O ₂ → .0855 + .4389 CH ₃ CHO + .4389 H ₂ O ₂ + .0456 CH ₃ COOH + .285 + .0855 CH ₄ + .0855 CO ₂ + .0342 + .0513 CH ₃ OH + .0228 CH ₃ C(O)OO + .57 HCHO + .2709 CO + .0688 HO ₂ + .1591 HOCH ₂ OOH + .43 CH ₃ CHO + .3766 OH + .3766 POHORG	6.5E-15*EXP(-1900./temp)	Taraborrelli (2013a)
G4302	TrGC	C ₃ H ₆ + OH → HYPROPO2 + POHORG	K_3rd(temp, cair, 8.E-27, 3.5, 3.E-11, 0., 0.5)	Atkinson et al. (1999)
G4303	TrGNC	C ₃ H ₆ + NO ₃ → PRONO3BO2	4.6E-13*EXP(-1155./temp)	Atkinson et al. (1999)
G4304	TrGC	iC ₃ H ₇ O ₂ + HO ₂ → iC ₃ H ₇ OOH	1.9E-13*EXP(1300./temp)	Atkinson (1997)*
G4305	TrGNC	iC ₃ H ₇ O ₂ + NO → .96 CH ₃ COCH ₃ + .96 HO ₂ + .96 NO ₂ + .04 iC ₃ H ₇ ONO ₂	2.7E-12*EXP(360./temp)	Atkinson et al. (1999)
G4306	TrGC	iC ₃ H ₇ O ₂ → CH ₃ COCH ₃ + .8 HO ₂	4.E-14*RD2	Rickard and Pascoe (2009)*
G4307	TrGC	iC ₃ H ₇ OOH + OH → .27 iC ₃ H ₇ O ₂ + .73 CH ₃ COCH ₃ + .73 OH + H ₂ O + .73 POHORG + POHORG	1.66E-11 + 0.6*k_CH300H_OH	Rickard and Pascoe (2009)*
G4311	TrGC	CH ₃ COCH ₃ + OH → CH ₃ COCH ₂ O ₂ + H ₂ O + POHORG	1.33E-13+3.82E-11*EXP(-2000./temp)	Sander et al. (2003)
G4312e	TrGC	CH ₃ COCH ₂ O ₂ + HO ₂ → .15 OH + .15 CH ₃ C(O)OO + .15 HCHO + .85 CH ₃ COCH ₂ O ₂ H + .15 POHORG	8.6E-13*EXP(700./temp)	Taraborrelli (2013a)
G4313	TrGNC	CH ₃ COCH ₂ O ₂ + NO → CH ₃ C(O)OO + HCHO + NO ₂	2.9E-12*EXP(300./temp)	Sander et al. (2003)
G4314	TrGC	CH ₃ COCH ₂ O ₂ → .6 CH ₃ C(O)OO + .6 HCHO + .2 MGLYOX + .2 CH ₃ COCH ₂ OH	7.5E-13*EXP(500./temp)*2.*RD2	Tyndall et al. (2001)
G4321	TrGNC	CH ₃ COCH ₂ O ₂ + NO ₃ → CH ₃ C(O)OO + HCHO + NO ₂	KR02ND3	Rickard and Pascoe (2009)
G4315a	TrGC	CH ₃ COCH ₂ O ₂ H + OH → CH ₃ COCH ₂ O ₂ + H ₂ O + POHORG	0.6*k_CH300H_OH	Rickard and Pascoe (2009)*
G4315b	TrGC	CH ₃ COCH ₂ O ₂ H + OH → MGLYOX + OH + H ₂ O + POHORG + POHORG	ks*fsooh*fco	Taraborrelli (2013a)
G4316e	TrGC	CH ₃ COCH ₂ OH + OH → + H ₂ O + POHORG	1.60E-12*EXP(305./temp)	Taraborrelli (2013a)
G4336ea	TrGC	→ MGLYOX + HO ₂	0.8485	Taraborrelli (2013a)
G4317e	TrGC	MGLYOX + OH → .4 CH ₃ O ₂ + .6 CH ₃ C(O)OO + 1.4 CO + POHORG	1.9E-12*EXP(575./temp)	Baeza-Romero et al. (2007),IU-PAC (2013)
G4331	TrGNC	MGLYOX + NO ₃ → CH ₃ C(O)OO + CO + HNO ₃	KNG3AL*2.4	Rickard and Pascoe (2009)
G4320	TrGNC	iC ₃ H ₇ ONO ₂ + OH → CH ₃ COCH ₃ + NO ₂ + POHORG	6.2E-13*EXP(-230./temp)	Atkinson et al. (1999)
G4322	TrGC	HYPROPO2 → CH ₃ CHO + HCHO + HO ₂	8.80E-13*RD2	Rickard and Pascoe (2009)
G4323	TrGC	HYPROPO2 + HO ₂ → HYPROPO2H	KR02HD2*0.520	Rickard and Pascoe (2009)
G4324	TrGNC	HYPROPO2 + NO → CH ₃ CHO + HCHO + HO ₂ + NO ₂	KR02ND	Rickard and Pascoe (2009)
G4325	TrGNC	HYPROPO2 + NO ₃ → CH ₃ CHO + HCHO + HO ₂ + NO ₂	KR02ND3	Rickard and Pascoe (2009)

7

Table 1: Gas phase reactions (... continued)

#	labels	reaction	rate coefficient	reference
G4326a	TrGC	HYPROPO2H + OH → HYPROPO2 + POHORG	0.6*k_CH300H_OH	Rickard and Pascoe (2009)
G4326b	TrGC	HYPROPO2H + OH → CH ₃ COCH ₂ OH + OH + POHORG + POHORG	ks*fsoh*fpch2oh+kt*ftooh*fpch2oh	Taraborrelli (2013a)
G4327	TrGNC	PRONO3BO2 + HO ₂ → PR2O2HNO3	KR02HD2*0.520	Rickard and Pascoe (2009)
G4328	TrGNC	PRONO3BO2 + NO → NOA + HO ₂ + NO ₂	KR02ND0	Rickard and Pascoe (2009)
G4329	TrGNC	PRONO3BO2 + NO ₃ → NOA + HO ₂ + NO ₂	KR02ND3	Rickard and Pascoe (2009)
G4330a	TrGNC	PR2O2HNO3 + OH → PRONO3BO2 + POHORG	1.90E-12*EXP(190./temp)	Rickard and Pascoe (2009)
G4330b	TrGNC	PR2O2HNO3 + OH → NOA + OH + POHORG + POHORG	kt*ftooh*fch2ono2	Rickard and Pascoe (2009)
G4332	TrGNC	NOA + OH → MGLYOX + NO ₂ + POHORG	ks*fco*fono2+kp*fco	Taraborrelli (2013a)
G4333e	TrGC	HOCH2COCHO + OH → .8609 + .8609 CO + .1391 + .1391 HO ₂ + POHORG	1.9E-12*EXP(575./temp)+ks*fsoh*fco	Taraborrelli (2013a)
G4334e	TrGNC	HOCH2COCHO + NO ₃ → + CO + HNO ₃	KN03AL*2.4	Taraborrelli (2013a)
G4337e	TrGC	+ OH → CH ₃ C(O)OO + H ₂ O + CO ₂ + POHORG	4.9E-14*EXP(276./temp)	Mellouki and Taraborrelli (2013a)
G4338e	TrGC	→ HCHO +	R02*2.0E-12	Taraborrelli (2013a)
G4339e	TrGC	+ HO ₂ → .15 HCHO + .15 + .15 OH + .85 + .15 POHORG	KR02HD2*0.520	Taraborrelli (2013a)
G4340e	TrGC	+ NO → HCHO + + NO ₂	KR02ND0	Taraborrelli (2013a)
G4341e	TrGC	+ OH → HOCH2COCHO + OH + POHORG + POHORG	ks*fsooh*fco	Taraborrelli (2013a)
G4342e	TrGC	+ OH → + POHORG	.6*k_CH300H_OH	Taraborrelli (2013a)
G4343e	TrGC	+ OH → + HO ₂ + POHORG	0.9295*1.60E-12*EXP(305./temp)	Taraborrelli (2013a)
G4344e	TrGC	→ 0.6 + 0.6 HCHO + 0.2 + 0.2 HOCH2COCHO	2.00E-12*R02	Taraborrelli (2013a)
G4345e	TrGC	+ NO → + HCHO + NO ₂	KR02ND0	Taraborrelli (2013a)
G4346e	TrGC	+ HO ₂ → 0.85 + 0.15 + 0.15 HCHO + 0.15 OH + .15 POHORG	KR02HD2*0.520	Taraborrelli (2013a)
G4347e	TrGC	+ NO ₃ → + HCHO + NO ₂	KR02ND3	Taraborrelli (2013a)
G4348e	TrGC	+ OH → + CO + H ₂ O + POHORG	kt*fco*fco	Taraborrelli (2013a)
G4349e	TrGC	+ OH → + OH + H ₂ O + POHORG + POHORG	ks*fsooh*fco	Taraborrelli (2013a)
G4350e	TrGC	+ OH → + H ₂ O + POHORG	0.6*k_CH300H_OH	Taraborrelli (2013a)
G4351e	TrGC	+ NO ₃ → + CO + HNO ₃	KN03AL*2.4	Taraborrelli (2013a)
G4352e	TrGC	+ OH → + CO + POHORG	2*kt*fco*fco	Taraborrelli (2013a)
G4353e	TrGC	+ OH → .72 CO + .72 CH ₃ CHO + .72 HO ₂ + .21 + .07 CH ₃ CHO + .07 HO ₂ + .07 CO ₂ + POHORG	7.6E-11	Hatakeyama et al. (1985), Taraborrelli (2013a)*

8

Table 1: Gas phase reactions (... continued)

#	labels	reaction	rate coefficient	reference
G4354e	TrGC	+ OH → CO + + POHORG	1E-10*acho	Hatakeyama et al. (1985), Taraborrelli (2013a)*
G4355e	TrGC	+ OH → CO + + POHORG	7.6E-11*acoch3	Hatakeyama et al. (1985), Taraborrelli (2013a)*
G4400	TrGC	nC ₄ H ₁₀ + OH → LC ₄ H ₉ O ₂ + H ₂ O + POHORG	1.81E-17*temp*temp*EXP(114./temp)	Atkinson (2003)*
G4401	TrGC	LC ₄ H ₉ O ₂ → 0.254 CO ₂ + 0.5552 MEK + 0.5552 HO ₂ + 0.3178 CH ₃ CHO + 0.4448 C ₂ H ₅ O ₂	2.5E-13*R02	Rickard and Pascoe (2009)*
G4402	TrGC	LC ₄ H ₉ O ₂ + HO ₂ → LC ₄ H ₉ OOH	KR02HD2*0.625	Rickard and Pascoe (2009)
G4403	TrGNC	LC ₄ H ₉ O ₂ + NO → 0.9172 NO ₂ + 0.233 CO ₂ + 0.5092 MEK + 0.5092 HO ₂ + 0.2915 CH ₃ CHO + 0.408 C ₂ H ₅ O ₂ + 0.0828 LC4H9NO3	KR02ND0	Rickard and Pascoe (2009)*
G4404	TrGC	LC ₄ H ₉ OOH + OH → 0.2285796 LC ₄ H ₉ O ₂ + 0.7117253 MEK + 0.1193902 CO ₂ + 0.0596951 C ₂ H ₅ O ₂ + 0.7714204 OH + H ₂ O + .7714204 POHORG + POHORG	2.636E-11	Rickard and Pascoe (2009)*
G4405e	TrGC	MVK + O ₃ → .87 MGLYOX + 0.5481 CO + 0.1392 HO ₂ + 0.1392 OH + 0.3219 HOCH2OOH + .13 HCHO + 0.04680 OH + 0.04680 CO + 0.07280 CH ₃ C(O)OO + .026 CH ₃ CHO + .026 CO ₂ + .026 HCHO + .026 HO ₂ + 0.02402 MGLYOX + 0.02402 H ₂ O ₂ + 0.007176 + 0.1860 POHORG	8.5E-16*EXP(-1520./temp)	Taraborrelli (2013a)
G4406e	TrGC	MVK + OH → LHMVKABO2 + POHORG	2.6E-12*EXP(610./temp)	Taraborrelli (2013a)*
G4413	TrGC	MEK + OH → LMEKO2 + H ₂ O + POHORG	3.24E-18*temp*temp*EXP(414./temp)	Rickard and Pascoe (2009)*
G4414ea	TrGC	LMEKO2 + HO ₂ → LMEKOOH	KR02HD2*0.625*rcoch2o2_ooH	Taraborrelli (2013a)
G4414eb	TrGC	LMEKO2 + HO ₂ → 0.538 HCHO + 0.538 CO ₂ + 0.459 HOCH ₂ CH ₂ O ₂ + 0.079 C ₂ H ₅ O ₂ + 0.462 CH ₃ C(O)OO + 0.462 CH ₃ CHO + OH + POHORG	KR02HD2*0.625*rcoch2o2_oh	Taraborrelli (2013a)
G4415	TrGNC	LMEKO2 + NO → 0.538 HCHO + 0.538 CO ₂ + 0.459 HOCH ₂ CH ₂ O ₂ + 0.079 C ₂ H ₅ O ₂ + 0.462 CH ₃ C(O)OO + 0.462 CH ₃ CHO + NO ₂	KR02ND0	Rickard and Pascoe (2009)*
G4416	TrGC	LMEKOOH + OH → 0.40851 CH ₃ COCH ₂ O ₂ + 0.350196 BIACET + 0.807212 OH + 0.048506 C ₂ H ₅ O ₂ + 0.505522 CO ₂ + 0.192788 LMEKO2 + H ₂ O + .807212 POHORG + POHORG	3.786E-11	Rickard and Pascoe (2009)*
G4417	TrGNC	LC4H9NO3 + OH → 0.91423 MEK + 0.08577 C ₂ H ₅ O ₂ + 0.17154 CO ₂ + NO ₂ + H ₂ O + POHORG	9.598E-13	Rickard and Pascoe (2009)*

9

B. Chemical mechanism – MTM

Table 1: Gas phase reactions (... continued)

#	labels	reaction	rate coefficient	reference
G4418	TrGNC	MPAN + OH → CH ₃ COCH ₂ OH + CO + NO ₂ + POHORG	3.2E-11	Orlando et al. (2002)
G4419	TrGNC	MPAN → MACO3 + NO ₂	k_PAN_M	see note
G4420	TrGC	LMEKO2 → 0.538 HCHO + 0.538 CO ₂ + 0.459 HOCH ₂ CH ₂ O ₂ + 0.079 C ₂ H ₅ O ₂ + 0.462 CH ₃ C(O)OO + 0.462 CH ₃ CHO	1.483E-12*R02	Rickard and Pascoe (2009)*
G4421e	TrGC	MACR + OH → .45 MACO3 + .55 MACRO2 + POHORG	8.E-12*EXP(380./temp)	Orlando et al. (1999b), Taraborrelli (2013a)
G4422e	TrGC	MACR + O ₃ → 0.5481 CO + 0.1392 HO ₂ + 0.1392 OH + 0.3219 HOCH ₂ OOH + .87 MGLYOX + .13 HCHO + .13 OH + .065 + .065 CO + .065 CH ₃ C(O)OO + 0.2692 POHORG	1.36E-15*EXP(-2112./temp)	Taraborrelli (2013a)
G4423	TrGNC	MACR + NO ₃ → MACO3 + HNO ₃	KN03AL*2.0	Rickard and Pascoe (2009)
G4424e	TrGC	MACO3 → .7 + .3 MACO2H	1.00E-11*R02	Taraborrelli (2013a)
G4425e	TrGC	MACO3 + HO ₂ → + OH + POHORG	KAPH02*rc03_oh	Taraborrelli (2013a)
G4425et2	TrGC	MACO3 + HO ₂ → MACO3H	KAPH02*rc03_ohh	Taraborrelli (2013a)
G4425et3	TrGC	MACO3 + HO ₂ → MACO2H + O ₃	KAPH02*rc03_o3	Taraborrelli (2013a)
G4426e	TrGNC	MACO3 + NO → + NO ₂	8.70E-12*EXP(290./temp)	Taraborrelli (2013a)
G4427	TrGNC	MACO3 + NO ₂ → MPAN	k_CH3CO3_N02	Rickard and Pascoe (2009)
G4428e	TrGNC	MACO3 + NO ₃ → + NO ₂	KR02N03*1.60	Taraborrelli (2013a)
G4429e	TrGC	MACRO2 → .7 CH ₃ COCH ₂ OH + .7 HO ₂ + .3 MACROH	9.20E-14*R02	Taraborrelli (2013a)
G4430e	TrGC	MACRO2 + HO ₂ → + OH + POHORG	KR02H02*0.625*rc0ch2o2_oh	Taraborrelli (2013a)
G4430et2	TrGC	MACRO2 + HO ₂ → MACROOH	KR02H02*0.625*rc0ch2o2_ohh	Taraborrelli (2013a)
G4431e	TrGNC	MACRO2 + NO → .85 + .85 NO ₂ + .15	KR02N0	Taraborrelli (2013a)
G4432e	TrGNC	MACRO2 + NO ₃ → + NO ₂	KR02N03	Taraborrelli (2013a)
G4433ea	TrGC	MACROOH + OH → MACRO2 + POHORG	0.6*k_CH300H_OH	Taraborrelli (2013a)
G4433eb	TrGC	MACROOH + OH → CO + OH + CH ₃ COCH ₂ OH + POHORG + POHORG	kt*fco*ftch2oh*falk	Taraborrelli (2013a)
G4433ec	TrGC	MACROOH + OH → CO + MGLYOX + HO ₂ + POHORG	ks*fsoh*fpch2oh + krohro	Taraborrelli (2013a)
G4434e	TrGC	MACROH + OH → CH ₃ COCH ₂ OH + CO + HO ₂ + POHORG	kt*fco*ftch2oh*falk	Taraborrelli (2013a)
G4434et2	TrGC	→ .85 CH ₃ COCH ₂ OH + .885 CO + .115 MGLYOX + .115 HCHO + HO ₂	KDEC	Taraborrelli (2013a)

10

Table 1: Gas phase reactions (... continued)

#	labels	reaction	rate coefficient	reference
G4435e	TrGC	MACO2H + OH → CH ₃ COCH ₂ OH + HO ₂ + CO ₂ + POHORG	(kadt*kadp)*aco2h*kco2h	Taraborrelli (2013a)
G4436e	TrGC	MACO3H + OH → CH ₃ COCH ₂ OH + CO ₂ + OH + POHORG + POHORG	0.6*k_CH300H_OH*(kadt*kadp)*aco2h	Taraborrelli (2013a)
G4437e	TrGC	LHMVKABO2 → .024 CO ₂ H ₃ CHO + .072 + .072 HCHO + .5280 CH ₃ C(O)OO + .5280 HOCH ₂ CHO + .176 BIACETOH + .2 HO ₁₂ CO ₃ C4	1.014E-12*R02	Taraborrelli (2013a)*
G4438e	TrGC	LHMVKABO2 + HO ₂ → OH + HOCH ₂ CHO + CH ₃ C(O)OO + POHORG	KR02H02*0.625*.88*rc0ch2o2_oh	Taraborrelli (2013a)
G4438et2	TrGC	LHMVKABO2 + HO ₂ → LHMVKABOOH	KR02H02*0.625*(.12+.88*rc0ch2o2_ohh)	Taraborrelli (2013a)
G4439ea	TrGNC	LHMVKABO2 + NO → .12 + .88 HOCH ₂ CHO + .88 CH ₃ C(O)OO + .12 HCHO + NO ₂	KR02N0*(1.-0.11)	Taraborrelli (2013a)*
G4439eb	TrGNC	LHMVKABO2 + NO →	KR02N0*0.11	Taraborrelli (2013a)
G4440e	TrGNC	LHMVKABO2 + NO ₃ → .12 MGLYOX + .88 HOCH ₂ CHO + .88 CH ₃ C(O)OO + .12 HCHO + .12 HO ₂ + NO ₂	KR02N03	Taraborrelli (2013a)*
G4441e	TrGC	LHMVKABOOH + OH → .12 CO ₂ H ₃ CHO + .88 BIACETOH + OH + POHORG + POHORG	0.6*k_CH300H_OH*.12*ks*fsoh*fpch2oh+.88*kt*ft0oh*fpch2oh*fco	Taraborrelli (2013a)*
G4449e	TrGC	CO ₂ H ₃ CHO + OH → CO ₂ H ₃ CO ₃ + POHORG	kt*fco*falk	Taraborrelli (2013a)
G4449et2	TrGC	CO ₂ H ₃ CHO + OH → + HO ₂ + H ₂ O + POHORG	kt*fco*ftoh*fcho	Taraborrelli (2013a)
G4450	TrGNC	CO ₂ H ₃ CHO + NO ₃ → CO ₂ H ₃ CO ₃ + HNO ₃	KN03AL*4.0	Rickard and Pascoe (2009)
G4451e	TrGC	CO ₂ H ₃ CO ₃ → + CO ₂	1.00E-11*R02	Taraborrelli (2013a)
G4452e	TrGC	CO ₂ H ₃ CO ₃ + HO ₂ → OH + + CO ₂ + POHORG	KAPH02*rc03_oh	Taraborrelli (2013a)
G4452et2	TrGC	CO ₂ H ₃ CO ₃ + HO ₂ → + O ₃	KAPH02*rc03_o3	Taraborrelli (2013a)
G4452et3	TrGC	CO ₂ H ₃ CO ₃ + HO ₂ → CO ₂ H ₃ CO ₃ H	KAPH02*rc03_ohh	Taraborrelli (2013a)
G4453e	TrGNC	CO ₂ H ₃ CO ₃ + NO → + NO ₂ + CO ₂	KAPN0	Taraborrelli (2013a)
G4454e	TrGNC	CO ₂ H ₃ CO ₃ + NO ₃ → + NO ₂ + CO ₂	KR02N03*1.60	Taraborrelli (2013a)
G4455e	TrGC	CO ₂ H ₃ CO ₃ H + OH → 0.5127 CO ₂ H ₃ CO ₃ + 0.4873 CH ₃ C(O)OO + 0.4873 CO + 0.4873 CO ₂ + 0.4873 OH + POHORG + 0.4873 POHORG	kt*fco2h*fco*ftoh+0.6*k_CH300H_OH	Taraborrelli (2013a)*
G4455t2	TrGC	+ OH → + HO ₂ + POHORG	kt*fco2h*fco*ftoh+kco2h	Taraborrelli (2013a)
G4456a	TrGC	HO ₁₂ CO ₃ C4 + OH → BIACETOH + HO ₂ + POHORG	kt*ftoh*falk*fco	Taraborrelli (2013a)
G4456b	TrGC	HO ₁₂ CO ₃ C4 + OH → CO ₂ H ₃ CHO + HO ₂ + POHORG	ks*fsoh*falk	Taraborrelli (2013a)
G4457e	TrGC	→ .65 CH ₃ O ₂ + .65 CO + .65 HCHO + .35 OH + .35 CH ₃ COCH ₂ O ₂ + CO ₂ + .35 POHORG	KDEC	Taraborrelli (2013a)

11

Table 1: Gas phase reactions (... continued)

#	labels	reaction	rate coefficient	reference
G4458e	TrGC	LHMVKABO2 → .88 MGLYOX + .88 HCHO + .12 + .12 CH ₃ C(O)OO + OH + POHORG	KHSD	Taraborrelli (2013a)
G4459e	TrGNC	MACRO2 → MGLYOX + HCHO + OH + POHORG	KHSB	Taraborrelli (2013a)
G4460e	TrGNC	+ OH → .7 MGLYOX + .7 HCOOH + .7 NO ₃ + .3 CO ₂ H ₃ CHO + .3 NO ₂ + H ₂ O + POHORG	5.6E-12	Taraborrelli (2013a)
G4461e	TrGC	+ OH → .08 CH ₃ COOH + .08 HCHO + .15 NO ₂ + .07 HCOOH + .07 MGLYOX + .85 CH ₃ COCH ₂ OH + .85 NO ₃ + .93 CO ₂ + H ₂ O + POHORG	5.E-11	Taraborrelli (2013a)
G4462e	TrGC	→ .9 + .1 CH ₃ C(O)OO + .01 GLYOX + .18 CO + .09 HO ₂ + OH + POHORG	k16HS	Taraborrelli (2013a)*
G4463e	TrGC	→ + OH + POHORG	K16HS	Taraborrelli (2013a)
G4500e	TrGC	C ₅ H ₈ + O ₃ → .3508 MACR + 0.01518 MACO2H + .2440 MVK + .7085 HCHO + .11 HOCH ₂ OOH + .1275 C ₃ H ₆ + .1575 CH ₃ C(O)OO + .0510 CH ₃ O ₂ + 0.2625 HO ₂ + .27 OH + .09482 H ₂ O ₂ + .255 CO ₂ + .522 CO + 0.07182 HCHO + .03618 + .01782 CO + .27 POHORG	1.03E-14*EXP(-1995./temp)	Taraborrelli (2013a)*
G4501e	TrGC	C ₅ H ₈ + OH → .63 + .30 + .07 + POHORG	2.7E-11*EXP(390./temp)*(1.-iseg)	Taraborrelli (2013a)*
G4502	TrGNC	C ₅ H ₈ + NO ₃ → NISOPO2	3.15E-12*EXP(-450./temp)	Rickard and Pascoe (2009)
G4503e	TrGC	+ O ₂ → LISOPACO2	5.530E-13	Taraborrelli (2013a)*
G4504e	TrGC	+ O ₂ → ISOPBO2	3.E-12	Taraborrelli (2013a)*
G4505e	TrGC	+ O ₂ →	6.780E-13	Taraborrelli (2013a)*
G4506e	TrGC	+ O ₂ → ISOPDO2	3.E-12	Taraborrelli (2013a)*
G4507e	TrGC	LISOPACO2 → + O ₂	3.1E12*exp(-7900./temp)*.6+ 7.8E13*exp(-8600./temp)*.4	Taraborrelli (2013a)*
G4508e	TrGC	ISOPBO2 → + O ₂	3.7E14*exp(-9570./temp) +4.2E14*exp(-9970./temp)	Taraborrelli (2013a)*
G4509e	TrGC	→ + O ₂	5.65E12*exp(-8410./temp)*.42+ 1.4E14*exp(-9110./temp)*.58	Taraborrelli (2013a)*
G4510e	TrGC	ISOPDO2 → + O ₂	5.0E14*exp(-10120./temp) +8.25E14*exp(-10220./temp)	Taraborrelli (2013a)*
G4511e	TrGC	LISOPACO2 → + HO ₂	K16HS	Taraborrelli (2013a)
G4512e	TrGC	→ + HO ₂	K16HS	Taraborrelli (2013a)
G4513et3	TrGC	LISOPACO2 → .9 LHC4ACCHO + .8 HO ₂ + .1 ISOPAOH	2.4E-12*RD2	Rickard and Pascoe (2009)
G4514t2	TrGC	LISOPACO2 + HO ₂ → LISOPACOOH	.706*KR02H02	Rickard and Pascoe (2009)

12

Table 1: Gas phase reactions (... continued)

#	labels	reaction	rate coefficient	reference
G4515et2	TrGNC	LISOPACO2 + NO → 0.95 LHC4ACCHO + 0.95 HO ₂ + 0.95 NO ₂ + .05 LISOPACNO3	KR02N0	Lockwood et al. (2010),Taraborrelli (2013a)
G4506et3	TrGNC	LISOPACO2 + NO ₃ → LHC4ACCHO + HO ₂ + NO ₂	KR02N03	Rickard and Pascoe (2009)
G4507et3	TrGC	→ .9 LHC4ACCHO + .8 HO ₂ + .1 ISOPAOH	2.4E-12*RD2	Rickard and Pascoe (2009)
G4511et3	TrGC	+ HO ₂ → LISOPACOOH	.706*KR02H02	Rickard and Pascoe (2009)
G4512et3	TrGNC	+ NO → 0.95 LHC4ACCHO + 0.95 HO ₂ + 0.95 NO ₂ + .05 LISOPACNO3	KR02N0	Lockwood et al. (2010),Taraborrelli (2013a)
G4513et4	TrGNC	+ NO ₃ → LHC4ACCHO + HO ₂ + NO ₂	KR02N03	Rickard and Pascoe (2009)
G4514e	TrGC	LISOPACOOH + OH → LISOPACO2 + POHORG	0.6*k_CH300H_OH	Taraborrelli (2013a)
G4514et2	TrGC	LISOPACOOH + OH → + HO ₂ + POHORG	ks*fally1*fsoh	Taraborrelli (2013a)
G4514et3	TrGC	LISOPACOOH + OH → LHC4ACCHO + OH + POHORG + POHORG	ks*fs0oh*fally1+krohro	Taraborrelli (2013a)
G4514et4	TrGC	LISOPACOOH + OH → + OH + POHORG + POHORG	(kadt+kads)*ach2oh*ach2ooh	Taraborrelli (2013a)
G4515	TrGC	ISOPAOH + OH → LHC4ACCHO + HO ₂ + POHORG	(kadt+kads)*ach2oh*ach2oh+ ks*fs0oh*fally1+krohro	Taraborrelli (2013a)
G4516e	TrGNC	LISOPACNO3 + OH → + POHORG	9.5E-11	Paulot et al. (2009a),Taraborrelli (2013a)
G4517e	TrGC	ISOPBO2 → .8 MVK + .8 HCHO + .8 HO ₂ + .2 ISOPBOH	8.E-13*RD2	Rickard and Pascoe (2009)
G4518	TrGC	ISOPBO2 + HO ₂ → ISOPBOOH	.706*KR02H02	Rickard and Pascoe (2009)
G4519e	TrGNC	ISOPBO2 + NO → .947 MVK + .947 HCHO + .947 HO ₂ + .947 NO ₂ + .053 ISOPBNO3	KR02N0	Lockwood et al. (2010),Taraborrelli (2013a)
G4520e	TrGNC	ISOPBO2 + NO ₃ → MVK + .75 HCHO + .75 HO ₂ + .25 CH ₃ O ₂ + NO ₂	KR02N03	Rickard and Pascoe (2009)
G4521ea	TrGC	ISOPBOOH + OH → + OH + POHORG + POHORG	(kads+kadp)*ach2ooh	Paulot et al. (2009b),Taraborrelli (2013a)
G4521eb	TrGC	ISOPBOOH + OH → ISOPBO2 + POHORG	0.6*k_CH300H_OH	Taraborrelli (2013a)
G4521ec	TrGC	ISOPBOOH + O ₃ → 0.1368 MACROOH + 0.1368 H ₂ O ₂ + 0.2280 HO ₂ + 0.4332 CH ₃ COCH ₂ OH + 0.2280 CO ₂ + 0.6384 OH + 0.2052 CO + .57 HCHO + .43 MACROOH + 0.06880 HO ₂ + 0.06880 OH + 0.2709 CO + 0.1591 HOCH ₂ OOH + 0.7072 POHORG	1.E-17	Taraborrelli (2013a)*
G41911	TrGC	ISOPBOOH + OH → MGLYOX + HOCH ₂ CHO + POHORG	krohro+ks*falk*fs0h	Taraborrelli (2013a)
G4522e	TrGC	ISOPBOH + OH → MVK + .75 HCHO + .75 HO ₂ + .25 CH ₃ O ₂ + POHORG	ks*falk*fs0h+(kadp+kads)*ach2oh	Taraborrelli (2013a)

13

B. Chemical mechanism – MTM

Table 1: Gas phase reactions (... continued)

#	labels	reaction	rate coefficient	reference
G4523e	TrGNC	ISOPBNO3 + OH → + POHORG	1.3E-11	Paulot et al. (2009a),Taraborrelli (2013a)
G4524	TrGC	ISOPDO2 → .8 MACR + .8 HCHO + .8 HO2 + .1 HCOC5 + .1 ISOPDOH	2.9E-12* <i>R02</i>	Rickard and Pascoe (2009)
G4525	TrGC	ISOPDO2 + HO2 → ISOPDOOH	.706* <i>KR02H02</i>	Rickard and Pascoe (2009)
G4526e	TrGNC	ISOPDO2 + NO → .85 MACR + .85 HCHO + .85 HO2 + .85 NO2 + .15 ISOPDNO3	<i>KR02N0</i>	Lockwood et al. (2010),Taraborrelli (2013a)
G4527	TrGNC	ISOPDO2 + NO3 → MACR + HCHO + HO2 + NO2	<i>KR02N03</i>	Rickard and Pascoe (2009)
G4528ea	TrGC	ISOPDOOH + OH → + OH + POHORG + POHORG	(<i>kadt+kadp</i>)* <i>ach2ooh</i>	Paulot et al. (2009b),Taraborrelli (2013a)
G4528eb	TrGC	ISOPDOOH + OH → ISOPDO2 + POHORG	0.6*k_ <i>CH300H_OH</i>	Taraborrelli (2013a)
G4528ec	TrGC	ISOPDOOH + OH → HCOC5 + OH + POHORG + POHORG	<i>kt*ftoh*fallyl*fpch2oh</i>	Taraborrelli (2013a)
G4528ed	TrGC	ISOPDOOH + OH → CH3COCH2OH + GLYOX + OH + POHORG + POHORG	<i>ks*fpch2oh*fsoh</i>	Taraborrelli (2013a)
G45222	TrGC	ISOPDOOH + O3 → 1.393 OH + 1.393 POHORG + BIACETOH + .67 HCHO + 0.05280 HO2 + 0.2079 CO + 0.1221 HOCH2OOH	1.E-17	Taraborrelli (2013a)*
G4529e	TrGC	ISOPDOH + OH → HCOC5 + HO2 + POHORG	2.* <i>krohro</i> +(<i>kt*ftoh*fallyl*ks*fsoh</i>)* <i>fpch2oh</i> +(<i>kadt+kadp</i>)* <i>ach2oh</i>	Taraborrelli (2013a)
G4530e	TrGNC	ISOPDNO3 + OH → + POHORG	1.3E-11	Paulot et al. (2009a),Taraborrelli (2013a)
G4531	TrGNC	NISOP02 → .8 NC4CHO + .6 HO2 + .2 LISOPACNO3	1.3E-12* <i>R02</i>	Rickard and Pascoe (2009)
G4532	TrGNC	NISOP02 + HO2 → NISOP0OH	.706* <i>KR02H02</i>	Rickard and Pascoe (2009)
G4533	TrGNC	NISOP02 + NO → NC4CHO + HO2 + NO2	<i>KR02N0</i>	Rickard and Pascoe (2009)
G4534	TrGNC	NISOP02 + NO3 → NC4CHO + HO2 + NO2	<i>KR02N03</i>	Rickard and Pascoe (2009)
G4535	TrGNC	NISOP0OH + OH → NC4CHO + OH + POHORG + POHORG	1.03E-10	Rickard and Pascoe (2009)
G4536	TrGNC	NC4CHO + OH → LNISO3 + POHORG	4.16E-11	Rickard and Pascoe (2009)
G4537e	TrGNC	NC4CHO + O3 → .27 NOA + .027 HCOCO2H + .0162 GLYOX + .0162 H2O2 + .1458 + .0405 HCOOH + .0405 CO + .8758 OH + .8758 POHORG + .365 MGLYOX + .73 NO2 + 0.7705 HCHO + .4055 CO2 + .73 GLYOX	2.40E-17	Taraborrelli (2013a)*
G4538	TrGNC	NC4CHO + NO3 → LNISO3 + HNO3	<i>KN03AL*4.25</i>	Rickard and Pascoe (2009)
G4539	TrGNC	LNISO3 + HO2 → LNISOOH	.5*.706* <i>KR02H02</i> + .5* <i>KAPH02</i>	Rickard and Pascoe (2009)

14

Table 1: Gas phase reactions (... continued)

#	labels	reaction	rate coefficient	reference
G4540e	TrGNC	LNISO3 + NO → NOA + .5 + .5 CO + .5 HO2 + NO2 + .5 CO2	.5* <i>KAPN0</i> +.5* <i>KR02N0</i>	Rickard and Pascoe (2009)
G4541e	TrGNC	LNISO3 + NO3 → NOA + .5 + .5 CO + .5 HO2 + NO2 + .5 CO2	1.3* <i>KR02N03</i>	Rickard and Pascoe (2009)
G4542	TrGNC	LNISOOH + OH → LNISO3 + POHORG	2.65E-11	Rickard and Pascoe (2009)
G4543e	TrGC	LHC4ACCHO + OH → LC578O2 + POHORG	(<i>kadttertprim+kads</i>)* <i>acho*ach2oh</i>	Taraborrelli (2013a)
G4543et2	TrGC	LHC4ACCHO + OH → LHC4ACCO3 + POHORG	<i>kcho</i>	Taraborrelli (2013a)
G4543et3	TrGC	LHC4ACCHO + OH → + HO2 + POHORG	<i>ks*fsoh*fallyl</i>	Taraborrelli (2013a)
G4544	TrGC	LHC4ACCHO + O3 → .2225 CH3C(O)OO + .89 CO + .0171875 HOCH2CO2H + .075625 H2O2 + .0171875 HCOCO2H + .2775 CH3COCH2OH + .6675 HO2 + .2603125 GLYOX + .2225 HCHO + .89 OH + .2603125 HOCH2CHO + .5 MGLYOX + .89 POHORG	2.40E-17	Rickard and Pascoe (2009)
G4545	TrGNC	LHC4ACCHO + NO3 → LHC4ACCO3 + HNO3	<i>KN03AL*4.25</i>	Rickard and Pascoe (2009)
G4546e	TrGC	LC578O2 → .25 CH3COCH2OH + .75 MGLYOX + .25 + .75 HOCH2CHO + .75 HO2	9.20E-14* <i>R02</i>	Rickard and Pascoe (2009)
G4547e	TrGC	LC578O2 + HO2 → MGLYOX + HOCH2CHO + OH + POHORG	<i>KR02H02*0.706*rcoch2o2_oh</i>	Rickard and Pascoe (2009)
G4547et2	TrGC	LC578O2 + HO2 → LC578OOH	<i>KR02H02*0.706*rcoch2o2_ooH</i>	Rickard and Pascoe (2009)
G4548e	TrGNC	LC578O2 + NO → .25 CH3COCH2OH + .75 MGLYOX + .25 + .75 HOCH2CHO + .75 HO2 + NO2	<i>KR02N0</i>	Rickard and Pascoe (2009)
G4549e	TrGNC	LC578O2 + NO3 → .25 CH3COCH2OH + .75 MGLYOX + .25 + .75 HOCH2CHO + .75 HO2 + NO2	<i>KR02N03</i>	Rickard and Pascoe (2009)
G4586e	TrGC	LC578O2 → .25 CH3COCH2OH + .75 MGLYOX + .25 HOCH2CHO + .75 HOCH2CHO + HO2 + OH + POHORG	<i>KHSB</i>	Taraborrelli (2013a)
G4550e	TrGC	LC578OOH + OH → LC578O2 + POHORG	0.6*k_ <i>CH300H_OH</i>	Taraborrelli (2013a)*
G4550et2	TrGC	LC578OOH + OH → + HO2 + POHORG	<i>kt*fof*ftch2oh*falk*</i> <i>kt*ftoh*fpch2oh*fpch2oh*</i> <i>ks*fsoh*fpch2oh</i>	Taraborrelli (2013a)*
G4551e	TrGC	LHC4ACCO3 → .3 LHC4ACCO2H + .7 OH + .35 MACRO2 + .35 LHMVKABO2 + .7 CO2 + .7 POHORG	1.00E-11* <i>R02</i>	Taraborrelli (2013a)*
G4552e	TrGC	LHC4ACCO3 + HO2 → 2 OH + .5 MACRO2 + .5 LHMVKABO2 + CO2 + 2 POHORG	<i>KAPH02*rc03_oh</i>	Taraborrelli (2013a)*
G4552et2	TrGC	LHC4ACCO3 + HO2 → LHC4ACCO3H	<i>KAPH02*rc03_ooH</i>	Taraborrelli (2013a)

15

Table 1: Gas phase reactions (... continued)

#	labels	reaction	rate coefficient	reference
G4552et3	TrGC	LHC4ACCO3 + HO ₂ → LHC4ACCO2H + O ₃	KAPH02*cco3_o3	Taraborrelli (2013a)
G4553e	TrGNC	LHC4ACCO3 + NO → .5 MACRO2 + .5 LHMVKABO2 + NO ₂ + CO ₂	KAPNO	Taraborrelli (2013a)*
G4554	TrGNC	LHC4ACCO3 + NO ₂ → LC5PAN1719	k_CH3CO3_NO2	Rickard and Pascoe (2009)
G4555e	TrGNC	LHC4ACCO3 + NO ₃ → .5 MACRO2 + .5 LHMVKABO2 + NO ₂ + CO ₂	1.6*KR02N03	Taraborrelli (2013a)*
G4556e	TrGC	LHC4ACCO2H + OH → OH + .5 MACRO2 + .5 LHMVKABO2 + CO ₂ + POHORG + POHORG	2.52E-11	Taraborrelli (2013a)
G4557	TrGC	LHC4ACCO3H + OH → LHC4ACCO3 + POHORG	2.88E-11	Rickard and Pascoe (2009)
G4558	TrGNC	LC5PAN1719 → LHC4ACCO3 + NO ₂	k_PAN_M	Rickard and Pascoe (2009)
G4559	TrGNC	LC5PAN1719 + OH → .5 MACROH + .5 HO12CO3C4 + CO + NO ₂ + POHORG	2.52E-11	Rickard and Pascoe (2009)
G4560a	TrGC	HCOC5 + OH → C59O2 + POHORG	3.81E-11	Rickard and Pascoe (2009)
G4560eb	TrGC	HCOC5 + O ₃ → BIACETOH + .335 H ₂ O ₂ + 0.67 HCHO + 0.2079 CO + 0.1221 HOCH2OOH + 0.05280 OH + 0.0528 POHORG	7.51E-16*EXP(-1521./temp)	Taraborrelli (2013a)
G4561	TrGC	C59O2 → CH ₃ COCH ₂ OH +	9.20E-14*R02	Taraborrelli (2013a)
G4562e	TrGC	C59O2 + HO ₂ → OH + CH ₃ COCH ₂ OH + POHORG	KR02H02*0.706*rcoch2o2_oh	Taraborrelli (2013a)
G4562et2	TrGC	C59O2 + HO ₂ → C59OOH	KR02H02*0.706*rcoch2o2_ooH	Taraborrelli (2013a)
G4563	TrGNC	C59O2 + NO → CH ₃ COCH ₂ OH + NO ₂	KR02N0	Taraborrelli (2013a)
G4564	TrGNC	C59O2 + NO ₃ → CH ₃ COCH ₂ OH + NO ₂	KR02N03	Taraborrelli (2013a)
G4565	TrGC	C59OOH + OH → C59O2 + POHORG	9.7E-12	Taraborrelli (2013a)
G4566e	TrGC	+ OH → LC578O2 + H ₂ O + POHORG	5.78E-11*EXP(-400/temp)	Paulot et al. (2009b), Taraborrelli (2013a)
G4567e	TrGC	ISOPBO2 → MVK + HCHO + OH + POHORG	KHSB	Taraborrelli (2013a)
G4568e	TrGC	ISOPDO2 → MACR + HCHO + OH + POHORG	KHSD	Taraborrelli (2013a)
G4577ea	TrGC	+ OH → .6 + .4 + POHORG	kadt*acho*ach2ooh	Taraborrelli (2013a)
G4577eb	TrGC	+ OH → .6 + .4 + POHORG	kads*acho*ach2ooh	Taraborrelli (2013a)
G4577e	TrGC	+ OH → + POHORG	kt*fo*falk*0.6*k_CH300H_OH	Taraborrelli (2013a)
G4577et2	TrGC	+ OH → OH + + POHORG + POHORG	ks*fsooh*fallyl	Taraborrelli (2013a)

16

Table 1: Gas phase reactions (... continued)

#	labels	reaction	rate coefficient	reference
G4577et3	TrGC	+ O ₂ → .4672 OH + .2336 + .2336 CO + 2336 CH ₃ C(O)OO + .4672 + .1728 MGLYOX + .1901 OH + .0864 GLYOX + .02765 + .02765 H ₂ O ₂ + .02592 CH ₃ OOH + .02592 CO ₂ + .01037 + .01555 HOCH2OOH + .01555 CO + .006912 + .2628 OH + .1314 MGLYOX + .1314 OH + .1314 + 0.2628 GLYOX + .0972 CH ₃ COCH ₂ O ₂ H + .00972 HCOCO ₂ H + .005832 GLYOX + .005832 H ₂ O ₂ + .05249 OH + .05249 + .01458 HCHO + .01458 CO ₂ + .01458 HCOOH + .01458 CO + 1.104 POHORG	2.4E-17	Taraborrelli (2013a)*
G4578e	TrGC	→ .78 CH ₃ COCH ₂ O ₂ H + .78 + .22 CO2H3CHO + .22 HCHO + .22 OH + .22 POHORG	8.00E-13*R02	Taraborrelli (2013a)
G4579e	TrGC	+ NO → .78 CH ₃ COCH ₂ O ₂ H + .78 + .22 CO2H3CHO + .22 HCHO + .22 OH + .22 POHORG + NO ₂	KR02N0	Taraborrelli (2013a)
G4580e	TrGC	+ HO ₂ →	KR02H02*0.706	Taraborrelli (2013a)
G4580ea	TrGC	→ CH ₃ COCH ₂ O ₂ H + GLYOX + OH + POHORG	KHSB	Taraborrelli (2013a)
G4581e	TrGC	→ OH + + POHORG	K15SHSDHB	Taraborrelli (2013a)
G4581et2	TrGC	+ OH → + OH + POHORG + POHORG	ks*fsooh*fpch2oh	Taraborrelli (2013a)
G4581et3	TrGC	+ OH → CH ₃ COCH ₂ O ₂ H + OH + 2 CO + 2 HO ₂ + POHORG + POHORG	kt*ftoh*fpch2oh*fpch2oh	Taraborrelli (2013a)
G4581et4	TrGC	+ OH → + POHORG	0.6*k_CH300H_OH	Taraborrelli (2013a)
G4581et6	TrGC	→ MGLYOX + + HO ₂	2.90E-12*R02	Taraborrelli (2013a)
G4581et7	TrGC	+ NO → MGLYOX + + HO ₂ + NO ₂	KR02N0	Taraborrelli (2013a)
G4581et8	TrGC	+ HO ₂ → .5 CH ₃ C(O)OO + .5 CO + .5 MGLYOX + .5 HO ₂ +	KR02H02*0.706	Taraborrelli (2013a)*
G4581et9	TrGC	→ MGLYOX + OH + + POHORG	KHSD	Taraborrelli (2013a)
G4581et10	TrGC	→ .625 MGLYOX + 2 CO + 1.625 HO ₂ + .375 CH ₃ C(O)OO + .375 CO ₂ + OH + POHORG	K15SHSDHB	Taraborrelli (2013a)*
G4582e	TrGC	LHC4ACCO3 → + HO ₂	K16HS	Taraborrelli (2013a)
G4583e	TrGC	+ OH → + POHORG	2*kt*fo*falk*(kadt*kads)*acho*acho	Taraborrelli (2013a)
G4584e	TrGC	+ HO ₂ → OH + POHORG + MGLYOX +	KR02H02*0.706*rcoch2o2_oh	Taraborrelli (2013a)
G4584et2	TrGC	+ HO ₂ →	KR02H02*0.706*rcoch2o2_ooH	Taraborrelli (2013a)
G4585e	TrGC	+ NO → NO ₂ + MGLYOX +	KR02N0	Taraborrelli (2013a)
G4585et2	TrGC	→ MGLYOX +	8.00E-13*R02	Taraborrelli (2013a)
G4585et3	TrGC	+ OH → MGLYOX + 2 CO + .5 OH + POHORG + .5 POHORG	2.*kt*fo*fch2oh*falk*kt*ftoh*fcho*fpch2oh	Taraborrelli (2013a)*

17

B. Chemical mechanism – MTM

Table 1: Gas phase reactions (... continued)

#	labels	reaction	rate coefficient	reference
G4587e	TrGC	+ NO → .21 NOA + .21 HOCH ₂ CHO + .21 HO ₂ + .49 HOI2CO3C4 + .49 HCHO + .49 NO ₂ + .045 + .045 HCHO + .255 CH ₃ COCH ₂ OH + .255 + .225 H ₂ O ₂ + NO ₂	KR02ND	Taraborrelli (2013a)
G4587et2	TrGC	→ .21 NOA + .21 HOCH ₂ CHO + .21 HO ₂ + .49 HOI2CO3C4 + .49 HCHO + .49 NO ₂ + .045 + .045 HCHO + .255 CH ₃ COCH ₂ OH + .255 + .225 H ₂ O ₂	8.00E-13*R02+KR02H02*0.706*c(ind_H02)	Taraborrelli (2013a)
G4587et3	TrGC	+ NO → .6 CH ₃ COCH ₂ OH + .6 HOCH ₂ CHO + .26 + .14 + .4 HCHO + .4 HO ₂ + 1.6 NO ₂	KR02ND	Taraborrelli (2013a)
G4587et4	TrGC	→ .6 CH ₃ COCH ₂ OH + .6 HOCH ₂ CHO + .26 + .14 + .4 HCHO + .4 HO ₂ + .6 NO ₂	2.9E-12*R02+KR02H02*0.706*c(ind_H02)	Taraborrelli (2013a)
G4588e	TrGNC	LISOPACNO3 + O ₃ → .8704 OH + .365 HO ₂ + .73 MGLYOX + .4325 + .135 CH ₃ COCH ₂ OH + .0675 GLYOX + .4325 NO ₂ + .0891 H ₂ O ₂ + .135 NOA + .0675 + .3866 HOCH ₂ CHO + .0405 CH ₃ OH + .0405 CO + .0054 + .8704 POHORG	4.E-16	Taraborrelli (2013a)
G4599e	TrGC	LISOPACOOH + O ₃ → 1.3272 OH + 0.36986 HO ₂ + .0432 H ₂ O ₂ + 0.23002 CO + .2025 CH ₃ OOH + .01215 HOCH ₂ OOH + 0.3704 HCHO + .00405 CH ₃ OH + .0405 CO ₂ + .1825 + .365 MGLYOX + .3866 + .135 CH ₃ COCH ₂ OH + .0675 GLYOX + .00324 + .3866 HOCH ₂ CHO + .135 CH ₃ COCH ₂ O ₂ H + .0675 + .0054 + 1.3272 POHORG	4.829E-16	Taraborrelli (2013a)
G4598et3	TrGC	+ OH → .62 CO2H3CHO + .62 OH + .62 CO ₂ + .38 MGLYOX + .38 HCOCO ₃ H + .38 HO ₂ + POHORG + .62 POHORG	kadt*acho*aco2h	Taraborrelli (2013a)*
G4598et4	TrGC	+ OH → .62 + 1.24 CO + 1.24 HO ₂ + .38 + .38 CO + .38 HO ₂ + .38 OH + .38 CO ₂ + POHORG + .38 POHORG	kads*acho*aco2h	Taraborrelli (2013a)*
G41311	TrGC	→ .7143 MACR + .2857 MVK + HCHO + HO ₂	2.40E-12*R02	Taraborrelli (2013a)
G41341	TrGC	+ NO → .7143 MACR + .2857 MVK + HCHO + HO ₂ + NO ₂	KR02ND	Taraborrelli (2013a)
G41351t2	TrGC	+ HO ₂ → .7143 MACR + .2857 MVK + HCHO + HO ₂	KR02H02*0.706	Taraborrelli (2013a)
G41361	TrGC	+ NO ₃ → .7143 MACR + .2857 MVK + HCHO + HO ₂	KR02ND3	Taraborrelli (2013a)
G41378	TrGC	+ NO ₂ →	9.39E9*EXP(-7322/temp)	Taraborrelli (2013a)

18

Table 1: Gas phase reactions (... continued)

#	labels	reaction	rate coefficient	reference
G41341t2	TrGC	→ .7143 MACR + .2857 MVK + HCHO + OH + POHORG	.7143*KHSD+.2857*KHSB	Taraborrelli (2013a)
G413112	TrGC	→ + HO ₂	8.00E-13*R02	Taraborrelli (2013a)
G413416	TrGC	+ NO → + HO ₂ + NO ₂	KR02ND	Taraborrelli (2013a)*
G413519	TrGC	+ HO ₂ →	KR02H02*0.706	Taraborrelli (2013a)
G413618	TrGC	+ NO ₃ → + HO ₂ + NO ₂	KR02ND3	Taraborrelli (2013a)
G413417	TrGC	→ + OH + POHORG	KHSB	Taraborrelli (2013a)
G413619	TrGC	+ OH → + POHORG	0.6*k_CH3OOH_OH	Taraborrelli (2013a)
G413621	TrGC	+ OH → MGLYOX + 2 CO + 2 HO ₂ + POHORG	kt*ftoh*falk*fpch2oh	Taraborrelli (2013a)*
G413622	TrGC	+ OH → .8405 HCHO + .8405 OH + .8405 CO2H3CHO + .1595 + .1595 HO ₂ + POHORG + .8405 POHORG	ks*fsoh*falk*ks*fsoh*falk	Taraborrelli (2013a)
G4136	TrGC	+ OH → CH ₃ C(O)OO + CO ₂ + 2 HCHO + POHORG	kt*fo*ftch2oh	Taraborrelli (2013a)*
G413610	TrGC	+ OH → GLYOX + CH ₃ C(O)OO + HCHO + POHORG	ks*fcho*fsoh	Taraborrelli (2013a)
G41361t2	TrGC	+ OH → MGLYOX + GLYOX + HO ₂ + POHORG	ks*fco*fsoh	Taraborrelli (2013a)
G45mbo1	TrGC	+ OH →	8.1E-12*EXP(610/TEMP)	Rickard and Pascoe (2009), Taraborrelli (2013b)
G45mbo2	TrGC	+ O ₃ → HCHO + .16 CH ₃ COCH ₃ + .16 HO ₂ + .16 CO + .16 OH + .84	1.0E-17*0.57	Rickard and Pascoe (2009), Taraborrelli (2013b)
G45mbo3	TrGC	+ O ₃ → + .63 CO + .37 HOCH ₂ OOH + .16 OH + .16 HO ₂	1.0E-17*0.43	Rickard and Pascoe (2009), Taraborrelli (2013b)
G45mbo4	TrGC	+ NO ₃ →	4.6E-14*EXP(-400/TEMP)	Rickard and Pascoe (2009), Taraborrelli (2013b)
G45mbo5	TrGC	+ HO ₂ →	KR02H02*0.706	Rickard and Pascoe (2009), Taraborrelli (2013b)
G45mbo6	TrGC	+ NO →	KR02ND*(0.064+0.026)/2.	Rickard and Pascoe (2009), Taraborrelli (2013b)
G45mbo7	TrGC	+ NO → HOCH ₂ CHO + CH ₃ COCH ₃ + HO ₂ + NO ₂	KR02ND*(0.936+0.974)/2*.67	Rickard and Pascoe (2009), Taraborrelli (2013b)
G45mbo8	TrGC	+ NO → + HCHO + HO ₂ + NO ₂	KR02ND*(0.936+0.974)/2*.33	Rickard and Pascoe (2009), Taraborrelli (2013b)
G45mbo9	TrGC	→ HOCH ₂ CHO + CH ₃ COCH ₃ + HO ₂	8.8E-13*R02*.67	Rickard and Pascoe (2009), Taraborrelli (2013b)
G45mbo10	TrGC	→ + HCHO + HO ₂	8.8E-13*R02*.33	Rickard and Pascoe (2009), Taraborrelli (2013b)

19

Table 1: Gas phase reactions (... continued)

#	labels	reaction	rate coefficient	reference
G45mbo11	TrGC	+ OH → + OH	.67*2.93E-11*.33*2.05E-12	Rickard and Pascoe (2009), Taraborrelli (2013b)*
G45mbo12	TrGC	+ OH →	.6*k_CH300H_OH	Rickard and Pascoe (2009), Taraborrelli (2013b)
G45mbo13	TrGC	+ hν → HOCH ₂ CHO + CH ₃ COCH ₃ + HO ₂ + OH	1.14*jx(ip_CH300H)*.67	Rickard and Pascoe (2009), Taraborrelli (2013b)
G45mbo14	TrGC	+ hν → + HCHO + HO ₂ + OH	1.14*jx(ip_CH300H)*.33	Rickard and Pascoe (2009), Taraborrelli (2013b)
G45mbo15	TrGC	+ OH → + NO ₂	.67*1.75E-12*.33*2.69E-12	Rickard and Pascoe (2009), Taraborrelli (2013b)*
G45mbo16	TrGC	+ OH → + HO ₂	3.79E-12	Rickard and Pascoe (2009)
G45mbo17	TrGC	+ hν → HCHO + HO ₂ +	J_ACETOL	Rickard and Pascoe (2009)
G45mbo18	TrGC	+ OH → CO +	1.38E-11	Rickard and Pascoe (2009)
G45mbo19	TrGC	+ hν → CO + HO ₂ +	jx(ip_MGLYOX)	Rickard and Pascoe (2009)
G45mbo20	TrGC	+ OH →	1.4E-11	Rickard and Pascoe (2009)
G45mbo21	TrGC	+ hν → CH ₃ COCH ₃ + HO ₂ + HO ₂ + CO	J_ACETOL	Rickard and Pascoe (2009)
G45mbo22	TrGC	+ HO ₂ → CH ₃ COCH ₃ + HO ₂ + OH	KAPHO2*rco3_oh	Rickard and Pascoe (2009), Taraborrelli (2013b)
G45mbo23	TrGC	+ HO ₂ → + O ₃	KAPHO2*rco3_o3	Rickard and Pascoe (2009), Taraborrelli (2013b)
G45mbo24	TrGC	+ HO ₂ →	KAPHO2*rco3_ooH	Rickard and Pascoe (2009), Taraborrelli (2013b)
G45mbo25	TrGC	+ NO → CH ₃ COCH ₃ + HO ₂ + NO ₂	KAPNO	Rickard and Pascoe (2009)
G45mbo26	TrGC	+ NO ₂ →	k_CH3CO3_NO2	Rickard and Pascoe (2009)
G45mbo27	TrGC	+ NO ₃ → CH ₃ COCH ₃ + HO ₂ + NO ₂	KRO2ND03*1.74	Rickard and Pascoe (2009)
G45mbo28	TrGC	→ CH ₃ COCH ₃ + HO ₂	1.00E-11*R02*0.7	Rickard and Pascoe (2009)
G45mbo29	TrGC	→	1.00E-11*R02*0.3	Rickard and Pascoe (2009)
G45mbo30	TrGC	+ OH → CH ₃ COCH ₃ + HO ₂	1.72E-12	Rickard and Pascoe (2009)
G45mbo31	TrGC	+ hν → CH ₃ COCH ₃ + HO ₂ + OH	1.14*jx(ip_CH300H)	Rickard and Pascoe (2009)
G45mbo32	TrGC	OH + →	4.80E-12	Rickard and Pascoe (2009)
G45mbo33	TrGC	→ + NO ₂	K_PAN_M	Rickard and Pascoe (2009)
G45mbo34	TrGC	+ OH → CH ₃ COCH ₃ + CO + NO ₂	4.75E-13	Rickard and Pascoe (2009)
G45mbo35	TrGC	+ HO ₂ →	KRO2HD2*0.706	Rickard and Pascoe (2009), Taraborrelli (2013b)

20

Table 1: Gas phase reactions (... continued)

#	labels	reaction	rate coefficient	reference
G45mbo36	TrGC	+ NO → .65 + .65 CH ₃ COCH ₃ + .65 HO ₂ + .35 + .35 HCHO + .35 NO ₂ + NO ₂	KRO2ND0	Rickard and Pascoe (2009), Taraborrelli (2013b)
G45mbo37	TrGC	+ NO ₂ → .65 + .65 CH ₃ COCH ₃ + .65 HO ₂ + .35 + .35 HCHO + .35 NO ₂ + NO ₂	KRO2ND03	Rickard and Pascoe (2009), Taraborrelli (2013b)
G45mbo38	TrGC	→ .65 + .65 CH ₃ COCH ₃ + .65 HO ₂ + .35 + .35 HCHO + .35 NO ₂	8.8E-13*R02	Rickard and Pascoe (2009), Taraborrelli (2013b)
G45mbo39	TrGC	+ OH → .65 + .35 + OH	.65*4.89E-12*.35*2.52E-12	Rickard and Pascoe (2009), Taraborrelli (2013b)
G45mbo40	TrGC	+ OH →	.6*k_CH300H_OH	Rickard and Pascoe (2009), Taraborrelli (2013b)
G45mbo41	TrGC	+ hν → + CH ₃ COCH ₃ + HO ₂ + OH	1.14*jx(ip_CH300H)*.65	Rickard and Pascoe (2009), Taraborrelli (2013b)
G45mbo42	TrGC	+ hν → + HCHO + NO ₂ + OH	1.14*jx(ip_CH300H)*.35	Rickard and Pascoe (2009), Taraborrelli (2013b)
G45mbo43	TrGC	+ OH → CH ₃ COCH ₃ + HCHO + CO ₂ + NO ₂	1.23E-12	Rickard and Pascoe (2009), Taraborrelli (2013b)*
G45mbo44	TrGC	+ OH →	4.26E-12	Rickard and Pascoe (2009)
G45mbo45	TrGC	+ HO ₂ → + NO ₂ + OH	KAPHO2*rco3_oh	Rickard and Pascoe (2009), Taraborrelli (2013b)
G45mbo46	TrGC	+ HO ₂ →	KAPHO2*(rco3_o3+rco3_ooH)	Rickard and Pascoe (2009), Taraborrelli (2013b)
G45mbo47	TrGC	+ NO → + NO ₂ + NO ₂	KAPNO	Rickard and Pascoe (2009)
G45mbo48	TrGC	+ NO ₂ →	k_CH3CO3_NO2	Rickard and Pascoe (2009)
G45mbo49	TrGC	+ NO ₃ → + NO ₂ + NO ₂	KRO2ND03*1.74	Rickard and Pascoe (2009)
G45mbo50	TrGC	→ + NO ₂	1.00E-11*R02	Rickard and Pascoe (2009)
G45mbo51	TrGC	+ OH →	4.50E-12	Rickard and Pascoe (2009)
G45mbo52	TrGC	→ + NO ₂ + OH	1.14*jx(ip_CH300H)	Rickard and Pascoe (2009)
G45mbo53	TrGC	+ OH → + CO + NO ₂ + NO ₂	1.27E-12	Rickard and Pascoe (2009)
G45mbo54	TrGC	→ + NO ₂	K_PAN_M	Rickard and Pascoe (2009)
G45mbo55	TrGC	→	1.60E-17*C(ind_H2D)*(0.08+0.15)	Rickard and Pascoe (2009), Taraborrelli (2013b)
G45mbo56	TrGC	→ + H ₂ O ₂	1.60E-17*C(ind_H2D)*0.77	Rickard and Pascoe (2009), Taraborrelli (2013b)
G45mbo57	TrGC	+ CO →	1.20E-15	Rickard and Pascoe (2009)
G45mbo58	TrGC	+ NO → + NO ₂	1.00E-14	Rickard and Pascoe (2009)

21

B. Chemical mechanism – MTM

Table 1: Gas phase reactions (... continued)

#	labels	reaction	rate coefficient	reference
G45mbo59	TrGC	+ NO ₂ → + NO ₃	1.00E-15	Rickard and Pascoe (2009)
G45mbo60	TrGC	+ SO ₂ → + H ₂ SO ₄	7.00E-14	Rickard and Pascoe (2009)
G410apin1	TrGC	+ OH →	1.47E-11*EXP(467/TEMP)*(.50+.25)	Vereecken et al. (2007), Taraborrelli (2013b)*
G410apin2	TrGC	+ OH → + HO ₂	1.47E-11*EXP(467/TEMP)*.25*.60	Vereecken et al. (2007), Taraborrelli (2013b)*
G410apin3	TrGC	+ OH →	1.47E-11*EXP(467/TEMP)*.25*.40	Vereecken et al. (2007), Taraborrelli (2013b)*
G410apin4	TrGC	+ NO → + HO ₂	KR02N0*0.770	Rickard and Pascoe (2009), Taraborrelli (2013b)
G410apin5	TrGC	+ NO →	KR02N0*0.230	Rickard and Pascoe (2009), Taraborrelli (2013b)
G410apin6	TrGC	+ HO ₂ →	KR02H02*0.914	Rickard and Pascoe (2009), Taraborrelli (2013b)
G410apin7	TrGC	→ + HO ₂	R02*(.33*9.20E-14+.67*8.80E-13)	Rickard and Pascoe (2009), Taraborrelli (2013b)
G410apin9	TrGC	+ OH → .33 + .67	.33*1.83E-11+.67*3.28E-11	Rickard and Pascoe (2009), Taraborrelli (2013b)
G410apin10	TrGC	+ hν → + HO ₂ + OH	1.14*jx(ip_CH300H)	Rickard and Pascoe (2009), Taraborrelli (2013b)
G410apin11	TrGC	+ OH → .33 + .67 + NO ₂	.33*5.50E-12+.67*3.64E-12	Rickard and Pascoe (2009), Taraborrelli (2013b)
G410apin12	TrGC	+ OH →	(kads+kadt)*acoch3	Vereecken et al. (2007), Taraborrelli (2013b)
G410apin13	TrGC	+ hν → + OH	1.14*jx(ip_CH300H)	Vereecken et al. (2007), Taraborrelli (2013b)
G410apin14	TrGC	+ NO → + HO ₂ + NO ₂	KR02N0	Vereecken et al. (2007), Taraborrelli (2013b)
G410apin15	TrGC	+ HO ₂ →	KR02H02*0.914	Vereecken et al. (2007), Taraborrelli (2013b)
G410apin16	TrGC	→ + HO ₂	R02*9.20E-14	Vereecken et al. (2007), Taraborrelli (2013b)
G410apin17	TrGC	+ OH → LCARBON	1E-11	Vereecken et al. (2007), Taraborrelli (2013b)

22

Table 1: Gas phase reactions (... continued)

#	labels	reaction	rate coefficient	reference
G410apin18	TrGC	+ hν → LCARBON + OH	1.14*jx(ip_CH300H)	Vereecken et al. (2007), Taraborrelli (2013b)
G410apin18t2	TrGC	+ OH →	4.20E-11*0.772	Rickard and Pascoe (2009), Taraborrelli (2013b)
G410apin19	TrGC	+ OH →	4.20E-11*0.228	Rickard and Pascoe (2009), Taraborrelli (2013b)
G410apin20	TrGC	→ + CO + HO ₂	jx(ip_HOCH2CHO)	Rickard and Pascoe (2009), Taraborrelli (2013b)
G410apin21	TrGC	+ NO ₃ → + HNO ₃	3.80E-14	Rickard and Pascoe (2009), Taraborrelli (2013b)
G410apin	TrGC	→ 0.3 + 0.7	1.00E-11*R02	Rickard and Pascoe (2009), Taraborrelli (2013b)
G410apint2	TrGC	+ HO ₂ →	KAPH02*rco3_ooh	Rickard and Pascoe (2009), Taraborrelli (2013b)
G410apint3	TrGC	+ HO ₂ → + O ₃	KAPH02*rco3_o3	Rickard and Pascoe (2009), Taraborrelli (2013b)
G410apint4	TrGC	+ HO ₂ → + OH	KAPH02*rco3_oh	Rickard and Pascoe (2009), Taraborrelli (2013b)
G410apint5	TrGC	+ NO ₂ →	k_CH3CO3_NO2	Rickard and Pascoe (2009), Taraborrelli (2013b)
G410apint6	TrGC	+ NO → + NO ₂	KAFNO	Rickard and Pascoe (2009), Taraborrelli (2013b)
G410apint7	TrGC	+ NO ₃ → + NO ₂	KR02N03*1.60	Rickard and Pascoe (2009), Taraborrelli (2013b)
G410apint8	TrGC	→ + NO ₂	k_PAN_M	Rickard and Pascoe (2009), Taraborrelli (2013b)
G410apint9	TrGC	+ OH → + CO + NO ₂	3.66E-12	Rickard and Pascoe (2009), Taraborrelli (2013b)
G410apint10	TrGC	→	1.30E-12*R02	Rickard and Pascoe (2009), Taraborrelli (2013b)
G410apint11	TrGC	+ NO →	KR02N0*0.157	Rickard and Pascoe (2009), Taraborrelli (2013b)
G410apint12	TrGC	+ HO ₂ →	KR02H02*0.890	Rickard and Pascoe (2009), Taraborrelli (2013b)

23

Table 1: Gas phase reactions (... continued)

#	labels	reaction	rate coefficient	reference
G410apint13	TrGC	+ NO → + NO ₂	KR02ND*0.843	Rickard and Pascoe (2009), Taraborrelli (2013b)
G410apint14	TrGC	+ hν → + NO ₂	J_IC3H7NO3+J_ACETOL	Rickard and Pascoe (2009), Taraborrelli (2013b)
G410apint15	TrGC	+ OH → + NO ₂	2.88E-12	Rickard and Pascoe (2009), Taraborrelli (2013b)
G410apint16	TrGC	+ hν → + OH	1.14*jx(ip_CH300H)+J_ACETOL	Rickard and Pascoe (2009), Taraborrelli (2013b)
G410apint17	TrGC	+ OH →	1.90E-12*EXP(190/TEMP)	Rickard and Pascoe (2009), Taraborrelli (2013b)
G410apint18	TrGC	+ OH → + OH	1.30E-11	Rickard and Pascoe (2009), Taraborrelli (2013b)
G410apint19	TrGC	→	6.70E-15*R02	Rickard and Pascoe (2009), Taraborrelli (2013b)
G410apint20	TrGC	+ NO → + NO ₂	KR02ND	Rickard and Pascoe (2009), Taraborrelli (2013b)
G410apint21	TrGC	+ HO ₂ →	KR02HD2*0.890	Rickard and Pascoe (2009), Taraborrelli (2013b)
G410apint22	TrGC	+ hν → + OH	1.14*jx(ip_CH300H)+J_ACETOL	Rickard and Pascoe (2009), Taraborrelli (2013b)
G410apint23	TrGC	+ OH →	1.05E-11	Rickard and Pascoe (2009), Taraborrelli (2013b)
G410apint24	TrGC	→ + CH ₃ COCH ₃	6.70E-15*R02	Rickard and Pascoe (2009), Taraborrelli (2013b)
G410apint25	TrGC	+ NO →	KR02ND*0.118	Rickard and Pascoe (2009), Taraborrelli (2013b)
G410apint26	TrGC	+ NO → + CH ₃ COCH ₃ + NO ₂	KR02ND*0.882	Rickard and Pascoe (2009), Taraborrelli (2013b)
G410apint27	TrGC	+ HO ₂ →	KR02HD2*0.890	Rickard and Pascoe (2009), Taraborrelli (2013b)
G410apint28	TrGC	+ hν → + CH ₃ COCH ₃ + OH	1.14*jx(ip_CH300H)+2.15*jx(ip_MGLYOX)	Rickard and Pascoe (2009), Taraborrelli (2013b)
G410apint29	TrGC	+ OH →	2.05E-11	Rickard and Pascoe (2009), Taraborrelli (2013b)

24

Table 1: Gas phase reactions (... continued)

#	labels	reaction	rate coefficient	reference
G410apint30	TrGC	+ OH →	6.65E-12	Rickard and Pascoe (2009), Taraborrelli (2013b)
G410apint31	TrGC	+ hν → + HO ₂	J_ACETOL	Rickard and Pascoe (2009), Taraborrelli (2013b)
G410apint32	TrGC	+ OH →	2.64E-11	Rickard and Pascoe (2009), Taraborrelli (2013b)
G410apint33	TrGC	+ hν → + CO + HO ₂	jx(ip_HOCH2CHO)	Rickard and Pascoe (2009), Taraborrelli (2013b)
G410apint34	TrGC	+ NO ₃ → + HNO ₃	KN03AL*8.5	Rickard and Pascoe (2009), Taraborrelli (2013b)
G410apint35	TrGC	+ hν → + OH	1.14*jx(ip_CH300H)+J_ACETOL	Rickard and Pascoe (2009), Taraborrelli (2013b)
G410apint36	TrGC	+ OH →	9.73E-12	Rickard and Pascoe (2009), Taraborrelli (2013b)
G410apint37	TrGC	→	1.00E-11*R02	Rickard and Pascoe (2009), Taraborrelli (2013b)
G410apint38	TrGC	+ NO → + NO ₂	KAPNO	Rickard and Pascoe (2009), Taraborrelli (2013b)
G410apint39	TrGC	+ NO ₂ →	k_CH3CO3_NO2	Rickard and Pascoe (2009), Taraborrelli (2013b)
G410apint40	TrGC	+ HO ₂ →	KAPH02*(rco3_ooH+rco3_o3)	Rickard and Pascoe (2009), Taraborrelli (2013b)
G410apint41	TrGC	+ HO ₂ → + OH	KAPH02*rco3_oh	Rickard and Pascoe (2009), Taraborrelli (2013b)
G410apint42	TrGC	→	6.70E-15*R02	Rickard and Pascoe (2009), Taraborrelli (2013b)
G410apint43	TrGC	+ HO ₂ →	KR02HD2*0.859	Rickard and Pascoe (2009), Taraborrelli (2013b)
G410apint44	TrGC	+ NO → + NO ₂	KR02ND	Rickard and Pascoe (2009), Taraborrelli (2013b)
G410apint45	TrGC	→ + NO ₂	k_PAN_M	Rickard and Pascoe (2009), Taraborrelli (2013b)
G410apint46	TrGC	+ OH → + CO + NO ₂	6.60E-12	Rickard and Pascoe (2009), Taraborrelli (2013b)

25

B. Chemical mechanism – MTM

Table 1: Gas phase reactions (... continued)

#	labels	reaction	rate coefficient	reference
G410apint47	TrGC	$\rightarrow + \text{OH}$	$1.14 \cdot jx(ip_CH300H) + J_ACETOL$	Rickard and Pascoe (2009), Taraborrelli (2013b)
G410apint48	TrGC	$+ \text{OH} \rightarrow$	$1.02E-11$	Rickard and Pascoe (2009), Taraborrelli (2013b)
G410apint49	TrGC	$+ h\nu \rightarrow + \text{OH}$	$1.14 \cdot jx(ip_CH300H) + J_ACETOL$	Rickard and Pascoe (2009), Taraborrelli (2013b)
G410apint50	TrGC	$+ \text{OH} \rightarrow$	$1.29E-11$	Rickard and Pascoe (2009), Taraborrelli (2013b)
G410apint51	TrGC	$\rightarrow + \text{CH}_3\text{COCH}_3$	$6.70E-15 \cdot R02$	Rickard and Pascoe (2009), Taraborrelli (2013b)
G410apint52	TrGC	$+ \text{NO} \rightarrow + \text{CH}_3\text{COCH}_3 + \text{NO}_2$	$KR02N0$	Rickard and Pascoe (2009), Taraborrelli (2013b)
G410apint53	TrGC	$+ \text{HO}_2 \rightarrow$	$KR02H02 \cdot 0.859$	Rickard and Pascoe (2009), Taraborrelli (2013b)
G410apint54	TrGC	$+ h\nu \rightarrow + \text{CH}_3\text{COCH}_3 + \text{OH}$	$1.14 \cdot jx(ip_CH300H) + jx(ip_HOCH2CHO)$	Rickard and Pascoe (2009), Taraborrelli (2013b)
G410apint55	TrGC	$+ \text{OH} \rightarrow$	$3.45E-11$	Rickard and Pascoe (2009), Taraborrelli (2013b)
G410apint56	TrGC	$+ \text{HO}_2 \rightarrow$	$KR02H02 \cdot 0.914$	Rickard and Pascoe (2009), Taraborrelli (2013b)
G410apint57	TrGC	$+ \text{NO} \rightarrow$	$KR02N0 \cdot 0.050$	Rickard and Pascoe (2009), Taraborrelli (2013b)
G410apint58	TrGC	$+ \text{NO} \rightarrow + \text{NO}_2$	$KR02N0 \cdot 0.950$	Rickard and Pascoe (2009), Taraborrelli (2013b)
G410apint59	TrGC	\rightarrow	$6.70E-15 \cdot R02$	Rickard and Pascoe (2009), Taraborrelli (2013b)
G410apint60	TrGC	$+ \text{OH} \rightarrow$	$2.75E-11$	Rickard and Pascoe (2009), Taraborrelli (2013b)
G410apint61	TrGC	$+ h\nu \rightarrow + \text{OH}$	$1.14 \cdot jx(ip_CH300H) + jx(ip_HOCH2CHO)$	Rickard and Pascoe (2009), Taraborrelli (2013b)
G410apint62	TrGC	$+ \text{OH} \rightarrow + \text{CH}_3\text{COCH}_3 + \text{NO}_2$	$2.25E-11$	Rickard and Pascoe (2009), Taraborrelli (2013b)
G410apint63	TrGC	$+ h\nu \rightarrow + \text{NO}_2$	$J_IC3H7N03 + jx(ip_HOCH2CHO)$	Rickard and Pascoe (2009), Taraborrelli (2013b)

26

Table 1: Gas phase reactions (... continued)

#	labels	reaction	rate coefficient	reference
G410apint64	TrGC	$+ \text{HO}_2 \rightarrow$	$KR02H02 \cdot 0.914$	Rickard and Pascoe (2009), Taraborrelli (2013b)
G410apint65	TrGC	$+ \text{NO} \rightarrow$	$KR02N0 \cdot 0.125$	Rickard and Pascoe (2009), Taraborrelli (2013b)
G410apint66	TrGC	$+ \text{NO} \rightarrow + \text{CH}_3\text{COCH}_3 + \text{NO}_2$	$KR02N0 \cdot 0.875$	Rickard and Pascoe (2009), Taraborrelli (2013b)
G410apint67	TrGC	$\rightarrow + \text{CH}_3\text{COCH}_3$	$6.70E-15 \cdot R02$	Rickard and Pascoe (2009), Taraborrelli (2013b)
G410apint68	TrGC	$+ \text{OH} \rightarrow$	$8.01E-11$	Rickard and Pascoe (2009), Taraborrelli (2013b)
G410apint69	TrGC	$+ h\nu \rightarrow + \text{CH}_3\text{COCH}_3 + \text{OH}$	$1.14 \cdot jx(ip_CH300H) + jx(ip_HOCH2CHO)$	Rickard and Pascoe (2009), Taraborrelli (2013b)
G410apint70	TrGC	$+ \text{OH} \rightarrow + \text{CH}_3\text{COCH}_3 + \text{NO}_2$	$7.03E-11$	Rickard and Pascoe (2009), Taraborrelli (2013b)
G410apint71	TrGC	$+ h\nu \rightarrow + \text{CH}_3\text{COCH}_3 + \text{NO}_2$	$J_IC3H7N03 + jx(ip_HOCH2CHO)$	Rickard and Pascoe (2009), Taraborrelli (2013b)
G410apint72	TrGC	$+ \text{NO}_3 \rightarrow + \text{HNO}_3$	$KN03AL \cdot 5.5$	Rickard and Pascoe (2009), Taraborrelli (2013b)
G410apint73	TrGC	$+ \text{OH} \rightarrow$	$6.70E-11$	Rickard and Pascoe (2009), Taraborrelli (2013b)
G410apint74	TrGC	$+ h\nu \rightarrow + \text{CH}_3\text{C}(\text{O})\text{OO}$	$2.15 \cdot jx(ip_MGLYOX)$	Rickard and Pascoe (2009), Taraborrelli (2013b)
G410apint75	TrGC	$+ \text{HO}_2 \rightarrow$	$KAPH02 \cdot (rco3_ooh + rco3_o3)$	Rickard and Pascoe (2009), Taraborrelli (2013b)
G410apint76	TrGC	$+ \text{HO}_2 \rightarrow + \text{OH}$	$KAPH02 \cdot rco3_oh$	Rickard and Pascoe (2009), Taraborrelli (2013b)
G410apint77	TrGC	$+ \text{NO} \rightarrow + \text{NO}_2$	$KAPN0$	Rickard and Pascoe (2009), Taraborrelli (2013b)
G410apint78	TrGC	$+ \text{NO}_2 \rightarrow$	K_CH3CO3_N02	Rickard and Pascoe (2009), Taraborrelli (2013b)
G410apint79	TrGC	\rightarrow	$1.00E-11 \cdot R02$	Rickard and Pascoe (2009), Taraborrelli (2013b)
G410apint80	TrGC	$+ \text{OH} \rightarrow$	$4.75E-12$	Rickard and Pascoe (2009), Taraborrelli (2013b)

27

Table 1: Gas phase reactions (... continued)

#	labels	reaction	rate coefficient	reference
G410apint81	TrGC	$+ h\nu \rightarrow + OH$	$1.14*jx(ip_CH300H)+2.15*jx(ip_MGLY0X)$	Rickard and Pascoe (2009), Taraborrelli (2013b)
G410apint82	TrGC	$+ HO_2 \rightarrow$	KR02HD2*0.770	Rickard and Pascoe (2009), Taraborrelli (2013b)
G410apint83	TrGC	$+ NO \rightarrow + HCHO + NO_2$	KR02ND	Rickard and Pascoe (2009), Taraborrelli (2013b)
G410apint84	TrGC	$\rightarrow + HCHO$	$2.00E-12*R02$	Rickard and Pascoe (2009), Taraborrelli (2013b)
G410apint85	TrGC	$+ OH \rightarrow + CO + NO_2$	$8.83E-13$	Rickard and Pascoe (2009), Taraborrelli (2013b)
G410apint86	TrGC	$\rightarrow + NO_2$	k_PAN_M	Rickard and Pascoe (2009), Taraborrelli (2013b)
G410apint87	TrGC	$+ OH \rightarrow$	$1.01E-11$	Rickard and Pascoe (2009), Taraborrelli (2013b)
G410apint88	TrGC	$+ h\nu \rightarrow + HCHO + OH$	$1.14*jx(ip_CH300H)+ 2.15*jx(ip_MGLY0X)$	Rickard and Pascoe (2009), Taraborrelli (2013b)
G410apint89	TrGC	$+ HO_2 \rightarrow$	KR02HD2*0.820	Rickard and Pascoe (2009), Taraborrelli (2013b)
G410apint90	TrGC	$+ NO \rightarrow + CH_3C(O)OO + NO_2$	KR02ND	Rickard and Pascoe (2009), Taraborrelli (2013b)
G410apint91	TrGC	$\rightarrow + CH_3C(O)OO$	$8.80E-13*R02$	Rickard and Pascoe (2009), Taraborrelli (2013b)
G410apint92	TrGC	$+ OH \rightarrow + OH$	$1.20E-10$	Rickard and Pascoe (2009), Taraborrelli (2013b)
G410apint93	TrGC	$+ h\nu \rightarrow + CH_3C(O)OO + OH$	$1.14*jx(ip_CH300H)+jx(ip_HOCH2CHO)$	Rickard and Pascoe (2009), Taraborrelli (2013b)
G410apint94	TrGC	$\rightarrow CH_3C(O)OO +$	$8.80E-13*R02$	Rickard and Pascoe (2009), Taraborrelli (2013b)
G410apint95	TrGC	$+ NO \rightarrow CH_3C(O)OO + + NO_2$	KR02ND	Rickard and Pascoe (2009), Taraborrelli (2013b)
G410apint96	TrGC	$+ HO_2 \rightarrow$	KR02HD2*0.706	Rickard and Pascoe (2009), Taraborrelli (2013b)
G410apint97	TrGC	$+ h\nu \rightarrow CH_3C(O)OO + + OH$	$1.14*jx(ip_CH300H)+jx(ip_HOCH2CHO)$	Rickard and Pascoe (2009), Taraborrelli (2013b)

28

Table 1: Gas phase reactions (... continued)

#	labels	reaction	rate coefficient	reference
G410apint98	TrGC	$+ OH \rightarrow$	$7.49E-11$	Rickard and Pascoe (2009), Taraborrelli (2013b)
G410apint99	TrGC	$+ OH \rightarrow$	$4.29E-11$	Rickard and Pascoe (2009), Taraborrelli (2013b)
G410apint100	TrGC	$+ h\nu \rightarrow + HO_2 + CO$	$jx(ip_HOCH2CHO)*2$	Rickard and Pascoe (2009), Taraborrelli (2013b)
G410apint101	TrGC	$+ NO_3 \rightarrow + HNO_3$	$2*KNO3AL*2.4$	Rickard and Pascoe (2009), Taraborrelli (2013b)
G410apint102	TrGC	$\rightarrow + HCHO + HO_2$	$8.80E-13*R02$	Rickard and Pascoe (2009), Taraborrelli (2013b)
G410apint103	TrGC	$+ NO \rightarrow$	KR02ND*0.098	Rickard and Pascoe (2009), Taraborrelli (2013b)
G410apint104	TrGC	$+ NO \rightarrow + HCHO + HO_2 + NO_2$	KR02ND*0.902	Rickard and Pascoe (2009), Taraborrelli (2013b)
G410apint105	TrGC	$+ HO_2 \rightarrow$	KR02HD2*0.770	Rickard and Pascoe (2009), Taraborrelli (2013b)
G410apint106	TrGC	$+ h\nu \rightarrow + HCHO + HO_2 + NO_2$	$2.15*jx(ip_MGLY0X)$	Rickard and Pascoe (2009), Taraborrelli (2013b)
G410apint107	TrGC	$+ OH \rightarrow + NO_2$	$7.11E-12$	Rickard and Pascoe (2009), Taraborrelli (2013b)
G410apint108	TrGC	$+ h\nu \rightarrow + HCHO + HO_2 + OH$	$1.14*jx(ip_CH300H)+2.15*jx(ip_MGLY0X)$	Rickard and Pascoe (2009), Taraborrelli (2013b)
G410apint109	TrGC	$+ OH \rightarrow + OH$	$8.69E-11$	Rickard and Pascoe (2009), Taraborrelli (2013b)
G410apint110	TrGC	$+ h\nu \rightarrow + HOCH_2CO_3$	J_ACETDL	Rickard and Pascoe (2009), Taraborrelli (2013b)
G410apint111	TrGC	$+ OH \rightarrow + HO_2$	$3.22E-12$	Rickard and Pascoe (2009), Taraborrelli (2013b)
G410apint112	TrGC	$\rightarrow CH_3C(O)OO + HCHO + CO$	$2.00E-12*R02$	Rickard and Pascoe (2009), Taraborrelli (2013b)
G410apint113	TrGC	$+ HO_2 \rightarrow$	KR02HD2*0.625	Rickard and Pascoe (2009), Taraborrelli (2013b)
G410apint114	TrGC	$+ NO \rightarrow CH_3C(O)OO + HCHO + CO + NO_2$	KR02ND	Rickard and Pascoe (2009), Taraborrelli (2013b)

29

B. Chemical mechanism – MTM

Table 1: Gas phase reactions (... continued)

#	labels	reaction	rate coefficient	reference
G410apint115	TrGC	+ OH → + OH	ks*fc0*fsooh	Rickard and Pascoe (2009), Taraborrelli (2013b)
G410apint116	TrGC	+ OH →	.6*k_CH3OOH_OH	Rickard and Pascoe (2009), Taraborrelli (2013b)
G410apint117	TrGC	+ hν → + OH + HO ₂	1.14*jx(ip_CH3OOH)	Rickard and Pascoe (2009), Taraborrelli (2013b)
G410apint118	TrGC	+ hν → CH ₃ C(O)OO + CO + OH + HCHO	J_ACETOL	Rickard and Pascoe (2009), Taraborrelli (2013b)
G410apint119	TrGC	+ hν → CH ₃ C(O)OO + HCOCO ₃	2.15*jx(ip_MGLYOX)	Rickard and Pascoe (2009), Taraborrelli (2013b)
G410apint120	TrGC	+ OH → + CO	1.33E-11	Rickard and Pascoe (2009), Taraborrelli (2013b)
G410apint121	TrGC	+ hν → + CO + HO ₂	jx(ip_MGLYOX)	Rickard and Pascoe (2009), Taraborrelli (2013b)
G410apint122	TrGC	+ NO ₃ → + CO + HNO ₃	KN03AL*5.5	Rickard and Pascoe (2009), Taraborrelli (2013b)
G410apint123	TrGC	+ OH →	6.65E-11	Rickard and Pascoe (2009), Taraborrelli (2013b)
G410apint124	TrGC	+ hν → + HO ₂ + CO	jx(ip_HOCH2CHO)	Rickard and Pascoe (2009), Taraborrelli (2013b)
G410apint125	TrGC	+ hν → CH ₃ C(O)OO +	2.15*jx(ip_MGLYOX)	Rickard and Pascoe (2009), Taraborrelli (2013b)
G410apint126	TrGC	+ NO ₃ → + HNO ₃	KN03AL*5.5	Rickard and Pascoe (2009), Taraborrelli (2013b)
G410apint127	TrGC	→	1.00E-11*RD2	Rickard and Pascoe (2009), Taraborrelli (2013b)
G410apint128	TrGC	+ NO → + NO ₂	KAPNO	Rickard and Pascoe (2009), Taraborrelli (2013b)
G410apint129	TrGC	+ NO ₂ →	k_CH3CO3_NO2	Rickard and Pascoe (2009), Taraborrelli (2013b)
G410apint130	TrGC	+ HO ₂ →	KAPHO2*(rco3_ooh+rco3_o3)	Rickard and Pascoe (2009), Taraborrelli (2013b)
G410apint131	TrGC	+ HO ₂ → + OH	KAPHO2*rco3_oh	Rickard and Pascoe (2009), Taraborrelli (2013b)

30

Table 1: Gas phase reactions (... continued)

#	labels	reaction	rate coefficient	reference
G410apint132	TrGC	+ hν → + OH	1.14*jx(ip_CH3OOH)+jx(ip_HOCH2CHO)	Rickard and Pascoe (2009), Taraborrelli (2013b)
G410apint133	TrGC	+ hν →	4.23E-12	Rickard and Pascoe (2009), Taraborrelli (2013b)
G410apint134	TrGC	→ + NO ₂	k_PAN_M	Rickard and Pascoe (2009), Taraborrelli (2013b)
G410apint135	TrGC	+ OH → + CO + NO ₂	3.12E-13	Rickard and Pascoe (2009), Taraborrelli (2013b)
G410apint136	TrGC	→ 0.7 + 0.3	1.00E-11*RD2	Rickard and Pascoe (2009), Taraborrelli (2013b)
G410apint137	TrGC	+ NO → + NO ₂	KAPNO	Rickard and Pascoe (2009), Taraborrelli (2013b)
G410apint138	TrGC	+ NO ₂ →	k_CH3CO3_NO2	Rickard and Pascoe (2009), Taraborrelli (2013b)
G410apint139	TrGC	+ HO ₂ →	KAPHO2*rco3_ooh	Rickard and Pascoe (2009), Taraborrelli (2013b)
G410apint140	TrGC	+ HO ₂ → + O ₃	KAPHO2*rco3_o3	Rickard and Pascoe (2009), Taraborrelli (2013b)
G410apint141	TrGC	+ HO ₂ → + CO ₂ + OH	KAPHO2*rco3_oh	Rickard and Pascoe (2009), Taraborrelli (2013b)
G410apint142	TrGC	→ + NO ₂	k_PAN_M	Rickard and Pascoe (2009), Taraborrelli (2013b)
G410apint143	TrGC	+ OH → GLYOX + CO + NO ₂	2.10E-11	Rickard and Pascoe (2009), Taraborrelli (2013b)
G410apint144	TrGC	+ OH →	2.14E-11	Rickard and Pascoe (2009), Taraborrelli (2013b)
G410apint145	TrGC	+ hν → + HO ₂	jx(ip_HOCH2CHO)	Rickard and Pascoe (2009), Taraborrelli (2013b)
G410apint146	TrGC	+ O ₃ →	1.01E-15*EXP(-732/TEMP)*.50*.18	Capouet et al. (2008)
G410apint147	TrGC	+ O ₃ →	1.01E-15*EXP(-732/TEMP)*.50*.16	Capouet et al. (2008)
G410apint148	TrGC	+ O ₃ → OH + + CO + HO ₂	1.01E-15*EXP(-732/TEMP)*.50*.66	Capouet et al. (2008)
G410apint149	TrGC	+ O ₃ →	1.01E-15*EXP(-732/TEMP)*.50*.12	Capouet et al. (2008)
G410apint150	TrGC	+ O ₃ → OH +	1.01E-15*EXP(-732/TEMP)*.50*(.22+.66)	Capouet et al. (2008)*
G410apint151	TrGC	→ + H ₂ O ₂	1.00E-17*c(ind_H2O)	Rickard and Pascoe (2009), Taraborrelli (2013b)

31

Table 1: Gas phase reactions (... continued)

#	labels	reaction	rate coefficient	reference
G410apint152	TrGC	+ CO →	1.20E-15	Rickard and Pascoe (2009), Taraborrelli (2013b)
G410apint153	TrGC	+ NO → + NO ₂	1.00E-14	Rickard and Pascoe (2009), Taraborrelli (2013b)
G410apint154	TrGC	+ NO ₂ → + NO ₃	1.00E-15	Rickard and Pascoe (2009), Taraborrelli (2013b)
G410apint155	TrGC	+ SO ₂ → + H ₂ SO ₄	7.00E-14	Rickard and Pascoe (2009), Taraborrelli (2013b)
G410apint156	TrGC	→	1.00E-17*c(ind_H2O)*(0.08+0.15)	Rickard and Pascoe (2009), Taraborrelli (2013b)
G410apint157	TrGC	→ + H ₂ O ₂	1.00E-17*c(ind_H2O)*0.77	Rickard and Pascoe (2009), Taraborrelli (2013b)
G410apint158	TrGC	+ CO →	1.20E-15	Rickard and Pascoe (2009), Taraborrelli (2013b)
G410apint159	TrGC	+ NO → + NO ₂	1.00E-14	Rickard and Pascoe (2009), Taraborrelli (2013b)
G410apint160	TrGC	+ NO ₂ → + NO ₃	1.00E-15	Rickard and Pascoe (2009), Taraborrelli (2013b)
G410apint161	TrGC	+ SO ₂ → + H ₂ SO ₄	7.00E-14	Rickard and Pascoe (2009), Taraborrelli (2013b)
G410apint162	TrGC	→ + HCHO	2.00E-12*R02	Rickard and Pascoe (2009), Taraborrelli (2013b)*
G410apint163	TrGC	+ NO → + HCHO + NO ₂	KR02N0	Rickard and Pascoe (2009), Taraborrelli (2013b)
G410apint164	TrGC	+ HO ₂ →	KR02H02*0.914	Rickard and Pascoe (2009), Taraborrelli (2013b)
G410apint165	TrGC	→ + HCHO + OH	1.14*jx(ip_CH300H)+jx(ip_HOCH2CHO)	Rickard and Pascoe (2009), Taraborrelli (2013b)
G410apint166	TrGC	+ OH → + OH	5.47E-11	Rickard and Pascoe (2009), Taraborrelli (2013b)
G410apint167	TrGC	+ hν → + HCHO + OH	J_ACETOL	Rickard and Pascoe (2009), Taraborrelli (2013b)
G410apint168	TrGC	+ OH → + CO	5.47E-11	Rickard and Pascoe (2009), Taraborrelli (2013b)

32

Table 1: Gas phase reactions (... continued)

#	labels	reaction	rate coefficient	reference
G410apint169	TrGC	+ hν → + CO + HO ₂	jx(ip_MGLYOX)+jx(ip_HOCH2CHO)	Rickard and Pascoe (2009), Taraborrelli (2013b)
G410apint170	TrGC	→ .56 + .14 + 0.3	1.00E-11*R02	Rickard and Pascoe (2009), Taraborrelli (2013b)
G410apint171	TrGC	+ HO ₂ →	KAPH02*rco3_ooH	Rickard and Pascoe (2009), Taraborrelli (2013b)
G410apint172	TrGC	+ HO ₂ → + O ₃	KAPH02*rco3_o3	Rickard and Pascoe (2009), Taraborrelli (2013b)
G410apint173	TrGC	+ HO ₂ → .80 + 0.20 + OH	KAPH02*rco3_oh	Rickard and Pascoe (2009), Taraborrelli (2013b)
G410apint174	TrGC	+ NO ₂ →	k_CH3CO3_NO2	Rickard and Pascoe (2009), Taraborrelli (2013b)
G410apint175	TrGC	+ NO → 0.80 + 0.20 + NO ₂	KAPNO	Rickard and Pascoe (2009), Taraborrelli (2013b)
G410apint176	TrGC	+ OH → 0.80 + 0.20	2.69E-11	Rickard and Pascoe (2009), Taraborrelli (2013b)
G410apint177	TrGC	+ hν → 0.80 + 0.20 + HO ₂	jx(ip_HOCH2CHO)	Rickard and Pascoe (2009), Taraborrelli (2013b)
G410apint178	TrGC	→ 0.80 + 0.20 + OH	1.14*jx(ip_CH300H)+jx(ip_HOCH2CHO)	Rickard and Pascoe (2009), Taraborrelli (2013b)
G410apint179	TrGC	+ OH →	3.00E-11	Rickard and Pascoe (2009), Taraborrelli (2013b)
G410apint180	TrGC	→ + NO ₂	k_PAN_M	Rickard and Pascoe (2009), Taraborrelli (2013b)
G410apint181	TrGC	+ OH → CH ₃ COCH ₃ + + CO + NO ₂	2.52E-11	Rickard and Pascoe (2009), Taraborrelli (2013b)
G410apint182	TrGC	→ 0.7 + 0.3	1.00E-11*R02	Rickard and Pascoe (2009), Taraborrelli (2013b)
G410apint183	TrGC	+ HO ₂ →	KAPH02*rco3_ooH	Rickard and Pascoe (2009), Taraborrelli (2013b)
G410apint184	TrGC	+ HO ₂ → + O ₃	KAPH02*rco3_o3	Rickard and Pascoe (2009), Taraborrelli (2013b)
G410apint185	TrGC	+ HO ₂ → + OH	KAPH02*rco3_oh	Rickard and Pascoe (2009), Taraborrelli (2013b)

33

B. Chemical mechanism – MTM

Table 1: Gas phase reactions (... continued)

#	labels	reaction	rate coefficient	reference
G410apint186	TrGC	+ NO → + NO ₂	KAPNO	Rickard and Pascoe (2009), Taraborrelli (2013b)
G410apint187	TrGC	+ NO ₂ →	k_CH3CO3_NO2	Rickard and Pascoe (2009), Taraborrelli (2013b)
G410apint188	TrGC	+ OH →	7.29E-12	Rickard and Pascoe (2009), Taraborrelli (2013b)
G410apint189	TrGC	→	1.30E-12•R02	Rickard and Pascoe (2009), Taraborrelli (2013b)
G410apint190	TrGC	+ HO ₂ →	KR02H02•0.859	Rickard and Pascoe (2009), Taraborrelli (2013b)
G410apint191	TrGC	+ NO → + NO ₂	KR02NO	Rickard and Pascoe (2009), Taraborrelli (2013b)*
G410apint192	TrGC	+ hν → + OH	1.14*jx(ip_CH300H)	Rickard and Pascoe (2009), Taraborrelli (2013b)
G410apint193	TrGC	+ OH →	1.04E-11	Rickard and Pascoe (2009), Taraborrelli (2013b)
G410apint194	TrGC	→ + NO ₂	k_PAN_M	Rickard and Pascoe (2009), Taraborrelli (2013b)
G410apint195	TrGC	+ OH → + CO + NO ₂	6.77E-12	Rickard and Pascoe (2009), Taraborrelli (2013b)
G410apint196	TrGC	→	9.20E-14•R02	Rickard and Pascoe (2009), Taraborrelli (2013b)*
G410apint197	TrGC	+ NO → + NO ₂	KR02NO	Rickard and Pascoe (2009), Taraborrelli (2013b)
G410apint198	TrGC	+ HO ₂ →	KR02H02•0.859	Rickard and Pascoe (2009), Taraborrelli (2013b)
G410apint199	TrGC	+ hν → + OH	1.14*jx(ip_CH300H)	Rickard and Pascoe (2009), Taraborrelli (2013b)
G410apint200	TrGC	+ OH →	1.09E-11	Rickard and Pascoe (2009), Taraborrelli (2013b)
G410apint201	TrGC	→ CH ₃ COCH ₃ +	6.70E-15•R02	Rickard and Pascoe (2009), Taraborrelli (2013b)*
G410apint202	TrGC	+ NO → CH ₃ COCH ₃ + + NO ₂	KR02NO	Rickard and Pascoe (2009), Taraborrelli (2013b)*

34

Table 1: Gas phase reactions (... continued)

#	labels	reaction	rate coefficient	reference
G410apint203	TrGC	+ HO ₂ →	KR02H02•0.859	Rickard and Pascoe (2009), Taraborrelli (2013b)
G410apint204	TrGC	+ hν → CH ₃ COCH ₃ + + OH	1.14*jx(ip_CH300H)+jx(ip_MGLY0X)	Rickard and Pascoe (2009), Taraborrelli (2013b)
G410apint205	TrGC	+ OH →	1.86E-11	Rickard and Pascoe (2009), Taraborrelli (2013b)
G410apint206	TrGC	+ NO ₃ → + HNO ₃	KNG3AL•8.5	Rickard and Pascoe (2009), Taraborrelli (2013b)
G410apint207	TrGC	+ OH →	2.63E-11	Rickard and Pascoe (2009), Taraborrelli (2013b)
G410apint208	TrGC	→ + CO + HO ₂	jx(ip_H0CH2CHO)	Rickard and Pascoe (2009), Taraborrelli (2013b)
G410apint209	TrGC	+ HO ₂ →	KAPH02•rco3_ooh	Rickard and Pascoe (2009), Taraborrelli (2013b)
G410apint210	TrGC	+ HO ₂ → + OH	KAPH02•rco3_oh	Rickard and Pascoe (2009), Taraborrelli (2013b)
G410apint211	TrGC	+ HO ₂ → + O ₃	KAPH02•rco3_o3	Rickard and Pascoe (2009), Taraborrelli (2013b)
G410apint212	TrGC	+ NO → + NO ₂	KAPNO	Rickard and Pascoe (2009), Taraborrelli (2013b)
G410apint213	TrGC	+ NO ₂ →	k_CH3CO3_NO2	Rickard and Pascoe (2009), Taraborrelli (2013b)
G410apint214	TrGC	+ NO ₃ → + NO ₂	KR02NO3•1.74	Rickard and Pascoe (2009), Taraborrelli (2013b)
G410apint215	TrGC	→	1.00E-11•R02•0.7	Rickard and Pascoe (2009), Taraborrelli (2013b)
G410apint216	TrGC	→	1.00E-11•R02•0.3	Rickard and Pascoe (2009), Taraborrelli (2013b)
G410apint217	TrGC	+ HO ₂ →	KR02H02•0.820	Rickard and Pascoe (2009), Taraborrelli (2013b)
G410apint218	TrGC	+ NO → + NO ₂	KR02NO	Rickard and Pascoe (2009), Taraborrelli (2013b)
G410apint219	TrGC	→	1.30E-12•R02	Rickard and Pascoe (2009), Taraborrelli (2013b)

35

Table 1: Gas phase reactions (... continued)

#	labels	reaction	rate coefficient	reference
G410apint220	TrGC	+ OH →	9.65E-12	Rickard and Pascoe (2009), Taraborrelli (2013b)
G410apint221	TrGC	+ hν → + OH	1.14*jx(ip_CH300H)	Rickard and Pascoe (2009), Taraborrelli (2013b)
G410apint222	TrGC	+ OH →	6.57E-12	Rickard and Pascoe (2009), Taraborrelli (2013b)
G410apint223	TrGC	+ OH → + CO + NO ₂	2.96E-12	Rickard and Pascoe (2009), Taraborrelli (2013b)
G410apint224	TrGC	→ + NO ₂	k_PAN_M	Rickard and Pascoe (2009), Taraborrelli (2013b)
G410apint225	TrGC	+ OH →	1.27E-11	Rickard and Pascoe (2009), Taraborrelli (2013b)
G410apint226	TrGC	+ hν → + OH	1.14*jx(ip_CH300H)	Rickard and Pascoe (2009), Taraborrelli (2013b)
G410apint227	TrGC	+ HO ₂ →	KR02HD2*0.820	Rickard and Pascoe (2009), Taraborrelli (2013b)
G410apint228	TrGC	+ NO → CH ₃ COCH ₃ + + NO ₂	KR02N0	Rickard and Pascoe (2009), Taraborrelli (2013b)
G410apint229	TrGC	→ CH ₃ COCH ₃ +	6.70E-15*R02	Rickard and Pascoe (2009), Taraborrelli (2013b)
G410apint230	TrGC	+ OH →	3.31E-11	Rickard and Pascoe (2009), Taraborrelli (2013b)
G410apint231	TrGC	+ hν → CH ₃ COCH ₃ + + OH	1.14*jx(ip_CH300H)	Rickard and Pascoe (2009), Taraborrelli (2013b)
G410apint232	TrGC	+ HO ₂ →	KR02HD2*0.625	Rickard and Pascoe (2009), Taraborrelli (2013b)
G410apint233	TrGC	+ NO → + HO ₂ + NO ₂	KR02N0	Rickard and Pascoe (2009), Taraborrelli (2013b)
G410apint234	TrGC	→ + HO ₂	8.80E-13*R02	Rickard and Pascoe (2009), Taraborrelli (2013b)
G410apint235	TrGC	+ OH →	7.46E-11	Rickard and Pascoe (2009), Taraborrelli (2013b)
G410apint236	TrGC	+ hν → + HO ₂ + OH	1.14*jx(ip_CH300H)	Rickard and Pascoe (2009), Taraborrelli (2013b)

36

Table 1: Gas phase reactions (... continued)

#	labels	reaction	rate coefficient	reference
G410apint237	TrGC	→	1.30E-12*R02	Rickard and Pascoe (2009), Taraborrelli (2013b)*
G410apint238	TrGC	+ HO ₂ →	KR02HD2*0.706	Rickard and Pascoe (2009), Taraborrelli (2013b)
G410apint239	TrGC	+ NO → + NO ₂	KR02N0	Rickard and Pascoe (2009), Taraborrelli (2013b)*
G410apint240	TrGC	+ hν → + OH	1.14*jx(ip_CH300H)+jx(ip_HOCH2CHO)	Rickard and Pascoe (2009), Taraborrelli (2013b)
G410apint241	TrGC	+ OH → + OH	1.01E-10	Rickard and Pascoe (2009), Taraborrelli (2013b)
G410apint242	TrGC	→ GLYOX +	8.80E-13*R02	Rickard and Pascoe (2009), Taraborrelli (2013b)*
G410apint243	TrGC	+ NO → GLYOX + + NO ₂	KR02N0	Rickard and Pascoe (2009), Taraborrelli (2013b)
G410apint244	TrGC	+ HO ₂ →	KR02HD2*0.706	Rickard and Pascoe (2009), Taraborrelli (2013b)
G410apint245	TrGC	+ OH →	1.33E-10	Rickard and Pascoe (2009), Taraborrelli (2013b)
G410apint246	TrGC	+ hν → + CO + HO ₂	jx(ip_HOCH2CHO)*2	Rickard and Pascoe (2009), Taraborrelli (2013b)
G410apint247	TrGC	+ NO ₃ → + HNO ₃	2*KNO3AL*5.5	Rickard and Pascoe (2009), Taraborrelli (2013b)
G410apint248	TrGC	+ hν → GLYOX + + OH	1.14*jx(ip_CH300H)+jx(ip_HOCH2CHO)	Rickard and Pascoe (2009), Taraborrelli (2013b)
G410apint249	TrGC	+ OH → + OH	9.23E-11	Rickard and Pascoe (2009), Taraborrelli (2013b)
G410apint250	TrGC	→	1.00E-11*R02	Rickard and Pascoe (2009), Taraborrelli (2013b)
G410apint251	TrGC	+ HO ₂ →	KAPH02	Rickard and Pascoe (2009), Taraborrelli (2013b)
G410apint252	TrGC	+ NO ₂ →	k_CH3CO3_NO2	Rickard and Pascoe (2009), Taraborrelli (2013b)
G410apint253	TrGC	+ NO → + NO ₂	KAPN0	Rickard and Pascoe (2009), Taraborrelli (2013b)

37

B. Chemical mechanism – MTM

Table 1: Gas phase reactions (... continued)

#	labels	reaction	rate coefficient	reference
G410apint254	TrGC	$\rightarrow + \text{HCHO}$	2.00E-12*R02	Rickard and Pascoe (2009), Taraborrelli (2013b)
G410apint255	TrGC	$+ \text{HO}_2 \rightarrow$	KR02HD2*0.625	Rickard and Pascoe (2009), Taraborrelli (2013b)
G410apint256	TrGC	$+ \text{NO} \rightarrow + \text{HCHO} + \text{NO}_2$	KR02ND	Rickard and Pascoe (2009), Taraborrelli (2013b)
G410apint257	TrGC	$+ \text{OH} \rightarrow + \text{CO} + \text{CO}$	2.64E-11	Rickard and Pascoe (2009), Taraborrelli (2013b)
G410apint258	TrGC	$+ h\nu \rightarrow + \text{HO}_2 + \text{CO} + \text{CO}$	$\text{jx}(\text{ip_MGLYOX})+2.15*\text{jx}(\text{ip_MGLYOX})$	Rickard and Pascoe (2009), Taraborrelli (2013b)
G410apint259	TrGC	$+ \text{OH} \rightarrow$	8.33E-11	Rickard and Pascoe (2009), Taraborrelli (2013b)
G410apint260	TrGC	$+ h\nu \rightarrow + \text{HCHO} + \text{OH}$	$1.14*\text{jx}(\text{ip_CH3OOH})+\text{jx}(\text{ip_HOCH2CHO})$ $+ \text{J_ACETOL}$	Rickard and Pascoe (2009), Taraborrelli (2013b)
G410apint261	TrGC	$+ \text{OH} \rightarrow$	7.55E-11	Rickard and Pascoe (2009), Taraborrelli (2013b)
G410apint262	TrGC	$+ h\nu \rightarrow + \text{OH}$	$1.14*\text{jx}(\text{ip_CH3OOH})+\text{jx}(\text{ip_HOCH2CHO})$ $+ \text{J_ACETOL}$	Rickard and Pascoe (2009), Taraborrelli (2013b)
G410apint263	TrGC	$\rightarrow + \text{NO}_2$	k_PAN_M	Rickard and Pascoe (2009), Taraborrelli (2013b)
G410apint264	TrGC	$+ \text{OH} \rightarrow + \text{CO} + \text{NO}_2$	7.19E-11	Rickard and Pascoe (2009), Taraborrelli (2013b)
G410apint265	TrGC	$+ \text{OH} \rightarrow$	3.39E-11	Rickard and Pascoe (2009), Taraborrelli (2013b)
G410apint266	TrGC	$+ h\nu \rightarrow + \text{HO}_2 + \text{CO}$	$\text{jx}(\text{ip_HOCH2CHO})$	Rickard and Pascoe (2009), Taraborrelli (2013b)
G410apint267	TrGC	$+ h\nu \rightarrow + \text{HO}_2 + \text{CO}$	$\text{jx}(\text{ip_MGLYOX})$	Rickard and Pascoe (2009), Taraborrelli (2013b)
G410apint268	TrGC	$+ \text{NO}_3 \rightarrow + \text{HNO}_3$	2*KND3AL*4.0	Rickard and Pascoe (2009), Taraborrelli (2013b)
G410apint269	TrGC	\rightarrow	1.00E-11*R02	Rickard and Pascoe (2009), Taraborrelli (2013b)
G410apint270	TrGC	$+ \text{HO}_2 \rightarrow$	KAPH02*rco3_ooh	Rickard and Pascoe (2009), Taraborrelli (2013b)

38

Table 1: Gas phase reactions (... continued)

#	labels	reaction	rate coefficient	reference
G410apint271	TrGC	$+ \text{HO}_2 \rightarrow + \text{OH}$	KAPH02*(1-rco3_ooh)	Rickard and Pascoe (2009), Taraborrelli (2013b)
G410apint272	TrGC	$+ \text{NO}_2 \rightarrow$	k_CH3CO3_NO2	Rickard and Pascoe (2009), Taraborrelli (2013b)
G410apint273	TrGC	$+ \text{NO} \rightarrow + \text{NO}_2$	KAPNO	Rickard and Pascoe (2009), Taraborrelli (2013b)
G410apint274	TrGC	$+ \text{OH} \rightarrow$	1.63E-11	Rickard and Pascoe (2009), Taraborrelli (2013b)
G410apint275	TrGC	$+ h\nu \rightarrow + \text{OH}$	$1.14*\text{jx}(\text{ip_CH3OOH})+\text{jx}(\text{ip_MGLYOX})$	Rickard and Pascoe (2009), Taraborrelli (2013b)
G410apint276	TrGC	$\rightarrow + \text{NO}_2$	k_PAN_M	Rickard and Pascoe (2009), Taraborrelli (2013b)
G410apint277	TrGC	$+ \text{OH} \rightarrow + \text{CO} + \text{NO}_2$	1.27E-11	Rickard and Pascoe (2009), Taraborrelli (2013b)*
G410apint278	TrGC	$\rightarrow 0.7 \text{HOCH}_2\text{CH}_2\text{O}_2 + 0.3$	1.00E-11*R02	Rickard and Pascoe (2009), Taraborrelli (2013b)
G410apint279	TrGC	$+ \text{NO} \rightarrow \text{HOCH}_2\text{CH}_2\text{O}_2 + \text{NO}_2$	KAPNO	Rickard and Pascoe (2009), Taraborrelli (2013b)
G410apint280	TrGC	$+ \text{HO}_2 \rightarrow$	KAPH02*rco3_ooh	Rickard and Pascoe (2009), Taraborrelli (2013b)
G410apint281	TrGC	$+ \text{HO}_2 \rightarrow \text{HOCH}_2\text{CH}_2\text{O}_2 + \text{OH}$	KAPH02*rco3_oh	Rickard and Pascoe (2009), Taraborrelli (2013b)
G410apint282	TrGC	$+ \text{HO}_2 \rightarrow + \text{O}_3$	KAPH02*rco3_o3	Rickard and Pascoe (2009), Taraborrelli (2013b)
G410apint283	TrGC	$+ \text{NO}_2 \rightarrow$	k_CH3CO3_NO2	Rickard and Pascoe (2009), Taraborrelli (2013b)
G410apint284	TrGC	$+ \text{OH} \rightarrow \text{HOCH}_2\text{CH}_2\text{O}_2$	1.39E-11	Rickard and Pascoe (2009), Taraborrelli (2013b)
G410apint285	TrGC	$+ \text{OH} \rightarrow$	1.73E-11	Rickard and Pascoe (2009), Taraborrelli (2013b)
G410apint286	TrGC	$+ h\nu \rightarrow \text{HOCH}_2\text{CH}_2\text{O}_2 + \text{OH}$	$1.14*\text{jx}(\text{ip_CH3OOH})$	Rickard and Pascoe (2009), Taraborrelli (2013b)
G410apint287	TrGC	$\rightarrow + \text{NO}_2$	k_PAN_M	Rickard and Pascoe (2009), Taraborrelli (2013b)

39

Table 1: Gas phase reactions (... continued)

#	labels	reaction	rate coefficient	reference
G410apint288	TrGC	+ OH → HOCH ₂ CHO + CO + NO ₂	4.51E-12	Rickard and Pascoe (2009), Taraborrelli (2013b)
G410apint289	TrGC	+ NO ₃ →	1.2E-12*EXP(490./temp)	Rickard and Pascoe (2009), Taraborrelli (2013b)
G410apint290	TrGC	→ + NO ₂	(.65*6.70E-15+.35*2.50E-13)*RD2	Rickard and Pascoe (2009), Taraborrelli (2013b)
G410apint291	TrGC	+ NO → + NO ₂ + NO ₂	KR02N0	Rickard and Pascoe (2009), Taraborrelli (2013b)
G410apint292	TrGC	+ HO ₂ →	KR02H02*0.914	Rickard and Pascoe (2009), Taraborrelli (2013b)
G410apint293	TrGC	+ NO ₃ → + NO ₂ + NO ₂	KR02N03	Rickard and Pascoe (2009), Taraborrelli (2013b)
G410apint294	TrGC	+ hν → + NO ₂ + OH	1.14*jx(ip_CH300H)	Rickard and Pascoe (2009), Taraborrelli (2013b)
G410apint295	TrGC	+ OH →	.65*6.87E-12+.35*1.23E-11	Rickard and Pascoe (2009), Taraborrelli (2013b)*
G410bpin	TrGC	+ OH →	1.47E-11*EXP(467/TEMP)*(0.8326*0.3+0.068)/(0.8326+0.068)	Vereecken and Peeters (2012)*
G410bpint2	TrGC	+ OH →	1.47E-11*EXP(467/TEMP)*0.8326*0.7/(0.8326+0.068)	Vereecken and Peeters (2012)*
G410bpint3	TrGC	+ HO ₂ →	KR02H02*0.914	Rickard and Pascoe (2009), Taraborrelli (2013b)
G410bpint4	TrGC	+ NO →	KR02N0*0.240	Rickard and Pascoe (2009), Taraborrelli (2013b)
G410bpint5	TrGC	+ NO → + HCHO + HO ₂ + NO ₂	KR02N0*0.760	Rickard and Pascoe (2009), Taraborrelli (2013b)
G410bpint6	TrGC	→ + HCHO + HO ₂	9.20E-14*RD2	Rickard and Pascoe (2009), Taraborrelli (2013b)
G410bpint7	TrGC	+ OH →	1.33E-11	Rickard and Pascoe (2009), Taraborrelli (2013b)
G410bpint8	TrGC	+ hν → + HCHO + HO ₂ + OH	1.14*jx(ip_CH300H)	Rickard and Pascoe (2009), Taraborrelli (2013b)
G410bpint9	TrGC	+ OH → + HCHO + NO ₂	4.70E-12	Rickard and Pascoe (2009), Taraborrelli (2013b)

40

Table 1: Gas phase reactions (... continued)

#	labels	reaction	rate coefficient	reference
G410bpint10	TrGC	+ NO → + CH ₃ COCH ₃ + NO ₂	KR02N0*0.892	Vereecken and Peeters (2012), Taraborrelli (2013b)
G410bpint11	TrGC	+ NO →	KR02N0*0.108	Vereecken and Peeters (2012), Taraborrelli (2013b)
G410bpint12	TrGC	+ HO ₂ →	KR02H02*0.914	Vereecken and Peeters (2012), Taraborrelli (2013b)
G410bpint13	TrGC	→ + CH ₃ COCH ₃	1.60E-13*RD2	Vereecken and Peeters (2012), Taraborrelli (2013b)
G410bpint14	TrGC	→	5.68E10*exp(-8745/TEMP)	Vereecken and Peeters (2012), Taraborrelli (2013b)*
G410bpint15	TrGC	+ NO → + NO ₂	KR02N0*0.890	Vereecken and Peeters (2012), Taraborrelli (2013b)
G410bpint16	TrGC	+ NO →	KR02N0*0.110	Vereecken and Peeters (2012), Taraborrelli (2013b)
G410bpint17	TrGC	+ HO ₂ →	KR02H02*0.820	Vereecken and Peeters (2012), Taraborrelli (2013b)
G410bpint18	TrGC	→	2.50E-13*RD2	Vereecken and Peeters (2012), Taraborrelli (2013b)
G410bpint19	TrGC	→ + HO ₂	5.7E10*exp(-2949/TEMP)	Vereecken and Peeters (2012), Taraborrelli (2013b)*
G410bpint20	TrGC	→ + OH	9.17E10*exp(-8706/TEMP)	Vereecken and Peeters (2012), Taraborrelli (2013b)*
G410bpint21	TrGC	+ NO → + NO ₂	KR02N0*0.747	Vereecken and Peeters (2012), Taraborrelli (2013b)
G410bpint22	TrGC	+ NO →	KR02N0*0.253	Vereecken and Peeters (2012), Taraborrelli (2013b)
G410bpint23	TrGC	+ HO ₂ →	KR02H02*0.914	Vereecken and Peeters (2012), Taraborrelli (2013b)
G410bpint24	TrGC	→	8.80E-13*RD2	Vereecken and Peeters (2012), Taraborrelli (2013b)
G410bpint25	TrGC	+ NO → + NO ₂	KR02N0*0.893	Vereecken and Peeters (2012), Taraborrelli (2013b)
G410bpint26	TrGC	+ NO →	KR02N0*0.107	Vereecken and Peeters (2012), Taraborrelli (2013b)

41

B. Chemical mechanism – MTM

Table 1: Gas phase reactions (... continued)

#	labels	reaction	rate coefficient	reference
G410bpint27	TrGC	+ HO ₂ →	KR02HD2*0.914	Vereecken and Peeters (2012), Taraborrelli (2013b)
G410bpint28	TrGC	→	5.00E-12*R02	Vereecken and Peeters (2012), Taraborrelli (2013b)
G410bpint29	TrGC	+ OH →	1.55E-11	Lewis et al. (2005), Rickard and Pascoe (2009), Taraborrelli (2013b)
G410bpint30	TrGC	+ HO ₂ →	KR02HD2*0.890	Rickard and Pascoe (2009), Taraborrelli (2013b)
G410bpint31	TrGC	+ NO → + NO ₂	KR02NO	Rickard and Pascoe (2009), Taraborrelli (2013b)
G410bpint32	TrGC	→	2.00E-12*R02	Rickard and Pascoe (2009), Taraborrelli (2013b)
G410bpint33	TrGC	+ OH → + OH	2.63E-11	Rickard and Pascoe (2009), Taraborrelli (2013b)
G410bpint34	TrGC	+ hν → + OH	1.14*jx(ip_CH300H)	Rickard and Pascoe (2009), Taraborrelli (2013b)
G410bpint35	TrGC	+ OH →	3.07E-12	Rickard and Pascoe (2009), Taraborrelli (2013b)
G410bpint36	TrGC	+ O ₃ → + .63 CO + .37 HOCH2OOH + .16 OH + .16 HO ₂	1.5E-17*.051/(1-.027)	Nguyen et al. (2009), Taraborrelli (2013b)
G410bpint37	TrGC	+ O ₃ →	1.5E-17*.368/(1-.027)	Nguyen et al. (2009), Taraborrelli (2013b)
G410bpint38	TrGC	+ O ₃ → + OH	1.5E-17*.283/(1-.027)	Nguyen et al. (2009), Taraborrelli (2013b)
G410bpint40	TrGC	+ O ₃ → + CO ₂	1.5E-17*(.104+.167)/(1-.027)	Nguyen et al. (2009), Taraborrelli (2013b)*
G410bpint41	TrGC	+ OH →	3.04E-12	Rickard and Pascoe (2009), Taraborrelli (2013b)
G410bpint42	TrGC	+ HO ₂ →	KR02HD2*0.859	Rickard and Pascoe (2009), Taraborrelli (2013b)
G410bpint43	TrGC	+ NO →	KR02NO*0.138	Rickard and Pascoe (2009), Taraborrelli (2013b)
G410bpint44	TrGC	+ NO → + NO ₂	KR02NO*0.862	Rickard and Pascoe (2009), Taraborrelli (2013b)

42

Table 1: Gas phase reactions (... continued)

#	labels	reaction	rate coefficient	reference
G410bpint45	TrGC	→	2.50E-13*R02	Rickard and Pascoe (2009), Taraborrelli (2013b)
G410bpint46	TrGC	+ OH → + OH	1.62E-11	Rickard and Pascoe (2009), Taraborrelli (2013b)
G410bpint47	TrGC	+ hν → + OH	1.14*jx(ip_CH300H)	Rickard and Pascoe (2009), Taraborrelli (2013b)
G410bpint48	TrGC	+ OH → + NO ₂	1.84E-12	Rickard and Pascoe (2009), Taraborrelli (2013b)
G410bpint49	TrGC	→ + NO ₂	J_IC3H7NO3	Rickard and Pascoe (2009), Taraborrelli (2013b)
G410bpint50	TrGC	+ OH →	3.94E-12	Rickard and Pascoe (2009), Taraborrelli (2013b)
G410bpint51	TrGC	→ + H ₂ O ₂	6.00E-18*c(ind_H2O)	Rickard and Pascoe (2009), Taraborrelli (2013b)
G410bpint52	TrGC	+ CO →	1.2E-15	Rickard and Pascoe (2009), Taraborrelli (2013b)
G410bpint53	TrGC	+ NO → + NO ₂	1.E-14	Rickard and Pascoe (2009), Taraborrelli (2013b)
G410bpint54	TrGC	+ NO ₂ → + NO ₃	1.E-15	Rickard and Pascoe (2009), Taraborrelli (2013b)
G410bpint55	TrGC	+ SO ₂ → + H ₂ SO ₄	7.E-14	Rickard and Pascoe (2009), Taraborrelli (2013b)
G410bpint56	TrGC	+ NO ₃ →	2.51E-12	Rickard and Pascoe (2009), Taraborrelli (2013b)
G410bpint57	TrGC	+ HO ₂ →	KR02HD2*0.914	Rickard and Pascoe (2009), Taraborrelli (2013b)
G410bpint58	TrGC	+ NO → + HCHO + NO ₂ + NO ₂	KR02NO	Rickard and Pascoe (2009), Taraborrelli (2013b)
G410bpint59	TrGC	+ NO ₃ → + HCHO + NO ₂ + NO ₂	KR02NO3	Rickard and Pascoe (2009), Taraborrelli (2013b)
G410bpint60	TrGC	→ + HCHO + NO ₂	9.20E-14*R02*0.7	Rickard and Pascoe (2009), Taraborrelli (2013b)
G410bpint61	TrGC	→	9.20E-14*R02*0.3	Rickard and Pascoe (2009), Taraborrelli (2013b)*

43

Table 1: Gas phase reactions (... continued)

#	labels	reaction	rate coefficient	reference
G410bpint62	TrGC	+ OH →	9.58E-12	Rickard and Pascoe (2009), Taraborrelli (2013b)
G410bpint63	TrGC	+ hν → + HCHO + NO ₂ + OH	1.14*jx(ip_CH300H)	Rickard and Pascoe (2009), Taraborrelli (2013b)
G410apint296	TrGC	+ OH →	8.7E-11*(.50*.25)	Wolfe et al. (2011), Taraborrelli (2013b)*
G410apint297	TrGC	+ OH → + HO ₂	8.7E-11*.25*.60	Wolfe et al. (2011), Taraborrelli (2013b)
G410apint298	TrGC	+ OH →	8.7E-11*.25*.40	Wolfe et al. (2011), Taraborrelli (2013b)
G410apint299	TrGC	+ O ₃ →	2.E-16*.50*.18	Wolfe et al. (2011), Taraborrelli (2013b)
G410apint300	TrGC	+ O ₃ →	2.E-16*.50*.16	Wolfe et al. (2011), Taraborrelli (2013b)
G410apint301	TrGC	+ O ₃ → OH + + CO + HO ₂	2.E-16*.50*.66	Wolfe et al. (2011), Taraborrelli (2013b)
G410apint302	TrGC	+ O ₃ →	2.E-16*.50*.12	Wolfe et al. (2011), Taraborrelli (2013b)
G410apint303	TrGC	+ O ₃ → OH +	2.E-16*.50*(.22+.66)	Wolfe et al. (2011), Taraborrelli (2013b)*
G410apint304	TrGC	+ NO ₃ →	9.5E-12	Wolfe et al. (2011), Taraborrelli (2013b)
G410myrc	TrGC	+ OH → + POHORG	9.19E-12*exp(1071./temp)*0.64	Hites and Turner (2009), Orlando et al. (2000), Taraborrelli (2013b)
G410myrct2	TrGC	+ OH → + POHORG	9.19E-12*exp(1071./temp)*0.36	Hites and Turner (2009), Orlando et al. (2000), Taraborrelli (2013b)
G410myrct3	TrGC	+ O ₃ → .25 CH ₃ COCH ₃ + .75 OH + .75 CH ₃ COCH ₂ O ₂	4.7E-16	Atkinson and Arey (2003), Taraborrelli (2013b)
G410myrct4	TrGNC	+ +.75 POHORG + NO ₃ →	1.1E-11	Atkinson and Arey (2003), Taraborrelli (2013b)
G410myrct5	TrGC	→ CH ₃ COCH ₃ + HO ₂ +	8.E-13*RD2	Taraborrelli (2013b)
G410myrct6	TrGC	+ HO ₂ →	KR02HD2	Taraborrelli (2013b)

44

Table 1: Gas phase reactions (... continued)

#	labels	reaction	rate coefficient	reference
G410myrct7	TrGCN	+ NO → .80 CH ₃ COCH ₃ + .80 HO ₂ + .80 + .80 NO ₂ + .20	KR02ND	Taraborrelli (2013b)*
G410myrct8	TrGCJ	+ hν → CH ₃ COCH ₃ + OH + HO ₂ + + POHORG	1.14*jx(ip_CH300H)	Taraborrelli (2013b)
G410myrct9	TrGC	+ OH → + POHORG	1.55E-10	Baker et al. (2004), Taraborrelli (2013b)
G410myrct10	TrGC	+ NO ₃ → CH ₃ COCH ₃ + NISOP02	4.7E-13	Baker et al. (2004), Taraborrelli (2013b)
G410myrct11	TrGC	+ OH → iC ₃ H ₇ ONO ₂ + + POHORG	1.55E-10	see note
G410myrct12	TrGC	→	1.E-12*RD2	Taraborrelli (2013b)
G410myrct13	TrGC	+ HO ₂ →	KR02HD2	Taraborrelli (2013b)
G410myrct14	TrGC	+ NO → .8 + .8 NO ₂ + .2	KR02ND	Taraborrelli (2013b)
G410myrct15	TrGC	→ + HO ₂	K16HS	Taraborrelli (2013b)
G410myrct16	TrGC	→ CH ₃ COCH ₃ + + .43 MVK + .27 MACR + .7 HCHO + .29 LHC4ACCHO + HO ₂	KDEC	Taraborrelli (2013b)
G410myrct17	TrGC	+ OH → CH ₃ COCH ₃ + HO ₂ + + ISOPBNO3 + POHORG	kadt*kads	Taraborrelli (2013b)
G410myrct18	TrGC	+ hν → + OH + POHORG	1.14*jx(ip_CH300H)	Taraborrelli (2013b)
G410myrct19	TrGC	+ OH → + .43 ISOPBOOH + .27 ISOPDOOH + .29 LISOPACOOH + CH ₃ COCH ₃ + HO ₂ + POHORG	kadt*kads	Taraborrelli (2013b)
G410myrct20	TrGCJ	+ hν → OH + + HO ₂ + POHORG	J_HPALD	Taraborrelli (2013b)
G410myrct21	TrGC	+ OH → + HO ₂ + CH ₃ COCH ₃ + POHORG	kadt*kads	Taraborrelli (2013b)
G410myrct22	TrGC	+ OH → + + HCHO + GLYOX + HO ₂ + POHORG	(kadt*kads)*acho*ach2ooh	Taraborrelli (2013b)
G410myrct23	TrGC	+ O ₃ → + .25 CH ₃ COCH ₃ + .75 OH + .75 CH ₃ COCH ₂ O ₂ + .75 POHORG	4.7E-16	Taraborrelli (2013b)
G410myrct24	TrGC	+ OH → + + POHORG	1.55E-10	Baker et al. (2004), Taraborrelli (2013b)
G410myrct25	TrGC	+ NO ₃ → + NISOP02	4.7E-13	Baker et al. (2004), Taraborrelli (2013b)
G410myrct26	TrGC	→	1.E-12*RD2	Taraborrelli (2013b)
G410myrct27	TrGC	+ HO ₂ → + .43 ISOPBOOH + .27 ISOPDOOH + .29 LISOPACOOH	KR02HD2	Taraborrelli (2013b)
G410myrct28	TrGC	+ NO → .8 + .8 NO ₂ + .2 + .2 ISOPBNO3	KR02ND	Taraborrelli (2013b)
G410myrct29	TrGC	→ + HO ₂	K16HS	Taraborrelli (2013b)
G410myrct30	TrGC	→ + .43 MVK + .27 MACR + .7 HCHO + .29 LHC4ACCHO + HO ₂	KDEC	Taraborrelli (2013b)

45

B. Chemical mechanism – MTM

Table 1: Gas phase reactions (... continued)

#	labels	reaction	rate coefficient	reference
G410myrct31	TrGCJ	+ hν → + OH + + HO ₂ + POHORG	J_HPALD	Taraborrelli (2013b)
G410myrct32	TrGC	+ OH → + .3 + .2 + .3 + .2 + POHORG	(kadt+kads)*acho*ach2ooh	Taraborrelli (2013b)
G410myrct33	TrGC	→	1.E-12*RD2	Taraborrelli (2013b)
G410myrct34	TrGC	+ HO ₂ →	KR02H02	Taraborrelli (2013b)
G410myrct35	TrGC	+ NO → .8 + .8 NO ₂ + .2 CH ₃ COCH ₃ + .2 + .2	KR02N0	Taraborrelli (2013b)
G410myrct36	TrGC	ISOPBNO3 → + HO ₂	K16HS	Taraborrelli (2013b)
G410myrct37	TrGC	→ CH ₃ COCH ₃ + + .43 MVK + .27 MACR + .7 HCHO + .29 LHCACCHO + HO ₂ + OH + POHORG	KDEC	Taraborrelli (2013b)
G410myrct38	TrGCJ	+ hν → + OH + POHORG	1.14*jx(ip_CH300H)	Taraborrelli (2013b)
G410myrct39	TrGCJ	+ hν → CH ₃ COCH ₃ + HO ₂ + + .43 ISOPBOOH + .27 ISOPDOOH + .29 LISOPACOOH + OH + POHORG	1.14*jx(ip_CH300H)	Taraborrelli (2013b)
G410myrct40	TrGCJ	+ hν → CH ₃ COCH ₃ + OH + + OH + + HO ₂ + 2	J_HPALD	Taraborrelli (2013b)
G410myrct41	TrGC	POHORG + OH → CH ₃ COCH ₃ + OH + + .3 + .2 + .3 + .2 + POHORG + POHORG	(kadt+kads)*acho*ach2ooh	Taraborrelli (2013b)
G410myrct42	TrGC	+ OH → + H ₂ O + POHORG	4.4E-12*EXP(365./temp)	Taraborrelli (2013b)*
G410myrct43	TrGC	+ hν → HCHO + HO ₂ + HO ₂ + CO	jx(ip_CH3CHO)	Taraborrelli (2013b)
G410myrct44	TrGC	+ NO ₃ → HNO ₃ +	KN03AL	Taraborrelli (2013b)
G410myrct45	TrGC	→ HCHO + HO ₂ + CO ₂	1.00E-11*0.7*RD2	Taraborrelli (2013b)
G410myrct46	TrGC	→	1.00E-11*0.3*RD2	Taraborrelli (2013b)
G410myrct47	TrGC	+ HO ₂ → OH + HCHO + HO ₂ + CO ₂ + POHORG	KAPH02*0.44	Taraborrelli (2013b)
G410myrct48	TrGC	+ HO ₂ →	KAPH02*0.41	Taraborrelli (2013b)
G410myrct49	TrGC	+ HO ₂ → + O ₃	KAPH02*0.15	Taraborrelli (2013b)
G410myrct50	TrGC	+ NO ₂ →	k_CH3CO3_NO2	Taraborrelli (2013b)
G410myrct51	TrGC	+ NO → NO ₂ + HCHO + HO ₂ + CO ₂	KAFNO	Taraborrelli (2013b)
G410myrct52	TrGC	+ NO ₃ → NO ₂ + HCHO + HO ₂ + CO ₂	KR02N03*1.60	Taraborrelli (2013b)
G410myrct53	TrGC	+ OH → HCHO + HO ₂ + CO ₂ + POHORG	4.2E-14*exp(850./temp)	Taraborrelli (2013b)*
G410myrct54	TrGC	+ hν → HCHO + HO ₂ + OH + CO ₂ + POHORG	1.14*jx(ip_CH300H)	Taraborrelli (2013b)
G410myrct55	TrGC	+ OH → + H ₂ O + POHORG	0.6*k_CH300H_OH	Taraborrelli (2013b)
G410myrct56	TrGC	→ + NO ₂	k_PAN_M	Taraborrelli (2013b)
G410myrct57	TrGC	+ OH → HCHO + CO + NO ₂ + POHORG	9.50E-13*EXP(-650./temp)	Taraborrelli (2013b)
G410afarn	TrGC	+ OH → + POHORG	2.7E-11*EXP(390./temp)	Taraborrelli (2013b)*
G410afarnt2	TrGC	+ OH → + POHORG	2.*1.9E-11*exp(450./temp)	Taraborrelli (2013b)*

46

Table 1: Gas phase reactions (... continued)

#	labels	reaction	rate coefficient	reference
G410afarnt3	TrGC	+ O ₃ → + .25 CH ₃ COCH ₃ + .75 OH + .75 CH ₃ COCH ₂ O ₂ + .75 POHORG	6.51E-15*exp(-829./temp)	Taraborrelli (2013b)*
G410afarnt4	TrGC	+ O ₃ → + + .75 OH + .75 POHORG	6.51E-15*exp(-829./temp)	Taraborrelli (2013b)*
G410afarnt5	TrGNC	+ NO ₃ →	2E-12*2*9.37E-12	Taraborrelli (2013b)*
G410afarnt6	TrGC	→	8.E-13*RD2	Taraborrelli (2013b)
G410afarnt7	TrGC	+ HO ₂ →	KR02H02	Taraborrelli (2013b)
G410afarnt8	TrGC	+ NO → .75 + .75 NO ₂ + .25	KR02N0	Taraborrelli (2013b)
G410afarnt9	TrGCJ	+ hν → + OH + POHORG	1.14*jx(ip_CH300H)	Taraborrelli (2013b)
G410afarnt10	TrGC	+ OH → + + POHORG	2.7E-11*EXP(390./temp)	Taraborrelli (2013b)
G410afarnt11	TrGC	+ OH → .5 + .5 + + POHORG	2.*1.9E-11*exp(450./temp)	Taraborrelli (2013b)
G410afarnt12	TrGC	→ .5 + .5 + .5 + .5 CH ₃ COCH ₃ + HO ₂	KDEC	Taraborrelli (2013b)
G410afarnt13	TrGC	→	1.E-12*RD2	Taraborrelli (2013b)
G410afarnt14	TrGC	+ HO ₂ →	KR02H02	Taraborrelli (2013b)
G410afarnt15	TrGC	+ NO → .75 + .75 NO ₂ + .25	KR02N0	Taraborrelli (2013b)
G410afarnt16	TrGC	→ + HO ₂ +	K16HS	Taraborrelli (2013b)
G410afarnt17	TrGC	→ +	KDEC	Taraborrelli (2013b)
G410afarnt18	TrGC	+ OH → + HO ₂ + ISOPBNO3 + POHORG	kadt*kads	Taraborrelli (2013b)
G410afarnt19	TrGC	+ hν → + OH + POHORG	1.14*jx(ip_CH300H)	Taraborrelli (2013b)
G410afarnt20	TrGC	+ OH → + + POHORG	kadt*kads	Taraborrelli (2013b)
G410afarnt21	TrGC	+ O ₃ → + + .75 OH + .75 POHORG	2.*6.51E-15*exp(-829./temp)	Taraborrelli (2013b)*
G410afarnt22	TrGC	+ OH → + POHORG	1.9E-11*exp(450./temp)	Taraborrelli (2013b)*
G410afarnt23	TrGC	+ OH → + POHORG	2.7E-11*EXP(390./temp)	Taraborrelli (2013b)*
G410afarnt24	TrGC	+ O ₃ → + + .75 OH + .75 POHORG	6.51E-15*exp(-829./temp)	Taraborrelli (2013b)*
G410afarnt25	TrGNC	+ NO ₃ →	2E-12	Taraborrelli (2013b)*
G410afarnt26	TrGNC	+ NO ₃ →	9.37E-12	Taraborrelli (2013b)*
G410afarnt27	TrGC	→	8.E-13*RD2	Taraborrelli (2013b)
G410afarnt28	TrGC	+ HO ₂ →	KR02H02	Taraborrelli (2013b)
G410afarnt29	TrGC	+ NO → .75 + .75 NO ₂ + .25	KR02N0	Taraborrelli (2013b)
G410afarnt30	TrGCJ	+ hν → + OH + POHORG	1.14*jx(ip_CH300H)	Taraborrelli (2013b)
G410afarnt31	TrGC	+ OH → + HO ₂ + + POHORG	2.7E-11*EXP(390./temp)	Taraborrelli (2013b)*
G410afarnt32	TrGC	+ OH → + + POHORG	1.9E-11*exp(450./temp)	Taraborrelli (2013b)*
G410afarnt33	TrGC	→ + + HO ₂	KDEC	Taraborrelli (2013b)
G410afarnt34	TrGC	→	1.E-12*RD2	Taraborrelli (2013b)
G410afarnt35	TrGC	+ HO ₂ →	KR02H02	Taraborrelli (2013b)
G410afarnt36	TrGC	+ NO → .75 + .75 NO ₂ + .25	KR02N0	Taraborrelli (2013b)

47

Table 1: Gas phase reactions (... continued)

#	labels	reaction	rate coefficient	reference
G410afarnt37	TrGC	$\rightarrow + + \text{HO}_2 +$	K16HS	Taraborrelli (2013b)
G410afarnt38	TrGC	$\rightarrow +$	KDEC	Taraborrelli (2013b)
G410afarnt39	TrGC	$+ \text{OH} \rightarrow + \text{HO}_2 + \text{ISOPBNO}_3 + \text{POHORG}$	kadt*kads	Taraborrelli (2013b)
G410afarnt40	TrGC	$+ \text{h}\nu \rightarrow + \text{OH} + \text{POHORG}$	1.14*jx(ip_CH300H)	Taraborrelli (2013b)
G410afarnt41	TrGC	$+ \text{OH} \rightarrow + + \text{POHORG}$	kadt*kads	Taraborrelli (2013b)
G410afarnt42	TrGC	$+ \text{O}_3 \rightarrow + + .75 \text{ OH} + .75 \text{ POHORG}$	6.51E-15*exp(-829./temp)	Taraborrelli (2013b)
G410afarnt43	TrGC	$+ \text{OH} \rightarrow + \text{POHORG}$	1.37E-10	Smith et al. (1996), Taraborrelli (2013b)*
G410afarnt44	TrGC	$+ \text{O}_3 \rightarrow .25 \text{ CH}_3\text{COCH}_3 + .125 + .25 \text{ GLYOX}$ $+ .25 \text{ CH}_3\text{COCH}_2\text{O}_2 + .125 \text{ H}_2\text{O}_2 + .75 \text{ OH} + .75$ $\text{CH}_3\text{COCH}_2\text{O}_2 + .75 + .75 \text{ POHORG}$	3.9E-16	Grosjean et al. (1996), Taraborrelli (2013b)*
G410afarnt45	TrGC	$+ \text{NO}_3 \rightarrow$	7E-12	Smith et al. (1996), Taraborrelli (2013b)
G410afarnt46	TrGC	$\rightarrow \text{CH}_3\text{COCH}_3 + + \text{HO}_2$	8.E-13*R02	Taraborrelli (2013b)
G410afarnt47	TrGC	$+ \text{HO}_2 \rightarrow$	KR02H02	Taraborrelli (2013b)
G410afarnt48	TrGC	$+ \text{NO} \rightarrow .25 + .75 \text{ CH}_3\text{COCH}_3 + .75 + .75 \text{ HO}_2 + .75$ NO_2	KR02N0	Taraborrelli (2013b)
G410afarnt49	TrGC	$+ \text{OH} \rightarrow + \text{POHORG}$	0.6*k_CH300H_OH	Taraborrelli (2013b)
G410afarnt50	TrGC	$+ \text{OH} \rightarrow + \text{HO}_2 + \text{POHORG}$	kt*ftoh*falk*falk	Taraborrelli (2013b)
G410afarnt51	TrGCJ	$+ \text{h}\nu \rightarrow \text{CH}_3\text{COCH}_3 + + \text{OH} + \text{POHORG}$	1.14*jx(ip_CH300H)	Taraborrelli (2013b)
G410afarnt52	TrGCJ	$+ \text{h}\nu \rightarrow \text{CH}_3\text{COCH}_3 + \text{CH}_3\text{COCH}_2\text{O}_2 + + \text{OH} +$ POHORG	1.14*jx(ip_CH300H)+2.77*jx(ip_HOCH2CHO)	Taraborrelli (2013b)*
G410afarnt53	TrGC	$+ \text{OH} \rightarrow + \text{HO}_2 + \text{POHORG}$	kt*ftoh*falk*fch2ono2	Taraborrelli (2013b)
G410afarnt54	TrGC	$+ \text{h}\nu \rightarrow \text{CH}_3\text{COCH}_3 + \text{NO}_2 + \text{CH}_3\text{COCH}_2\text{O}_2 +$	2.84*J_IC3H7N03	Taraborrelli (2013b)
G410afarnt55	TrGC	$+ \text{OH} \rightarrow \text{CH}_3\text{COCH}_2\text{O}_2 + + \text{POHORG}$	2.E-11	Fruekilde et al. (1997), Taraborrelli (2013b)*
G410afarnt56	TrGCJ	$+ \text{h}\nu \rightarrow \text{CH}_3\text{COCH}_2\text{O}_2 + + \text{HO}_2$	jx(ip_CH3CHO)+jx(ip_CH3COCH3)	Taraborrelli (2013b)

48

*Notes:

Rate coefficients for three-body reactions are defined via the function $k_3rd(T, M, k_0^{300}, n, k_{inf}^{300}, m, f_c)$. In the code, the temperature T is called `temp` and the concentration of "air molecules" M is called `cair`. Using the auxiliary variables $k_0(T)$, $k_{inf}(T)$, and k_{ratio} , k_3rd is defined as:

$$k_0(T) = k_0^{300} \times \left(\frac{300\text{K}}{T}\right)^n \quad (1)$$

$$k_{inf}(T) = k_{inf}^{300} \times \left(\frac{300\text{K}}{T}\right)^m \quad (2)$$

$$k_{ratio} = \frac{k_0(T)M}{k_{inf}(T)} \quad (3)$$

$$k_3rd = \frac{k_0(T)M}{1 + k_{ratio}} \times f_c \left(\frac{1}{1 + (\log_{10}(k_{ratio}/N))^2}\right) \quad (4)$$

A similar function, called k_3rd_iupac here, is used by Atkinson et al. (2005) for three-body reactions. It has the same function parameters as k_3rd and it is defined as:

$$k_0(T) = k_0^{300} \times \left(\frac{300\text{K}}{T}\right)^n \quad (5)$$

$$k_{inf}(T) = k_{inf}^{300} \times \left(\frac{300\text{K}}{T}\right)^m \quad (6)$$

$$k_{ratio} = \frac{k_0(T)M}{k_{inf}(T)} \quad (7)$$

$$N = 0.75 - 1.27 \times \log_{10}(f_c) \quad (8)$$

$$k_3rd_iupac = \frac{k_0(T)M}{1 + k_{ratio}} \times f_c \left(\frac{1}{1 + (\log_{10}(k_{ratio}/N))^2}\right) \quad (9)$$

G2110: The rate coefficient is: $k_H02_H02 = (1.5E-12 \cdot \text{EXP}(19./\text{temp}) + 1.7E-33 \cdot \text{EXP}(1000./\text{temp}) \cdot \text{cair}) \cdot (1. + 1.4E-21 \cdot \text{EXP}(2200./\text{temp}) \cdot \text{c}(\text{ind}_$

H20)). The value for the first (pressure-independent) part is from Christensen et al. (2002), the water term from Kircher and Sander (1984).

G3109: The rate coefficient is: $k_N03_N02 = k_3rd(\text{temp}, \text{cair}, 2.E-30, 4.4, 1.4E-12, 0.7, 0.6)$.

G3110: The rate coefficient is defined as backward reaction divided by equilibrium constant.

G3206: The rate coefficient is: $k_HNO3_OH = 2.4E-14 \cdot \text{EXP}(460./\text{temp}) + 1./ (1./ (6.5E-34 \cdot \text{EXP}(1335./\text{temp}) \cdot \text{cair}) + 1./ (2.7E-17 \cdot \text{EXP}(2199./\text{temp})))$

G3207: The rate coefficient is defined as backward reaction divided by equilibrium constant.

G4107: The rate coefficient is: $k_CH300H_OH = 3.8E-12 \cdot \text{EXP}(200./\text{temp})$.

G4109: The same temperature dependence assumed as for $\text{CH}_3\text{CHO} + \text{NO}_3$.

G4206: The product $\text{C}_2\text{H}_5\text{OH}$, which reacts only with OH, is substituted by its degradation products $\approx 0.1 \text{ HOCH}_2\text{CH}_2\text{O}_2 + 0.9 \text{ CH}_3\text{CHO} + 0.9 \text{ HO}_2$.

G4207: The rate constant $8.01E-12$ is for the H abstraction in alpha to the $-\text{OOH}$ group (Rickard and Pascoe, 2009) and $0.6 \cdot k_CH300H_OH$ is for the $\text{C}_2\text{H}_5\text{O}_2$ channel. The branching ratios are calculated from the terms of the rate coefficient at 298 K.

G4218: The rate coefficient is the same as for the CH_3O_2 channel in G4107 ($\text{CH}_3\text{OOH} + \text{OH}$).

G4221: The rate coefficient $\text{isk_PAN_M} = k_CH3CO3_H02/9.E-29 \cdot \text{EXP}(-14000./\text{temp})$, i.e. the rate coefficient is defined as backward reaction divided by equilibrium constant.

G4300: The product $\text{NC}_3\text{H}_7\text{O}_2$ is substituted with its degradation products $\text{C}_2\text{H}_5\text{O}_2 + \text{CO}_2 + \text{HO}_2$.

G4304: The value for the generic $\text{RO}_2 + \text{HO}_2$ reaction from Atkinson (1997) is used here.

G4306: The MCM (Rickard and Pascoe, 2009) products are 0.2 IPROPOL + 0.2 CH_3COCH_3 + 0.6 IC3H7O. IPROPOL and IC3H7O are substituted with their degradation products. We assume IPROPOL to be oxidized entirely to $\text{CH}_3\text{COCH}_3 + \text{HO}_2$ by OH. IC3H7O + O_2 produces the same products.

G4307: Analogous to G4207 for both rate coefficient and branching ratios.

G4400: $\text{LC}_2\text{H}_5\text{O}_2$ represents $0.127 \text{ NC}_4\text{H}_9\text{O}_2 + 0.873 \text{ SC}_4\text{H}_9\text{O}_2$.

G4401: $\text{NC}_4\text{H}_9\text{O}$ and $\text{SC}_4\text{H}_9\text{O}$ are substituted with 2 $\text{CO}_2 + \text{C}_2\text{H}_5\text{O}_2$ and 0.636 $\text{MEK} + \text{HO}_2$ and 0.364 $\text{CH}_3\text{CHO} + \text{C}_2\text{H}_5\text{O}_2$, respectively. The stoichiometric coefficients on the right side are weighted averages.

G4403: The alkyl nitrate yield is the weighted average yield for the two isomers forming from $\text{NC}_4\text{H}_9\text{O}_2$ and $\text{SC}_4\text{H}_9\text{O}_2$.

G4404: The product distribution is the weighted average of the single isomer hydroperoxides. It is calculated from the rate constants of single channels and the ratio of the isomers $\text{NC}_4\text{H}_9\text{O}_2$ and $\text{SC}_4\text{H}_9\text{O}_2$. The overall rate constant for this reaction is calculated as weighted average of the channels rate constants.

The relative weight of the products from $\text{NC}_4\text{H}_9\text{OOH}$ and $\text{SC}_4\text{H}_9\text{OOH}$ are then 0.0887 and 0.9113. The channels producing RO_2 are given the rate coefficient $0.6 \cdot k_CH300H_OH$ as for G4107. For $\text{NC}_4\text{H}_9\text{OOH}$ the products are $0.327 \text{ NC}_4\text{H}_9\text{O}_2 + 0.673 \text{ C}_3\text{H}_7\text{CHO} + 0.673 \text{ OH}$. $\text{C}_3\text{H}_7\text{CHO}$ is then substituted with 2 $\text{CO}_2 + \text{C}_2\text{H}_5\text{O}_2$. Hence, $0.327 \text{ NC}_4\text{H}_9\text{O}_2 + 1.346 \text{ CO}_2 + 0.673 \text{ C}_2\text{H}_5\text{O}_2 + 0.673 \text{ OH}$. For $\text{SC}_4\text{H}_9\text{OOH}$ the products are $0.219 \text{ SC}_4\text{H}_9\text{O}_2 + 0.781 \text{ MEK} + 0.781 \text{ OH}$.

G4413: LMEKO2 represents $0.459 \text{ MEKAO}_2 + 0.462 \text{ MEKBO}_2 + 0.079 \text{ MEKCO}_2$.

G4415: Alkyl nitrate formation is neglected. The products of MEKAO and MEKCO are substituted with

49

B. Chemical mechanism – MTM

HCHO + CO ₂ + HOCH ₂ CH ₂ O ₂ and HCHO + CO ₂ + C ₂ H ₅ O ₂ .	G4416: LMEKOOH is assumed having the composition 0.459 MEKAOOH + 0.462 MEKBOOH + 0.079 MEKCOOH. MEKAOOH + OH gives 0.89 CO ₂ C ₃ CHO + 0.89 OH + 0.11 MEKAO ₂ + H ₂ O. CO ₂ C ₃ CHO is substituted with CH ₃ COCH ₂ O ₂ + CO ₂ and the products become 0.89 CH ₃ COCH ₂ O ₂ + 0.89 CO ₂ + 0.89 OH + 0.11 MEKAO ₂ + H ₂ O. MEKBOOH + OH gives 0.758 BIACET + 0.758 OH + 0.242 MEKBO ₂ + H ₂ O. MEKCOOH + OH gives 0.614 EGLYOX + 0.614 OH + 0.386 MEKCO ₂ + H ₂ O. EGLYOX is substituted with C ₂ H ₅ O ₂ + 2 CO ₂ and the products become 0.614 C ₂ H ₅ O ₂ + 1.228 CO ₂ + 0.614 OH + 0.386 MEKCO ₂	G4417: The rate coefficient is the combination of the ones for the two isomers weighted by the relative abundances for NC4H9NO ₃ and SC4H9NO ₃ , respectively. Product distribution is calculated accordingly. NC4H9NO ₃ + OH gives C3H7CHO + NO ₂ + H ₂ O with C3H7CHO being substituted with 2 CO ₂ + C ₂ H ₅ O ₂ . After substitution is obtained 2 CO ₂ + C ₂ H ₅ O ₂ + NO ₂ + H ₂ O. SC4H9NO ₃ + OH gives MEK + NO ₂ + H ₂ O. For the product distribution NC4H9NO ₃ and SC4H9NO ₃ account for 0.08577 and 0.91423, respectively.	G4419: The same value as for PAN is assumed.	G4420: Products are as in G4415. Only the main channels for each isomer are considered. Rate constant is the weighted average for the isomers.	G4455: CH ₃ COCOCO ₃ H assumed to photolyse quickly and give CH ₃ CO ₃ + CO + CO ₂ + OH	G45222: HYBIACETOOA approximated to yield BIACETOH only. CH ₃ COCHOHCH ₂ OH's main reaction with OH yields BIACETOH recycling OH = _z substitution with BIACETOH	G413621: PEROXYRINGC2OHC3OD substituted	G4136: CH ₃ COCH ₂ O ₂ CH ₂ CO ₃ - _z CH ₃ CO ₃ + CO ₂ + 2 HCHO
---	--	--	--	--	--	--	---	---

50

Table 2: Photolysis reactions

#	labels	reaction	rate coefficient	reference
J1000	StTrGJ	O ₂ + hν → O(³ P) + O(³ P)	jx(ip_02)	see note
J1001a	StTrGJ	O ₃ + hν → O(¹ D)	jx(ip_01D)	see note
J1001b	StTrGJ	O ₃ + hν → O(³ P)	jx(ip_03P)	see note
J2101	StTrGJ	H ₂ O ₂ + hν → 2 OH + 2 POHOG	JX(ip_H2O2)	see note
J3101	StTrGNJ	NO ₂ + hν → NO + O(³ P)	jx(ip_N02)	see note
J3103a	StTrGNJ	NO ₃ + hν → NO ₂ + O(³ P)	jx(ip_N020)	see note
J3103b	StTrGNJ	NO ₃ + hν → NO	jx(ip_N002)	see note
J3104a	StTrGNJ	N ₂ O ₅ + hν → NO ₂ + NO ₃	jx(ip_N2O5)	see note
J3200	TrGJ	HONO + hν → NO + OH + PONOX	JX(ip_HONO)	see note
J3201	StTrGNJ	HNO ₃ + hν → NO ₂ + OH + PONOX	JX(ip_HNO3)	see note
J3202	StTrGNJ	HNO ₄ + hν → .667 NO ₂ + .667 HO ₂ + .333 NO ₃ + .333 OH + .333 PONOX	JX(ip_HNO4)	see note
J4100e	StTrGJ	CH ₃ OOH + hν → HCHO + OH + HO ₂ + POHORG	1.14*jx(ip_CH3OOH)	see note
J4101a	StTrGJ	HCHO + hν → H ₂ + CO	jx(ip_COH2)	see note
J4101b	StTrGJ	HCHO + hν → H + CO + HO ₂	jx(ip_CHOH)	see note
J4104e	StTrGJ	HOCH ₂ OOH + hν → OH + HO ₂ + HCOOH + POHORG	1.14*jx(ip_CH3OOH)	see note
J4200e	TrGCJ	C ₂ H ₅ OOH + hν → CH ₃ CHO + HO ₂ + OH + POHORG	1.14*jx(ip_CH3OOH)	see note
J4201	TrGCJ	CH ₃ CHO + hν → CH ₃ O ₂ + HO ₂ + CO	jx(ip_CH3CHO)	see note
J4202e	TrGCJ	CH ₃ C(O)OOH + hν → CH ₃ O ₂ + OH + CO ₂ + POHORG	1.14*jx(ip_CH3CO3H)	see note
J4204e	TrGNCJ	PAN + hν → .6 CH ₃ C(O)OO + .6 NO ₂ + .4 CH ₃ O ₂ + .4 CO ₂ + .4 NO ₃	jx(ip_PAN)	see note
J4205ae	TrGCJ	HOCH ₂ CHO + hν → HCHO + 2 HO ₂ + CO	jx(ip_HOCH2CHO)*0.70	Taraborrelli (2013a)
J4205be	TrGCJ	HOCH ₂ CHO + hν → 1.16 OH + .84 + .1 HCHO + .1 CO + .06 GLYOX + 1.16 POHORG	jx(ip_HOCH2CHO)*0.15	Taraborrelli (2013a)
J4205ce	TrGCJ	HOCH ₂ CHO + hν → CH ₃ OH + CO	jx(ip_HOCH2CHO)*0.15	Taraborrelli (2013a)
J4206e	TrGCJ	+ hν → OH + HCHO + CO + HO ₂ + POHORG	1.14*jx(ip_CH3OOH)+jx(ip_HOCH2CHO)	Taraborrelli (2013a)
J4206et2	TrGCJ	HOCH ₂ CO ₃ H + hν → HCHO + HO ₂ + OH + CO ₂ + POHORG	1.14*jx(ip_CH3OOH)	Rickard and Pascoe (2009)*
J4207	TrGCJ	PHAN + hν → HOCH ₂ CO ₃ + NO ₂	jx(ip_PAN)	see note
J4208	TrGCJ	GLYOX + hν → 2 CO + 2 HO ₂	jx(ip_GLYOX)	see note
J4209	TrGNCJ	HCOCO ₂ H + hν → 2 HO ₂ + CO + CO ₂	jx(ip_MGLYOX)	Rickard and Pascoe (2009)*

51

Table 2: Photolysis reactions (... continued)

#	labels	reaction	rate coefficient	reference
J4210e	TgNCJ	HCOC ₃ H + hν → HO ₂ + CO + OH + CO ₂ + POHORG	1.14*jx(ip_CH300H)*jx(ip_HOCH2CHO)	Rickard and Pascoe (2009)*
J4211e	TgCJ	HYETHO2H + hν → HOCH ₂ CH ₂ O + OH + POHORG	1.14*jx(ip_CH300H)	Rickard and Pascoe (2009)*
J4212	TgCJ	ETHOHN ₃ + hν → HO ₂ + 2 HCHO + NO ₂	J_IC3H7N ₃	see note
J4213e	TgCJ	+ hν → OH + HCHO + CO ₂ + OH + 2 POHORG	2*1.14*jx(ip_CH300H)	Taraborrelli (2013a)
J4214e	TgC	+ hν → OH + HCHO + HO ₂ + CO ₂ + POHORG	1.14*jx(ip_CH300H)	Taraborrelli (2013a)
J4215e	TgC	+ hν → .4 CO ₂ + .8 H + .34 CO + .34 OH + .34 HO ₂ + .16 HCHO + .16 O(³ P) + .1 HCOOH + CO + .34 POHORG	J_ketene* 0.36	Taraborrelli (2013a)
J4216e	TgC	+ hν → CH ₃ O ₂ + HCOOH + OH + POHORG	1.14*jx(ip_CH300H)	Taraborrelli (2013a)
J4217e	TgCJ	+ hν → HO ₂ + CO + HCHO + NO ₂	1.59*J_IC3H7N ₃ +jx(ip_CH3COCH ₃)	Taraborrelli (2013a)
J4300e	TgCJ	iC ₃ H ₇ OOH + hν → CH ₃ COCH ₃ + HO ₂ + OH + POHORG	1.14*jx(ip_CH300H)	von Kuhlmann (2001)*
J4301	TgCJ	CH ₃ COCH ₃ + hν → CH ₃ C(O)OO + CH ₃ O ₂	jx(ip_CH3COCH ₃)	see note
J4302	TgCJ	CH ₃ COCH ₂ OH + hν → CH ₃ C(O)OO + HCHO + HO ₂	J_ACETOL	see note
J4303	TgCJ	MGLYOX + hν → CH ₃ C(O)OO + CO + HO ₂	jx(ip_MGLYOX)	see note
J4304e	TgCJ	CH ₃ COCH ₂ O ₂ H + hν → CH ₃ C(O)OO + HCHO + OH + POHORG	1.14*jx(ip_CH300H)+J_ACETOL	Taraborrelli (2013a)
J4305e	TgCJ	+ hν → + HCHO + OH + POHORG	1.14*jx(ip_CH300H)+J_ACETOL	Taraborrelli (2013a)
J4306	TgNCJ	iC ₃ H ₇ ONO ₂ + hν → CH ₃ COCH ₃ + NO ₂ + HO ₂	J_IC3H7N ₃	von Kuhlmann et al. (2003)*
J4307	TgCJ	NOA + hν → CH ₃ C(O)OO + HCHO + NO ₂	J_IC3H7N ₃ +jx(ip_CH3COCH ₃)	see note
J4309e	TgCJ	HYPROPO2H + hν → CH ₃ CHO + HCHO + HO ₂ + OH + POHORG	1.14*jx(ip_CH300H)	Taraborrelli (2013a)
J4310e	TgNCJ	PR2O2HNO ₃ + hν → NOA + HO ₂ + OH + POHORG	1.14*jx(ip_CH300H)	Taraborrelli (2013a)
J4311e	TgCJ	HOCH ₂ COCHO + hν → + CO + HO ₂	jx(ip_MGLYOX)	Taraborrelli (2013a)
J4312e	TgCJ	+ hν → .5 CH ₃ CHO + .8 CO ₂ + .4 CH ₃ C(O)OO + .3 HO ₂ + .1 CH ₃ COOH + .1 OH + .2 CO + .1 POHORG	JX(IP_MGLYOX)	Taraborrelli (2013a)
J4313e	TgCJ	+ hν → + HCHO + OH + POHORG	1.14*jx(ip_CH300H)+J_ACETOL	Taraborrelli (2013a)
J4314e	TgCJ	+ hν → + CO + HO ₂	JX(IP_MGLYOX)	Taraborrelli (2013a)
J4315e	TgCJ	+ hν → + HO ₂ + CO	2*JX(IP_MGLYOX)	Taraborrelli (2013a)
J4316e	TgC	+ hν → CH ₃ C(O)OO + OH + POHORG + CO ₂	JX(IP_MGLYOX)+1.14*jx(ip_CH300H)	Taraborrelli (2013a)
J4317e	TgC	+ hν → C ₂ H ₄ + CO	J_ketene*0.36*2.	Taraborrelli (2013a)*
J4400e	TgCJ	LC ₄ H ₉ OOH + hν → OH + 0.254 CO ₂ + 0.5552 MEK + 0.5552 HO ₂ + 0.3178 CH ₃ CHO + 0.4448 C ₂ H ₅ O ₂ + POHORG	1.14*jx(ip_CH300H)	Rickard and Pascoe (2009)*
J4401	TgCJ	MVK + hν → C ₃ H ₆ + CO	jx(ip_MVK)	Taraborrelli (2013a)*

52

Table 2: Photolysis reactions (... continued)

#	labels	reaction	rate coefficient	reference
J4403	TgCJ	MEK + hν → CH ₃ C(O)OO + C ₂ H ₅ O ₂	0.42*jx(ip_CHOH)	von Kuhlmann et al. (2003)*
J4404e	TgCJ	LMEKOOH + hν → 0.538 HCHO + 0.538 CO ₂ + 0.459 HOCH ₂ CH ₂ O ₂ + 0.079 C ₂ H ₅ O ₂ + 0.462 CH ₃ C(O)OO + 0.462 CH ₃ CHO + OH + POHORG	1.14*jx(ip_CH300H)+J_ACETOL	Rickard and Pascoe (2009)*
J4405	TgCJ	BIACET + hν → 2 CH ₃ C(O)OO	2.15*jx(ip_MGLYOX)	see note
J4406	TgNCJ	LC4H9NO ₃ + hν → NO ₂ + 0.254 CO ₂ + 0.5552 MEK + 0.5552 HO ₂ + 0.3178 CH ₃ CHO + 0.4448 C ₂ H ₅ O ₂	J_IC3H7N ₃	see note
J4407e	TgNCJ	MPAN + hν → .6 MACO ₃ + .6 NO ₂ + .4 + .4 NO ₃	jx(ip_PAN)	Taraborrelli (2013a)*
J4409e	TgCJ	CO2H3CO3H + hν → + OH + CO ₂ + POHORG	1.14*jx(ip_CH300H)	Taraborrelli (2013a)
J4410	TgCJ	CO2H3CO3H + hν → CH ₃ C(O)OO + HO ₂ + HCOCO ₂ H	J_ACETOL	Rickard and Pascoe (2009)*
J4410t2	TgCJ	+ hν → CH ₃ C(O)OO + HCOCO ₂ H + HO ₂	J_ACETOL	Taraborrelli (2013a)
J4411	TgCJ	MACR + hν → .5 MACO ₃ + .5 + .5 CO + HO ₂	jx(ip_MACR)	see note
J4412e	TgCJ	MACROOH + hν → + OH + POHORG	1.14*jx(ip_CH300H)+ 2.77*jx(ip_HOCH2CHO)	see note
J4414	TgCJ	MACROH + hν → CH ₃ COCH ₂ OH + CO + HO ₂ + HO ₂	2.77*jx(ip_HOCH2CHO)	see note
J4415e	TgCJ	MACO3H + hν → + OH + POHORG	1.14*jx(ip_CH300H)	Taraborrelli (2013a)
J4416e	TgCJ	LHMVKABOOH + hν → .12 + .88 CH ₃ C(O)OO + .88 HOCH ₂ CHO + .12 HCHO + OH + POHORG	1.14*jx(ip_CH300H)+J_ACETOL	Taraborrelli (2013a)
J4418e	TgCJ	CO2H3CHO + hν → + CO + HO ₂	jx(ip_HOCH2CHO)+J_ACETOL	Taraborrelli (2013a)
J4419	TgCJ	HO12CO3C4 + hν → CH ₃ C(O)OO + HOCH ₂ CHO + HO ₂	J_ACETOL	Rickard and Pascoe (2009)*
J4420e	TgCJ	BIACETOH + hν → CH ₃ C(O)OO +	2.15*jx(ip_MGLYOX)	Taraborrelli (2013a)
J4421e	TgC	+ hν → .5 OH + .25 + .25 CH ₃ C(O)OO + .5 + .5 CO + .5 POHORG	J_KETENE	Taraborrelli (2013a)
J4422e	TgC	+ hν → .0192 + .1848 H ₂ O ₂ + .2208 MGLYOX + .36 OH + .36 CO + .56 CH ₃ C(O)OO + .2 CH ₃ CHO + .2 CO ₂ + .2 HCHO + .2 HO ₂ + .36 POHORG	J_KETENE*0.5	Taraborrelli (2013a)
J4422et2	TgC	+ hν → + CO	J_KETENE*0.5	Taraborrelli (2013a)
J4423e	TgCJ	+ hν → CH ₃ C(O)OO + CO + CO + HO ₂	jx(ip_MGLYOX)	Taraborrelli (2013a)
J4424e	TgCJ	+ hν → CH ₃ C(O)OO +	2.15*jx(ip_MGLYOX)	Taraborrelli (2013a)
J4424et2	TgC	+ hν → CH ₃ C(O)OO + CO + CO ₂ + HO ₂	3.15*jx(ip_MGLYOX)	Taraborrelli (2013a)
J4502et2	TgCJ	LISOPACOOH + hν → LHC4ACCHO + HO ₂ + OH + POHORG	1.14*jx(ip_CH300H)	Rickard and Pascoe (2009)*

53

B. Chemical mechanism – MTM

Table 2: Photolysis reactions (... continued)

#	labels	reaction	rate coefficient	reference
J4503et2	TgNCJ	LISOPACNO3 + hν → LHC4ACCHO + HO ₂ + NO ₂	0.59*J_IC3H7NO3	see note
J4504e	TgCJ	ISOPBOOH + hν → MVK + HCHO + HO ₂ + OH + POHORG	1.14*jx(ip_CH300H)	Rickard and Pascoe (2009)*
J4505e	TgNCJ	ISOPBNO3 + hν → MVK + HCHO + HO ₂ + NO ₂	2.84*J_IC3H7NO3	see note
J4506e	TgCJ	ISOPDOOH + hν → MACR + HCHO + HO ₂ + OH + POHORG	1.14*jx(ip_CH300H)	Rickard and Pascoe (2009)*
J4507	TgNCJ	ISOPDNO3 + hν → MACR + HCHO + HO ₂ + NO ₂	J_IC3H7NO3	see note
J4508e	TgNCJ	NISOPPOOH + hν → NC4CHO + HO ₂ + OH + POHORG	1.14*jx(ip_CH300H)	Rickard and Pascoe (2009)*
J4509	TgNCJ	NC4CHO + hν → NOA + 2 CO + 2 HO ₂	jx(ip_MACR)	see note
J4510e	TgNCJ	LNISOOH + hν → NOA + OH + .5 + .5 CO + .5 HO ₂ + .5 CO ₂ + POHORG	1.14*jx(ip_CH300H)	Taraborrelli et al. (2009)*
J4511e	TgCJ	LHC4ACCHO + hν → .5 LHC4ACCO3 + .5 HO ₂ + .5 OH + .25 MACRO2 + .25 LHMVKABO2 + .5 POHORG	jx(ip_MACR)	Taraborrelli (2013a)*
J4512e	TgCJ	LC578OOH + hν → .25 CH ₃ COCH ₂ OH + .75 MGLYOX + .25 + .75 HOCH ₂ CHO + .75 HO ₂ + OH + POHORG	1.14*jx(ip_CH300H) + 2.77*jx(ip_HOCH2CHO)	Taraborrelli (2013a)
J4513e	TgCJ	LHC4ACCO3H + hν → OH + .5 MACRO2 + .5 LHMVKABO2 + OH + 2 POHORG + CO ₂	J_HPALD	Taraborrelli (2013a)*
J4514	TgNCJ	LC5PAN1719 + hν → .6 LHC4ACCO3 + .6 NO ₂ + .2 MACRO2 + .2 LHMVKABO2 + .4 CO ₂ + .4 NO ₃	jx(ip_PAN)	see note
J4515e	TgCJ	HCOC5 + hν → +	0.5*jx(ip_MVK)	Taraborrelli (2013a)
J4516e	TgCJ	C59OOH + hν → CH ₃ COCH ₂ OH + OH + POHORG	J_ACETOL+1.14*jx(ip_CH300H)	Taraborrelli (2013a)
J4517e	TgCJ	+ hν → LHC4ACCO3 + OH + POHORG	J_HPALD	Taraborrelli (2013a)
J4518e	TgCJ	+ hν → .62 + .38 + OH + CO ₂ + POHORG	J_HPALD	Taraborrelli (2013a)
J4519e	TgCJ	+ hν → CH ₃ COCH ₂ O ₂ H + OH + 2 CO + HO ₂ + POHORG	2.77*JX(IP_HOCH2CHO)	Taraborrelli (2013a)
J4520e	TgCJ	+ hν → .5 CH ₃ COCH ₂ O ₂ H + .5 + .5 CO ₂ H ₃ CHO + .5 HCHO + 1.5 OH + 1.5 POHORG	2*1.14*JX(IP_CH300H)	Taraborrelli (2013a)
J4523e	TgCJ	+ hν → MGLYOX + OH + POHORG	1.14*JX(IP_CH300H)	Taraborrelli (2013a)
J4524e	TgCJ	+ hν → CO ₂ H ₃ CHO + CO + HO ₂ + OH + POHORG	2*2.77*JX(IP_HOCH2CHO)	Taraborrelli (2013a)*
J4525	TgCJ	+ hν → + HO ₂ + OH + POHORG	1.14*JX(IP_CH300H)	Taraborrelli (2013a)
J4526	TgCJ	+ hν → HCHO + OH + HO ₂ + CO ₂ H ₃ CHO + POHORG	1.14*JX(IP_CH300H)	Taraborrelli (2013a)*
J4525e	TgCJ	+ hν → .5 + .5 + CO + HO ₂ + OH + POHORG	jx(ip_ND2)*0.1*0.5	Taraborrelli (2013a)
J4526e	TgCJ	+ hν → CH ₃ C(O)OO + HCHO + GLYOX + HO ₂	1.14*JX(IP_CH300H)+J_ACETOL	Taraborrelli (2013a)
J4527e	TgCJ	+ hν → CH ₃ C(O)OO + HCHO + HCHO + CO + HO ₂	jx(ip_HOCH2CHO)	Taraborrelli (2013a)

54

*Notes:

J-values are calculated with an external module and then supplied to the MECCA chemistry.

Values that originate from the Master Chemical Mechanism (MCM) by Rickard and Pascoe (2009) are translated according in the following way:

J(11) → jx(ip_C0H2)
 J(12) → jx(ip_C0H)
 J(15) → jx(ip_HOCH2CHO)
 J(18) → jx(ip_MACR)
 J(22) → jx(ip_ACETOL)
 J(23)+J(24) → jx(ip_MVK)
 J(31)+J(32)+J(33) → jx(ip_GLYOX)
 J(34) → jx(ip_MGLYOX)
 J(41) → jx(ip_CH300H)
 J(53) → J(C₃H-ONO₂)
 J(54) → J(C₃H-ONO₂)
 J(55) → J(C₃H-ONO₂)
 J(56)+J(57) → jx(ip_N04)

J4207: It is assumed that J(PHAN) is the same as J(PAN).

J4212: It is assumed that J(ETHOHNO3) is the same as J(iC₃H₇ONO₂).

J4302: Following von Kuhlmann et al. (2003), we use J(CH₃COCH₂OH) = 0.11*jx(ip_C0H). As an additional factor, the quantum yield of 0.65 is taken from Orlando et al. (1999a).

J4306: Following von Kuhlmann et al. (2003), we use J(iC₃H₇ONO₂) = 3.7*jx(ip_PAN).

J4307: NOA contains the chromophores of both CH₃COCH₃ and a nitrate group. It is assumed here that the J values are additive, i.e.: J(NOA) = J(CH₃COCH₃) + J(iC₃H₇ONO₂).

J4401: Romero et al.(2005)

J4406: It is assumed that J(LC4H9NO3) is the same as J(iC₃H₇ONO₂).

J4407: It is assumed that J(MPAN) is the same as J(PAN).

J4405: It is assumed that J(BIACET) is 2.15 times larger than J(MGLYOX), consistent with the photolysis rate coefficients used in the MCM (Rickard and Pascoe, 2009).

J4414: It is assumed that J(MACROH) is 2.77 times larger than J(HOCH₂CHO), consistent with the photolysis rate coefficients used in the MCM (Rickard and Pascoe, 2009).

J4505: It is assumed that J(ISOPBNO3) = 2.84 × J(iC₃H₇ONO₂), consistent with the photolysis rate coefficients used in the MCM (Rickard and Pascoe, 2009).

J4509: It is assumed that J(NC4CHO) is the same as J(MACR).

J4514: It is assumed that J(LC5PAN1719) is the same as J(PAN).

J4526: decomposition of a dialkoxy radical

55

References

- Atkinson, R.: Gas-phase tropospheric chemistry of volatile organic compounds: 1. Alkanes and alkenes, *J. Phys. Chem. Ref. Data*, 26, 215–290, 1997.
- Atkinson, R.: Kinetics of the gas-phase reactions of OH radicals with alkanes and cycloalkanes, *Atmos. Chem. Phys.*, 3, 2233–2307, 2003.
- Atkinson, R. and Arey, J.: Atmospheric Degradation of Volatile Organic Compounds, *Chemical Reviews*, 103(12), 4605–4638, 2003.
- Atkinson, R., Baulch, D. L., Cox, R. A., Hampson, Jr., R. F., Kerr, J. A., Hynes, R. G., Jenkin, M. E., Rossi, M. J., and Troe, J.: Summary of evaluated kinetic and photochemical data for atmospheric chemistry: Web version August 1999, <http://www.iupac-kinetic.ch.cam.ac.uk>, 1999.
- Atkinson, R., Baulch, D. L., Cox, R. A., Crowley, J. N., Hampson, Jr., R. F., Hynes, R. G., Jenkin, M. E., Kerr, J. A., Rossi, M. J., and Troe, J.: Summary of evaluated kinetic and photochemical data for atmospheric chemistry: Web version March 2005, <http://www.iupac-kinetic.ch.cam.ac.uk>, 2005.
- Atkinson, R., Baulch, D. L., Cox, R. A., Crowley, J. N., Hampson, R. F., Hynes, R. G., Jenkin, M. E., Rossi, M. J., and Troe, J.: Evaluated kinetic and photochemical data for atmospheric chemistry: Volume II—gas phase reactions of organic species, *Atmos. Chem. Phys.*, 6, 3625–4055, 2006.
- Baeza-Romero, M. T., Glowacki, D. R., Blitz, M. A., Heard, D., Pilling, M. J., Rickard, A., and Seakins, P.: A combined experimental and theoretical study of the reaction between methylglyoxal and OH/OD radical: OH regeneration, *Phys. Chem. Chem. Phys.*, 9, 4114–4128, doi:10.1039/b702916k, 2007.
- Baker, J., Arey, J., and Atkinson, R.: Kinetics of the Gas-Phase Reactions of OH Radicals, NO₃ Radicals and O₃ with Three C₇-Carbonyls Formed From The Atmospheric Reactions of Myrcene, Ocimene and Terpinolene, *J. Atmos. Chem.*, pp. 241–260, 2004.
- Baulch, D. L., Bowman, C. T., Cobos, C., Cox, R. A., Just, T., Kerr, J. A., Pilling, M. J., Stocker, D., Troe, J., Tsang, W., Walker, R. W., and Warnatz, J.: Evaluated Kinetic Data for Combustion Modeling: Supplement II, *J. Phys. Chem. Ref. Data*, 34, 757–1397, 2005.
- Canosa-Mas, C. E., King, M. D., Lopez, R., Percival, C. J., Wayne, R. P., Shallcross, D. E., Pyle, J. A., and Daele, V.: Is the reaction between CH₃(O)O₂ and NO₃ important in the night-time troposphere?, *J. Chem. Soc. Faraday Trans.*, 92, 2211–2222, 1996.
- Capouet, M., Müller, J.-F., Ceulemans, K., Compernelle, S., Vereecken, L., and Peeters, J.: Modeling aerosol formation in alpha-pinene photo-oxidation experiments, *J. Geophys. Res.*, 8, doi:10.1029/2007JD008995, 2008.
- Christensen, L. E., Okumura, M., Sander, S. P., Salawitch, R. J., Toon, G. C., Sen, B., Blavier, J.-F., and Jucks, K. W.: Kinetics of HO₂ + HO₂ → H₂O₂ + O₂: Implications for stratospheric H₂O₂, *Geophys. Res. Lett.*, 29, doi:10.1029/2001GL014525, 2002.
- Feierabend, K. J., Zhu, L., Talukdar, R. K., and Burkholder, J. B.: Rate coefficients for the OH + HC(O)C(O)H (Glyoxal) reaction between 210 and 390 K, *J. Phys. Chem. A*, 112, 73–82, 2008.
- Fruekilde, P., Hjorth, J., Jensen, N., Kotzias, D., and Larsen, B.: Ozonolysis at vegetation surfaces: a source of acetone, 4-oxopentanal, 6-methyl-5-hepten-2-one, and geranyl acetone in the troposphere, *Atmos. Environ.*, doi:10.1016/S1352-2310(97)00485-8, 1997.
- Grosjean, E., Grosjean, D., and Seinfeld, J. H.: Gas-Phase Reaction of Ozone with Trans-2-Hexenal, Trans-2-Hexenyl Acetate, Ethylvinyl Ketone, and 6-Methyl-5-Hepten-2-One, *Int. J. Chem. Kinetics*, pp. 373–382, 1996.
- Hatakeyama, S., Honda, S., and Akinoto, H.: Rate constants and mechanism for reactions of ketenes with OH radicals in air at 299±2K, *Bull. Chem. Soc. Jpn.*, pp. 2157–2162, 1985.
- Hermans, I., Müller, J.-F., Nguyen, T. L., Jacobs, P. A., and Peeters, J.: Kinetics of α-Hydroxyalkylperoxy Radicals in Oxidation Processes. HO₂-Initiated Oxidation of Ketones/Aldehydes near the Tropopause, *J. Phys. Chem. A*, pp. 4303–4311, doi:10.1021/jp044080v, 2005.
- Hites, R. A. and Turner, A. M.: Rate Constants for the Gas-Phase β-Myrcene+OH and Isoprene+OH Reactions as a Function of Temperature, *Int. J. Chem. Kinetics*, pp. 407–413, 2009.
- IUPAC: Evaluated Kinetic Data, <http://iupac-pole-ether.fr/>, 2013.
- Jenkin, M. E., Hurley, M. D., and Wallington, T. J.: Investigation of the radical product channel of the CH₃C(O)O₂ + HO₂ reaction in the gas phase, *Phys. Chem. Chem. Phys.*, 9, 3149–3162, doi:10.1039/b702757e, 2007.
- Kircher, C. C. and Sander, S. P.: Kinetics and mechanism of HO₂ and DO₂ disproportionations, *J. Phys. Chem.*, 88, 2082–2091, 1984.
- Lewis, P. J., Bennett, K. A., and Harvey, J. N.: A computational study of the atmospheric oxidation of

56

- nopinone, *Phys. Chem. Chem. Phys.*, pp. 1643–1649, doi:10.1039/b418909d, 2005.
- Lockwood, A. L., Shepson, P. B., Fiddler, M. N., and Alaghmand, M.: Isoprene nitrates: preparation, separation, identification, yields, and atmospheric chemistry, *Atmos. Chem. Phys.*, 10, 6169–6178, doi:10.5194/acp-10-6169-2010, 2010.
- McCabe, D. C., Gierczak, T., Talukdar, R. K., and Ravishankara, A. R.: Kinetics of the reaction OH + CO under atmospheric conditions, *Geophys. Res. Lett.*, 28, 3135–3138, 2001.
- Mellouki, A. and Mu, Y.: On the atmospheric degradation of pyruvic acid in the gas phase, *J. Photochem. Photobiol. A: Chem.*, doi:10.1016/S1010-6030(03)00070-4, 2003.
- Mollner, A. K., Valluvadasan, S., Feng, L., Sprague, M. K., Okumura, M., Milligan, D. B., Bloss, W. J., Sander, S. P., Martien, P. T., Harley, R. A., McCoy, A. B., and Carter, W. P. L.: Rate of Gas Phase Association of Hydroxyl Radical and Nitrogen Dioxide, *Science*, doi:10.1126/science.1193030, 2010.
- Nguyen, T. L., Peeters, J., and Vereecken, L.: Theoretical study of the gas-phase ozonolysis of β-pinene (C₁₀H₁₆), *Phys. Chem. Chem. Phys.*, doi:10.1039/b822984h, 2009.
- Orlando, J. J. and Tyndall, G. S.: The atmospheric chemistry of the HC(O)CO radical, *Int. J. Chem. Kinetics*, 33, 149–156, 2001.
- Orlando, J. J., Tyndall, G. S., Bilde, M., Ferronato, C., Wallington, T. J., Vereecken, L., and Peeters, J.: Laboratory and Theoretical Study of the Oxy Radicals in the OH- and Cl-Initiated Oxidation of Ethene, *J. Phys. Chem. A*, 102, 8116–8123, 1998.
- Orlando, J. J., Tyndall, G. S., Frachebourg, J. M., Estupinan, E. G., Haberkorn, S., and Zimmer, A.: The rate and mechanism of the gas-phase oxidation of hydroxyacetone, *Atmos. Environ.*, 33, 1621–1629, 1999a.
- Orlando, J. J., Tyndall, G. S., and Paulson, S. E.: Mechanism of the OH-initiated oxidation of methacrolein, *Geophys. Res. Lett.*, 26, 1999b.
- Orlando, J. J., Noziere, B., Tyndall, G. S., Orzechowska, G. E., Paulson, S. E., and Rudich, Y.: Product studies of the OH- and ozone-initiated oxidation of some monoterpenes, *J. Geophys. Res.*, pp. 11561–11572, 2000.
- Orlando, J. J., Tyndall, G. S., Bertman, S. B., Chen, W., and Burkholder, J. B.: Rate coefficient for the reaction of OH with CH₂=C(CH₃)C(O)OONO₂ (MPAN), *Atmos. Environ.*, 36, 1895–1900, 2002.
- Paulot, F., Crounse, J. D., Kjaergaard, H. G., Kroll, J. H., Seinfeld, J. H., and Wennberg, P. O.: Isoprene photooxidation: new insights into the production of acids and organic nitrates, *Atmos. Chem. Phys.*, 9, 1479–1501, 2009a.
- Paulot, F., Crounse, J. D., Kjaergaard, H. G., Kürten, A., St. Clair, J. M., Seinfeld, J. H., and Wennberg, P. O.: Unexpected Epoxide Formation in the Gas-Phase Photooxidation of Isoprene, *Science*, 325, doi:10.1126/science.1172910, 2009b.
- Rickard, A. and Pascoe, S.: The Master Chemical Mechanism (MCM), <http://mcm.leeds.ac.uk>, 2009.
- Sander, S. P., Finlayson-Pitts, B. J., Friedl, R. R., Golden, D. M., Huie, R. E., Kolb, C. E., Kurylo, M. J., Molina, M. J., Moortgat, G. K., Orkin, V. L., and Ravishankara, A. R.: Chemical Kinetics and Photochemical Data for Use in Atmospheric Studies, Evaluation Number 14, JPL Publication 02-25, Jet Propulsion Laboratory, Pasadena, CA, 2003.
- Sander, S. P., Friedl, R. R., Golden, D. M., Kurylo, M. J., Moortgat, G. K., Keller-Rudek, H., Wine, P. H., Ravishankara, A. R., Kolb, C. E., Molina, M. J., Finlayson-Pitts, B. J., Huie, R. E., and Orkin, V. L.: Chemical Kinetics and Photochemical Data for Use in Atmospheric Studies, Evaluation Number 15, JPL Publication 06-2, Jet Propulsion Laboratory, Pasadena, CA, <http://jpldataeval.jpl.nasa.gov>, 2006.
- Sivakumaran, V., Hölscher, D., Dillon, T. J., and Crowley, J. N.: Reaction between OH and HCHO: temperature dependent rate coefficients (202–399 K) and product pathways (298 K), *Phys. Chem. Chem. Phys.*, 5, 4821–4827, 2003.
- Smith, A. M., Rigler, E., Kwok, E. S. C., and Atkinson, R.: Kinetics and Products of the Gas-Phase Reactions of 6-Methyl-5-hepten-2-one and trans-Cinnamaldehyde with OH and NO₃ Radicals and O₃ at 296(±2K), *Internat. Sci. Technol.*, pp. 1781–1785, 1996.
- Taraborrelli, D.: MIM3, *Geosci. Model Dev.*, (in preparation), 2013a.
- Taraborrelli, D.: MTM, *Atmos. Chem. Phys.*, (in preparation), 2013b.
- Taraborrelli, D., Lawrence, M. G., Butler, T. M., Sander, R., and Lelieveld, J.: Mainz Isoprene Mechanism 2 (MIM2): an isoprene oxidation mechanism for regional and global atmospheric modelling, *Atmos. Chem. Phys.*, 9, 2751–2777, <http://www.atmos-chem-phys.net/9/2751/>, 2009.

57

- Tyndall, G. S., Cox, R. A., Granier, C., Lesclaux, R., Moortgat, G. K., Pilling, M. J., Ravishankara, A. R., and Wallington, T. J.: The atmospheric chemistry of small organic peroxy radicals, *J. Geophys. Res.*, 106D, 12157–12182, 2001.
- Vereecken, L. and Peeters, J.: A theoretical study of the OH-initiated gas-phase oxidation mechanism of β -pinene ($C_{10}H_{16}$): first generation products, *Phys. Chem. Chem. Phys.*, pp. 3802–3815, doi:10.1039/c2cp23711c, 2012.
- Vereecken, L., Müller, J.-F., and Peeters, J.: Low-volatility poly-oxygenates in the OH-initiated atmospheric oxidation of α -pinene: impact of non-traditional peroxy radical chemistry, *Phys. Chem. Chem. Phys.*, 9, 5241–5248, doi:10.1039/b708023a, 2007.
- von Kuhlmann, R.: Tropospheric photochemistry of ozone, its precursors and the hydroxyl radical: A 3D-modeling study considering non-methane hydrocarbons, Ph.D. thesis, Johannes Gutenberg-Universität, Mainz, Germany, 2001.
- von Kuhlmann, R., Lawrence, M. G., Crutzen, P. J., and Rasch, P. J.: A model for studies of tropospheric ozone and nonmethane hydrocarbons: Model description and ozone results, *J. Geophys. Res.*, 108D, doi:10.1029/2002JD002893, 2003.
- Wolfe, G. M., Thornton, J. A., Bouvier-Brown, N. C., Goldstein, A. H., Park, J.-H., McKay, M., Matross, D. M., Mao, J., Brune, W. H., LaFranchi, B. W., Browne, E. C., Min, K.-E., Wooldridge, P. J., Cohen, R. C., Crouse, J. D., Faloona, I. C., Gilman, J. B., Kuster, W. C., de Gouw, J. A., Huisman, A., and Keutsch, F. N.: The Chemistry of Atmosphere-Forest Exchange (CAFE) Model Part 2: Application to BEARPEX-2007 observations, *Atmos. Chem. Phys.*, 11, 1269–1294, doi:10.5194/acp-11-1269-2011, 2011.

C. Data sheets

C.1. Pen-ray line source – LOT-QuantumDesign, Europe

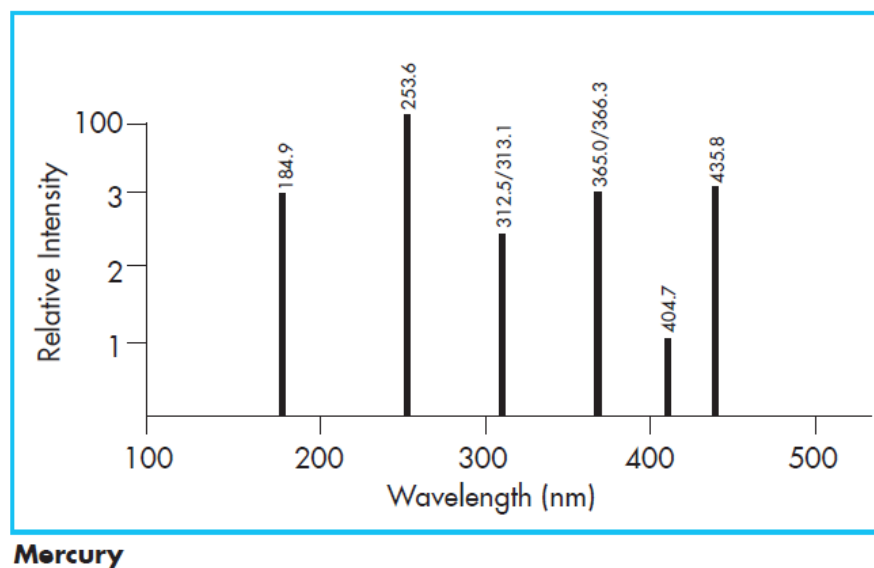


Abbildung C.1.: Discontinuous spectrum of the pen-ray line source used for calibration of the HORUS instrument (Taken from manual, LOT-QuantumDesign, Europe, www.lot-qd.com)

C.2. NIST NO standard

National Institute of Standards & Technology
Certificate of Analysis
Standard Reference Material® 2627a
Nitric Oxide in Nitrogen
 (Nominal Amount-of-Substance Fraction – 5 µmol/mol)
This certificate reports the certified values for Lot 48-H-XX.

This Standard Reference Material (SRM) is a primary gas mixture for which the amount-of-substance fraction, expressed as concentration [1], may be related to secondary working standards. The SRM is intended for the calibration of instruments used for nitric oxide determinations and for other uses.

This SRM mixture is supplied in a DOT 3AL specification aluminum (6061 alloy) cylinder with a water volume of 6 L. Mixtures are shipped with a nominal pressure exceeding 12.4 MPa (1800 psig) which provides the user with 0.65 m³ (23.0 ft³) of useable mixture. The cylinder is the property of the purchaser and is equipped with a CGA-660 stainless steel valve, which is the recommended outlet for this nitric oxide mixture.

Certified Value: This SRM mixture has been certified for the concentrations of nitric oxide (NO) and total oxides of Nitrogen (NO_x) in a nitrogen (N₂) matrix. The certified values, given below, apply to the identified cylinder and NIST sample number.

Nitric Oxide (NO) Concentration:	4.91 µmol/mol ± 0.04 µmol/mol
Total oxides of Nitrogen (NO _x) Concentration:	5.09 µmol/mol ± 0.04 µmol/mol

Cylinder Number: CAL016555 NIST Sample Number: 48-H-61

The uncertainty of the certified value includes the estimated uncertainties in the NIST standards, the analytical comparisons to the lot standard (LS), and the uncertainty of comparing the LS with each of the mixtures comprising this lot. This uncertainty is expressed as an expanded uncertainty $U = k u$, with u determined by experiment and a coverage factor $k = 2$. The true value for the nitric oxide and total oxides of nitrogen amount-of-substance fraction is asserted to lie in the interval defined by the certified value $\pm U$ with a level of confidence of approximately 95 % [2].

Expiration of Certification: This certification is valid from this certificate issue date until 31 December 2011, within the measurement uncertainties specified, provided the SRM is handled and stored in accordance with the instructions given in this certificate.

Hydrotest Date: May 2005 Blend Date: September 2005

Cylinder and Gas Handling Information: A high-purity, two-stage pressure regulator with a stainless steel diaphragm and CGA-660 outlet should be used to safely reduce the pressure and to deliver this SRM mixture to the instrument. The regulator should be evacuated and purged to prevent accidental contamination of the SRM by repeatedly (minimum five times) opening the valve and pressurizing the regulator, then closing the valve and releasing the pressure safely into a vent line. This SRM should NOT be used after the internal pressure drops below 0.8 MPa (100 psig). This SRM should be stored under normal laboratory conditions within the temperature range of 15 °C and 30 °C.

The analytical measurements leading to the certification of this current SRM lot were performed by W.J. Thorn III of the NIST Analytical Chemistry Division.

Stephen A. Wise, Chief
 Analytical Chemistry Division

Robert L. Watters, Jr., Chief
 Measurement Services Division

Gaithersburg, MD 20899
 Certificate Issue Date: 02 June 2008

SRM 2627a Page 1 of 2

Abbildung C.2.: National Institute of Standards & Technology - NO standard used for actinic flux density calibration of the mercury lamp that was applied for calibration of the HORUS instrument.

C.3. Dew Point Generator - LI-610 & H₂O-Monitor - LI-7000

CERTIFICATE of CALIBRATION

LI-610 Portable Dew Point Generator

Serial Number: **DPG-629B**

Standards Used:
Precision Thermistor Serial Number: #2
Multimeter: **Hewlett Packard Model 3468A Serial Number: 2137A16238**
Platinum RTD Probe Serial Number: **Minco Model S7297PAIL120S Serial Number: 1194**
Standard Resistor: **Julie Research Model NB-102 Serial Number: 1156**

The copper condenser block temperature is used to calibrate the LI-610. The temperature of the condenser block can be measured with greater accuracy and resolution than the dew point of the output air stream as measured by a dew point hygrometer.

The water temperature inside the condenser block is established by the block temperature, and air brought to saturation at the water temperature will have a dew point equal to the water temperature. Design testing has confirmed that air leaving the LI-610 is saturated at flow rates up to 2 liters min⁻¹, with a dew point equal to the block and water temperature.

The platinum Resistance-Temperature-Detector (RTD) mounted on the copper condenser block is calibrated at two temperatures: 0 °C and 49.90 °C. The slight non-linearity of the RTD is corrected electronically. A precision thermistor is used to calibrate the condenser block at 0 °C and 49.90 °C, as it offers much greater sensitivity than the RTD.
See the instruction manual for more information on calibration standards.

Cooling Block Temperature errors after calibration:
At 0 °C **.00 °C.**
At 25 °C **-0.02 °C.**
At 49.90 °C **.00 °C.**

This certifies that the dew point generated will be within ± .2 °C of the setting when operated according to the instructions.

Date of Calibration: November 20, 2003
Calibration Technician: *Jermy Tucke*

LI-COR Biosciences | LI-COR, Inc. • Environmental • 4421 Superior Street • P.O. Box 4425 • Lincoln, NE 68504
Phone: 402-467-3576 • FAX: 402-467-2819 • Toll-free 1-800-447-3576 (U.S. & Canada)
E-mail: envsales@licor.com • www.licor.com

Abbildung C.3.: Certificate of Calibration, Dew Point Generator Licor, LI-610. Calibrated against NIST-traceable standard.

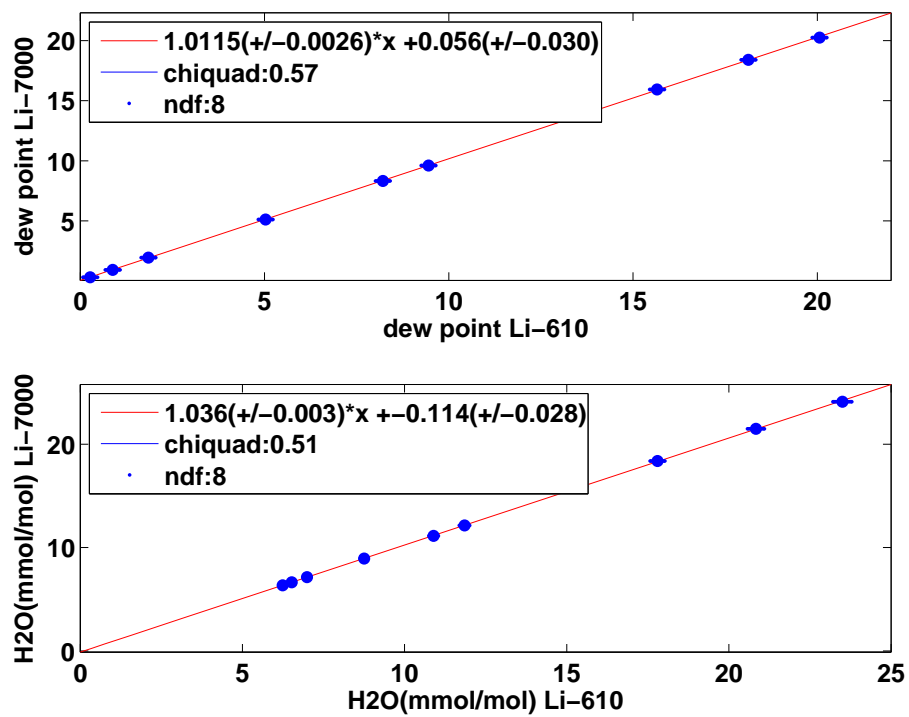



Abbildung C.4.: Calibration of the H₂O-Monitor - Licor, LI-7000, using the Dew Point Generator Licor, LI-610. Date of calibration: 10th of June, 2010.

C.4. Gas Flow Calibrator – DryCal, BIOS, USA



Heuvelweg 283a Tel. +31 (0)24 379 2120
 6600BH Heteren Fax +31 (0)24 379 1993
 The Netherlands Web: www.tpf-control.nl

Calibration Certificate

Cal Date : 08 June 2010
Page : 1 of 1

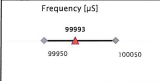
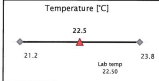
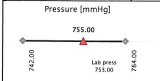
GENERAL DETAILS

Customer name : Westphal Mess- und Regeltechnik	Manufacturer : Bios International
Customer ref : R10-000379	Product : DC-2 base
Internal ref. : 12875	Serial no. : 104451
	Revision : 1.15

AS RECEIVED TEST DATA

Temperature, pressure and frequency are tested following the Bios procedure PR04-05 Rev. E

Tool Number	Description	Cal. Date	Due Date	Cert.
DVW001	Frequency counter	10/8/2009	10/8/2010	
T00101	PF100 sensor	9/11/2009	9/11/2010	
P00107	UN3 pressure ind.	11/27/2009	11/27/2010	409752

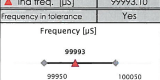
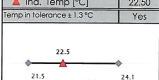
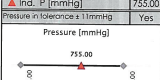
<table border="1" style="width: 100%; border-collapse: collapse;"> <tr> <th>Ind. freq. [μS]</th> <td>99993.10</td> </tr> <tr> <th>Temp in tolerance ± 0.3 °C</th> <td>Yes</td> </tr> </table> <p style="font-size: 8px;">Frequency [μS]</p> 	Ind. freq. [μS]	99993.10	Temp in tolerance ± 0.3 °C	Yes	<table border="1" style="width: 100%; border-collapse: collapse;"> <tr> <th>Ind. Temp [°C]</th> <td>22.50</td> </tr> <tr> <th>Temp in tolerance ± 0.3 °C</th> <td>Yes</td> </tr> </table> <p style="font-size: 8px;">Temperature [°C]</p> 	Ind. Temp [°C]	22.50	Temp in tolerance ± 0.3 °C	Yes	<table border="1" style="width: 100%; border-collapse: collapse;"> <tr> <th>Ind. P. (mmHg)</th> <td>755.00</td> </tr> <tr> <th>Pressure in tolerance ± 11 mmHg</th> <td>Yes</td> </tr> </table> <p style="font-size: 8px;">Pressure (mmHg)</p> 	Ind. P. (mmHg)	755.00	Pressure in tolerance ± 11 mmHg	Yes
Ind. freq. [μS]	99993.10													
Temp in tolerance ± 0.3 °C	Yes													
Ind. Temp [°C]	22.50													
Temp in tolerance ± 0.3 °C	Yes													
Ind. P. (mmHg)	755.00													
Pressure in tolerance ± 11 mmHg	Yes													

◆ Minimum value / Maximum value ▲ Measured / Indicated value

AS SHIPPED TEST DATA


Temperature, pressure and frequency are tested following the Bios procedure PR04-05 Rev. E

Tool Number	Description	Cal. Date	Due Date	Cert.
DVW001	Frequency counter	10/8/2009	10/8/2010	
T00101	PF100 sensor	9/11/2009	9/11/2010	
P00107	UN3 pressure ind.	11/27/2009	11/27/2010	409752

<table border="1" style="width: 100%; border-collapse: collapse;"> <tr> <th>Ind. freq. [μS]</th> <td>99993.10</td> </tr> <tr> <th>Temp in tolerance ± 0.3 °C</th> <td>Yes</td> </tr> </table> <p style="font-size: 8px;">Frequency [μS]</p> 	Ind. freq. [μS]	99993.10	Temp in tolerance ± 0.3 °C	Yes	<table border="1" style="width: 100%; border-collapse: collapse;"> <tr> <th>Ind. Temp [°C]</th> <td>22.50</td> </tr> <tr> <th>Temp in tolerance ± 0.3 °C</th> <td>Yes</td> </tr> </table> <p style="font-size: 8px;">Temperature [°C]</p> 	Ind. Temp [°C]	22.50	Temp in tolerance ± 0.3 °C	Yes	<table border="1" style="width: 100%; border-collapse: collapse;"> <tr> <th>Ind. P. (mmHg)</th> <td>755.00</td> </tr> <tr> <th>Pressure in tolerance ± 11 mmHg</th> <td>Yes</td> </tr> </table> <p style="font-size: 8px;">Pressure (mmHg)</p> 	Ind. P. (mmHg)	755.00	Pressure in tolerance ± 11 mmHg	Yes
Ind. freq. [μS]	99993.10													
Temp in tolerance ± 0.3 °C	Yes													
Ind. Temp [°C]	22.50													
Temp in tolerance ± 0.3 °C	Yes													
Ind. P. (mmHg)	755.00													
Pressure in tolerance ± 11 mmHg	Yes													


◆ Minimum value / Maximum value ▲ Measured / Indicated value

Technician Name : Khalid Harkach
Printed date : 08/06/2010
Certificate no. 12876



This report shall not be reproduced except in full, without the written approval of TPF Control. Results only relate to the items calibrated.
 This report is produced by an electronic data system and is valid without signature.
 Form BMS-41.03 / Rev A dated 11 aug 08

Abbildung C.5.: Certificate of Calibration, DryCal, DC-LC-1 & HC-LC-1, BIOS International, USA. Calibrated against NIST-traceable standard.



TPF CONTROL
CALIBRATION
RVA K 140

CALIBRATION CERTIFICATE

12877

AS FOUND RESULTS

Lab. Temperature 20.8 °C		Lab. Pressure 1004.2 mbar	
INSTRUMENT READING (ml/min)	LAB STANDARD READING (Flow)(ml/min)	Flow (ml/min)	Flow (ml/min)
99.45	99.25	800101	800101
101.70	100.51	800101	800101
485.45	498.24	800101	800101

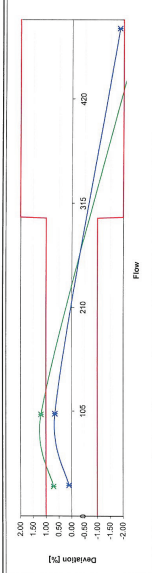
DEVIATION (ERROR)		UNCERTAINTY	
Of Rate [%]	Flow (ml/min)	Limit [%]	Flow [%]
0.20	0.20	1.00	0.32%
1.19	1.20	1.00	0.32%
-2.57	-12.79	2.00	0.33%

CALIBRATION RESULTS AFTER ADJUSTMENT

Lab. Temperature 20.8 °C		Lab. Pressure 1004.3 mbar	
INSTRUMENT READING (ml/min)	LAB STANDARD READING (Flow)(ml/min)	Flow (ml/min)	Flow (ml/min)
30.76	30.72	800101	800101
102.25	101.59	800101	800101
4911.5	500.40	800102	800102


DEVIATION (ERROR)		UNCERTAINTY	
Of Rate [%]	Flow (ml/min)	Limit [%]	Flow [%]
0.10	0.03	1.00	0.33%
0.65	0.66	1.00	0.34%
-1.85	-9.23	2.00	0.32%

GRAPH DEVIATION vs FLOW



Remarks:
The deviation is determined by: Deviation = $\frac{\text{Instrument reading} - \text{Lab. Standard reading}}{\text{Lab. Standard reading}} \times 100\%$

Form BMS 4.1/09 - Rev.0 dated 1/05/10 Page 2 of 2



TPF CONTROL
CALIBRATION
RVA K 140

CALIBRATION CERTIFICATE

12878

AS FOUND RESULTS

Lab. Temperature 31.2 °C		Lab. Pressure 1004.5 mbar	
INSTRUMENT READING (ml/min)	LAB STANDARD READING (Flow)(ml/min)	Flow (ml/min)	Flow (ml/min)
511.20	498.41	800101	800101
5034.00	5023.65	800104	800104
50100.00	49622.00	800104	800104

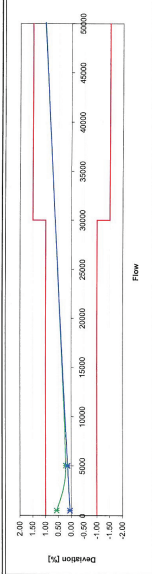
DEVIATION (ERROR)		UNCERTAINTY	
Of Rate [%]	Flow (ml/min)	Limit [%]	Flow [%]
0.56	2.79	1.00	0.32%
0.21	10.35	1.00	0.37%
1.00	498.00	1.50	0.38%

CALIBRATION RESULTS AFTER ADJUSTMENT

Lab. Temperature 20.7 °C		Lab. Pressure 1004.4 mbar	
INSTRUMENT READING (ml/min)	LAB STANDARD READING (Flow)(ml/min)	Flow (ml/min)	Flow (ml/min)
491.25	491.05	800101	800101
5012.00	5005.30	800104	800104
50080.00	49573.50	800104	800104

DEVIATION (ERROR)		UNCERTAINTY	
Of Rate [%]	Flow (ml/min)	Limit [%]	Flow [%]
0.04	0.21	1.00	0.32%
0.13	6.70	1.00	0.37%
1.02	506.50	1.50	0.37%



GRAPH DEVIATION vs FLOW



Remarks:
The deviation is determined by: Deviation = $\frac{\text{Instrument reading} - \text{Lab. Standard reading}}{\text{Lab. Standard reading}} \times 100\%$

Form BMS 4.1/09 - Rev.0 dated 1/05/10 Page 2 of 2

C.4. Gas Flow Calibrator – DryCal, BIOS, USA

CALIBRATION CERTIFICATE



12878

Applicant	Westphal Mess- und Regeltechnik
Customer name	E. Reuveni
Contact	Laurfweg 20
Address	85521 - Ollsburnn Germany
Order reference applicant	RO-000379
Order reference TPF Control	12875
Instrument Information (I01)	
Instrument	Primary flow Calibrator
Manufacturer	Bios International
Serial no.	10404
Model	DC-FC-1
Revision	E
Calibration method	The device under test is connected in a parallel setup to the mentioned flow calibrator to compare flow readings. An appropriate warm up time is incorporated. Bios-Drycal products a flow source is used to generate a flow. (According to standard, if reading device under test.)
Period of calibration	8 Jun 2010
Calibration result	The result of the calibration are presented on page 2 of 2. The reported uncertainty of measurement is based on the standard uncertainty multiplied by a coverage factor k=2 which provides a confidence level of approximately 95%. The standard uncertainty of measurement has been determined in accordance with EA-402.
Calibration traceability	The measurements have been executed using standards for which the traceability to international standards has been demonstrated towards the BVA.
Remarks	
Certificate issue date	Wijchen, 8 Jun 2010
Calibration technician	Technical Manager Rik van de Bovenkamp

TPF Control B.V.
 Nieuwegeweg 282a
 3821 LK Amstelveen (NL)
 Tel. +31 20 371 1043
 Fax. +31 20 371 1043
 Web: www.tpf-control.nl

BVA is member of the European Co-operation for Accreditation (EA) and is one of the signatories to the International Agreement on the Recognition of Mutual Acceptance Arrangements with the mutual recognition of the listed over-accurate calibration certificates.
 For more information, please contact us directly.

Page 1 of 2

CALIBRATION CERTIFICATE

12877

Applicant	Westphal Mess- und Regeltechnik
Customer name	E. Reuveni
Contact	Laurfweg 20
Address	85521 - Ollsburnn Germany
Order reference applicant	RO-000379
Order reference TPF Control	12875
Instrument Information (I01)	
Instrument	Primary flow Calibrator
Manufacturer	Bios International
Serial no.	10404
Model	DC-FC-1
Revision	F
Calibration method	The device under test is connected in a parallel setup to the mentioned flow calibrator to compare flow readings. An appropriate warm up time is incorporated. Bios-Drycal products a flow source is used to generate a flow. (According to standard, if reading device under test.)
Period of calibration	8 Jun 2010
Calibration result	The result of the calibration are presented on page 2 of 2. The reported uncertainty of measurement is based on the standard uncertainty multiplied by a coverage factor k=2 which provides a confidence level of approximately 95%. The standard uncertainty of measurement has been determined in accordance with EA-402.
Calibration traceability	The measurements have been executed using standards for which the traceability to international standards has been demonstrated towards the BVA.
Remarks	
Certificate issue date	Wijchen, 8 Jun 2010
Calibration technician	Technical Manager Rik van de Bovenkamp

TPF Control B.V.
 Nieuwegeweg 282a
 3821 LK Amstelveen (NL)
 Tel. +31 20 371 1043
 Fax. +31 20 371 1043
 Web: www.tpf-control.nl

BVA is member of the European Co-operation for Accreditation (EA) and is one of the signatories to the International Agreement on the Recognition of Mutual Acceptance Arrangements with the mutual recognition of the listed over-accurate calibration certificates.
 For more information, please contact us directly.

Page 1 of 2

C.5. Optical Fiber – Thorlabs GmbH, Germany



TECS-Coated Silica/Silica Fiber Specifications

Core Diameter	μm	200 ± 8	365 ± 14	550 ± 19	910 ± 30
Clad Diameter	μm	240 ± 5	400 ± 8	600 ± 10	1000 ± 15
Coating Diameter	μm	260 ± 6	425 ± 10	630 ± 10	1035 ± 15
Buffer Diameter ¹	μm	400 ± 30	730 ± 30	1040 ± 30	1400 ± 50
Maximum Attenuation @ 820nm	dB/km	12	12	12	12
Maximum Core Offset	μm	5	7	9	10
Numerical Aperture ²		0.22 ± 0.02	0.22 ± 0.02	0.22 ± 0.02	0.22 ± 0.02
Acceptance Angle (Full)		25°	25°	25°	25°
Maximum Power Capability					
– CW ³	kW	0.2	0.7	1.5	5.0
– Pulsed ⁴	MW	1.0	3.4	7.6	25.1
Operating Temperature @ 820nm		-60°C to +125°C	-60°C to +125°C	-60°C to +125°C	-60°C to +125°C
Proof Test Level	ksi	100	100	100	100
Minimum Bend Diameter					
– Recommended Short Term ⁵	mm	24	40	60	100
– Recommended Long Term ⁶	mm	48	80	120	200
Standard Length	m	1100	500	300	50
Type					
Low-OH ⁺	Part Number	FG-200-LCR	FG-365-LER	FG-550-LER	FG-910-LER
	Stock Number	98-0400-1367-8	98-0400-1361-1	98-0400-1362-9	98-0400-3373-4
High-OH ⁺	Part Number	FG-200-UCR	FG-365-UER	FG-550-UER	FG-910-UER
	Stock Number	98-0400-1368-6	98-0400-1369-4	98-0400-1370-2	98-0400-3635-6

¹ Standard buffer coating is Tefzel® 210.

² 2 meters, 50% intensity, uncoated and mode stripped.

³ Based on 1 MW/cm² for 1064nm Nd:YAG laser and input spot size equal to 80 percent of the core diameter.

⁴ Based on 5 GW/cm² for 1064nm Nd:YAG laser with 10 nsec. pulse length and input spot size equal to 80 percent of the core diameter.

⁵ Recommended geometric strain during installation is 100% of proof test level, based on statistical analysis of fiber failures.

⁶ Recommended geometric strain is 50% of proof test level, based on statistical analysis of fiber failures.

Abbildung C.6.: Specifications of coated silica fiber used for transportation of the 308 nm UV light within HORUS. (Taken from manual, Thorlabs GmbH, Europe, Germany, www.thorlabs.com)

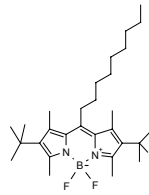
C.6. Laser Dye Pyrromethene-597 – Exciton, USA



PO Box 31126
Dayton, OH 45437
Tel: 937.252.2989 Fax: 937.258.3937
E-mail: info@exciton.com
www.exciton.com

PYRROMETHENE 597-3C9

Synonym: 2,6-di-tert-butyl-8-nonyl-1,3,5,7-tetramethylpyrromethene- BF₂ Complex
Catalog No.: 05971 **CAS Registry Number:** N/A
Chemical Formula: C₃₀H₄₈N₂BF₂ **MW:** 486.54
Appearance: Red-orange solid **Melting Point:** 247°C



Suggested Use: lithography, fl hydrocarbon probe or tagant, electro-luminescence, DVD (digital video data)

Solubility Limits (g/l) (room temperature):

Ethanol	3.7	EPH	very soluble
Heptane	≥10.3	PPH	very soluble
Ethyl Acetate	very soluble	Toluene	very soluble
Acetonitrile	very soluble	THF	very soluble
p-Dioxane	very soluble	Dow Corning 200 Silicone Oil	0.47

Spectral Information:

$\lambda_{\text{max,abs}}$ = 524nm (ethanol), 525nm (methylene chloride), 527.8nm (diesel fuel)
 $\lambda_{\text{max,e}}$ = 588nm (ethanol), 585nm (methylene chloride), 590nm (diesel fuel)

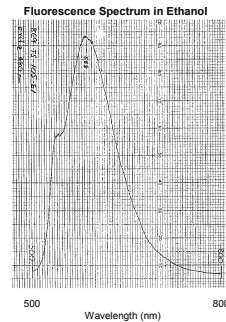
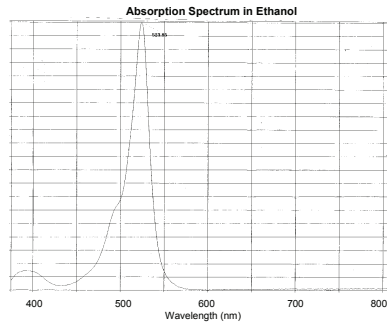


Abbildung C.7.: Pyrromethene-597 laser dye, Exciton, USA, www.exciton.com

D. Abbreviations

BVOC	<i>Biogenic Volatile Organic Compound</i>
BEARPEX09	<i>Biosphere Effects on AeRosols and Photochemistry EXperiment 2009, USA</i>
CAABA/MECCA	<i>Chemistry As A Boxmodel Application / Module Efficiently Calculating the Chemistry of the Atmosphere</i>
CABINEX	<i>Community Atmosphere Biosphere INteractions EXperiments, USA</i>
CIMS	<i>Chemical Ionisation Mass Spectroscopy</i>
CRD	<i>Cavity Ring Down</i>
DOAS	<i>Differential Optical Absorption Spectroscopy</i>
GABRIEL	<i>Guyanas Atmosphere-Biosphere Exchange and Radicals Intensive Experiment with the Learjet, Oct. 2005, Suriname</i>
GTHOS	<i>Ground-based Tropospheric Hydrogen Oxides Sensor</i>
HOPE12	<i>HOhenpeissenberg Photochemistry Experiment</i>
HORUS	<i>HydrOxyl Radical Measurement Unit based on fluorescence Spectroscopy</i>
HO _x COMP	<i>HO_x Intercomparison Campaign 2005, Jülich, Germany</i>
HUMPPA-COPEC	<i>Hyytiälä United Measurements of Photochemistry and Particles in Air – Comprehensive Organic Precursor Emission and Concentration study, Finland</i>
IPI	<i>InletPreInjector</i>
LIF	<i>Laser Induced Fluorescence</i>
LIF-FAGE	<i>Laser Induced Fluorescence - Fluorescence Assay by Gas Expansion</i>
NMHC	<i>Non-Methane HydroCarbons</i>
MCM	<i>Master Chemical Mechanism</i>
MCP	<i>Micro Channel Plate</i>
MIESR	<i>Matrix Isolation Electron Spin Resonance</i>
MIM	<i>Mainz Isoprene Mechanism</i>
MTM	<i>Mainz Terpene Mechanism</i>

D. Abbreviations

OP3	<i>Oxidant and Particle Photochemical Processes</i> above a Southeast Asian Tropical Rainforest
PARADE	<i>P</i> Articles and <i>R</i> Adicals: <i>D</i> iel observations of the impact of urban and biogenic <i>E</i> missions
PROPHET	<i>P</i> rogram for <i>R</i> esearch on <i>O</i> xidants: <i>P</i> Hotochemistry, <i>E</i> missions, and <i>T</i> ransport, USA
PTR-MS	<i>P</i> roton <i>T</i> ransfer <i>R</i> eaction <i>M</i> ass <i>S</i> pectroscopy
SMEAR II	<i>S</i> tation for <i>M</i> easuring <i>F</i> orest <i>E</i> cosystem- <i>A</i> tmosphere <i>R</i> elations
SOS99	<i>S</i> outhern <i>O</i> xidants <i>S</i> tudy 1999
TexAQS	<i>T</i> exas <i>A</i> ir <i>Q</i> uality <i>S</i> tudy
Trace-P	<i>T</i> ransport and <i>C</i> hemical <i>E</i> volution over the <i>P</i> acific
UTC	<i>U</i> niversal <i>T</i> ime <i>C</i> oordinates
VOC	<i>V</i> olatile <i>O</i> rganic <i>C</i> ompound

Bibliography

- Atkinson, R., Baulch, D. L., Cox, R. A., Crowley, J. N., Hampson, R. F., Hynes, R. G., Jenkin, M. E., Rossi, M. J., Troe, J., and Subcommittee, I.: Evaluated kinetic and photochemical data for atmospheric chemistry: Volume II - gas phase reactions of organic species, *Atmospheric Chemistry and Physics*, 6, 3625–4055, doi:10.5194/acp-6-3625-2006, <http://www.atmos-chem-phys.net/6/3625/2006/>, 2006.
- Aumont, B., Chervier, F., and Laval, S.: Contribution of HONO sources to the NO_x/HO_x/O₃ chemistry in the polluted boundary layer, *Atmospheric Environment*, 37, 487–498, doi:[http://dx.doi.org/10.1016/S1352-2310\(02\)00920-2](http://dx.doi.org/10.1016/S1352-2310(02)00920-2), <http://www.sciencedirect.com/science/article/pii/S1352231002009202>, 2003.
- Bailey, A., Heard, D., Henderson, D., and Paul, P.: Collisional quenching of OH by H₂O between 211 and 294 K and the development of a unified model for quenching, *Chemical Physics Letters*, 302, 132–138, doi:[http://dx.doi.org/10.1016/S0009-2614\(99\)00076-7](http://dx.doi.org/10.1016/S0009-2614(99)00076-7), <http://www.sciencedirect.com/science/article/pii/S0009261499000767>, 1999.
- Bailey, A. E., Heard, D. E., Paul, P. H., and Pilling, M. J.: Collisional quenching of OH ($A^2\Sigma^+$, $v' = 0$) by N₂, O₂ and CO₂ between 204 and 294 K. Implications for atmospheric measurements of OH by laser-induced fluorescence, *J. Chem. Soc., Faraday Trans.*, 93, 2915–2920, doi:10.1039/A701582H, <http://dx.doi.org/10.1039/A701582H>, 1997.
- Benning, L. and Wahner, A.: Measurements of Atmospheric Formaldehyde (HCHO) and Acetaldehyde (CH₃CHO) during POPCORN 1994 Using 2,4-DNPH Coated Silica Cartridges, *Journal of Atmospheric Chemistry*, 31, 105–117, doi:10.1023/A:1005884116406, <http://dx.doi.org/10.1023/A%3A1005884116406>, 1998.
- Berresheim, H., Elste, T., Tremmel, H. G., Allen, A. G., Hansson, H.-C., Rosman, K., Dal Maso, M., Mäkelä, J. M., Kulmala, M., and O'Dowd, C. D.: Gas-aerosol relationships of H₂SO₄, MSA, and OH: Observations in the coastal marine boundary layer at Mace Head, Ireland, *Journal of Geophysical Research: Atmospheres*, 107, PAR 5–1–PAR 5–12, doi:10.1029/2000JD000229, <http://dx.doi.org/10.1029/2000JD000229>, 2002.
- Bohn, B., Corlett, G. K., Gillmann, M., Sanghavi, S., Stange, G., Tensing, E., Vrekoussis, M.,

- Bloss, W. J., Clapp, L. J., Kortner, M., Dorn, H.-P., Monks, P. S., Platt, U., Plass-Dülmer, C., Mihalopoulos, N., Heard, D. E., Clemitshaw, K. C., Meixner, F. X., Prevot, A. S. H., and Schmitt, R.: Photolysis frequency measurement techniques: results of a comparison within the ACCENT project, *Atmospheric Chemistry and Physics*, 8, 5373–5391, doi:10.5194/acp-8-5373-2008, <http://www.atmos-chem-phys.net/8/5373/2008/>, 2008; B.Bohn, personal communication, 2012.
- Brune, W. H., Mao, J., and Ren, X.: OH and HO₂ Measurements in Blodgett Forest, CA during BEARPEX 2009, abstract A51G-02 presented at 2010 Fall Meeting, AGU, San Francisco, Calif., 13-17 Dec., 2010.
- Cantrell, C. A., Edwards, G. D., Stephens, S., Mauldin, L., Kosciuch, E., Zondlo, M., and Eisele, F.: Peroxy radical observations using chemical ionization mass spectrometry during TOPSE, *Journal of Geophysical Research: Atmospheres*, 108, doi:10.1029/2002JD002715, <http://dx.doi.org/10.1029/2002JD002715>, 2003.
- Chan, C. Y., Hard, T. M., Mehrabzadeh, A. A., George, L. A., and O'Brien, R. J.: Third-generation FAGE instrument for tropospheric hydroxyl radical measurement, *Journal of Geophysical Research: Atmospheres*, 95, 18 569–18 576, doi:10.1029/JD095iD11p18569, <http://dx.doi.org/10.1029/JD095iD11p18569>, 1990.
- Criegee, R.: Mechanism of Ozonolysis, *Angewandte Chemie International Edition in English*, 14, 745–752, doi:10.1002/anie.197507451, <http://dx.doi.org/10.1002/anie.197507451>, 1975.
- Crouse, J. D., Paulot, F., Kjaergaard, H. G., and Wennberg, P. O.: Peroxy radical isomerization in the oxidation of isoprene, *Phys. Chem. Chem. Phys.*, 13, 13 607–13 613, doi:10.1039/C1CP21330J, <http://dx.doi.org/10.1039/C1CP21330J>, 2011.
- Crowley, J. N., Ammann, M., Cox, R. A., Hynes, R. G., Jenkin, M. E., Mellouki, A., Rossi, M. J., Troe, J., and Wallington, T. J.: Evaluated kinetic and photochemical data for atmospheric chemistry: Volume V - heterogeneous reactions on solid substrates, *Atmospheric Chemistry and Physics*, 10, 9059–9223, doi:10.5194/acp-10-9059-2010, <http://www.atmos-chem-phys.net/10/9059/2010/>, 2010.
- Crutzen, P.: A discussion of the chemistry of some minor constituents in the stratosphere and troposphere, *Pure and applied geophysics*, 106-108, 1385–1399, doi:10.1007/BF00881092, <http://dx.doi.org/10.1007/BF00881092>, 1973.
- Dentener, F., Williams, J., and Metzger, S.: Aqueous Phase Reaction of HNO₄: The Impact on Tropospheric Chemistry, *Journal of Atmospheric Chemistry*, 41, 109–133, doi:10.1023/A:1014233910126, <http://dx.doi.org/10.1023/A%3A1014233910126>, 2002.
- Dieke, G. and Crosswhite, H.: The ultraviolet bands of OH Fundamental data, *Journal of Quantitati-*

- ve Spectroscopy and Radiative Transfer, 2, 97 – 199, doi:[http://dx.doi.org/10.1016/0022-4073\(62\)90061-4](http://dx.doi.org/10.1016/0022-4073(62)90061-4), <http://www.sciencedirect.com/science/article/pii/0022407362900614>, 1962.
- Dillon, T.: Interactive comment on “Detection of HO_2 by laser-induced fluorescence: calibration and interferences from RO_2 radicals” by H. Fuchs et al., Atmos. Meas. Tech. Discuss., 4, 1255, 2011.
- Dillon, T. J. and Crowley, J. N.: Direct detection of OH formation in the reactions of HO_2 with $CH_3C(O)O_2$ and other substituted peroxy radicals, Atmospheric Chemistry and Physics, 8, 4877–4889, doi:10.5194/acp-8-4877-2008, <http://www.atmos-chem-phys.net/8/4877/2008/>, 2008.
- Dorn, H., Brandenburger, U., Brauers, T., and Hausmann, M.: A new in situ laser long-path absorption instrument for the measurement of tropospheric OH radicals., Journal of the Atmospheric Sciences, 52, 3373–3380, <http://search.ebscohost.com/login.aspx?direct=true&db=aph&AN=9512310260&site=ehost-live&scope=site>, 1995.
- Eisele, F. L. and Tanner, D. J.: Ion-assisted tropospheric OH measurements, Journal of Geophysical Research: Atmospheres, 96, 9295–9308, doi:10.1029/91JD00198, <http://dx.doi.org/10.1029/91JD00198>, 1991.
- Evans, M., Shallcross, D., Law, K., Wild, J., Simmonds, P., Spain, T., Berrisford, P., Methven, J., Lewis, A., McQuaid, J., Pilling, M., Bandy, B., Penkett, S., and Pyle, J.: Evaluation of a Lagrangian box model using field measurements from EASE (Eastern Atlantic Summer Experiment) 1996, Atmospheric Environment, 34, 3843 – 3863, doi:10.1016/S1352-2310(00)00184-9, <http://www.sciencedirect.com/science/article/pii/S1352231000001849>, 2000.
- Faloona, I., Tan, D., Brune, W. H., Jaegle, L., Jacob, D. J., Kondo, Y., Koike, M., Chatfield, R., Pueschel, R., Ferry, G., Sachse, G., Vay, S., Anderson, B., Hannon, J., and Fuelberg, H.: Observations of HO_x and its relationship with NO_x in the upper troposphere during SONEX, Journal of Geophysical Research: Atmospheres, 105, 3771–3783, doi:10.1029/1999JD900914, <http://dx.doi.org/10.1029/1999JD900914>, 2000.
- Faloona, I., Tan, D., Leshner, R., Hazen, N., Frame, C., Simpas, J., Harder, H., Martinez, M., Di Carlo, P., Ren, X., and Brune, W.: A Laser-induced Fluorescence Instrument for Detecting Tropospheric OH and HO_2 : Characteristics and Calibration, Journal of Atmospheric Chemistry, 47, 139–167, doi:10.1023/B:JOCH.0000021036.53185.0e, <http://www.ingentaconnect.com/content/klu/joch/2004/00000047/00000002/05257331>, 2004.
- FAO: Global forest resources assessment 2010, FAO forestry paper, FAO, Rome, <http://www.fao.org/docrep/013/i1757e/i1757e.pdf>, available online., 2010.
- Fehsenfeld, F., Calvert, J., Fall, R., Goldan, P., Guenther, A. B., Hewitt, C. N., Lamb, B., Liu, S., Trainer, M., Westberg, H., and Zimmerman, P.: Emissions of volatile organic compounds from

Bibliography

- vegetation and the implications for atmospheric chemistry, *Global Biogeochemical Cycles*, 6, 389–430, doi:10.1029/92GB02125, <http://dx.doi.org/10.1029/92GB02125>, 1992.
- Felton, C. C., Sheppard, J. C., and Campbell, M. J.: Measurements of the diurnal OH cycle by a ^{14}C -tracer method, *Nature*, 335, 53–55, <http://dx.doi.org/10.1038/335053a0>, 1988.
- Freeman, A. J.: Configuration Interaction Study of the Electronic Structure of the OH Radical by the Atomic and Molecular Orbital Methods, *The Journal of Chemical Physics*, 28, 230–243, doi:10.1063/1.1744098, <http://link.aip.org/link/?JCP/28/230/1>, 1958.
- Fuchs, H., Bohn, B., Hofzumahaus, A., Holland, F., Lu, K. D., Nehr, S., Rohrer, F., and Wahner, A.: Detection of HO_2 by laser-induced fluorescence: calibration and interferences from RO_2 radicals, *Atmospheric Measurement Techniques*, 4, 1209–1225, doi:10.5194/amt-4-1209-2011, <http://www.atmos-meas-tech.net/4/1209/2011/>, 2011.
- Fuchs, H., Hofzumahaus, A., Rohrer, F., Bohn, B., Brauers, T., Dorn, H.-P., Haseler, R., Holland, F., Kaminski, M., Li, X., Lu, K., Nehr, S., Tillmann, R., Wegener, R., and Wahner, A.: Experimental evidence for efficient hydroxyl radical regeneration in isoprene oxidation, *Nature Geosci*, advance online publication, –, <http://dx.doi.org/10.1038/ngeo1964>, 2013.
- Goldan, P. D., Kuster, W. C., and Fehsenfeld, F. C.: Nonmethane hydrocarbon measurements during the Tropospheric OH Photochemistry Experiment, *Journal of Geophysical Research: Atmospheres*, 102, 6315–6324, doi:10.1029/96JD01868, <http://dx.doi.org/10.1029/96JD01868>, 1997.
- Griffith, S. M., Hansen, R. F., Dusanter, S., Stevens, P. S., Alaghmand, M., Bertman, S. B., Carroll, M. A., Erickson, M., Galloway, M., Grossberg, N., Hottle, J., Hou, J., Jobson, B. T., Kammrath, A., Keutsch, F. N., Lefer, B. L., Mielke, L. H., O'Brien, A., Shepson, P. B., Thurlow, M., Wallace, W., Zhang, N., and Zhou, X. L.: OH and HO_2 radical chemistry during PROPHET 2008 and CABINEX 2009; Part 1: Measurements and model comparison, *Atmospheric Chemistry and Physics*, 13, 5403–5423, doi:10.5194/acp-13-5403-2013, <http://www.atmos-chem-phys.net/13/5403/2013/>, 2013.
- Guenther, A., Hewitt, C. N., Erickson, D., Fall, R., Geron, C., Graedel, T., Harley, P., Klinger, L., Lerdau, M., McKay, W. A., Pierce, T., Scholes, B., Steinbrecher, R., Tallamraju, R., Taylor, J., and Zimmerman, P.: A global model of natural volatile organic compound emissions, *Journal of Geophysical Research: Atmospheres*, 100, 8873–8892, doi:10.1029/94JD02950, <http://dx.doi.org/10.1029/94JD02950>, 1995.
- Hall, B. D. and Claiborn, C. S.: Measurements of the dry deposition of peroxides to a Canadian boreal forest, *Journal of Geophysical Research: Atmospheres*, 102, 29 343–29 353, doi:10.1029/97JD01113, <http://dx.doi.org/10.1029/97JD01113>, 1997.

- Hard, T. M., O'Brien, R. J., Cook, T. B., and Tsongas, G. A.: Interference suppression in HO fluorescence detection, *Appl. Opt.*, 18, 3216–3217, doi:10.1364/AO.18.003216, <http://ao.osa.org/abstract.cfm?URI=ao-18-19-3216>, 1979.
- Hari, P. and Kulmala, M.: Station for Measuring Ecosystem-Atmosphere Relations (SMEAR II), *Boreal Environ. Res.*, 10, 315–322, 2005.
- Hasson, A. S., Tyndall, G. S., and Orlando, J. J.: A Product Yield Study of the Reaction of HO₂ Radicals with Ethyl Peroxy (C₂H₅O₂), Acetyl Peroxy (CH₃C(O)O₂), and Acetonyl Peroxy (CH₃C(O)CH₂O₂) Radicals, *The Journal of Physical Chemistry A*, 108, 5979–5989, doi:10.1021/jp048873t, <http://pubs.acs.org/doi/abs/10.1021/jp048873t>, 2004.
- Heard, D. E. and Pilling, M. J.: Measurement of OH and HO₂ in the Troposphere, *Chemical Reviews*, 103, 5163–5198, doi:10.1021/cr020522s, <http://pubs.acs.org/doi/abs/10.1021/cr020522s>, 2003.
- Hofzumahaus, A., Aschmutat, U., Hessling, M., Holland, F., and Ehhalt, D. H.: The measurement of tropospheric OH radicals by laser-induced fluorescence spectroscopy during the POPCORN Field Campaign, *Geophysical Research Letters*, 23, 2541–2544, doi:10.1029/96GL02205, <http://dx.doi.org/10.1029/96GL02205>, 1996.
- Hofzumahaus, A., Rohrer, F., Lu, K., Bohn, B., Brauers, T., Chang, C.-C., Fuchs, H., Holland, F., Kita, K., Kondo, Y., Li, X., Lou, S., Shao, M., Zeng, L., Wahner, A., and Zhang, Y.: Amplified Trace Gas Removal in the Troposphere, *Science*, 324, 1702–1704, 2009.
- Holland, F., Aschmutat, U., Hessling, M., Hofzumahaus, A., and Ehhalt, D.: Highly Time Resolved Measurements of OH during POPCORN Using Laser-Induced Fluorescence Spectroscopy, *Journal of Atmospheric Chemistry*, 31, 205–225, doi:10.1023/A:1005868520002, <http://dx.doi.org/10.1023/A%3A1005868520002>, 1998.
- Holland, F., Hofzumahaus, A., Schäfer, J., Kraus, A., and Pätz, H.-W.: Measurements of OH and HO₂ radical concentrations and photolysis frequencies during BERLIOZ, *Journal of Geophysical Research: Atmospheres*, 108, PHO 2–1–PHO 2–23, doi:10.1029/2001JD001393, <http://dx.doi.org/10.1029/2001JD001393>, 2003.
- Hosaynali Beygi, Z., Fischer, H., Harder, H. D., Martinez, M., Sander, R., Williams, J., Brookes, D. M., Monks, P. S., and Lelieveld, J.: Oxidation photochemistry in the Southern Atlantic boundary layer: unexpected deviations of photochemical steady state, *Atmospheric Chemistry and Physics*, 11, 8497–8513, doi:10.5194/acp-11-8497-2011, <http://www.atmos-chem-phys.net/11/8497/2011/>, 2011.
- Jaegle, L., Jacob, D. J., Brune, W. H., Faloon, I., Tan, D., Heikes, B. G., Kondo, Y., Sachse,

Bibliography

- G. W., Anderson, B., Gregory, G. L., Singh, H. B., Pueschel, R., Ferry, G., Blake, D. R., and Shetter, R. E.: Photochemistry of HO_x in the upper troposphere at northern midlatitudes, *Journal of Geophysical Research: Atmospheres*, 105, 3877–3892, doi:10.1029/1999JD901016, <http://dx.doi.org/10.1029/1999JD901016>, 2000.
- Janzen, E. G., Nutter Jr., D. E., Davis, E. R., Blackburn, B. J., Poyer, J. L., and McCay, P. B.: On spin trapping hydroxyl and hydroperoxyl radicals, *Canadian Journal of Chemistry*, 56, 2237–2242, doi:10.1139/v78-368, <http://www.nrcresearchpress.com/doi/abs/10.1139/v78-368>, 1978.
- Jenkin, M. E., Hurley, M. D., and Wallington, T. J.: Investigation of the radical product channel of the CH₃C(O)O₂ + HO₂ reaction in the gas phase, *Phys. Chem. Chem. Phys.*, 9, 3149–3162, doi:10.1039/B702757E, <http://dx.doi.org/10.1039/B702757E>, 2007.
- Junkermann, W., Platt, U., and Volz-Thomas, A.: A photoelectric detector for the measurement of photolysis frequencies of ozone and other atmospheric molecules, *Journal of Atmospheric Chemistry*, 8, 203–227, doi:10.1007/BF00051494, <http://dx.doi.org/10.1007/BF00051494>, 1989.
- Karl, T., Hansel, A., Cappellin, L., Kaser, L., Herdinger-Blatt, I., and Jud, W.: Selective measurements of isoprene and 2-methyl-3-buten-2-ol based on NO⁺ ionization mass spectrometry, *Atmospheric Chemistry and Physics*, 12, 11 877–11 884, doi:10.5194/acp-12-11877-2012, <http://www.atmos-chem-phys.net/12/11877/2012/>, 2012.
- Kesselmeier, J. and Staudt, M.: Biogenic Volatile Organic Compounds (VOC): An Overview on Emission, Physiology and Ecology, *Journal of Atmospheric Chemistry*, 33, 23–88, doi:10.1023/A:1006127516791, <http://dx.doi.org/10.1023/A/3A1006127516791>, 1999.
- Kim, S., Wolfe, G. M., Mauldin, L., Cantrell, C., Guenther, A., Karl, T., Turnipseed, A., Greenberg, J., Hall, S. R., Ullmann, K., Apel, E., Hornbrook, R., Kajii, Y., Nakashima, Y., Keutsch, F. N., DiGangi, J. P., Henry, S. B., Kaser, L., Schnitzhofer, R., Graus, M., Hansel, A., Zheng, W., and Flocke, F. F.: Evaluation of HO_x sources and cycling using measurement-constrained model calculations in a 2-methyl-3-butene-2-ol (MBO) and monoterpene (MT) dominated ecosystem, *Atmospheric Chemistry and Physics*, 13, 2031–2044, doi:10.5194/acp-13-2031-2013, <http://www.atmos-chem-phys.net/13/2031/2013/>, 2013.
- Kleffmann, J., Heland, J., Kurtenbach, R., Lorzer, J., and Wiesen, P.: A new instrument (LOPAP) for the detection of nitrous acid (HONO), *Environmental Science and Pollution Research*, 9, 48–54, 2002.
- Kleffmann, J., Gavriolaiei, T., Hofzumahaus, A., Holland, F., Koppmann, R., Rupp, L., Schlosser, E., Siese, M., and Wahner, A.: Daytime formation of nitrous acid: A major source of OH radicals in a forest, *Geophysical Research Letters*, 32, n/a–n/a, doi:10.1029/2005GL022524, <http://dx.doi.org/10.1029/2005GL022524>, 2005.

- doi.org/10.1029/2005GL022524, 2005.
- Klippel, T., Fischer, H., Bozem, H., Lawrence, M. G., Butler, T., Jöckel, P., Tost, H., Martinez, M., Harder, H., Regelin, E., Sander, R., Schiller, C. L., Stickler, A., and Lelieveld, J.: Distribution of hydrogen peroxide and formaldehyde over Central Europe during the HOOVER project, *Atmospheric Chemistry and Physics*, 11, 4391–4410, doi:10.5194/acp-11-4391-2011, <http://www.atmos-chem-phys.net/11/4391/2011/>, 2011.
- Kubistin, D.: *OH- und HO₂-Radikale über dem tropischen Regenwald*, Ph.D. thesis, Johannes Gutenberg-Universität Mainz, Germany, 2009.
- Kubistin, D., Harder, H., Martinez, M., Rudolf, M., Sander, R., Bozem, H., Eerdeken, G., Fischer, H., Gurk, C., Klüpfel, T., Königstedt, R., Parchatka, U., Schiller, C. L., Stickler, A., Taraborrelli, D., Williams, J., and Lelieveld, J.: Hydroxyl radicals in the tropical troposphere over the Suriname rainforest: comparison of measurements with the box model MECCA, *Atmospheric Chemistry and Physics*, 10, 9705–9728, doi:10.5194/acp-10-9705-2010, <http://www.atmos-chem-phys.net/10/9705/2010/>, 2010.
- Kulmala, M., Hämeri, K., Aalto, P. P., Mäkelä, J. M., Pirjola, L., Nilsson, E. D., Buzorius, G., Rannik, U., Maso, M. D., Seidl, W., Hoffman, T., Janson, R., Hansson, H.-C., Viisanen, Y., Laaksonen, A., and O’Dowd, C. D.: Overview of the international project on biogenic aerosol formation in the boreal forest (BIOFOR), *Tellus B*, 53, 324–343, doi:10.1034/j.1600-0889.2001.530402.x, <http://dx.doi.org/10.1034/j.1600-0889.2001.530402.x>, 2001.
- Langhoff, S. R., van Dishoeck, E. F., Wetmore, R., and Dalgarno, A.: Radiative lifetimes and dipole moments of the $A_2\Sigma^+$, $B_2\Sigma^+$, and $C_2\Sigma^+$ states of OH, *The Journal of Chemical Physics*, 77, 1379–1390, doi:10.1063/1.443962, <http://link.aip.org/link/?JCP/77/1379/1>, 1982.
- Leighton, P.: *Photochemistry of air pollution*, New York and London., Academic Press, 1961.
- Lelieveld, J., Peters, W., Dentener, F. J., and Krol, M. C.: Stability of tropospheric hydroxyl chemistry, *Journal of Geophysical Research: Atmospheres*, 107, ACH 17–1–ACH 17–11, doi:10.1029/2002JD002272, <http://dx.doi.org/10.1029/2002JD002272>, 2002.
- Lelieveld, J., Butler, T. M., Crowley, J. N., Dillon, T. J., Fischer, H., Ganzeveld, L., Harder, H., Lawrence, M. G., Martinez, M., Taraborrelli, D., and Williams, J.: Atmospheric oxidation capacity sustained by a tropical forest, *Nature*, 452, 737–740, <http://dx.doi.org/10.1038/nature06870>, 2008.
- Levy II, H.: Normal Atmosphere: Large Radical and Formaldehyde Concentrations Predicted, *Science*, 173, pp. 141–143, <http://www.jstor.org/stable/1732208>, 1971.
- Lowe, D. C. and Schmidt, U.: Formaldehyde (HCHO) measurements in the nonurban atmosphere,

- Journal of Geophysical Research: Oceans, 88, 10 844–10 858, doi:10.1029/JC088iC15p10844, <http://dx.doi.org/10.1029/JC088iC15p10844>, 1983.
- Lu, K. D., Rohrer, F., Holland, F., Fuchs, H., Bohn, B., Brauers, T., Chang, C. C., Häseler, R., Hu, M., Kita, K., Kondo, Y., Li, X., Lou, S. R., Nehr, S., Shao, M., Zeng, L. M., Wahner, A., Zhang, Y. H., and Hofzumahaus, A.: Observation and modelling of OH and HO₂ concentrations in the Pearl River Delta 2006: a missing OH source in a VOC rich atmosphere, *Atmospheric Chemistry and Physics*, 12, 1541–1569, doi:10.5194/acp-12-1541-2012, <http://www.atmos-chem-phys.net/12/1541/2012/>, 2012.
- Mao, J., Ren, X., Zhang, L., Van Duin, D. M., Cohen, R. C., Park, J.-H., Goldstein, A. H., Paulot, F., Beaver, M. R., Crounse, J. D., Wennberg, P. O., DiGangi, J. P., Henry, S. B., Keutsch, F. N., Park, C., Schade, G. W., Wolfe, G. M., Thornton, J. A., and Brune, W. H.: Insights into hydroxyl measurements and atmospheric oxidation in a California forest, *Atmospheric Chemistry and Physics*, 12, 8009–8020, doi:10.5194/acp-12-8009-2012, <http://www.atmos-chem-phys.net/12/8009/2012/>, 2012.
- Martinez, M., Harder, H., Kovacs, T. A., Simpas, J. B., Bassis, J., Leshner, R., Brune, W. H., Frost, G. J., Williams, E. J., Stroud, C. A., Jobson, B. T., Roberts, J. M., Hall, S. R., Shetter, R. E., Wert, B., Fried, A., Alicke, B., Stutz, J., Young, V. L., White, A. B., and Zamora, R. J.: OH and HO₂ concentrations, sources, and loss rates during the Southern Oxidants Study in Nashville, Tennessee, summer 1999, *J. Geophys. Res.*, 108, 4617–, <http://dx.doi.org/10.1029/2003JD003551>, 2003.
- Martinez, M., Harder, H., Ren, X., Leshner, R. L., and Brune, W. H.: Measuring atmospheric naphthalene with laser-induced fluorescence, *Atmospheric Chemistry and Physics*, 4, 563–569, doi:10.5194/acp-4-563-2004, <http://www.atmos-chem-phys.net/4/563/2004/>, 2004.
- Martinez, M., Harder, H., Kubistin, D., Rudolf, M., Bozem, H., Eerdekens, G., Fischer, H., Klüpfel, T., Gurk, C., Königstedt, R., Parchatka, U., Schiller, C. L., Stickler, A., Williams, J., and Lelieveld, J.: Hydroxyl radicals in the tropical troposphere over the Suriname rainforest: airborne measurements, *Atmospheric Chemistry and Physics*, 10, 3759–3773, doi:10.5194/acp-10-3759-2010, <http://www.atmos-chem-phys.net/10/3759/2010/>, 2010.
- Mihelcic, D., Ehhalt, D., Kullessa, G., Klomfass, J., Trainer, M., Schmidt, U., and Röhrs, H.: Measurements of free radicals in the atmosphere by matrix isolation and electron paramagnetic resonance, *pure and applied geophysics*, 116, 530–536, doi:10.1007/BF01636905, <http://dx.doi.org/10.1007/BF01636905>, 1978.
- Mogensen, D., Smolander, S., Sogachev, A., Zhou, L., Sinha, V., Guenther, A., Williams, J., Nieminen, T., Kajos, M. K., Rinne, J., Kulmala, M., and Boy, M.: Modelling atmospheric OH-

- reactivity in a boreal forest ecosystem, *Atmospheric Chemistry and Physics*, 11, 9709–9719, doi:10.5194/acp-11-9709-2011, <http://www.atmos-chem-phys.net/11/9709/2011/>, 2011.
- Nölscher, A. C., Williams, J., Sinha, V., Custer, T., Song, W., Johnson, A. M., Axinte, R., Bozem, H., Fischer, H., Pouvesle, N., Phillips, G., Crowley, J. N., Rantala, P., Rinne, J., Kulmala, M., Gonzales, D., Valverde-Canossa, J., Vogel, A., Hoffmann, T., Ouwersloot, H. G., Vilà-Guerau de Arellano, J., and Lelieveld, J.: Summertime total OH reactivity measurements from boreal forest during HUMPPA-COPEC 2010, *Atmospheric Chemistry and Physics*, 12, 8257–8270, doi:10.5194/acp-12-8257-2012, <http://www.atmos-chem-phys.net/12/8257/2012/>, 2012.
- Novelli, A., Hens, K., Tatum Ernest, C., Trawny, K., Rudolf, M., Kubistin, D., Hosaynali Beygi, Z., Fischer, H., Williams, J. and Paasonen, P., Sipilä, M., Keronen, P., Petäjä, T., Elste, T., Plass-Duelmer, C., Vereecken, L., Martinez, M., Lelieveld, J., and Harder, H.: The role of stabilised Criegee intermediate in gas phase H_2SO_4 formation, abstract A24D-04 presented at 2012 Fall Meeting, AGU, San Francisco, Calif., 3-7 Dec., 2012.
- Ortgies, G., Gericke, K.-H., and Comes, F. J.: Is UV laser induced fluorescence a method to monitor tropospheric OH?, *Geophysical Research Letters*, 7, 905–908, doi:10.1029/GL007i011p00905, <http://dx.doi.org/10.1029/GL007i011p00905>, 1980.
- Paulot, F., Crounse, J. D., Kjaergaard, H. G., K \ddot{A} rtten, A., St. Clair, J. M., Seinfeld, J. H., and Wennberg, P. O.: Unexpected Epoxide Formation in the Gas-Phase Photooxidation of Isoprene, *Science*, 325, 730–733, doi:10.1126/science.1172910, <http://www.sciencemag.org/content/325/5941/730.abstract>, 2009.
- Peeters, J., Vereecken, L., and Fantechi, G.: The detailed mechanism of the OH-initiated atmospheric oxidation of [small alpha]-pinene: a theoretical study, *Phys. Chem. Chem. Phys.*, 3, 5489–5504, doi:10.1039/B106555F, <http://dx.doi.org/10.1039/B106555F>, 2001.
- Peeters, J., Nguyen, T. L., and Vereecken, L.: HOx radical regeneration in the oxidation of isoprene, *Phys. Chem. Chem. Phys.*, 11, 5935–5939, doi:10.1039/B908511D, <http://dx.doi.org/10.1039/B908511D>, 2009.
- Penkett, S. A., Monks, P. S., Carpenter, L. J., Clemitshaw, K. C., Ayers, G. P., Gillett, R. W., Galbally, I. E., and Meyer, C. P.: Relationships between ozone photolysis rates and peroxy radical concentrations in clean marine air over the Southern Ocean, *Journal of Geophysical Research: Atmospheres*, 102, 12805–12817, doi:10.1029/97JD00765, <http://dx.doi.org/10.1029/97JD00765>, 1997.
- Petäjä, T., Mauldin III, R. L., Kosciuch, E., McGrath, J., Nieminen, T., Paasonen, P., Boy, M., Adamov, A., Kotiaho, T., and Kulmala, M.: Sulfuric acid and OH concentrations in a boreal

- forest site, *Atmospheric Chemistry and Physics*, 9, 7435–7448, doi:10.5194/acp-9-7435-2009, <http://www.atmos-chem-phys.net/9/7435/2009/>, 2009.
- Pöschl, U., von Kuhlmann, R., Poisson, N., and Crutzen, P. J.: Development and Intercomparison of Condensed Isoprene Oxidation Mechanisms for Global Atmospheric Modeling, *Journal of Atmospheric Chemistry*, 37, 29–52, <http://dx.doi.org/10.1023/A:1006391009798>, 10.1023/A:1006391009798, 2000.
- Pugh, T. A. M., MacKenzie, A. R., Hewitt, C. N., Langford, B., Edwards, P. M., Furneaux, K. L., Heard, D. E., Hopkins, J. R., Jones, C. E., Karunaharan, A., Lee, J., Mills, G., Misztal, P., Moller, S., Monks, P. S., and Whalley, L. K.: Simulating atmospheric composition over a South-East Asian tropical rainforest: performance of a chemistry box model, *Atmospheric Chemistry and Physics*, 10, 279–298, doi:10.5194/acp-10-279-2010, <http://www.atmos-chem-phys.net/10/279/2010/>, 2010a.
- Pugh, T. A. M., MacKenzie, A. R., Langford, B., Nemitz, E., Misztal, P. K., and Hewitt, C. N.: The influence of small-scale variations in isoprene concentrations on atmospheric chemistry over a tropical rainforest, *Atmospheric Chemistry and Physics Discussions*, 10, 18 197–18 234, doi:10.5194/acpd-10-18197-2010, <http://www.atmos-chem-phys-discuss.net/10/18197/2010/>, 2010b.
- Regelin, E., Harder, H., Martinez, M., Kubistin, D., Tatum Ernest, C., Bozem, H., Klippel, T., Hosaynali-Beygi, Z., Fischer, H., Sander, R., Jöckel, P., Königstedt, R., and Lelieveld, J.: HO_x measurements in the summertime upper troposphere over Europe: a comparison of observations to a box model and a 3-D model, *Atmospheric Chemistry and Physics Discussions*, 12, 30 619–30 660, doi:10.5194/acpd-12-30619-2012, <http://www.atmos-chem-phys-discuss.net/12/30619/2012/>, 2012.
- Reiner, T., Hanke, M., and Arnold, F.: Atmospheric peroxy radical measurements by ion molecule reaction-mass spectrometry: A novel analytical method using amplifying chemical conversion to sulfuric acid, *Journal of Geophysical Research: Atmospheres*, 102, 1311–1326, doi:10.1029/96JD02963, <http://dx.doi.org/10.1029/96JD02963>, 1997.
- Ren, X., Harder, H., Martinez, M., Faloona, I., Tan, D., Leshner, R., Di Carlo, P., Simpas, J., and Brune, W.: Interference Testing for Atmospheric HO_x Measurements by Laser-induced Fluorescence, *Journal of Atmospheric Chemistry*, 47, 169–190, doi:10.1023/B:JOCH.0000021037.46866.81, <http://dx.doi.org/10.1023/B:3AJUCH.0000021037.46866.81>, 2004.
- Ren, X., Olson, J. R., Crawford, J. H., Brune, W. H., Mao, J., Long, R. B., Chen, Z., Chen, G., Avery, M. A., Sachse, G. W., Barrick, J. D., Diskin, G. S., Huey, L. G., Fried, A., Cohen, R. C., Heikes, B., Wennberg, P. O., Singh, H. B., Blake, D. R., and Shetter, R. E.: HO_x chemistry

- during INTEX-A 2004: Observation, model calculation, and comparison with previous studies, *Journal of Geophysical Research: Atmospheres*, 113, 2156–2202, doi:10.1029/2007JD009166, <http://dx.doi.org/10.1029/2007JD009166>, 2008.
- Rinne, J., Markkanen, T., Ruuskanen, T. M., Petäjä, T., Keronen, P., Tang, M., Crowley, J. N., Rannik, U., and Vesala, T.: Effect of chemical degradation on fluxes of reactive compounds - a study with a stochastic Lagrangian transport model, *Atmospheric Chemistry and Physics*, 12, 4843–4854, doi:10.5194/acp-12-4843-2012, <http://www.atmos-chem-phys.net/12/4843/2012/>, 2012.
- Rohrer, F. and Berresheim, H.: Strong correlation between levels of tropospheric hydroxyl radicals and solar ultraviolet radiation, *Nature*, 442, 184–187, <http://dx.doi.org/10.1038/nature04924>, 2006.
- Sander, R., Baumgaertner, A., Gromov, S., Harder, H., Jöckel, P., Kerkweg, A., Kubistin, D., Regelin, E., Riede, H., Sandu, A., Taraborrelli, D., Tost, H., and Xie, Z.-Q.: The atmospheric chemistry box model CAABA/MECCA-3.0, *Geoscientific Model Development*, 4, 373–380, doi:10.5194/gmd-4-373-2011, <http://www.geosci-model-dev.net/4/373/2011/>, 2011a.
- Sander, S. P., Abbatt, J., Barker, J. R., Burkholder, J. B., Friedl, R. R., Golden, D. M., Huie, R. E., Kolb, C. E., Kurylo, M. J., Moortgat, G. K., Orkin, V. L., and Wine, P. H.: Chemical Kinetics and Photochemical Data for Use in Atmospheric Studies, Evaluation No. 17, JPL Publication Jet - Propulsion Laboratory, Pasadena, 10, <http://jpldataeval.jpl.nasa.gov>, 2011b.
- Sandu, A. and Sander, R.: Technical note: Simulating chemical systems in Fortran90 and Matlab with the Kinetic PreProcessor KPP-2.1, *Atmospheric Chemistry and Physics*, 6, 187–195, <http://www.atmos-chem-phys.net/6/187>, 2006.
- Schlosser, E., Brauers, T., Dorn, H.-P., Fuchs, H., Häsel, R., Hofzumahaus, A., Holland, F., Wahner, A., Kanaya, Y., Kajii, Y., Miyamoto, K., Nishida, S., Watanabe, K., Yoshino, A., Kubistin, D., Martinez, M., Rudolf, M., Harder, H., Berresheim, H., Elste, T., Plass-Dülmer, C., Stange, G., and Schurath, U.: Technical Note: Formal blind intercomparison of OH measurements: results from the international campaign HOxComp, *Atmospheric Chemistry and Physics*, 9, 7923–7948, doi:10.5194/acp-9-7923-2009, <http://www.atmos-chem-phys.net/9/7923/2009/>, 2009.
- Schuster, G., Labazan, I., and Crowley, J. N.: A cavity ring down/cavity enhanced absorption device for measurement of ambient NO₃ and N₂O₅, *Atmospheric Measurement Techniques*, 2, 1–13, doi:10.5194/amt-2-1-2009, <http://www.atmos-meas-tech.net/2/1/2009/>, 2009.
- Seinfeld, J. H. and Pandis, S. N.: *Atmospheric Chemistry and Physics - From Air Pollution to Climate Change* (2nd Edition), John Wiley & Sons, <http://www.knovel.com/web/portal/browse/>

- display?_EXT_KNOVEL_DISPLAY_bookid=2126, 2006.
- Sinha, V., Williams, J., Crowley, J. N., and Lelieveld, J.: The Comparative Reactivity Method – a new tool to measure total OH Reactivity in ambient air, *Atmospheric Chemistry and Physics*, 8, 2213–2227, doi:10.5194/acp-8-2213-2008, <http://www.atmos-chem-phys.net/8/2213/2008/>, 2008.
- Sinha, V., Williams, J., Lelieveld, J., Ruuskanen, T., Kajos, M., Patokoski, J., Hellen, H., Hakola, H., Mogensen, D., Boy, M., Rinne, J., and Kulmala, M.: OH Reactivity Measurements within a Boreal Forest: Evidence for Unknown Reactive Emissions, *Environmental Science & Technology*, 44, 6614–6620, doi:10.1021/es101780b, <http://pubs.acs.org/doi/abs/10.1021/es101780b>, 2010.
- Stone, D., Evans, M. J., Edwards, P. M., Commane, R., Ingham, T., Rickard, A. R., Brookes, D. M., Hopkins, J., Leigh, R. J., Lewis, A. C., Monks, P. S., Oram, D., Reeves, C. E., Stewart, D., and Heard, D. E.: Isoprene oxidation mechanisms: measurements and modelling of OH and HO₂ over a South-East Asian tropical rainforest during the OP3 field campaign, *Atmospheric Chemistry and Physics*, 11, 6749–6771, doi:10.5194/acp-11-6749-2011, <http://www.atmos-chem-phys.net/11/6749/2011/>, 2011.
- Tan, D., Faloon, I., Simpas, J., Brune, W., Shepson, P., Couch, T., Sumner, A., Carroll, M., Thornberry, T., Apel, E., Riemer, D., and Stockwell, W.: HO_x budgets in a deciduous forest: Results from the PROPHET summer 1998 campaign, *Journal of Geophysical Research*, 106, No. D20, 24 407–24 427, doi:10.1029/2001JD900016, 2001.
- Tanner, D. J. and Eisele, F. L.: Present OH measurement limits and associated uncertainties, *Journal of Geophysical Research: Atmospheres*, 100, 2883–2892, doi:10.1029/94JD02609, <http://dx.doi.org/10.1029/94JD02609>, 1995.
- Tanner, D. J., Jefferson, A., and Eisele, F. L.: Selected ion chemical ionization mass spectrometric measurement of OH, *Journal of Geophysical Research: Atmospheres*, 102, 6415–6425, doi:10.1029/96JD03919, <http://dx.doi.org/10.1029/96JD03919>, 1997.
- Taraborrelli, D., Lawrence, M. G., Butler, T. M., Sander, R., and Lelieveld, J.: Mainz Isoprene Mechanism 2 (MIM2): an isoprene oxidation mechanism for regional and global atmospheric modelling, *Atmospheric Chemistry and Physics*, 9, 2751–2777, doi:10.5194/acp-9-2751-2009, <http://www.atmos-chem-phys.net/9/2751/2009/>, 2009.
- Taraborrelli, D., Lawrence, M. G., Crowley, J. N., Dillon, T. J., Gromov, S., Grosz, C. B. M., Vereecken, L., and Lelieveld, J.: Hydroxyl radical buffered by isoprene oxidation over tropical forests, *Nature Geosci*, advance online publication, –, <http://dx.doi.org/10.1038/ngeo1405>, 2012.

- Tarvainen, V., Hakola, H., Hellén, H., Bäck, J., Hari, P., and Kulmala, M.: Temperature and light dependence of the VOC emissions of Scots pine, *Atmospheric Chemistry and Physics*, 5, 989–998, doi:10.5194/acp-5-989-2005, <http://www.atmos-chem-phys.net/5/989/2005/>, 2005.
- Tatum Ernest, C., Novelli, A., Trawny, K., Hens, K., Rudolf, M., Elste, T., Werner, A., Englert, J., Gilge, S., Plass-Dülmer, C., Lelieveld, J., Martinez, M., and Harder, H.: OH and HO₂ Measurements in a Rural Mid-Latitude Environment during HOPE2012, paper presented at the Atmospheric Chemical Mechanisms Conference, Davis, CA, 10 to 13 December 2012, <https://sites.google.com/site/atmoschemmech2012/>, 2012.
- Thornton, J. A., Wooldridge, P. J., Cohen, R. C., Martinez, M., Harder, H., Brune, W. H., Williams, E. J., Roberts, J. M., Fehsenfeld, F. C., Hall, S. R., Shetter, R. E., Wert, B. P., and Fried, A.: Ozone production rates as a function of NO_x abundances and HO_x production rates in the Nashville urban plume, *Journal of Geophysical Research: Atmospheres*, 107, ACH 7–1–ACH 7–17, doi:10.1029/2001JD000932, <http://dx.doi.org/10.1029/2001JD000932>, 2002.
- Vereecken, L., Muller, J.-F., and Peeters, J.: Low-volatility poly-oxygenates in the OH-initiated atmospheric oxidation of [small alpha]-pinene: impact of non-traditional peroxy radical chemistry, *Phys. Chem. Chem. Phys.*, 9, 5241–5248, doi:10.1039/B708023A, <http://dx.doi.org/10.1039/B708023A>, 2007.
- Vereecken, L., Harder, H., and Novelli, A.: The reaction of Criegee intermediates with NO, RO₂, and SO₂, and their fate in the atmosphere, *Phys. Chem. Chem. Phys.*, 14, 14682–14695, doi:10.1039/C2CP42300F, <http://dx.doi.org/10.1039/C2CP42300F>, 2012.
- Vesala, T., Haataja, J., Aalto, P., Altimir, N., Buzorius, G., Garam, E., Hämeri, K., Ilvesniemi, H., Jokinen, V., Keronen, P., Lahti, T., Markkanen, T., Mäkelä, J. M., E., N., Palmroth, S., Palva, L., Pohja, T., Pumpanen, J., Rannik, U., Siivola, E., Ylitalo, H., Hari, P., and Kulmala, M.: Long-term field measurements of atmosphere-surface interaction in boreal forest combining forest ecology, micrometeorology, aerosol physics and atmospheric chemistry, *Trends in Heat, Mass & Momentum Transfer*, 4, 17–35, 1998.
- Wang, C. C. and Davis, L. I.: Measurement of Hydroxyl Concentrations in Air Using a Tunable uv Laser Beam, *Phys. Rev. Lett.*, 32, 349–352, doi:10.1103/PhysRevLett.32.349, <http://link.aps.org/doi/10.1103/PhysRevLett.32.349>, 1974.
- Watanabe, T., Yoshida, M., Fujiwara, S., Abe, K., Onoe, A., Hirota, M., and Igarashi, S.: Spin trapping of hydroxyl radical in the troposphere for determination by electron spin resonance and gas chromatography/mass spectrometry, *Analytical Chemistry*, 54, 2470–2474, doi:10.1021/ac00251a015, <http://pubs.acs.org/doi/abs/10.1021/ac00251a015>, 1982.

Bibliography

- Weinstock, B.: Carbon Monoxide - Residence Time in the Atmosphere, *Science*, 166, 224–225, doi: {10.1126/science.166.3902.224}, 1969.
- Wennberg, P., Cohen, R., Hazen, N., Lapson, L., Allen, N., Hanisco, T., Oliver, J., Lanham, N., Demusz, J., and Anderson, J.: An aircraft-borne, laser-induced fluorescence instrument for the in situ detection of hydroxyl and hydroperoxyl radicals, *Rev. Sci. Instrum.*, 65, 1858–1876, 1994.
- Whalley, L. K., Edwards, P. M., Furneaux, K. L., Goddard, A., Ingham, T., Evans, M. J., Stone, D., Hopkins, J. R., Jones, C. E., Karunaharan, A., Lee, J. D., Lewis, A. C., Monks, P. S., Moller, S. J., and Heard, D. E.: Quantifying the magnitude of a missing hydroxyl radical source in a tropical rainforest, *Atmospheric Chemistry and Physics*, 11, 7223–7233, doi:10.5194/acp-11-7223-2011, <http://www.atmos-chem-phys.net/11/7223/2011/>, 2011.
- Whalley, L. K., Blitz, M. A., Desservettaz, M., Seakins, P. W., and Heard, D. E.: Reporting the sensitivity of Laser Induced Fluorescence instruments used for HO₂ detection to an interference from RO₂ radicals and introducing a novel approach that enables HO₂ and certain RO₂ types to be selectively measured, *Atmospheric Measurement Techniques Discussions*, 6, 6249–6292, doi: 10.5194/amtd-6-6249-2013, <http://www.atmos-meas-tech-discuss.net/6/6249/2013/>, 2013.
- White, J.: Long Optical Paths of Large Aperture, *J. Opt. Soc. Amer.*, 32, 285–288, 1942.
- Williams, J.: Organic Trace Gases in the Atmosphere: An Overview, *Environ. Chem.*, 1, 125–136, <http://dx.doi.org/10.1071/EN04057>, 2004.
- Williams, J., Pöschl, U., Crutzen, P., Hansel, A., Holzinger, R., Warneke, C., Lindinger, W., and Lelieveld, J.: An Atmospheric Chemistry Interpretation of Mass Scans Obtained from a Proton Transfer Mass Spectrometer Flown over the Tropical Rainforest of Surinam, *Journal of Atmospheric Chemistry*, 38, 133–166, doi:10.1023/A:1006322701523, <http://dx.doi.org/10.1023/A/3A1006322701523>, 2001.
- Williams, J., Crowley, J., Fischer, H., Harder, H., Martinez, M., Petäjä, T., Rinne, J., Bäck, J., Boy, M., Dal Maso, M., Hakala, J., Kajos, M., Keronen, P., Rantala, P., Aalto, J., Aaltonen, H., Paatero, J., Vesala, T., Hakola, H., Levula, J., Pohja, T., Herrmann, F., Auld, J., Mesarchaki, E., Song, W., Yassaa, N., Nölscher, A., Johnson, A. M., Custer, T., Sinha, V., Thieser, J., Pouvesle, N., Taraborrelli, D., Tang, M. J., Bozem, H., Hosaynali-Beygi, Z., Axinte, R., Oswald, R., Novelli, A., Kubistin, D., Hens, K., Javed, U., Trawny, K., Breitenberger, C., Hidalgo, P. J., Ebben, C. J., Geiger, F. M., Corrigan, A. L., Russell, L. M., Ouwersloot, H. G., Vilà-Guerau de Arellano, J., Ganzeveld, L., Vogel, A., Beck, M., Bayerle, A., Kampf, C. J., Bertelmann, M., Köllner, F., Hoffmann, T., Valverde, J., González, D., Riekkola, M.-L., Kulmala, M., and Lelieveld, J.: The summertime Boreal forest field measurement intensive (HUMPPA-COPEC-2010): an overview of

- meteorological and chemical influences, *Atmospheric Chemistry and Physics*, 11, 10 599–10 618, doi:10.5194/acp-11-10599-2011, <http://www.atmos-chem-phys.net/11/10599/2011/>, 2011.
- Yassaa, N., Song, W., Lelieveld, J., Vanhatalo, A., Bäck, J., and Williams, J.: Diel cycles of isoprenoids in the emissions of Norway spruce, four Scots pine chemotypes, and in Boreal forest ambient air during HUMPPA-COPEC-2010, *Atmospheric Chemistry and Physics*, 12, 7215–7229, doi:10.5194/acp-12-7215-2012, <http://www.atmos-chem-phys.net/12/7215/2012/>, 2012.
- York, D., Evensen, N. M., Martínez, M. L., and Delgado, J. D. B.: Unified equations for the slope, intercept, and standard errors of the best straight line, *American Journal of Physics*, 72, 367–375, doi:10.1119/1.1632486, <http://link.aip.org/link/?AJP/72/367/1>, 2004.

Danksagung

[Die elektronische Version dieser Dissertation enthält aus Gründen des Datenschutzes keine Danksagung.]

Curriculum Vitae

Name Korbinian Hens
Date of Birth 24th of September 1983 in Wiesbaden-Dotzheim, Germany
Nationality German

Education

Since Feb. 2009 PhD student at the Max-Planck Institute for Chemistry in the department of Airchemistry, in cooperation with the J. Gutenberg-University Mainz, Germany, Member in the graduate programme of the International Max-Planck-Research School for Atmospheric Chemistry and Physics

May 2008 - Feb. 2009 M.Sc. (German diploma), J. Gutenberg-University Mainz, Germany, Topic of thesis: „Der bodennahe, vertikale, turbulente Transport von ²²²Rn, ²²⁰Rn und anderen Spurengasen im Stammraum eines Fichtenbestandes“, supervisor: Prof. Dr. M. Wendisch

Oct. 2003 - Feb. 2009 Study of physics at the J. Gutenberg-University of Mainz, Germany

1994 - 2003 Secondary school at Rabanus-Maurus-Gymnasium, Mainz, Germany

Field campaigns

July - Aug. 2010 *Hyytiälä United Measurements of Photochemistry and Particles in Air – Comprehensive Organic Precursor Emission and Concentration study (HUMPPA-COPEC-2010)*

Aug. - Oct. 2007 *ExchanGE processes in mountainous Regions (EGER)*

May - July 2008

Aug. 2006 *LIndenberg REacTive Trace gas prOfiles (LIBRETTO)*

Publications and Conference Contributions

Foken, T., Meixner, F. X., Falge, E., Zetzsch, C., Serafimovich, A., Bargsten, A., Behrendt, T., Biermann, T., Breuninger, C., Dix, S., Gerken, T., Hunner, M., Lehmann-Pape, L., **Hens, K.**, Jocher, G., Kesselmeier, J., Lüers, J., Mayer, J.-C., Moravek, A., Plake, D., Riederer, M., Rütz, F., Scheibe, M., Siebicke, L., Sörgel, M., Staudt, K., Trebs, I., Tsokankunku, A., Welling, M., Wolff, V., and Zhu, Z.: Coupling processes and exchange of energy and reactive and non-reactive trace gases at a forest site - results of the EGER experiment, *Atmos. Chem. Phys.*, 12, 1923-1950, doi:10.5194/acp-12-1923-2012, 2012.

Hens, K., Novelli, A., Paasonen, P., Sipilä, M., Petäjä, T., Nölscher, A., Keronen, P., Trawny, K., Kubistin, D., Oswald, R., Axinte, R., Hosaynali Beygi, Z., Auld, J., Klüpfel, T., Mesarchaki, E., Song, W., Valverde Canossa, J., González Orozco, D., Königstedt, R., Bohn, B., Rudolf, M., Fischer, H., Williams, J., Crowley, J., Martinez, M., Harder, H.: Hydroxyl radical measurements in a boreal forest during HUMPPA-COPEC 2010, *Geophysical Research Abstracts*, Vol. 14, EGU2012-9051, 2012, EGU General Assembly 2012.

Novelli, A., **Hens, K.**, Paasonen, P., Sipilä, M., Petäjä, T., Keronen, P., Auld, J., Beygi, Z. H., Axinte, R., Trawny, K., Kubistin, D., Tatum Ernest, C., Rudolf, M., Adame, J. A., Fischer, H., Williams, J., Vereecken, L., Martinez, M. and Harder, H.: Assessment of the role of stabilized Criegee Intermediates in OH radical measurements by LIF, *Geophysical Research Abstracts*, Vol. 14, EGU2012-9491, 2012, EGU General Assembly 2012.

Tatum-Ernest, C., Novelli, A., Trawny, K., **Hens, K.**, Rudolf, M., Elste, T., Werner, A., Englert, J., Gilge, S., Plass-Dülmer, C., Lelieveld, J., Martinez, M., and Harder, H.: OH and HO₂ Measurements in a Rural Mid-Latitude Environment during HOPE2012, paper presented at the Atmospheric Chemical Mechanisms Conference, Davis, CA, 10 to 13 December 2012, <https://sites.google.com/site/atmoschemmech2012/>, 2012.

Novelli, A., **Hens, K.**, Tatum-Ernest, C., Trawny, K., Rudolf, M., Kubistin, D., Hosaynali Beygi, Z., Fischer, H., Williams, J. and Paasonen, P., Sipilä, M., Keronen, P., Petäjä, T., Elste, T., Plass-Dülmer, C., Vereecken, L., Martinez, M., Lelieveld, J., and Harder, H.: The

role of stabilised Criegee intermediate in gas phase H₂SO₄ formation, Abstract A24D-04 presented at 2012 Fall Meeting, AGU, San Francisco, Calif., 3-7 Dec., 2012.

Hens, K., Tatum Ernest, C., Novelli, A., Paasonen, P., Sipilä, M., Petäjä, T., Nölscher, A., Keronen, P., Trawny, K., Kubistin, D., Oswald, R., Axinte, R., Hosaynali Beygi, Z., Auld, J., Klüpfel, T., Mesarchaki, E., Song, W., Valverde Canossa, J., González Orozco, D., Königs-
tedt, R., Bohn, B., Rudolf, M., Fischer, H., Williams, J., Crowley, J., Martinez, M., Harder, H.: Hydroxyl radical measurements and oxidation capacity in a boreal forest environment, Abstract A33K-0299 presented at 2012 Fall Meeting, AGU, San Francisco, Calif., 3-7 Dec., 2012.

Williams, J., Crowley, J., Fischer, H., Harder, H., Martinez, M., Petäjä, T., Rinne, J., Bäck, J., Boy, M., Dal Maso, M., Hakala, J., Kajos, M., Keronen, P., Rantala, P., Aalto, J., Aaltonen, H., Paatero, J., Vesala, T., Hakola, H., Levula, J., Pohja, T., Herrmann, F., Auld, J., Mesarchaki, E., Song, W., Yassaa, N., Nölscher, A., Johnson, A. M., Custer, T., Sinha, V., Thieser, J., Pouvesle, N., Taraborrelli, D., Tang, M. J., Bozem, H., Hosaynali-Beygi, Z., Axinte, R., Oswald, R., Novelli, A., Kubistin, D., **Hens, K.**, Javed, U., Trawny, K., Breitenberger, C., Hidalgo, P. J., Ebben, C. J., Geiger, F. M., Corrigan, A. L., Russell, L. M., Ouwersloot, H. G., Vilà-Guerau de Arellano, J., Ganzeveld, L., Vogel, A., Beck, M., Bayerle, A., Kampf, C. J., Bertelmann, M., Köllner, F., Hoffmann, T., Valverde, J., González, D., Riekkola, M.-L., Kulmala, M., and Lelieveld, J.: The summertime Boreal forest field measurement intensive (HUMPPA-COPEC-2010): an overview of meteorological and chemical influences, *Atmos. Chem. Phys.*, 11, 10599-10618, doi:10.5194/acp-11-10599-2011, 2011.

Hens, K., Meixner, F.X., Riederer, M., Moravek, A., Bargsten, A., Zhu, Z., Andrea, M.O.: Trace gas exchange at the forest floor, *Geophysical Research Abstracts*, Vol. 11, EGU2009-5911, 2009, EGU General Assembly 2009.

Riederer, M., **Hens, K.**, Meixner, F.X., Foken, T.: Fluxes of reactive and non-reactive trace gases close to the forest floor, *Geophysical Research Abstracts*, Vol. 11, EGU2009-3248-4, 2009, EGU General Assembly 2009.

Meixner, F.X., Scheibe, M., **Hens, K.**, Feig, G.T., Andreae, M.O.: An unconventional ap-

proach to estimate the exchange of reactive trace gases at the soil - trunk space interface of a steep mountain forest site, Geophysical Research Abstracts, Vol. 11, EGU2009-9739, 2009, EGU General Assembly 2009.

Sörgel, M., Trebs, I., Moravek, A., **Hens, K.**, Zetzsch, C.: Simultaneous measurements of HONO below and above a spruce forest canopy, Geophysical Research Abstracts, Vol. 11, EGU2009-10191, 2009, EGU General Assembly 2009.

Mayer, J.-C., **Hens, K.**, Rummel, U., Meixner, F. X., and Foken, T.: Moving measurement platforms - specific challenges and corrections, Meteorol. Z., 18, 477-488, doi:10.1127/0941-2948/2009/0401, 2009.

Pape, L., Ammann, C., Nyfeler-Brunner, A., Spirig, C., **Hens, K.**, and Meixner, F. X.: An automated dynamic chamber system for surface exchange measurement of non-reactive and reactive trace gases of grassland ecosystems, Biogeosciences, 6, 405-429, doi:10.5194/bg-6-405-2009, 2009.

Hens, K., „Der bodennahe, vertikale, turbulente Transport von ^{222}Rn , ^{220}Rn und anderen Spurengasen im Stammraum eines Fichtenbestandes“, Diplomarbeit, J. Gutenberg-University, Mainz, Germany, 2009.